# Development of a Wearable Sensor-Based Framework for the Classification and Quantification of High Knee Flexion Exposures in Childcare

by

Annemarie Florence Laudanski

A thesis
presented to the University of Waterloo
in fulfillment of the
thesis requirement for the degree of
Doctor of Philosophy
in
Kinesiology

Waterloo, Ontario, Canada, 2022

# Examining Committee Membership

The following served on the Examining Committee for this thesis. The decision of the Examining committee is by majority vote.

External Examiner: **Henk Luinge**, Ph.D.
Sensor Fusion Manager
Sciosense

Supervisor: **Stacey M. Acker**, Ph.D.
Associate Professor, Dept. of Kinesiology and Health Sciences
Faculty of Health, University of Waterloo

Internal-External Member: **Arash Arami**, Ph.D.
Assistant Professor, Dept. of Mechanical and Mechatronics Engineering
Faculty of Engineering, University of Waterloo

Internal Member: **Clark R. Dickerson**, Ph.D.
Professor, Dept. of Kinesiology and Health Sciences
Faculty of Health, University of Waterloo

Internal Member: **Monica R. Maly**, Ph.D.
Professor, Dept. of Kinesiology and Health Sciences
Faculty of Health, University of Waterloo

# Author's Declaration

This thesis consists of material all of which I authored or co-authored: see Statement of Contributions included in the thesis. This is a true copy of the thesis, including any required final revisions, as accepted by my examiners.

I understand that my thesis may be made electronically available to the public.

# Statement of Contributions

This thesis contains an edited version of one manuscript written for publication which I hereby declare to be from my own work under the supervision of Dr. Stacey M. Acker. The contribution of author Jessa M. Buchman-Pearle was to data analysis. Each author additionally provided intellectual input on manuscript drafts.

Laudanski, A. F., Buchman-Pearle, J. M., & Acker, S. M. (2022). Quantifying high flexion postures in occupational childcare as they relate to the potential for increased risk of knee osteoarthritis. *Ergonomics*, *65*(2), 253–264.

# Abstract

Repetitive cyclic and prolonged joint loading in high knee flexion postures has been associated with the progression of degenerative knee joint diseases and knee osteoarthritis (OA). Despite this association, high flexion postures, where the knee angle exceeds 120°, are commonly performed within occupational settings. While work related musculoskeletal disorders have been studied across many occupations, the risk of OA development associated with the adoption of high knee flexion postures in childcare workers has until recently been unexplored; and therefore, occupational childcare has not appeared in any systematic reviews seeking to prove a causal relationship between occupational exposures and the risk of knee OA development. Therefore, the overarching goal of this thesis was to explore the adoption of high flexion postures in childcare settings and to develop a means by which these could be measured using non-laboratory-based technologies. The global objectives of this thesis were to (i) identify the postural demands of occupational childcare as they relate to high flexion exposures at the knee, (ii) apply, extend, and validate sensor to segment alignment algorithms through which lower limb flexion-extension kinematics could be measured in multiple high knee flexion postures using inertial measurement units (IMUs), and (iii) develop a machine learning based classification model capable of identifying each childcare-inspired high knee flexion posture. In-line with these global objectives, four independent studies were conducted.

### *Study I – Characterization of Postures of High Knee Flexion and Lifting Tasks Associated with Occupational Childcare*

**Background:** High knee flexion postures, despite their association with increased incidences of osteoarthritis, are frequently adopted in occupational childcare. High flexion exposure thresholds (based on exposure frequency or cumulative daily exposure) that relate to increased incidences of OA have previously been proposed; yet our understanding of how the specific postural requirements of this childcare compare to these thresholds remains limited.

**Objectives:** This study sought to define and quantify high flexion postures typically adopted in childcare to evaluate any increased likelihood of knee osteoarthritis development.

**Methods:** Video data of eighteen childcare workers caring for infant, toddler, and preschool-aged children over a period of approximately 3.25 hours were obtained for this investigation from a larger cohort study conducted across five daycares in Kingston, Ontario, Canada. Each video was segmented to identify the start and end of potential high knee flexion exposures. Each identified posture was quantified by duration and frequency. An analysis of postural adoption by occupational task was subsequently performed to determine which task(s) might pose the greatest risk for cumulative joint trauma.

**Results:** A total of ten postures involving varying degrees of knee flexion were identified, of which 8 involved high knee flexion. Childcare workers caring for children of all ages were found to adopt high knee flexion postures for durations of 1.45±0.15 hours and frequencies of 128.67±21.45 over the 3.25 hour observation period, exceeding proposed thresholds for incidences of knee osteoarthritis development. Structured activities, playing, and feeding tasks were found to demand the greatest adoption of high flexion postures.

**Conclusions:** Based on the findings of this study, it is likely that childcare workers caring for children of all ages exceed cumulative exposure- and frequency-based thresholds associated with increased incidences of knee OA development within a typical working day.

### *Study II – Evaluating the Robustness of Automatic IMU Calibration for Lower Extremity Motion Analysis in High Knee Flexion Postures*

**Background:** While inertial measurement units promise an out- of-the-box, minimally intrusive means of objectively measuring body segment kinematics in any setting, in practice their

implementation requires complex calculations in order to align each sensor with the coordinate system of the segment to which they are attached.

**Objectives:** This study sought to apply and extend previously proposed alignment algorithms to align inertial sensors with the segments on which they are attached in order to calculate flexion-extension angles for the ankle, knee, and hip during multiple childcare-inspired postures.

**Methods:** The Seel joint axis algorithm and the Constrained Seel Knee Axis (CSKA) algorithm were implemented for the sensor to segment calibration of acceleration and angular velocity data from IMUs mounted on the lower limbs and pelvis, based on a series of calibration movements about each joint. Further, the Iterative Seel spherical axis (ISSA) extension to this implementation was proposed for the calibration of sensors about the ankle and hip. The performance of these algorithms was validated across fifty participants during ten childcare-inspired movements performed by comparing IMU- and gold standard optical-based flexion-extension angle estimates.

**Results:** Strong correlations between the IMU- and optical-based angle estimates were reported for all joints during each high flexion motion with the exception of a moderate correlation reported for the ankle angle estimate during child chair sitting. Mean RMSE between protocols were found to be 6.61° ± 2.96° for the ankle, 7.55° ± 5.82° for the knee, and 14.64° ± 6.73° for the hip.

**Conclusions:** The estimation of joint kinematics through the IMU-based CSKA and ISSA algorithms presents an effective solution for the sensor to segment calibration of inertial sensors, allowing for the calculation of lower limb flexion-extension kinematics in multiple childcare-inspired high knee flexion postures.

***Study III – A Multi-Dimensional Dynamic Time Warping Distance-Based Framework for the Recognition of High Knee Flexion Postures in Inertial Sensor Data***

**Background:** The interpretation of inertial measures as they relate to occupational exposures is non-trivial. In order to relate the continuously collected data to the activities or postures performed by the sensor wearer, pattern recognition and machine learning based algorithms can be applied. One difficulty in applying these techniques to real-world data lies in the temporal and

scale variability of human movements, which must be overcome when seeking to classify data in the time-domain.

**Objectives:** The objective of this study was to develop a sensor-based framework for the detection and measurement of isolated childcare-specific postures (identified in Study I). As a secondary objective, the classification accuracy movements performed under loaded and unloaded conditions were compared in order to assess the sensitivity of the developed model to potential postural variabilities accompanying the presence of a load.

**Methods:** IMU-based joint angle estimates for the ankle, knee, and hip were time and scale normalized prior to being input to a multi-dimensional Dynamic Time Warping (DTW) distance-based Nearest Neighbour algorithm for the identification of twelve childcare inspired postures. Fifty participants performed each posture, when possible, under unloaded and loaded conditions. Angle estimates from thirty-five participants were divided into development and testing data, such that 80% of the trials were segmented into movement templates and the remaining 20% were left as continuous movement sequences. These data were then included in the model building and testing phases while the accuracy of the model was validated based on novel data from fifteen participants.

**Results:** Overall accuracies of 82.3% and 55.6% were reached when classifying postures on testing and validation data respectively. When adjusting for the imbalances between classification groups, mean balanced accuracies increased to 86% and 74.6% for testing and validation data respectively. Sensitivity and specificity values revealed the highest rates of misclassifications occurred between flatfoot squatting, heels-up squatting, and stooping. It was also found that the model was not capable of identifying sequences of walking data based on a single step motion template. No significant differences were found between the classification of loaded and unloaded motion trials.

**Conclusions:** A combination of DTW distances calculated between motion templates and continuous movement sequences of lower limb flexion-extension angles was found to be effective in the identification of isolated postures frequently performed in childcare. The developed model was successful at classifying data from participants both included and

precluded from the algorithm building dataset and insensitive to postural variability which might be caused by the presence of a load.

### *Study IV – Evaluating the Feasibility of Applying the Developed Multi-Dimensional Dynamic Time Warping Distance-Based Framework to the Measurement and Recognition of High Knee Flexion Postures in a Simulated Childcare Environment*

**Background:** While the simulation of high knee flexion postures in isolation (in Study III) provided a basis for the development of a multi-dimensional Dynamic Time Warping based nearest neighbour algorithm for the identification of childcare-inspired postures, it is unlikely that the postures adopted in childcare settings would be performed in isolation.

**Objectives:** This study sought to explore the feasibility of extending the developed classification algorithm to identify and measure postures frequently adopted when performing childcare specific tasks within a simulated childcare environment.

**Methods:** Lower limb inertial motion data was recorded from twelve participants as they interacted with their child during a series of tasks inspired by those identified in Study I as frequently occurring in childcare settings. In order to reduce the error associated with gyroscopic drift over time, joint angles for each trial were calculated over 60 second increments and concatenated across the duration of each trial. Angle estimates from ten participants were time windowed in order to create the inputs for the development and testing of two model designs wherein: (*A*) the model development data included all templates generated from Study III as well as continuous motion windows here collected, or (*B*) only the model development data included only windows of continuous motion data. The division of data into the development and testing datasets for each 5-fold cross-validated classification model was performed in one of two ways wherein the data was divided: (*a*) through stratified randomized partitioning of windows such that 80% were assigned to model development and the remaining 20% were reserved for testing, or (*b*) by partitioning all windows from a single trial of a single participant for testing while all remaining windows were assigned to the model development dataset. When the classification of continuously collected windows was tested (using division strategy *b*), a logic-based correction module was introduced to eliminate any erroneous predictions. Each model design (*A* and *B*) was developed and tested using both data division strategies (*a* and *b*) and subsequently their

performance was evaluated based on the classification of all data windows from the two subjects reserved for validation.

**Results**: Classification accuracies of 42.2% and 42.5% were achieved when classifying the testing data separated through stratified random partitioning (division strategy *a*) using models that included (model *A*, 159 classes) or excluded (model *B*, 149 classes) the templates generated from Study III, respectively. This classification accuracy was found to decrease when classifying a test partition which included all windows of a single trial (division strategy *b*) to 35.4% when using model *A* (where templates from Study III were included in the model development dataset); however, this same trial was classified with an accuracy of 80.8% when using model *B* (whose development dataset included only windows of continuous motion data). This accuracy was however found to be highly dependent on the motions performed in a given trial and logic-based corrections were not found to improve classification accuracies. When validating each model by identifying postures performed by novel subjects, classification accuracies of 24.0% and 26.6% were obtained using development data which included (model *A*) and excluded (model *B*) templates from Study III, respectively. Across all novel data, the highest classification accuracies were observed when identifying static postures, which is unsurprising given that windows of these postures were most prevalent in the model development datasets.

**Conclusions:** While classification accuracies above those achievable by chance were achieved, the classification models evaluated in this study were incapable of accurately identifying the postures adopted during simulated childcare tasks to a level that could be considered satisfactory to accurately report on the postures assumed in a childcare environment. The success of the classifier was highly dependent on the number of transitions occurring between postures while in high flexion; therefore, more classifier development data is needed to create templates for these novel transition movements. Given the high variability in postural adoption when caring for and interacting with children, additional movement templates based on continuously collected data would be required for the successful identification of postures in occupational settings.

### *Global Conclusions*

Childcare workers exceed previously reported thresholds for high knee flexion postures based on cumulative exposure and frequency of adoption associated with increased incidences of knee OA

development within a typical working day. Inertial measurement units provide a unique means of objectively measuring postures frequently adopted when caring for children which may ultimately permit the quantification of high knee flexion exposures in childcare settings and further study of the relationship between these postures and the risk of OA development in occupational childcare. While the results of this thesis demonstrate that IMU based measures of lower limb kinematics can be used to identify these postures in isolation, further work is required to expand the classification model and enable the identification of such postures from continuously collected data.

# Acknowledgments

I find myself in the most fortunate of scenarios to have so many people to thank for their ongoing support throughout the completion of this thesis. Without all of you, I would not be the person I am today, nor would I have found the passion for academia that now drives me to my next adventure. TL;DR: Thank you all so very much!

First, I must take the opportunity to thank my supervisor, Dr. Stacey Acker, who took the risk of accepting a student three years removed from academia and full of wild dreams of working almost exclusively in the realms of machine learning and wearable sensing into her research program. Without your continued support, encouragement, and sometimes what felt like unfounded trust, I would not be where I am today. Stacey, you've always encouraged me to be the best academic possible while being an exemplar model of compassion and understanding on topics far beyond those presented in these pages. I am so fortunate to have worked with you and will forever value your insight and your mentorship. Thank you for your time and investment in my future, and for believing in me, so much so that I finally started believing in myself.

Thank you also to my committee members, Drs. Arash Arami, Clark Dickerson, and Monica Maly. Your insights and support throughout this thesis have been incredibly appreciated. Arash, without your input I would not have made the connections responsible for driving many of the ideas behind this research, thank you for taking the time and risk on me. Clark, thank you for bringing your knowledge and wit to this thesis. Working with you made for an enjoyable experience while ensuring the outcomes of this thesis were applicable to a broad audience. Monica, I am so thankful for your ongoing support, from initially accepting this position while on parental leave to your continued encouragement each step of the way. Your smile and kind

words have supported me far more than I think you know, and I am truly appreciative to have had the opportunity to work with you. Thank you all for your time and insight over the years and for your unique perspectives, thorough review, and discussion of this work.

I would be remiss if I did not additionally thank the mentorship I received from outside the University of Waterloo during this degree. Dr. Bjoern Eskofier, thank you for allowing me to join the MaD lab for a brief period during which I felt entirely welcomed and overwhelmed by the thought-provoking conversations and knowledge being shared on a daily basis. Thank you also for your encouragement and support of this work, you have helped shape my thesis and the research I hope to continue pursuing and for that I am forever grateful. Dr. Anselmo Frizera Neto, thank you for taking the time to meet with me so regularly in the peak of the pandemic, and moreover, for humanizing research when I needed it most. Your mentorship will forever impact my approach to academia and has made me a better writer, researcher, and mentor.

To my fellow students, both past and present, graduate studies would not have been the same, and likely would not have been possible without you. The pandemic related lockdowns truly highlighted how important each quick hallway chat and after work drink were to my mental health. I'm so glad we were able to return to (somewhat) normal for the completion of this document, as the return of these seemingly trivial interactions likely kept me sane while writing these pages. To all members of the BOHM lab past and present, thank you for your work and dedication in advancing high knee flexion research and your support of my own crazy thoughts and ideas, I've grown so much with you all and will cherish the memories forever. I could go on to thank each friend I've made individually but doing so might result in a record-breaking and braggadocios acknowledgement section, which I would like to avoid, and so; To all of you, you know who you are, thank you for lifting me up, and recognizing the achievements I've made, often before I recognized them myself. Your friendship and support have meant the world.

I would like to formally acknowledge my funding sources, without whom this research would not have been possible: the Natural Sciences and Engineering Council of Canada (NSERC), the Ontario government, the International Society of Biomechanics, and the Ross and Doris Dixon Charitable Foundation for the Doctoral Thesis Completion Award.

Finally, I must humbly acknowledge that none of this would have been possible without my ultimate supporters, Matthew Mascioli and my dog Macs. The roller coaster of emotions which accompanied this thesis was at many times greater than I could bear alone, and in those moments your love helped me push through. Macs, you were the best friend I could have asked for and spending nearly two years at home with you was the silver lining to a global pandemic. There are no words to express my thanks to you, sweet boy.

# Dedication

In loving memory of Macs.

# Table of Contents

# List of Figures

# List of Tables

# List of Abbreviations

| | |
|---|---|
| 3D | Three Dimensional |
| 95% CI | 95% Confidence Interval |
| ACS | Adult Sized Chair Sitting |
| ANN | Artificial Neural Network |
| ANOVA | Analysis of Variance |
| BMI | Body Mass Index |
| CCS | Child Sized Chair Sitting |
| CLS | Crossed Leg Sitting |
| CS | Coordinate System |
| CSKA | Constrained Seel Knee Axis |
| DAK | Double Arm Supported Kneeling |
| DK | Dorsiflexed Kneeling |
| DoF | Degree of Freedom |
| DTW | Dynamic Time Warping |
| FD | Frequency Domain |
| FFT | Fast Fourier Transform |
| FLRS | Floor Sitting |
| FS | Flatfoot Squatting |
| HS | Heels-Up Squatting |
| IMU | Inertial Measurement Unit |
| ISSA | Iterative Seel Spherical Axis |
| kNN | *k*-Nearest Neighbour |

| | |
|---|---|
| LDA | Linear Discriminate Analysis |
| LM | Levenberg-Marquardt |
| mDTW | Multi-Dimensional Dynamic Time Warping |
| MEMS | Microelectromechanical System |
| MSK | Musculoskeletal |
| OA | Osteoarthritis |
| OR | Odds Ratio |
| PCA | Principle Component Analysis |
| PK | Plantarflexed Kneeling |
| PME | Percent Mean Error |
| RMSE | Root Mean Squared Error |
| RoM | Range of Motion |
| SAK | Single Arm Supported Kneeling |
| SD | Standard Deviation |
| SJA | Seel Joint Axis |
| SL | Side Leaning |
| SS | Side Sitting or Leaning |
| STD | Standing |
| STLS | Stool Sitting |
| STP | Stooping |
| SVM | Support Vector Machine |
| TD | Time Domain |
| TFD | Time Frequency Domain |
| WHO | World Health Organization |
| WLK | Walking |
| WSIB | Workplace Safety and Insurance Board |
| _A | Ascent |
| _AD | Ascent Descent |
| _AW | Ascent Walk |
| _D | Descent |
| _DA | Descent Ascent |
| _DS | Descent Static |

| | |
|---|---|
| _S | Static |
| _SA | Static Ascent |
| _W | Walk |
| _WD | Walk Descent |

# Chapter 1

# General Introduction

## 1.1 Scope of the Problem

High knee flexion postures (such as kneeling, squatting, or bending), where the flexion angle exceeds 120° are commonly adopted in occupational settings where workers are required to perform repetitive high flexion motions for a significant portion of their working hours (Coggon et al., 2000; Felson, 1994). These repetitive cyclic or prolonged joint loadings are known factors in the progressive degradation of knee joint tissue and increased incidences of knee osteoarthritis (OA) (Felson, 1988, 2013; Henriksen, Graven-Nielsen, Aaboe, Andriacchi, & Bliddal, 2010). Compounding this, when not in high flexion postures, workers are often required to lift and carry heavy or awkward loads which may independently contribute to increased risk of OA development (C. Cooper, McAlindon, Coggon, Egger, & Dieppe, 1994). Despite the growing incidence of knee OA worldwide and the financial burden these place on the healthcare system, little has been done to address the increased risk factors within occupational settings.

The study of occupational exposures of high knee flexion, to date, has focused primarily on observational or questionnaire based qualification of movement types and simulating occupational exposures within a laboratory-based environment (Grant, Habes, & Tepper, 1995; Jensen, Rytter, & Bonde, 2010; Klussmann et al., 2010; Schiphof, Boers, & Bierma-Zeinstra,

2008; Seidler et al., 2008). While some focus has been paid to floor layers, tile setters, and miners, the exposure to high flexion postures in childcare has only recently begun to be explored (Burford et al., 2017; Hendriksen, Korshøj, Skotte, & Holtermann, 2020). Given the primarily young, female demographic of childcare workers, the occupational exposures of this industry may predispose individuals towards the initiation or progression of musculoskeletal (MSK) diseases or knee OA (Erick & Smith, 2011; Grant et al., 1995). There is therefore a need to quantify childcare worker exposure to occupational high knee flexion postures. However, several challenges exist in studying the occupational demands of childcare. There is first a need to protect the privacy of the children under the care of the childcare worker, limiting the types of measurement tools which can be used. Consideration must also be given to the active nature of this occupation as well as the potential for occlusion of recording instrumentation due to children, toys, or furniture within laboratory or childcare settings. Due to these constraints, studies conducted on childcare workers have relied on self-reported measures through questionnaires or on the observation and measurement of a very small sample of childcare workers (Burford et al., 2017; Gratz, Claffey, King, & Scheuer, 2002; Y. Horng, Hsieh, Wu, Feng, & Lin, 2007; Labaj et al., 2016; Linnan et al., 2017; Okuno, Uketa, Nakaseko, & Tokunaga, 1997; Shimaoka et al., 1997). While the majority of recent studies have focused primarily on the association between lifting postures and back and shoulder pain in childcare workers, the prevalence of knee pain, with severity equal or greater to that of other body segments, has repeatedly been reported (Grant et al., 1995; Y. Horng et al., 2007; Labaj et al., 2016). This elevated reporting of pain development demonstrates a need for the objective measurement of occupational exposures within childcare settings in order to investigate any potential links between these exposures and increased risk of knee OA. Recent endeavours in Germany and Denmark have sought to quantify the physical work demands of childcare workers through wearable sensing (Burford et al., 2017; Holtermann, Hendriksen, Schmidt, Svendsen, & Rasmussen, 2020), however neither study employed computational methods specifically designed for the unique postural requirements of childcare, and as such may have under-reported the daily exposures experienced by childcare workers.

## 1.2 Thesis Overview

Given that little information is known about the postural requirements of the childcare industry, using a combination of observational and laboratory-based studies, the overarching goal of this thesis was to explore the adoption of high flexion postures in childcare settings and to develop a means by which these could be identified and measured using non-laboratory-based technologies. To achieve this, four studies aimed at observing and/or simulating potentially knee straining postures and the associated tasks for which they were performed were completed, with the aim of developing a wearable sensor-based framework through which the physical demands of this occupation could be quantified (Figure *1.1*). In the context of this thesis, the term knee straining will be used as it has been colloquially within the literature to refer to exposures of high knee flexion rather than referring to events which might lead to increased strain within the joint (including contact with the environment, lifting tasks, etc.).

The first study sought to characterize and document the high knee flexion postures frequently adopted in occupational childcare through the analysis of video-recordings obtained from a larger multi-center cohort study in Kingston, Ontario, Canada (Labaj et al., 2016). These data presented a unique opportunity for the characterization of knee straining exposures in childcare given that video-based collections are generally not welcomed within childcare facilities due to the privacy considerations of the children being cared for. The childcare specific tasks performed to elicit each potentially knee straining posture were additionally identified through this analysis, thereby defining the breadth of postural requirements on childcare workers and their potential association with increased risk of knee osteoarthritis development in these individuals.

In the second study, previously proposed algorithms for the alignment of inertial sensors to body segments were applied and extended for the measurement of high knee flexion joint kinematics for the ankle, knee, and hip using non-laboratory based wearable technologies. Postures identified in **Study 1** (Chapter 3) as potentially knee straining were simulated in isolation while inertial measures of segmental acceleration and angular velocity were captured. Once aligned to the body, these signals were combined using a custom complementary filter in order to estimate the flexion-extension angles throughout the childcare inspired postures and subsequently these estimates were evaluated in comparison to gold-standard optical-based

kinematic measures through differences in range of motion, root mean squared error, percent mean error, and the Pearson correlation coefficients. This evaluation established levels of confidence in the ankle, knee, and hip angle estimates and justified the use of inertial sensors for the quantification of high knee flexion postures in non-laboratory settings.

The third study built upon the postural characterizations established in **Study 1** (Chapter 3) and the kinematic measures derived in **Study 2** (Chapter 4) in order develop a sensor-based framework for the detection and measurement of childcare-specific postures performed in a controlled environment. Therefore, a multi-dimensional Dynamic Time Warping (mDTW) distance-based Nearest Neighbour classification algorithm was created for the identification of twelve groupings of childcare inspired postures performed under unloaded and loaded conditions. The performance of the classification model was evaluated when applied to the prediction of both novel movements performed by participants included in its development as well as movements performed by novel participants.

Finally, in the fourth study, the classification framework was evaluated through four models developed for the classification of pseudo-real-world data through the prediction of postures adopted when completing childcare inspired activities (derived from the findings of **Study 1,** Chapter 3) while caring for and interacting with a child within a laboratory-based simulated childcare environment. While the framework used in the development of these models was found to be stable in the classification of controlled movements **(Study 3**, Chapter 5), their performance was markedly lower when identifying the postures adopted during these childcare inspired activities. The study therefore demonstrates the limitations in applying laboratory-derived models to the classification of real-world movements and highlights areas for future development.

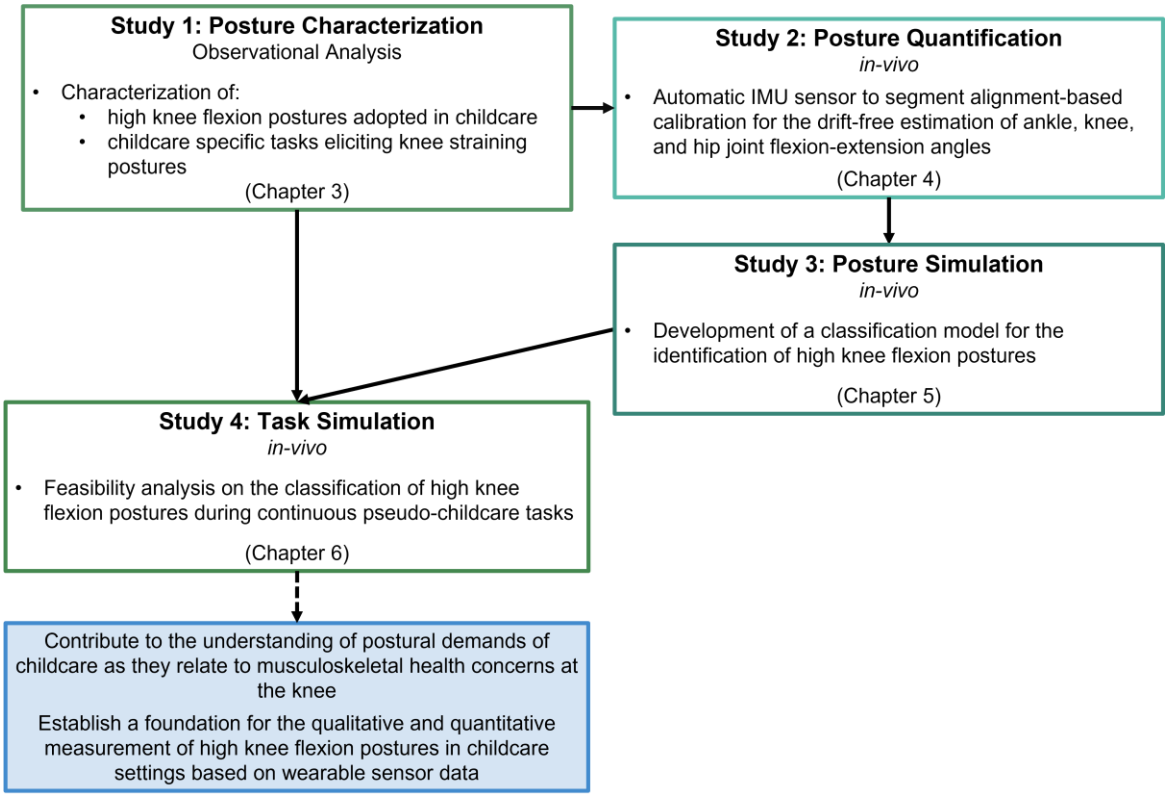


Figure 1.1 Connection and specific objectives of the four studies contained in this thesis and their contributions to the field.

## 1.3 Global Thesis Objectives

The research presented in this thesis has at its heart two global objectives. The first was to explore the adoption of high knee flexion postures within occupational childcare environments in order to further understand the associations, if any, between childcare related exposures and the potential for knee joint degeneration and OA development. The second objective was to establish a framework by which these commonly adopted postures could be identified and measured using non-laboratory-based wearable sensors. Together, these objectives would establish a foundation for the qualitative and quantitative measurement of high knee flexion exposures in childcare settings.

## 1.4 Specific Thesis Objectives

In order to accomplish the global thesis objectives, three specific objectives were therefore explored throughout this thesis:

1. To characterize the postural demands of occupational childcare as they related to high flexion exposures at the knee and identify the specific tasks which elicit the adoption of these postures in childcare settings (**Study 1**, Chapter 3)
2. To apply, extend, and validate sensor to segment alignment algorithms through which lower limb flexion-extension kinematics could be measured in multiple high knee flexion postures using inertial measurement units. (**Study 2**, Chapter 4)
3. To develop a machine learning based classification model capable of identifying each childcare-inspired high knee flexion posture (**Studies 3 & 4**, Chapter 5 and Chapter 6)

## 1.5 Significance

It remains unclear whether prolonged exposure to high flexion postures, frequent transitions through these postures, or high estimated cumulative exposures over an individual's career or lifetime result in the greatest damage to the knee, yet the currently available literature points to increased incidences of OA associated with each of these phenomena (Coggon et al., 2000; C. Cooper et al., 1994; D'Souza et al., 2008; Jensen et al., 2010; X. Wang et al., 2020). Similarly, despite the frequent adoption of high knee flexion postures in occupational childcare, the potential for MSK trauma among these workers has largely been unexplored (Grant et al., 1995; Holtermann et al., 2020; Labaj et al., 2016; Linnan et al., 2017). The overall goal of this thesis was therefore to bridge the gap between the mechanistic and occupational literature relating to childcare using *observational* and *in vivo* studies in combination with computational approaches to human motion measurement and posture recognition through wearable sensor-based data.

# Chapter 2

# Review of Literature

This thesis sought to develop a model capable of identifying high knee flexion postures and assessing knee osteoarthritis risk by comparing temporal characteristics of high flexion exposures to previously established thresholds from the current literature. This literature review will therefore be divided into three Subsections in order to familiarize the reader with the current state-of-the-art and motivation for the proposed work. The first Subsection will introduce knee OA as a debilitating disease aggravated by exposure to postures of high knee flexion. Subsequently, evidence will be provided in order to highlight the link between occupational postures of high knee flexion and risk of OA, as well as the literature gaps surrounding occupational childcare. Finally, a brief review of wearable inertial technologies as well as machine learning classification models will be conducted in order to present the potential for data acquisition and analysis outside of traditional laboratory-based settings through classification algorithms.

## 2.1 Knee Osteoarthritis Development

In order to address the motivation for creating an occupational exposure measurement tool, the link between high flexion postures and the potential for OA development must be explored. In

this Subsection, a general overview of disease development will be provided in order to establish a foundational understanding of OA as a musculoskeletal disorder that may be initiated as a function of occupational high flexion postures. OA affects each individual differently, however it typically manifests clinically as pain, limited mobility, and joint deformity, and is clinically characterized by the deterioration and loss of articular cartilage within the joint (Arokoski, Jurvelin, Väätäinen, & Helminen, 2000; Osteoarthritis Research Society International, 2018). There are known discrepancies between radiographic and symptomatic occurrences of knee OA, suggesting that structural degeneration and symptomatic progression of the disease are most likely associated with different biomechanical factors (Englund & Lohmander, 2004). While biomechanical studies have sought to analyze both symptomatic and non-symptomatic occurrences of OA, a greater burden is placed on the healthcare system by those individuals presenting with symptomatic OA due to the detrimental effects this disease has on quality of life and its association with an increased risk of mortality (Y. Wang et al., 2021). Symptomatic knee OA was reported to affect 9.6% of men and 18.0% of women aged 60 and greater in 2010 (Osteoarthritis Research Society International, 2018). The Canadian joint replacement registry annual report indicated degenerative arthritis was the most common reason for total knee replacement (99.4%), with 75,073 surgeries performed in Canada between 2019 and 2020, representing an increase in growth of 0.4% from the previous year (CIHI, 2021). 2020-2021 saw a 26.4% decrease in surgeries, with only 55,285 knee replacements performed in Canada. It is important to note that the Canadian Institute for Health Information estimates that approximately 48,000 knee and hip replacements were not performed between 2020-2021 due to the COVID 19 pandemic, and that the average annual increase in knee joint replacements prior to 2019 was 5% (CIHI, 2021, 2022). OA has also been shown to be the most common reason for total knee replacement in the United States, with the number of these surgeries doubling from 2000 to 2006 (DeFrances, Lucas, & Golosinskiy, 2008). The rapid increase in the number of total knee replacements stemming from cases of OA therefore suggests that this disease will present a growing problem to our health care and public health systems in the years to come (Y. Zhang & Jordan, 2010).

It is likely that the onset of joint degeneration leading to OA requires a host of conditions to be in place rather than a single triggering event. Numerous systemic and local risk factors for

knee OA development and progression have been identified from large epidemiological studies, yet the relationship among these factors remains poorly understood (Felson & Zhang, 1998; Y. Zhang & Jordan, 2010). Systematic factors include age, sex, racial characteristics, and genetics and are responsible for establishing the foundation for cartilage properties within the body. Local biomechanical factors include the magnitude and location of joint loading, history of joint injury, obesity resulting in excessive joint loading, and joint deformities and are a driving influence on the qualities of articular cartilage which will ultimately lead to its healthy remodelling or its breakdown (Felson & Zhang, 1998). Local biomechanical factors will influence the site and severity of OA development (Arokoski et al., 2000). Many environmental factors have also been shown to influence joint health (Arokoski et al., 2000). Occupational requirements including repetitive high flexion postures, potentially coupled with heavy lifting, have been related to increased incidences of knee OA (Coggon et al., 2000; Kellgren & Lawrence, 1958). The importance of these factors as they relate to OA risk for the purpose of this thesis will be explained in the subsequent Subsections to highlight the link between OA development and occupational high flexion exposures.

### 2.1.1.Anatomical Effects of OA

The knee is a synovial joint consisting of three articulating surfaces: two tibiofemoral articulations between the medial and lateral femoral and tibial condyles, and one patellofemoral articulation between the patella and femur. Given the incongruity of these articular surfaces, the surrounding muscles, ligaments, and tendons contribute to joint stability as well as flexion and extension, internal and external rotation, and abduction and adduction motions (Jackson, Wluka, Teichtahl, Morris, & Cicuttini, 2004; Moore, Dalley, & Agur, 2010). Two menisci of fibrocartilage lie between the medial and lateral articulating surfaces of the femur and tibia and contribute to force transmission, stress distribution, shock absorption, as well as joint stabilization within the knee joint (Hoshino & Wallace, 1987; McDermott, Masouros, & Amis, 2008).The articular surfaces of the femur, tibia, and patella are lined with cartilage, a permeable, mechanically viscoelastic structure (Laasanen et al., 2003). The smooth, irregularity free, external surfaces of healthy articular cartilage are well adapted to absorb and dissipate loads, thus creating a protective barrier and preventing any bone-on-bone contact (Kumar, 2001).

Incidences of knee osteoarthritis, which can be a debilitating disorder, are increasing in prevalence. Knee OA affects joint cartilage and the underlying subchondral bone of a joint (Felson, 1988, 2006). Healthy cartilage matrix is mainly composed of collagen fibers which provide tensile support for the tissue while negatively charged proteoglycans attract water molecules within the tissue which provide the compressive resistance and shock absorbing characteristics to cartilage (Maldonado & Nam, 2013). In the early stages of OA, even prior to cartilage surface deterioration, decreases in superficial proteoglycan concentrations are observed, along with increased water content, which contribute to a decreasing compressive modulus and expose the cartilage to greater strains under mechanical stress (Maldonado & Nam, 2013). Collagen synthesis rate, however, is observed to increase in early stages of OA, accompanied by a change from collagen type II to type I (Silver, Bradica, & Tria, 2002). While healthy cartilage is primarily composed of collagen type II, collagen type I is primarily found in subchondral bone tissue, therefore these new fiber types result in a decrease to the collagen's elastic modulus (Hollander et al., 1994; Venn & Maroudas, 1977). As the tissue's ability to store elastic energy decreases, fibrillation and fissure formation is observed (Silver et al., 2002). As OA advances and the composition of collagen type II and proteoglycans decrease, a decrease in cartilage stiffness leading to collagen network disorganization and softening are observed (Kempson, Spivey, Swanson, & Freeman, 1971).

It is hypothesized that once the superficial zone of the cartilage is lost, the underlying cartilage is subjected to abnormally high strains, and degenerative changes thus begin to extend into deeper cartilage zones (Arokoski et al., 2000). In healthy articular cartilage, it is the process of loading and joint movement which ensures the normal balance between nutrition synthesis and waste removal within the articular cartilage extracellular matrix and synovial fluid of the joint (Arokoski et al., 1996; Arokoski, Kiviranta, Jurvelin, Tammi, & Helminen, 1993; Oettmeier et al., 1992). Normal cartilage structure and properties are optimized for load-bearing function. Regular loading and unloading of a joint enhances proteoglycan synthesis (Arokoski et al., 2000) which directly affects the permeability of the cartilage. Areas of articular cartilage which are regularly subjected to high levels of shear stress, such as the patellar surface of the femur and the femoral condyles, show a higher degree of parallel collagen fibers and a thicker superficial zone in comparison to areas which are preferentially subjected to weight bearing such as the tibial

plateaus which have higher proteoglycan concentrations (Arokoski, Hyttinen, Helminen, & Jurvelin, 1999). Under high compressive loads, the cartilage behaves as an incompressible material, yet the loading will be influenced by the percentage of interstitial fluid flowing through or held within the collagen matrix. In dynamic loading scenarios, due to the relatively low permeability of the cartilage, this interstitial fluid remains trapped within the tissue, and pressurizes to support the majority of the load (Griffin & Guilak, 2005). While loading contributes to the balance and maintenance of healthy cartilage, some studies have shown that continuous compression, as observed in prolonged static loading, suppresses metabolic activity and diminishes proteoglycan synthesis ultimately leading to tissue damage through necrosis (Arokoski et al., 2000; Griffin & Guilak, 2005).

One frequently used measure of loading at the knee joint is ground reaction force. However, internal, site-specific loading of a joint is a function of internal geometry, bone alignment, and articular cartilage thickness as well as functional mechanical properties, therefore local loading at a joint may be very different between individuals despite identical global measures of external reaction forces (Moore et al., 2010). If changes and degeneration in structures within the knee are site specific, global measures of loading may not be representative of the loading conditions within the joint. It has been reported that roughly 68% of all instances of knee OA occur within the medial compartment (Felson et al., 2002). It is believed that these increased incidences are the result of increased loading and an imbalance in the proportion of medial to lateral loading, given the majority of reaction loads have been shown to pass medially to the knee joint center leading to compression of the medial tibial plateau (Andriacchi et al., 2004; Kinney et al., 2013). Internal adduction and abduction moments may compound or counteract, respectively, the effects of such external loads and moments on the knee. Given this general overview of the implication of joint loading in the development of OA, leading to changes at the anatomical level within the knee, it is evident that all sources of joint loading must be considered when exploring joint degeneration. In the following Subsection, the loading characteristics accompanying high knee flexion postures will further be explored.

### 2.1.2. High Knee Flexion Leading to the Loading of Unconditioned Tissues

While many factors have been shown to influence the potential for OA development, one of particular importance for this thesis is the adoption of postures involving high knee flexion. It has been postulated that high knee flexion postures, where a flexion angle of greater than 120$^{o}$ is attained, expose unconditioned cartilage to high joint contact forces (Andriacchi & Favre, 2014; Andriacchi et al., 2004). At low flexion angles, the tibia has been shown to rotate anteriorly, followed by posterior movement between 60$^{o}$ and 120$^{o}$. Beyond 120$^{o}$ posterior tibial translation is reduced and anterior tibial rotation can again be observed (Li et al., 2004; Qi et al., 2013). Between 30$^{o}$ and 120$^{o}$ of flexion, the lateral femoral condyle is observed to translate posteriorly while beyond 120$^{o}$, both the lateral and femoral condyles translate rapidly posteriorly (Qi et al., 2013). The lateral translation of the medial and lateral femoral condyles in high flexion has also been shown to result in a contact area decrease of roughly 25% between the femoral and tibial surfaces when compared to those in extension (Yao, Lancianese, Hovinga, Lee, & Lerner, 2008). Therefore, the posterior translation of tibiofemoral contacts accompanied by the decrease in contact area result in loads being transmitted through cartilage which is not typically loaded on a regular basis. To illustrate this change in cartilage loading, a comparison of loading locations between gait and high flexion lunging can be seen in Figure *2.1*.

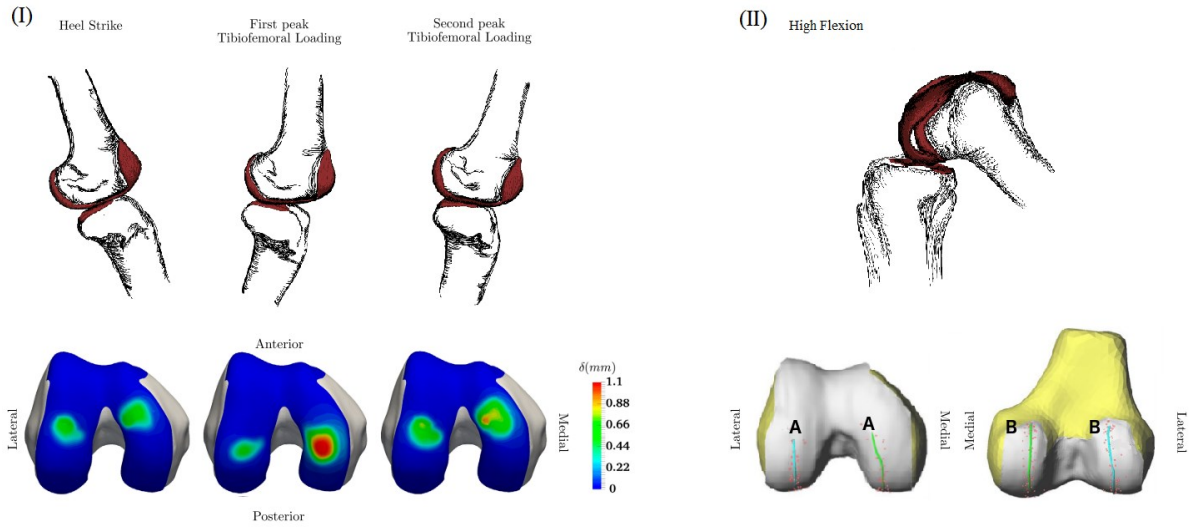


Figure 2.1 Loading instances for the medial and lateral femoral condyles during various phases of knee flexion. In the first row of both (I) and (II) the red represents articular cartilage of the femoral and tibial contact surfaces. In (I) instances of tibiofemoral contact from a typical gait cycle, with schematics of motion in the first row and loading location and deflections on the femoral condyles in the second row. Areas with non-zero deflection indicate where load is being applied. In (II) tibiofemoral contact in full flexion (greater than 140º) is shown in the first row, while the second row demonstrates the trajectory of contact points on the femoral condyles for various stages during an in vivo weight bearing lunge from (A) full extension through (B) maximum flexion. Adapted from Rakhsha et al (2018) and Qi et al (2013)

The human knee has adapted over the centuries for upright locomotion (Lovejoy, 2007). It has been suggested that this adaptation has resulted in a reduction of quadriceps force requirements for locomotion through an increased patellar moment arm due to anterior prolongations of the tibial condyles. These evolutionary changes have adapted the human knee through elongation of the femoral condyle, in order to reduce joint loading and stresses during extension through enhanced tibiofemoral cartilage congruity (Lovejoy, 2007). However, no such adaptation strategies have evolved for the reduction of loads in high flexion. The posterior extremities of the femoral condyles therefore may experience increased stresses in high flexion, resulting in inflammatory responses and degradation of cartilage over time (Andriacchi & Favre, 2014). Given the preferential conditioning of human cartilage for upright tasks and locomotion, the frequent adoption of high flexion postures in occupational settings may be of particular concern in the study of OA development. It is for this reason that the identification of high flexion postures will be a primary objective of this proposed work.

## 2.2 Occupation Related Risks for OA Development

While the previous Subsection outlined the biological effects of high knee flexion, recent research has begun to show links between exposures to occupational postures of high knee flexion and increased risks of knee pain and OA development, which will here be explored (Canetti, Schram, Orr, Knapik, & Pope, 2020; Coggon et al., 2000; C. Cooper et al., 1994; Jensen et al., 2010; Osteoarthritis Research Society International, 2018; Rytter, Egund, Jensen, & Bonde, 2009). It has been suggested that occupational workers such as miners (Kellgren & Lawrence, 1952; Schiphof et al., 2008), floor layers and tile setters (Coggon et al., 2000; C. Cooper et al., 1994; Jensen et al., 2010; Sandmark, Hogstedt, & Vingård, 2000), and childcare workers (Burford et al., 2017; Grant et al., 1995; Gratz et al., 2002; Holtermann et al., 2020; Y. Horng et al., 2007) might be at increased risk for occupational injury or OA development. Work-related musculoskeletal disorders, defined as a subset of MSK disorders arising from occupational exposures, may lead to work restrictions, work-time loss, or even work leave (Forde, Punnett, & Wegman, 2002).

Historically, OA was believed to be a chronic degenerative or "wear and tear" disease, wherein repetitive knee use alone might be sufficient to result in the gradual wear of articular cartilage as an individual ages (Hurley, 1999; Shrier, 2004). This theory has been shown to be espoused by many physicians, leading to a trivialization of the disease and a general lack of effective symptom management (Nissen et al., 2022). It is now widely accepted among the scientific community, however, that OA is an active dynamic whole joint disease, arising from cell stress and extracellular matrix degradation initiated by micro- and macro-injury leading to an imbalance between the destruction and repair of joint tissues (Kraus, Blanco, Englund, Karsdal, & Lohmander, 2015). Therefore, OA can be seen as a heterogeneous disease, resulting from a wide array of mechanistic pathways beginning with molecular derangement, advancing through anatomic and physiologic derangements, and ultimately resulting in join disfunction and damage (Kraus et al., 2015). Among those pathways, several mechanical factors arising from repetitive and prolonged occupational high flexion postures have been suggested as potential contributors to disease progression (Whitfield, Costigan, Stevenson, & Smallman, 2014). As previously mentioned in Subsection 2.1.1, static loading, as occurs in prolonged high flexion postures, is

known to be detrimental to cartilage health (Griffin & Guilak, 2005), potentially resulting from an increased loading of unconditioned tibiofemoral cartilage (C. Cooper et al., 1994; Nagura, Dyrby, Alexander, & Andriacchi, 2002). Additionally, increased risk of meniscal tears have been reported in individuals who kneel frequently (Snoeker, Bakker, Kegel, & Lucas, 2013), placing these individuals at higher risk over time to develop OA. Another pathway through which disease progression may occur is muscle dysfunction, based on the understanding that muscles are the main force absorption mechanism within a joint when properly contracting (Hurley, 1999; Shrier, 2004). Increased incidences of OA development following knee injuries are posited to be the result of instability and abnormal cartilage wear over time (Lindberg, Roos, & Gärdsell, 1993; Roos, Lohmander, Wingstrand, Lindberg, & Gärdsell, 1994) or of a disruption in normal muscle function, resulting in the malabsorption of loads, and eventually a disruption in the rate of articular cartilage degradation (Kraus et al., 2015; Shrier, 2004).

Regardless of the pathway of disease initiation, it remains unclear whether the risk of OA development is greater due to prolonged exposure to postures of high flexion, the number of transitions through these postures (descending into and ascending from high flexion postures), or the estimated cumulative exposures over an individual's career or lifetime. Current reports are quite contradictory in nature when indicating safe operating ranges for high flexion posture adoption. For example, OA risk inducing durations and frequencies have been reported to be between 30 minutes and 5 hours, with most between 1-2 hours (Coggon et al., 2000; C. Cooper et al., 1994; D'Souza et al., 2008; Jensen et al., 2010) and usually a maximum of 30 cycles per day (Coggon et al., 2000). These estimates, however, are typically based on retrospective self-reporting from individuals who have worked in various occupations, often polled long after they have left the workforce. Jensen et al. (2010) suggested that direct and repetitive loading of the knee joints, when working in extreme positions or when physical workload exceeds critical levels, may result in the formation of micro-injuries within the joint tissues, eventually leading to structural breakdown of the cartilage and OA development. Repetitive knee loading exposures have also been suggested to increase the risk of meniscal and ligamentous injuries, ultimately resulting in altered joint dynamics (C. Cooper et al., 1994). Work-related cumulative micro-traumas of the MSK system caused by any one of the previously mentioned possible injury mechanisms of OA have been referred to as cumulative trauma disorders and accounted for 69%

of all cases of MSK disorders within the service-providing industries from 2002-2004 according to the US bureau of labor statistics. Therefore, it appears as though no one mechanism results in the initiation of OA, but rather it seems that a combination of repetitive and prolonged loading over time may lead to an accumulation of damage, eventually resulting in OA development.

It has been reported that individuals in knee straining industries may spend between 41% and 65% of their working-hours in high flexion postures, moving between supported and unsupported kneeling or squatting predominantly (Jensen et al., 2010). Forces passing through the knee were found to vary throughout sustained high flexion, decreasing as individuals sat back towards their heels, yet increasing as weight was shifted forward into more reaching or forward leaning postures. It is known that high intensity or long duration loading in the knee such as during occupational high flexion postures may be excessive and result in joint breakdown (Richmond et al., 2013) however these incidences are not the only contributors to a worker's risk of OA development throughout a working day. When workers aren't in high flexion postures, they may be required to spend a considerable portion of time carrying heavy loads which also contribute to increased loading about the knee and risk of OA development (C. Cooper et al., 1994). While this increased loading is detrimental to knee health on its own, it is compounded by the exposures to high knee flexion, which may contribute to altering the biomechanical and neuromuscular balance within the joint. In fact, the combination of risk factor interactions based on high flexion postures and heavy loads were presented by Cooper et al. (1994) with an odds ratio and 95% confidence interval of 2.5 (1.1 - 5.5) for occupations involving repetitive high flexion alone versus 5.4 (1.4 – 21.0) for occupations involving repetitive knee flexion and heavy lifting. Recent systematic literature reviews have sought to expand on the data presented by Cooper et al. in order to capture risk metrics across multiple occupations. Canetti et al. (2020) found that activities such as squatting and kneeling (odds ratio [OR] = 1.69, 95% confidence interval [95% CI] 1.15-2.49) and lifting heavy loads (>10 kg/week; OR = 1.52, 95% CI 1.29-1.79) significantly contributed to the risk of knee OA across 28 studies, while Wang et al. (2020) found that kneeling (>30 minutes/day; OR = 1.29, 95% CI 1.05-1.57), squatting (>30 minutes/day; OR = 1.49, 95% CI 1.21-1.81), and lifting (>10kg/day; OR = 1.39, 95% CI 1.22-1.59) were all significantly associated with a higher risk of knee OA.

It may therefore be concluded that workers in occupations which require the frequent or extended adoption of postures of high knee flexion are at greater risk for knee OA development. Despite strong evidence to this association, little has been done to assess the risk-mitigating factors which could be implemented into such workplaces. Industry specific guidelines and recommendations based on individual job requirements are necessary in order to reverse the positive trend towards OA development in the ever-aging population. Given the lack of consensus in current exposure thresholds, means of obtaining quantitative exposure measures such as those proposed in the current thesis are needed in order to guide future studies seeking to distinguish which high flexion exposures are most likely to lead to increased OA risk and create guidelines on the safe adoption of high flexion postures in the workplace.

### 2.2.1.Occupational Risks in Childcare Workers

Despite findings linking occupational requirements to OA risk in several industries, the potential for MSK trauma among childcare workers has largely been unexplored (Grant et al., 1995; Holtermann et al., 2020; Labaj et al., 2016; Linnan et al., 2017) and therefore occupational childcare has not appeared in systematic reviews seeking to associate occupations with the risk of knee osteoarthritis development (Canetti et al., 2020; Perry, Garrett, Gronley, & Mulroy, 1995; X. Wang et al., 2020). Throughout the course of a standard work-shift, childcare workers are required to perform a number of tasks including but not limited to basic care (including feeding, changing of clothes and diapers, and comforting), leading play sessions, lifting and carrying children, toys, play equipment or furniture, bending to pick up children and toys, assuming awkward postures, sitting on the floor or in child-sized chairs, squatting in order to interact with children, and lifting children onto and off of cots and playground equipment (Burford et al., 2017; Gratz et al., 2002; Labaj, Diesbourg, Dumas, Plamondon, & Mecheri, 2019; Shimaoka et al., 1997). Due to the dynamic nature of interacting with children, completing a working shift will require a combination of standing, walking, bending, stooping, floor level interactions, and lifting. However, from a metabolic standpoint, each of these postures/ activities are considered to require light effort, and the handling of children is generally not believed to present handling difficulties or risks given that they are regarded as lightweight (Grant et al., 1995). In fact, though the physical demands of working with young children in childcare are an

integral part of the childcare day, most research on childcare health and safety issues has focused on disease transmission rather than MSK health (Gratz et al., 2002) or has focused on the children rather than the caregivers (King, Gratz, Scheuer, & Claffey, 1996). Only within the last fifteen years has the focus of childcare research shifted towards the risks of MSK injuries and pain in childcare workers, with focus on the spine (Y. Horng et al., 2007; Labaj et al., 2016) and recently the knee (Burford et al., 2017; Holtermann et al., 2020).

Based on a report by the US Bureau of Labor Statistics, in 2016 there were approximately 1.7 million childcare and preschool workers in the United States alone, of which 96% were female (Bureau of Labor Statistics, 2016). In 2013, a study of 2,695 Taiwanese childcare workers reported a 97.5% female population where 38.1% were between the ages of 21-30, and 33.7% were between 31-40 years of age (Cheng, Cheng, & Ju, 2013) while an average age of 39.9 ± 13 was reported for 674 American childcare workers in 2017 (Linnan et al., 2017). It has been reported that one out of every 100 childcare workers would report a non-fatal occupational injury (Wortman, 1999) and that 72% of injuries to childcare workers are attributed to overexertion (Brown & Gerberich, 1993). The incidence rate of MSK injuries in workers may however be significantly underreported in North America given that many childcare workers are employed by small businesses exempt from reporting to the Canadian Centre for Occupational Health and Safety or the Occupational Safety and Health Administration (Bright & Calabro, 1999; King, Gratz, & Kleiner, 2006). Given that floor level tasks, often performed in squatting or kneeling postures, as well as lifting tasks, have been associated with significantly increased risk of bursitis, meniscal abnormalities, and knee OA (Coggon et al., 2000; C. Cooper et al., 1994; Kivimaki, Riihimaki, & Hanninen, 1992; Virayavanich et al., 2013), and that females are already at increased risk for OA development (Felson, 1988; McKean et al., 2007), there is undoubtedly a risk to this occupational population which has yet to be explored.

Among the few studies that have sought to evaluate occupational risks in childcare workers, it was suggested that a lack of appropriate furniture for adults in childcare facilities results in the adoption of potentially stressful postures (Burford et al., 2017; Grant et al., 1995). Interestingly, an investigation of 54 childcare facilities revealed that despite design and physical setting differences between each location, the childcare environments were almost always designed to respond to the needs of the children alone, and neglected to consider the consequences for adult

working conditions (Markon & Le Beau, 1994). Despite ergonomic recommendations in the wake of this publication, it appears that the uptake of proposed interventions remains quite low (Burford et al., 2017; King et al., 2006, 1996). It is known that rising from positions of extreme knee flexion imposes substantial stresses on the ligaments of the knee, therefore the use of child-sized furniture in childcare may very likely be a contributing factor to the reported incidences of lower extremity injuries and pain (Calder, 1994; Gratz et al., 2002; Labaj, 2014). The absence of change in childcare settings therefore highlights a need for detailed analysis of specific childcare exposures and tasks in order to identify targeted interventions for reducing the OA related risks associated with the adoption of high knee flexion postures.

In a study by Grant et al. (1995), it was concluded that preschool workers studied were at increased risk of back and lower-extremity MSK disorders due to activities which required sustained periods of kneeling, stooping, squatting, or bending. Through questionnaires of 18 workers, it was found that 25% of working hours were spent squatting, kneeling, or sitting on the floor, and another 26% spent sitting on child-sized furniture. It was also indicated that as the age of the children for which care was being provided decreased, the frequency of adoption of awkward postures increased. In fact, employees were reportedly uninformed as to the potential risks associated with postures involving high knee flexion. This study suggests that improvements are necessary not only to the working environment for childcare workers but also to the training and guidelines provided to these employees on MSK injury prevention.

Recent studies have highlighted disparity in the demographic and health status of childcare workers in North American vs European countries. Holtermann et al. (2020) aimed to assess the physical work demands of 199 Danish childcare workers across 16 nurseries. These individuals were found to work on average 34.9h/ week, had an average body mass index (BMI) of 25.3 ± 5.4, and self-rated their physical exertion at work to be 5.9 ± 1.8 on a scale of 0-10 (Holtermann et al., 2020). In contrast, when assessing the health status and working conditions of 674 American childcare workers, these workers worked an average of 41.6 ± 11.8 hours/week, had an average BMI of 34.5 ± 9.0, and self reported the work environment as demanding (Linnan et al., 2017; Neshteruk et al., 2021). Despite these significant differences in demographics, to date no work has addressed the exposures and occupational requirements in North American childcare settings associated with increased risk of OA development at the knee. Therefore, this

proposed thesis will seek to develop a means by which baseline quantitative data from work-related tasks and postures, potentially associated with increased risk of acute and long-term injury, which are currently missing from the literature, can be measured in childcare settings.

## 2.3 Wearable Sensors for the Measurement of Occupational Exposures

Several challenges exist when seeking to study the occupational demands of childcare. Firstly, there is a need to protect the privacy of the children under the care of the childcare worker, limiting the types of measurement tools that can be used. Additionally, consideration to the active nature of this occupation as well as the potential for occlusion of recording instrumentation due to children, toys, or furniture within actual or simulated childcare settings must be made. Therefore, cameraless, wireless methods of recording exposures to high knee flexion postures in the childcare industry are required.

### 2.3.1. Inertial Measurement Units

Inertial measurement units (IMUs), also referred to as inertial sensors, are composed of three dimensional (3D) accelerometers, gyroscopes, and magnetometers and provide measures of acceleration, angular velocity, and the local magnetic field in their own local 3D coordinate system. The IMU signals present a means of objectively estimating the kinematic properties, within their inertial coordinate system, of any object to which they are rigidly attached. Although inertial sensors are now integrated throughout a broad range of applications, the early development of these devices dates back to the 19$^{th}$ century and the quest to measure the earth's rotation. In the early 1900s these devices were used for navigation purposes, yet by the end of the 20$^{th}$ century techniques for the development of micro electromechanical systems (MEMS) began to be applied to the creation of sensor based accelerometers and gyroscopes (Benser, 2015).

It is important to be aware that the measurements obtained from MEMS gyroscopes and accelerometers both are susceptible to biases which vary over time. The following is a brief overview of the error characteristics within these sensors, based on the technical report on inertial motion analysis by Woodman (2007), presented in order to frame the correction of drift

performed when estimating joint angles as part of Chapter 4. When at rest, or in a situation where a sensor is not experiencing any accelerations or rotations, the ideal gyroscope and accelerometer readings would be 0 °/s (or rads/s) and 9.8 $m/s^2$ (or 1 G, in the vertical direction) respectively. Practically however, MEMS sensors measure an offset from these true values, the average of which is referred to as the sensor bias. When sensor signals which contain bias are integrated, the resultant signal will contain an error which increases over time, and this error is referred to as drift. Sensor bias must therefore be compensated for prior to signal integration to avoid measurements polluted by drift, however this compensation is not a simple task, given the time varying properties of bias.

Both the accelerometer and gyroscope sensors are susceptible to a constant bias term, which when integrated would create a linear drift characteristic in the data (Woodman, 2007). This drift can be eliminated simply by taking a measure of the sensor at rest over a long duration and subtracting the bias, however the precise orientation of the sensor must be known during this correction given that the accelerometer signal, even at rest, will contain a measure of gravity.

Temperature changes, resulting from both fluctuations in the environment and also self-heating of the sensors, has been shown to cause non-linear changes in the bias of the gyroscope and accelerometer measurements (Woodman, 2007). Higher cost professional or research grade IMUs often contain internal temperature sensors from which temperature induced bias effects can be corrected for internally, however in lower cost sensors, these fluctuations must be acknowledged.

The bias of each sensor further changes with time due to flicker noise in the electronics, which is typically modeled as random walk noise (Woodman, 2007). Random walk series are unpredictable noise series yet differ from white noise in that each value will depend on the previous value plus some level of random variation, which in the case of flicker noise will fall within a 1/frequency spectrum (Stockwell, 2003). Woodman cautions that the random walk model however is only an acceptable approximation of this change in bias over short periods of time.

Finally, calibration errors, or errors in the scale factors, alignments, and output linearities affect the bias errors of both accelerometer and gyroscope sensors (Woodman, 2007). These

errors tend to only be produced when the sensors are accelerating or turning respectively (however they can affect the accelerometer at all times due to the gravitational acceleration) and lead to an accumulation of drift in the integrated signals, proportional to the rate and duration of the motions measured. Again, in professional or research grade IMUs, these calibration errors can be corrected for internally, however not all IMUs will be capable of executing this correction.

Beyond the bias term, the outputs of MEMS gyroscope and accelerometer sensors will be affected by thermo-mechanical white noise, fluctuating at a rate much higher than the sampling rate of the sensors (Woodman, 2007). When integrated, this noise introduces a zero-mean random walk error into the signal whose standard deviation grows proportionally to the square root of time for the gyroscope, and proportionally to $time^{3/2}$ for the accelerometer.

Given the outlined sources of error unique to data collected with IMUs, it is evident that researchers must be diligent in presenting sufficient information regarding the confounding variables which might influence study findings. Therefore, length of data collection trials, which impacts many of the bias errors, should be reported as should the manufacturer and generation of the IMU sensor given the differences in error compensation across sensor grades (Vitali & Perkins, 2020).

### 2.3.2.Sensor to Segment Alignment for Joint Axis Estimation

Over the past 40 years, efforts have been made across the scientific community to standardize the reporting of joint kinematics, such that these data would be clinically relevant and uniformly presented across publications (Grood & Suntay, 1983; Wu & Cavanagh, 1995b; Wu et al., 2002, 2005). These recommendations have focused solely on the use of optical motion capture, considered to be the current gold standard for human motion measurement, and cannot be applied to inertial motion capture which measures motion (linear accelerations and angular velocities) rather than position. As such, there is currently no convention by which anatomical frames should be defined based on inertial data, yet the alignment of the sensor measurement frames to those of the body (often referred to as sensor to segment alignment or calibration) is crucial in order to accurately calculate joint angles.

Numerous algorithms and calibration methods have been presented in the literature for deriving anatomical reference frames from inertial data. Through a systematic review of literature published in peer reviewed journals between 2000 and 2018, Vitali and Perkins (2020) suggest that these methods can be broadly grouped into four categories.

*Assumed Alignment*, where an IMU is attached to a body segment such that its sensor measurement frame is approximately aligned with the anatomical frame of that segment, appeared in 42% of the 112 articles analysed. This method was observed amongst the earliest studies published using IMU data given the simplicity in its execution however it remains commonly used to this day, especially in studies seeking to estimate rotations in a single degree of freedom (DoF) joint (Vitali & Perkins, 2020). It has been noted however that the accuracy of the IMU based joint angles derived using this method relies heavily on expert placement (Favre et al., 2006), which can make the application of such a method outside of laboratory settings quite difficult. *Functional Alignment*, the most observed method (47% of the reviewed articles), involves participants completing prescribed movement(s) or pose(s) from which a specific anatomical axis can be estimated in the sensor measurement frame. Most commonly, measured acceleration during a static standing posture, which reveals the direction of gravity, can be aligned with the superior-inferior axis of a body segment. As an example, this method is used in a proprietary full body biomechanical measurement system developed by the company Xsens, in which gravity is measured by each sensor during a standing "normal" pose (Laudanski, Brouwer, & Li, 2013; Reenalda, Maartens, Homan, & Buurke, 2016; J. Zhang, Novak, Brouwer, & Li, 2013). As an alternative, Favre et al. (2008) instructed participants to perform a hip abduction-adduction movement in addition to a static standing posture to determine the posterior-anterior axes of the shank and thigh in addition to the superior-inferior axes. The medial-lateral axes could then be derived from a cross-product of the two functionally defined axes for each segment. Similarly, Luinge et al. (2007) had participants perform a series of isolated movements about the elbow and shoulder in order to define the superior-inferior and posterior-anterior axes of both the upper arm and forearm, and again a cross product was performed to derive the third functional axis of each segment. While this method is computationally simple to employ, it has been noted that this means of defining anatomical frames is relatively repeatable within but not between participants (Fasel, Spörri, Schütz, Lorenzetti, & Aminian, 2017). Additionally, care

must be taken when working with impaired populations who may not be able to achieve the required movement(s) or pose(s).

*Model Based* methods involve the use of a kinematic or statistical model into which the IMU data are input in order to estimate the anatomical frames of a given segment. These models, despite their wide applicability given the lack of requirements for precise sensor alignment or the execution of functional alignment movements, made up only 7% of the reviewed articles, making their first appearance in the work of Seel et al. in 2014 (Seel, Raisch, & Schauer, 2014). Seel et al. (2014) proposed a means of estimating knee flexion-extension by modeling the knee as a 1 DoF hinge and combining this model with a least squares optimization in order to derive the alignment between IMUs mounted on the shank and thigh and their respective anatomical axes during arbitrary leg movements (Seel et al., 2014). Müller et al. (2017) applied similar principals to a 2 DoF model of the elbow joint with which flexion-extension and pronation-supination axes could be estimated based on arbitrary motions about the joint and a straight arm "zero pose". Works by Blesser et al. (2017) and Zimmerman et al. (2018) in contrast estimated anatomical axes for a 3 DoF knee joint through statistical modeling of the knee using deep learning (the combination of convolutional neural networks and long-short-term memory recurrent networks). These works suggest that a Model Based approach could prove useful in real-world applications, however given their novelty, these joint-specific alignment techniques require additional validation and testing prior to broad application.

Finally, a small subset of reviewed studies used *Augmented Data* methods, in which a data source other than the IMUs (e.g., optical motion capture or force platforms) was used in order to provide information needed to align the IMU measurement frame with each segment's anatomical frame. This method has not seen much uptake given the requirement for additional instrumentation. One exception is the work by Picerno et al. (2008), who proposed a means of defining the segmental anatomical axes for the lower limbs based on a similar calibration process to that of optical motion capture, wherein anatomical landmarks are identified using an additional IMU sensor from which the anatomical axes can be derived. This work has recently been extended to the upper limbs (Picerno et al., 2019) and offers a means of calibrating based on the identification of palpable anatomical landmarks without any active involvement from the participant.

The majority of papers in the systematic review of calibration procedures by Vitali et al. (2017) focused on calibration of the lower limbs (41% including the hip, 65% the knee, and 33% the ankle) (Vitali et al., 2017). Across all these sensor to segment calibration methods for the lower limbs, high accuracy in angle estimates were obtained when compared with optical motion capture: Favre et al. reported precisions of 4.4°, 2.7°, and 4.2° for flexion-extension, internal-external rotation, and abduction-adduction of the knee, respectively using the Assumed Alignment method (Favre et al., 2006); Seel et al. reported a root mean square error (RMSE) of 3.3° in knee flexion-extension using a Model Based method (Seel et al., 2014); and Picerno et al. reported RMSE between 2.5% and 4.8% of range of motion for flexion-extension and between 13.1% and 41.8% of range of motion for internal-external rotation using the Augmented Data method (Picerno et al., 2008). It is important to note that all these studies compared measurement systems during walking only. Cooper et al. (2009) found that measurement error increased from slow walking (1 mph) to running (5 mph), however, non-gait based validations have yet to be performed on any of these alignment methods for the lower limbs and therefore the errors associated with such motions are currently unknown. When comparing optical and inertial systems, another important point to consider is the placement of the optical reference markers relative to the inertial sensors (Seel et al., 2014). In studies where these reference markers are placed on the IMU the effects of soft tissue artefact are equally measured by both systems, yet when the markers and IMUs are not coincident this skin motion must be considered as a possible source for alignment discrepancies. Finally, it must be noted that validating the alignment models against optical motion capture, while commonly performed, is not a ground truth validation, given that optical data itself is prone to errors due to soft tissue movement as well as mistakes in palpation of anatomical landmarks leading to misalignment of the anatomical frames.

Once the sensor to segment alignment has been performed, joint angles can be calculated through varying means. For example, Seel et al. (2014) proposes a means of calculating the lower limb angles directly from the raw acceleration and angular velocity measures through sensor fusion while Cooper et al. (2009) utilize a Kalman filter to first derive the orientation of each sensor and subsequently compare these orientations to determine the angle of the knee. Both studies have in common the omission of the magnetometer from angle estimations, in order to avoid measurement errors due to the heterogeneity of magnetic fields in most indoor locations.

Further details on the relevant algorithm for this work will be explained in Chapter 4 and Chapter 6.

### 2.3.3.Movement Classification

Beyond accounting for potential sources of error, performing the sensor to segment alignment, and successfully estimating joint angles, one major obstacle exists in the application of IMUs for the measure of biomechanical data outside of laboratory settings. In order to use this technology as a means of monitoring and measuring occupational activities without supervision, machine learning algorithms are required to identify specific activities performed within the collected data.

Advances in pattern recognition and machine learning algorithms along with the growing availability of wearable sensor technologies have led to increased interest in human activity classification (Bao & Intille, 2004; Barth et al., 2015; Kaya & Gündüz-Öğüdücü, 2015; K. S. Kim, Choi, Moon, & Mun, 2010; Kluge et al., 2017; Laudanski, Brouwer, & Li, 2015; Miller, Beazer, & Hahn, 2013; Preece, Goulermas, Kenney, Howard, et al., 2009; Webb & Copsey, 2011). Through these types of classification algorithms, human movement can be studied outside of laboratory settings to gain objective measures of movement within the home or community. Human movement classification originally began with automatic gesture recognition based on video recording data or optical motion capture (Samadani & Kulic, 2014). Recently however, advances in the application of wireless sensors for motion analysis have led to classification applications using data based on wearable technologies alone. IMU data lends itself well to classification as it provides a surrogate measure of activity and postures and has been used in multiple classification models for measuring activities of daily living (Altun, Barshan, & Tunçel, 2010; Bussmann et al., 2001; Kluge et al., 2017; Leuenberger, Gonzenbach, Wiedmer, Luft, & Gassert, 2014; Usharani & Sakthivel, 2014; N. Wang, Ambikairajah, Lovell, & Celler, 2007). These classification models, in combination with kinematic data collected from inertial sensors, offer the potential to broaden biomechanical research and address new questions which could not previously be answered.

Typically, identification of human movements based on biological signals will rely on pattern recognition-based classification algorithms. IMU data are collected and pre-processed

(including signal filtering and normalization as necessary) and subsequently passed through a four-module classification model:

- *Data segmentation:* This module may be composed of a number of methods to further divide data into a series of time segments of finite length prior to feature extraction in order to improve accuracy and processing time.
- *Feature selection:* This module is responsible for the computation of specific, repeatable features which will serve as input to the classifier in order to efficiently identify the occurrence of specific activities. The selection of representative and descriptive features is of critical importance for the overall success of the classification model.
- *Classification:* The classification module is tasked with identifying combinations of signal features as belonging to pre-defined categories of motion. Due to variability in the speed of movement execution as well as individual movement styles, preferences, and flexibility, this classification module must be robust and well trained in order to ensure accurate feature labeling.
- *Correction:* The final module may be responsible for the application of post-processing methods such as majority voting or prior knowledge, in order to smooth classification outputs. The inclusion of additional knowledge serves as a feedback element to the classification module and may provide a means to eliminate non-biological misclassifications. This module may be omitted or even merged into the classification module depending on the desired application, it will therefore not be discussed further in depth in this literature review.

The ability of the classification model to accurately identify human movements is of the utmost importance. To date no thresholds have been established for the acceptability of biological signal classification performance, therefore it is difficult to determine how well a model should perform and the aim is thus placed on obtaining the highest possible accuracy (Asghari Oskoei & Hu, 2007). The ideal classification model would be robust and intuitively trained to accurately classify movement data from novel users. This performance metric requires that the model be trained on a wide selection of variable data from previous individuals in order to create a system robust to a variety of conditions. However, this may not be possible for all classification models, in which case an intra-subject classification scheme must be employed,

where training data is collected from each individual in order to classify their novel data using a personalized model. There are therefore a number of decisions which must be made in the development of a classification model, which will be discussed in detail in the following Subsections.

#### 2.3.3.1. Data Segmentation

Due to the continuous nature of inertial biomechanical signals, the length (number of frames) of data passed to a classification model must be controlled in order to increase the accuracy of classifications (Asghari Oskoei & Hu, 2007; Nazmi et al., 2016; Preece, Goulermas, Kenney, & Howard, 2009). Typically, classification methods employ windowing techniques to divide the sensor signals into small time segments (or windows) from which repeatable features will be extracted for movement identification (Preece, Goulermas, Kenney, Howard, et al., 2009). Classification is therefore performed separately for each window. In real-time applications, windows of data must be processed independently (without knowledge of any prior data) to create a continuous movement profile. In contrast, for off-line processing, windows can first be defined and subsequently processed concurrently through the classifier (typically using an overlap between windows) in order to create the movement profile for the entire signal (Preece, Goulermas, Kenney, & Howard, 2009). Therefore, window length and windowing technique must both be considered when performing data segmentation.

When segmenting data, it is important to consider that longer segments will minimize any signal bias and variance yet increase the processing duration (Asghari Oskoei & Hu, 2007). It has been shown that windows of greater than 300 ms present too great a delay for real-time applications (Englehart & Hudgins, 2003). For post-processing classifications, window lengths of multiple seconds have been used (Joshi, Nakamura, & Hahn, 2015; Lin, Joukov, & Kulić, 2018; Phinyomark, Phukpattaranont, & Limsakul, 2012; Yoshikawa, Mikawa, & Tanaka, 2007). In steady-state signals, Englehart and Hudgins (2003) demonstrated that a window length as short as 32 ms could be used without incurring significant decreases in classification accuracy, when a correction mode such as a majority voting structure was incorporated into the classification model. However, in transient signals (e.g., those that incorporate the inherent variability of human movement), classification accuracy was found to decrease with decreasing

window lengths. It therefore seems that there is no optimal window length for all data types and that the length of a data window must be optimized for the parameters input to the classification model.

There are two windowing techniques prominently used when segmenting biological data for classification: continuous and overlapping. In continuous, or adjacent, windowing, as shown in Figure *2.2* (a), a series of consecutive windows of predefined length serve as input for feature extraction and classification, and a sliding window technique is employed where continuous data is segmented into a series of windows of varying duration. While this method is often used in real-time applications, the classifier must account for the system processing delay in which the features are calculated, and the classification is performed. This processing delay leads to an idling period for the processor during the remaining window length (Ahmad, 2009). In order to overcome this calculation lull, the second windowing technique uses the idling time to generate new features and classification results. Known as the overlapping or sliding window technique, as can be seen in Figure *2.2* (b), new segments are created with a varying degree of overlap into the previous segment with a constant time increment, greater than the processing time yet shorter than that of the window length, in order to ensure continuous classification. However, the impact of overlapping windows on classification model performance is still debated. Englehart and Hudgins (2003) suggested that a greater overlap produced semi-redundant classification results which may in fact improve response time and accuracy, while Farina and Merletti (2000) showed an increase in processing time with no accompanied classification accuracy increase.

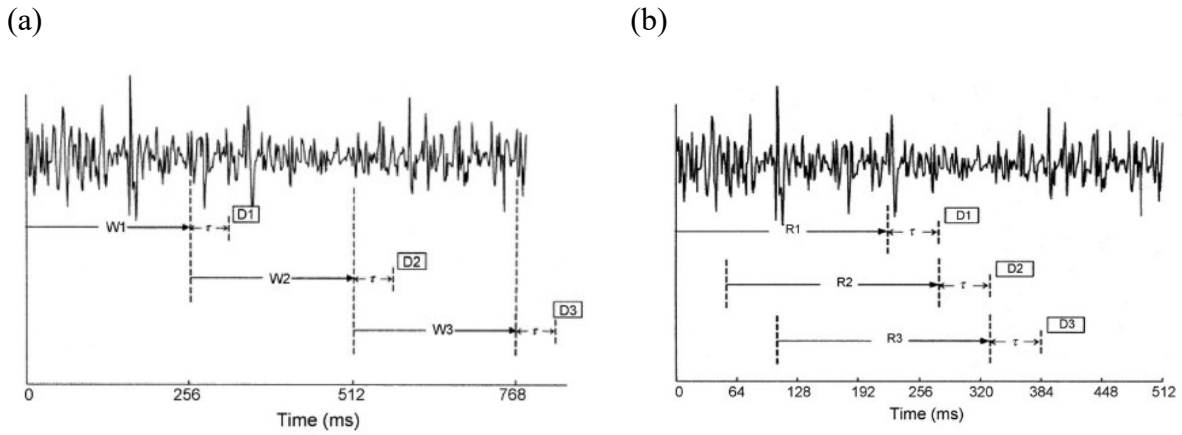


Figure 2.2 (a) Continuous and (b) overlapping windowing techniques adapted from Nayak and Das (2020)

#### 2.3.3.2. Feature Selection

In traditional applications of machine learning based classification models, the input of time series signals is computationally impractical due to the magnitude and randomness of these biological signals. Sensor-based signals are therefore manipulated to generate representative values within a smaller dimension, often referred to as signal features. In extracting these features, any unwanted or unnecessary signal characteristics, as they relate to classification, can be excluded. Pattern recognition in human motion therefore requires that repeatable features be extracted from each window of data in order to identify the occurrence of a specific activity (Graupe, Salahi, & Kohn, 1982; Phinyomark et al., 2012). In order for a classification algorithm to be successful, consideration must be paid to the nature of the input signals and movement types to be distinguished. Given that the classification of biological signals is performed on these representative features, the success of this classification therefore relies heavily on the selection and extraction of appropriate features for the signals in question. Features chosen for classification should ensure maximum class separability, through their complexity and robustness to variation over time (Phinyomark et al., 2012). Previous studies have utilized a wide variety of generated features in order to characterize the posture or activity assumed based on body worn sensors. Generally, features can be divided into three categories: time-domain (TD), frequency-domain (FD), and time-frequency-domain (TFD).

##### Time-Domain Features

Time-domain features are derived directly from the windowed sensor data, based on the time-varying signal amplitude. These TD features tend to be computationally simplistic and relatively easy to implement as they do not require any additional signal transformations (Preece, Goulermas, Kenney, Howard, et al., 2009; Theodoridis & Koutroumbas, 2003). Examples of TD features used for the classification of human movements based on inertial sensor signals include the maximum, minimum, mean, median, standard deviation (or variance), skewness, kurtosis, autocorrelation sequence, and inter-quartile range (Nazmi et al., 2016; Preece, Goulermas, Kenney, & Howard, 2009). Other studies have suggested the use of signal characteristics such as the number of peaks or zero crossings in both gyroscope and accelerometer data for the identification of key gait events such as toe off, heel strike, and stance phase (Casamassima et

al., 2014; Rebula, Ojeda, Adamczyk, & Kuo, 2013; Trung, Makihara, Nagahara, Mukaigawa, & Yagi, 2012). High and low pass filters have also been applied to time domain accelerometer data to separate signals based on a representation of frequency without the need for conversion of the signal into the frequency domain (Foerster & Fahrenberg, 2000; Lee, Park, Hong, Lee, & Kim, 2003). It should be noted, however, that due to the variability of sensor signals, a great number of time-domain features may be required to ensure classification accuracy (Huang et al., 2011; Miller et al., 2013).

Veltink et al. (1996) developed an alternative to the traditional TD features through a template-based classification scheme based on measures of signal morphology. They developed templates based on data from multiple single movement cycles of a dynamic activity (including slow, comfortable, and fast paced walking as well as ascending and descending stairs) and compared these templates to single cycle signals of each activity. Maximal circular cross-correlation coefficients between the unidentified signals and the templates were then calculated and used to identify the activity performed based on the maximum cross-correlation coefficient exceeding a pre-set threshold value (Veltink et al., 1996). This method was later employed by Ying et al. (2007) for the segmentation of individual steps in continuous gait data. Both these studies found success in identifying motions based on the templating of time domain data, however one major disadvantage to this approach lies in the fixed length of the motion template and the resultant inflexibility to variations in movement duration.

Dynamic Time Warping (DTW), as an alternative to cross-correlation, has therefore become popular for gait analysis. This technique, commonly used for computing the similarity between time series, allows for the identification of patterns of differing lengths through non-linear matching, such that subparts of the template are warped (either stretched or shortened) to optimally match a second waveform (Myers & Rabiner, 1981). Barth et al. (2013, 2015) present a novel application of DTW for the segmentation of single strides from standardized gait trials as well as during continuous and free walking movement sequences. This method has since been used for gait analyses in Parkinson's and Stroke survivors (Chang, Hsu, Yang, Lin, & Wu, 2016; Qiu, Liu, Zhao, Wang, & Jiang, 2018; Qiu, Wang, Zhao, Liu, & Jiang, 2018) as well as recent applications in hand gesture recognition (M. Kim, Cho, Lee, & Jung, 2019; Mekruksavanich, Jitpattanakul, Youplao, & Yupapin, 2020). These novel approaches to movement identification

based on time-domain template features offer an exciting and untapped means of classifying postures based on inertial data collected in real world settings.

## Frequency-Domain Features

Frequency-domain features may only be derived following the transformation of data from the time domain into the frequency domain, typically using a fast Fourier transform (FFT). The output of the FFT yields a series of coefficients representing the distribution of signal energy and the magnitude of the frequency components of the signal. FD features have often been used for the classification of wearable sensor data (Bao & Intille, 2004; Foerster, Smeja, & Fahrenberg, 1999; Joshi et al., 2015; Laudanski et al., 2015). The spectral distribution may be characterized through mean frequency (Phinyomark et al., 2012), median frequency (Foerster & Fahrenberg, 2000), spectral energy (Huynh & Schiele, 2005), mean power (Phinyomark et al., 2012), frequency-domain entropy (Bao & Intille, 2004), or by a subset of FFT components (Preece, Goulermas, Kenney, & Howard, 2009). While these features may be more computationally intensive to calculate, they may provide means of distinguishing between activities of varying intensity despite similarities in movement patterns.

## Time Frequency-Domain Features

Unlike TD or FD features, time-frequency-domain features generally represent the outcome of a dimensionality reduction method such as principle component analysis (PCA) or wavelet analysis (Phinyomark et al., 2012; Preece, Goulermas, Kenney, Howard, et al., 2009; Sapsanis, Georgoulas, & Tzes, 2013). These methods allow signals to be decomposed into a number of individual coefficients, each of which contain features on specific signal characteristics. In PCA, data is projected onto a new space, where the dimensions of the data are no longer correlated and its variances are maximized (Sapsanis et al., 2013; A. C. Tsai, Hsieh, Luh, & Lin, 2014). In wavelet analysis, each coefficient contains a specific frequency band and are thus well suited for the analysis and characterization of non-stationary signals (Preece, Goulermas, Kenney, Howard, et al., 2009). With each method, the derived coefficients can be used to form the feature vectors however when classifying short windows of data with similar variability within each, these TFD features alone may not prove optimal in distinguishing between movement types (Preece, Goulermas, Kenney, Howard, et al., 2009; Sapsanis et al., 2013)

### Feature Selection

Given the variability of individuals in performing a specific movement, considerable variability in features derived from body worn sensors is observed (Preece, Goulermas, Kenney, Howard, et al., 2009). Therefore, features must be selected so as to be highly discriminative between activities yet robust to variations within a given movement despite repetition or participant differences. For this reason, a combination of TD, FD, and TFD features may be utilized in order to form an initial representative feature vector for a given time window from which a machine learning algorithm could accurately distinguish the activity being performed.

Rather than manually selecting a subset of features to build a descriptive feature vector for classification, dimensionality reduction can be performed on a larger selection of features in order to determine which possess the greatest discriminative ability for the given classification problem. One proposed method of feature reduction is known as neighbourhood component analysis and relies on the gradient ascent technique to create relative weightings for each feature included in the development of a leave-one-out trained classifier. Each feature is given a weighting for its contribution to the successful classification and based on these weightings, a subset of the most important features for classification can be selected while eliminating any irrelevant or redundant features (W. Yang, Wang, & Zuo, 2012). In this way, the number of features used in the classification training and application are reduced and the generalizability of the classification model performance can be improved.

## 2.3.3.3. Classification

In order to identify specific postures or movements from wearable sensor data, extracted features must serve as input to a classification model. These models are often referred to as machine learning techniques as the developed algorithms are tasked with distinguishing patterns within the features associated with each activity (Preece, Goulermas, Kenney, Howard, et al., 2009). Given the variability of human movement and strategies adopted to complete similar tasks, it can be assumed that features extracted from inertial data will also be quite variable. The developed classifier must therefore be capable of distinguishing patterns regardless of signal variability without being overfit to any specific dataset (Asghari Oskoei & Hu, 2007). For each application an appropriate classification model must therefore be selected, ranging in complexity from basic

threshold-based models (Preece, Goulermas, Kenney, Howard, et al., 2009) to more complex algorithms such as Bayesian Theory (Young, Smith, Rouse, & Hargrove, 2013), Linear Discriminate Analysis (LDA) (Joshi et al., 2015; K. S. Kim et al., 2010; Miller et al., 2013), Fuzzy Logic (Kiguchi, Imada, & Liyanage, 2007), Support Vector Machine (H. Lau, Tong, & Zhu, 2009; Yoshikawa et al., 2007), *k*-Nearest Neighbour (*k*NN) (K. S. Kim et al., 2010; Lin, Samadani, & Kulić, 2016), and Artificial Neural Networks (Amsuss et al., 2014; C. Choi, Micera, Carpaneto, & Kim, 2009).

*The following Subsections provide an introduction to machine learning based classification models. This is not meant to be a comprehensive guide on this topic, however, should provide a basic understanding of the developed algorithms commonly used in biomechanical applications. The following Subsections were written broadly based on: Cervantes, Garcia-Lamont, Rodríguez-Mazahua, & Lopez, 2020; Preece, Goulermas, Kenney, Howard, et al., 2009; Tharwat, Gaber, Ibrahim, & Hassanien, 2017.*

## Threshold-Based Classification

Threshold-based classification models are quite simple, in that they involve the comparison of derived feature sets to predefined thresholds in order to distinguish if an activity is being performed or not. Threshold-based classifiers have been used for the identification of and distinction between static postures such as standing, sitting, and lying down based on relative segment angles calculated from acceleration signals of different body segments (Boyle, Karunanithi, Wark, Chan, & Colavitti, 2006; Bussmann et al., 2001; Preece, Goulermas, Kenney, Howard, et al., 2009). Najafi et al (2002; 2003) applied this method to the identification of transitions between lying, sitting, and standing using accelerometer and gyroscope data. It is noted however that the threshold-based algorithms are highly sensitive to the threshold value selected, and the determination of this value can be non-trivial when seeking to differentiate between multiple similar motions.

## Bayesian Theory Classification

Bayesian decision theory is based on the evaluation of trade-offs between the classification of feature sets into various classes through probability and cost analysis. Therefore a prior knowledge of the density of each class as well as an understanding of the nature, or distribution,

of each class as they relate to the probability of the future classifications can be used to influence the likelihood of a specific activity being identified over another in order to achieve successful classifications (Duda, Hart, & Stork, 2000). Penalties can be applied based on previously calculated probabilities in order to influence subsequent classifications and minimize the probability of error. Unfortunately, class densities are often unknown in inertial data, making it difficult to apply Bayesian Theory to human activity classification.

## Linear Discriminate Analysis

Linear Discriminate Analysis (LDA) was developed to reduce the dimensionality of features by producing linear combinations of these features through which the ratio of between class variance can be maximized (Tharwat et al., 2017). There are two possible forms of LDA: class-dependent and class-independent. In class-dependent LDA each class to be identified will have a separate lower dimensional space onto which its data will be projected whereas in class-independent LDA all data will be projected into the same lower dimensional space from which classes will be distinguished. Assuming that for each class the data is normally distributed, and the variance distribution is the same, the mean and variance of each class are estimated based on a set of previously labeled training data. The data is then combined to construct a lower dimensional space maximizing the between-class variance (distance between the means) while minimizing the within-class variance (the variance of samples from the group mean). The probability of a new feature set belonging to each class is then calculated and a class prediction is made for the given data sample as the class with the highest probability (Tharwat et al., 2017; Webb, 2002). While Linear Discriminate Analyses have been used as classification models, as by Crema et al. (2017) for the identification of various gym based exercises based on a single wrist worn IMU, this technique suffers from the *small sample problem* wherein if the dimensions of the data itself are much greater than the number of samples collected the within-class matrices will be singular. Therefore LDA is often used for dimensionality reduction and the creation of time frequency-domain features which can serve as input to other classification models (Sarcevic, Kincses, & Pletl, 2019).

## Fuzzy Logic

Fuzzy Logic classification stems from the definition of features into fuzzy sets, where a particular sample of data may be assigned to one or more class based on approximate rather than absolute knowledge. In traditional theory of classification, each data sample attributed to a class would be attributed a unique value as a label identifying that class, whereas the class membership of each feature set in a Fuzzy Logic classifier ranges between 0 and 1 based on a series of membership functions (Preece, Goulermas, Kenney, Howard, et al., 2009). Once each data sample has been assigned its membership weightings, a series of if-then statements known as rules can be applied in order to determine the appropriate class outputs, known as a fuzzy truth. The class with the highest fuzzy truth is generally taken as the classification result. Fuzzy Logic is well suited to the classification of human data given the dynamic nature of human movement and ambiguities in labelling data windows during movement transitions. These algorithms have previously been used in the classification of falls based on accelerometer data (Boissy, Choquette, Hamel, & Noury, 2007), the monitoring and recognition of daily activities in stroke survivors (Massé et al., 2015), and more recently for the fuzzy labeling of temporal windows which served as inputs to more traditional classification models for the identification of activities of daily living (Medina, Espinilla, Paggeti, & Quero, 2019).

## Support Vector Machine

Support Vector Machines (SVMs) function by projecting the feature sets of data onto higher dimensional planes through the use of kernel functions in order to find the optimal linear separation between classes for a given classification problem, which equate to nonlinear functions in the original feature space (Duda et al., 2000; Preece, Goulermas, Kenney, Howard, et al., 2009; Webb & Copsey, 2011). The optimal separation between hyperplanes is typically solved for through custom optimization solutions making this classification model useful across many applications. SVMs have been proven to perform well for the classification of high-dimensional problems or when processing small sample sets (Cervantes et al., 2020). Given that the decision functions by which the hyperplanes are distinguished are determined directly on the training data, these models strike a balance between computational complexity and minimizing the risk of misclassification, while maintaining high generalizability. It must be noted that with large data sets there is a very high computational cost of SVMs given that the training kernel

matrix grows quadratically with the size of the dataset, thus making the time to train a SVM on large data very slow (Cervantes et al., 2020). Additionally, given that Support Vector Machines were originally designed to solve binary classification problems, in order to apply SVM to multi-class problems, the classification must be framed as multiple binary classifications (Hsu & Lin, 2002).

Support Vector Machines have been used in multiple classification applications from image recognition to bioinformatics applications in cancer classification due to their generalizability and high fidelity. IMU data have been classified using SVMs for the detection of walking modes in stroke survivors (H. Lau et al., 2009), the detection of pathological gait patterns in total hip arthroplasty recipients (Teufl et al., 2021), and the prediction of falls pre-impact (Aziz, Russell, Park, & Robinovitch, 2014). SVMs have also recently been applied for the classification of inertial data collected through smartphones in order to identify activities of daily living such as sitting, standing, walking, and stair ambulating in healthy adults (Nurhanim, Elamvazuthi, Izhar, & Ganesan, 2017; Swarnakar, Agrawal, & Goel, 2021).

## *k* Nearest Neighbour

In *k*-Nearest Neighbour classification, algorithm building data features are used to construct and populate a multi-dimensional feature space wherein each dimension corresponds to a unique feature (Duda et al., 2000; Preece, Goulermas, Kenney, Howard, et al., 2009). Each feature set is therefore represented by a single point in this feature space corresponding to a particular class or activity. Unknown samples of data can then be represented in the feature space and the classes of its *k* nearest points (or neighbours) are identified. The unknown sample will be assigned a class based on the majority of the *k*-Nearest Neighbours. The choice of value assigned to *k* will impact the locality of the classification. While values of *k* typically range from 1 through a small percentage of the training data points, and typically will always be an odd number in order to avoid ties in classification, a value of 1 will lead to multiple small neighbourhoods spread throughout the multidimensional data space while larger values of *k* will lead to larger neighbourhoods which ignore isolated samples located within groupings of other classes (Kramer, 2013).

The choice of value for *k,* which yields an optimal classification rate, is often referred to as model selection and can be achieved through various methods ranging in complexity from trial and error to cross-validation procedures. Cross-validation is often employed in order to avoid overfitting of the model to the training data. This can be performed through a *k*-fold cross-validation where the training data is divided into *k* sets, and for each iteration, the model will be trained on $k - 1$ sets and tested on the remaining set such that all observations are ultimately used for training the model (Kramer, 2013). During this cross-validation, the value of *k* can be iterated so as to observe the classification losses associated with varying sizes of neighbourhood and ultimately select a *k* value which minimizes classification error.

To determine the class of an unknown data sample based on a series of labeled training samples in multidimensional space, distances between these samples must be calculated. Multiple distance functions have been employed in the literature for classification problems (Hu, Huang, Ke, & Tsai, 2016). Most commonly in biomechanical applications, Euclidean distances are calculated, wherein a straight line distance is measured between each training sample and the unknown point (Kramer, 2013). However, the choice of distance function is critical in ensuring separation between classes and the complexity of distance metrics can be varied depending on the data sample to be classified.

Due to their computational simplicity and instance based classification scheme, *k*-Nearest Neighbour algorithms have been used in multiple applications including the identification of activities performed by construction workers (Akhavian & Behzadan, 2016) and of different behaviours while sitting (Sinha, Patro, Plawiak, & Prakash, 2021) both assessed using smartphone data, as well as the differentiation between everyday activities and falls (T. Zhang, Wang, Xu, & Liu, 2006), and the classification of ambulatory behavior based on accelerometry (Bussmann et al., 2001), to name a few.

## Artificial Neural Network

An Artificial Neural Network (ANN) can be thought of as a mathematical mesh of hidden layers, creating connections between its input and outputs through a series of nodes (Duda et al., 2000; Preece, Goulermas, Kenney, Howard, et al., 2009). These algorithms are provided feature sets as input in conjunction with some form of optimization criteria controlling the weighting of each

layer in addition to the potential incorporation of feedforward and feedback loops in order to optimize classification accuracy. Once trained, ANNs can be used to estimate outputs for any set of inputs. Neural Networks have been used in traditional classification applications such as the identification of exercise movements (Um, Babakeshizadeh, & Kulić, 2017), the assessment of locomotion modes including walking, running, and stair ambulation based on pressure insole data (K. Zhang et al., 2005), or the identification and assessment of gait post stroke (L. Wang, Sun, Li, & Liu, 2018) and recently in the estimation of kinematic and kinetic parameters such as joint angles and moments (Mundt et al., 2021) and centre of mass and centre of pressure inclination angles during walking (A. Choi, Jung, & Mun, 2019) based solely on inertial data. While ANNs are growing in popularity for human motion classification, they present a significant limitation in that the creator has no access to the hidden layers, therefore, they are often referred to as black boxes. Due to this, the classification process and results can be quite difficult to understand, especially for a user or clinician outside of the field of biomechanics.

## Additional Considerations

Machine learning algorithms may follow either supervised or unsupervised development (Duda et al., 2000; Webb, 2002). In supervised learning, the model must be provided with a wide variety of feature sets, each identified, or labelled, as belonging to a specific class type. These data are used to train the classification algorithm to recognize each class through feature patterns unique to each group. Once this training has been completed, unlabeled feature sets can be passed through the algorithm and assigned a class or activity label. In unsupervised learning, or clustering, feature sets are passed to the machine learning algorithm unlabeled. The algorithm is therefore tasked with finding clusters or groupings between feature sets based on a series of patterns or cost-functions.

Cross-validation is often adopted in activity classification applications in order to perform between- and or within-participant comparisons (Duda et al., 2000). For between-participant evaluations, the chosen classifier is trained with data from a portion of all participants and tested on the remaining participants. This train-test cycle is iterated until all participants have been included in both the training and testing data sets and the classification accuracies for each iteration are calculated for the correctly identified windows of data. The overall accuracy can

then be calculated as the average accuracy across all train-test cycles. In contrast, within-participant evaluations involve the training of a classifier on a portion of feature sets for a given participant and testing is performed on the remaining windows of data. This process is repeated until all windows have been included in both the training and testing datasets and iterated for each participant's data. Overall accuracy in within-participant validation is calculated as the average of all cycles for all participants.

While overall classification accuracy is most frequently reported when discussing classification performance, sensitivity and specificity are often also reported in order to provide more detailed information on the classification of individual activity classes (Preece, Goulermas, Kenney, Howard, et al., 2009). Sensitivity represents a classifier's ability to correctly identify windows of a given activity class while specificity represents the classifier's ability to correctly reject windows of other activity classes. Both the sensitivity and specificity values can be calculated based on the confusion matrix which provides a summary of the predicted and true instances of each class passed through the developed classifier.

#### 2.3.3.4. Applications

Despite the growing use of wearable technologies and machine learning algorithms for the classification of human movement, the majority of studies differ in the type and number of activities to be classified, type and number of features employed, classification model selection, and in the location, type, and number of body-worn sensors included (Camomilla, Bergamini, Fantozzi, & Vannozzi, 2018; Lima, Souto, El-khatib, Jalali, & Gama, 2019; Picerno et al., 2021; Rast & Labruyère, 2020). This variability in nearly all aspects of current machine learning applications leads to difficulties in comparing classifier performance and accuracies between studies. Additionally, the majority of classification studies to date have relatively low sample sizes, making generalizability of findings quite difficult (Rast & Labruyère, 2020). The choice of derived features or classifiers therefore currently remains specific to a given application or study, often driven by accuracy, ease of development, processing speed, and personal preference.

In a comparative study, Sinha et al. (2021) demonstrated that *k*NN and SVM classifiers were able to identify with 99% accuracy five different postural behaviours while sitting, both outperforming a Naïve Bayes classifier (reported accuracy of 92% overall). Bao and Intille

(2004) compared the classification of 20 different activities of daily living based on full body accelerometer data and found that *k*NN and Decision tree models outperformed Naïve Bayes classification (accuracies of 84%, 83%, and 52% respectively were reported). Pirttikangas et al. (2006) also sought to classify 17 activities of daily living based on accelerometers worn on the wrists, thigh and around the neck and reported similar classification accuracies between a neural network and *k*NN classifier (93% and 90% respectively). Despite these comparative studies, to date no single combination of features and classification algorithm has proved superior for all applications, and the applications to which these machine learning algorithms have been applied have included only a subset of possible uses. The use of machine learning classification models for the study of occupational postures of high knee flexion has not been explored but such a system could prove an invaluable tool in the measurement of exposures within occupational settings. Therefore, a machine learning model will be developed for the offline classification of postures of high knee flexion adopted in occupational childcare to ultimately gain quantitative exposure data on childcare postures potentially related to increased risk of knee OA development.

# Chapter 3

# Characterization of Postures of High Knee Flexion Associated with Occupational Childcare

Components of this chapter have been published; however additional detail have been provided in the results.

Laudanski, A. F., Buchman-Pearle, J. M., & Acker, S. M. (2022). Quantifying high flexion postures in occupational childcare as they relate to the potential for increased risk of knee osteoarthritis. *Ergonomics*, *65*(2), 253–264.

## 3.1 Introduction

Repetitive joint loading due to occupational high knee flexion postures has been associated with the development of degenerative knee joint disease and knee osteoarthritis (Felson, 1988; Henriksen, Creaby, Lund, Juhl, & Christensen, 2014). These high flexion postures include any pose where the knee flexion angle exceeds 120° from a neutral standing posture, which would be considered 0° knee flexion. This pose-related increase in risk has been observed in men and women of both Eastern and Western cultures despite variance in purpose and frequency of exposure to these postures (Coggon et al., 2000). In Eastern populations, including Chinese, Japanese, Korean, and Vietnamese nationalities, high knee flexion postures tend to be assumed frequently during activities of daily living for socializing, eating, rest, and religious practices

(Akagi, 2005). In contrast, the adoption of high knee flexion postures in Western cultures occurs primarily in occupational settings, where workers are required to perform repetitive high flexion motions for a significant portion of their working hours (Coggon et al., 2000; Felson, 1994; Kingston, Tennant, Chong, & Acker, 2016). As such, workers such as miners (Kellgren & Lawrence, 1952; Schiphof et al., 2008), floor layers and tile setters (Coggon et al., 2000; C. Cooper et al., 1994; Jensen et al., 2010; Sandmark et al., 2000), and childcare workers (Grant et al., 1995; Gratz et al., 2002; Y. Horng et al., 2007) have been suggested to be at increased risk for occupational knee injury or OA development. Further, childcare workers have a compounded risk due to the primarily female demographic (where females represent 96.1% of the childcare workforce across Canada, and 96.7% of the workforce in the province of Ontario) and the known higher likelihood of OA development in females compared to males (Felson, 1988; McKean et al., 2007; Statistics Canada, 2016; The Social Research Centre, 2017). Despite the association between postures of high knee flexion and knee pain and OA development, few guidelines exist to address the occupational adoption of such movements and their relation to injury and disease mechanisms.

Jensen et al. (2010) suggested that direct and repetitive loading of the knee joints, when working in extreme positions or when physical workload exceeds critical levels, may result in formation of micro-injuries within the joint tissues, eventually leading to structural breakdown of the cartilage and OA development. Work-related musculoskeletal disorders, arising from occupational exposures, may lead to work restrictions, work-time loss, or even work leave (Forde et al., 2002). Repetitive high flexion knee loading exposures have also been suggested to increase the risk of meniscal and ligamentous injuries, ultimately resulting in altered joint dynamics (C. Cooper et al., 1994; Gaudreault, Hagemeister, Poitras, & de Guise, 2013; Kajaks & Costigan, 2015; Tennant, Chong, & Acker, 2018). Altered joint dynamics have independently been associated with loadings observed, in animal experiments, to be a contributing factor to joint damage and the initiation or progression of knee osteoarthritis during gait in populations exhibiting knee pain yet no radiographic evidence of joint degeneration (Radin, Yang, Riegger, Kish, & O'Connor, 1991). Special attention should therefore be paid to decreasing the occurrence of high knee flexion postures in occupational settings.

While it is accepted that mechanical factors may contribute to disease progression, it remains unclear whether the increased risk of OA development stems from prolonged exposure to high flexion postures, frequent transitions through these postures (descending into and ascending from high flexion postures), or from high estimated cumulative exposures over an individual's career or lifetime. Current reports are quite contradictory when indicating safe operating ranges for high flexion posture adoption and levels of exposure associated with increased incidences of OA have been reported for both frequency and duration. Based on retrospective self-reported exposures, reported durations of exposure associated with increased OA incidences range between 30 minutes and 5 hours total time spent in high flexion postures in a single workday, with most between 1-2 hours (Coggon et al., 2000; C. Cooper et al., 1994; D'Souza et al., 2008; Jensen, 2008; Tennant et al., 2018). The most commonly reported frequency threshold, beyond which incidences of OA are elevated, was 30 cycles per day (Coggon et al., 2000).

The bulk of published research on childcare related exposures has focused on the risk of neck, shoulder, and back injury (Brown & Gerberich, 1993; Grant et al., 1995; Y. Horng et al., 2007; Labaj et al., 2016, 2019); however, in 2019, the Workplace Safety and Insurance Board (WSIB) of Ontario reported that across all occupations, injuries to the legs (excluding ankles and feet) represented 9% of all lost time claims, less common only than reports involving the lower back or multiple body parts (WSIB Ontario, 2019). In childcare specifically, claims related to the lower extremities alone were found to represent 25% of lost time claims received between 2010 and 2019, with acute injuries to the knee alone representing 8% of all approved claims, amounting to $211,609 in benefit cost and 1215.6 lost days (WSIB Ontario, 2020). Despite clear evidence of lower limb and knee injuries in the Canadian workforce, to our knowledge only two studies have analyzed the physical demands of childcare as they relate to the adoption of high knee flexion postures (Burford et al., 2017; Holtermann et al., 2020).

In a study of 199 Danish childcare workers, Holtermann et al. recorded motions over an average of 3.6 days (with 6.5 mean working hours per day) using physical observations and a previously proposed method of classifying accelerometer data for static posture detection (Hendriksen et al., 2020; Holtermann et al., 2020). Childcare workers, caring for children ages 0-3, spent on average 4.1% of their working hours in knee straining postures (squatting or kneeling), with 7.4% of workers performing these postures for greater than 10% of the work day

(Holtermann et al., 2020). Findings related to increased risk of musculoskeletal pain due to the physical demands of childcare were inconclusive, yet the authors did recommend cautionary minimization of kneeling and squatting exposures. In contrast, Burford et al. analyzed 24 preschools in Germany and identified 9 locations as having an intermediate or high need for intervention to reduce the exposure to biomechanical risk factors (Burford et al., 2017). Using a wearable sensor-based postural classification system to monitor 12 childcare workers for approximately 4 hours per day over 2 days, knee straining exposures (including squatting, supported and unsupported plantarflexed kneeling, sitting on heels (dorsiflexed kneeling), and crawling) were identified (Burford et al., 2017; Ditchen, Ellegast, Gawliczek, Hartmann, & Rieger, 2015). It was reported that 8.4% ± 9% of working hours pre-intervention were spent in high flexion postures when caring for children aged 1-5 years, and that a combination of awareness training and new furnishings could significantly reduce these exposures to 3.1% ± 4.5% (Burford et al., 2017). While previous observations have identified increased yet variable adoption of high flexion postures in occupational childcare, the broader classification tools used in these studies may have failed to identify unique postures which are adopted when caring for children, such as crawling while kneeling or sitting on child sized furniture. Furthermore, caring for children of differing ages can require childcare workers to perform highly variable tasks, yet no study has analyzed differences in exposures by task or age grouping despite previous recommendations for the reporting of data in homogeneous exposure groups (Tak, Paquet, Woskie, Buchholz, & Punnett, 2009). Finally, despite the established frequency-based increases in incidence levels of OA for high flexion postures, transitions into, out of, and between such postures have not to date been quantified in the literature despite the reported incidences of knee injuries in childcare.

To objectively identify the high knee flexion exposures which may contribute to increasing the risk of knee injury in childcare workers, a comprehensive analysis is required. Therefore, using video observations collected in childcare centres in Kingston, Ontario, Canada, the objectives of this study were to identify the postural demands of occupational childcare as they relate to high flexion exposures at the knee when caring for children of different ages and independence levels, to quantify the frequency and duration of these postures and compare these with the current thresholds associated with increased incidences of OA, and finally to associate

the identified high knee flexion postures with the childcare related tasks during which they were assumed. Given the consistent reports of knee injury and pain in childcare workers (Grant et al., 1995), these findings will provide foundational knowledge of the high flexion postures assumed in occupational childcare to evaluate the potential for increased risk of knee OA development within this occupation.

## 3.2 Methods

The video observations presented in this study were collected as part of a larger cohort previously reported on by Labaj et al. (Labaj et al., 2016, 2019). Eighteen childcare workers (n = 17 females, 1 male) were recruited and observed through video recordings as they completed approximately half of a working shift in one of five daycares in Kingston, Ontario, Canada. Childcare workers were divided based on the age of the children with which they worked: Infant (0 to ~1.5 years), Toddler (~1.5 to ~2.5 years), and Preschool (~2.5 to ~4 years). These divisions were imposed by the daycare centres, however it is believed that noting differences between the occupational tasks related to caring for children of different ages is important given the varying levels of independence in each age category as well as the rapid growth and weight increase in children from Infant to Preschool ages (WHO Multicentre Growth Reference Study Group, 2006). Continuous video recordings from a primarily sagittal view were previously collected using a handheld video camera (Sony Handycam DCR-SR82) with a capture rate of 30 frames/second for a duration of approximately 3.25 hours (195 ± 25.0 minutes) for each participant. This duration was selected to capture the majority of tasks childcare workers completed with the children over the course of a traditional working day (including outdoor play, meal assistance, toileting, and naptime assistance). Working shifts were divided based on a midday nap and recordings were captured in the morning prior to the nap (Labaj, 2014; Labaj et al., 2016). Recruited participants were required to have a minimum of one year of working experience within a daycare or to have completed a required education program for an Early Childhood Educator diploma including mandatory placements. Informed consent was obtained from each participant prior to collections, which were approved by the General Research Ethics Board of Queen's University. This secondary analysis was approved by the University of Waterloo Research Ethics Board.

While previous sensor based research studies have suggested categorizing knee straining postures under the umbrellas of kneeling (both supported and unsupported), squatting, and crawling (Burford et al., 2017; Holtermann et al., 2020), all unique exposures which were believed to be knee straining were identified in this study. Therefore, to quantify all childcare related knee straining exposures, each video was segmented using VLC Media Player (Version 3.0.0) by the start and end time of each posture, where any posture which appeared to have the potential of being knee straining, or in which any segment in addition to the foot was located on the ground would be identified. For example, in addition to obvious high knee flexion activities, postures such as those involving bending and reaching forward, which at times can include increased knee flexion, were also recorded. Additionally, the total number of instances of each posture were noted to capture the transitions into and out of high flexion, as these transitions present an independent increase in likelihood of OA development (Tennant, Maly, Callaghan, & Acker, 2014).

For instances when the identified posture was performed in a plane approximately perpendicular to the camera axis with clear visibility of the hip, knee, and ankle, the peak knee flexion angle achieved was calculated. This analysis was performed using Kinovea (Version 8.27) to report the knee flexion angle attained in each high flexion posture across childcare workers. Previous validation work has suggested that knee angles calculated using Kinovea are accurate to within $\pm 2.5^{\circ}$ of those measured with a gold standard optical motion capture system, and that these estimates are not affected by camera projection angles between $45^{\circ}$ and $90^{\circ}$ (Fernández-González et al., 2020; Puig et al., 2019). Nevertheless, frames from which the flexion angles were calculated in this study were chosen conservatively in an attempt to ensure the best possible views were chosen from which to calculate the angle results (Puig et al., 2019). Any posture with a third quartile exceeding $120^{\circ}$ in any of the age ranges was considered to be a high knee flexion posture. Adoption frequencies and durations were only reported in the results for postures which were identified as high flexion.

Each adopted posture identified in postural segmentation was associated with one of twelve childcare tasks previously identified by Labaj et al. (Labaj et al., 2019). These tasks were determined based on questionnaire responses and examination of workers such that they were

consistent across child age groups (Table *3.1* Childcare tasks performed by individuals caring for children in all age categories previously identified by Labaj et al.).

For each participant, the frequency and duration of each posture determined to elicit knee flexion angles greater than 120° were calculated using the recorded start and end times, over the entire period of video collection (Matlab 9.7 – The Mathworks, Release R2019b, Natick, MA). Mean cumulative exposure duration, mean duration per exposure instance, and mean frequency of adoption for each high flexion posture were calculated across all workers by child age category. The frequencies and durations were then compared to previously reported exposure thresholds (Coggon et al., 2000; D'Souza et al., 2008) to determine any potential links between childcare related postures and increased incidences of OA development. For exposure duration, the most commonly reported adoption thresholds for high flexion postures are between 1 and 2 hours (Coggon et al., 2000; D'Souza et al., 2008). These thresholds are assumed to have been suggested for a standard 8-hour working period and were therefore scaled based on the length of the videos collected, to be compared with the results of this study. The length of the videos collected was on average 3.25 hours. To be conservative, the thresholds were scaled to a 3.5 hour time period. Thus, the scaled exposure duration thresholds became 0.44 to 0.88 hours. The proposed frequency threshold of 30 cycles was treated similarly, resulting in a scaled threshold of 13 cycles in 3.5 hours (Coggon et al., 2000).

Table 3.1 Childcare tasks performed by individuals caring for children in all age categories previously identified by Labaj et al. (2016).

| Task Name | Action |
|---|---|
| **Activity** | Lead or instructed structured activity |
| **Bathroom** | Any activity in the bathroom including hand washing, toileting, etc. |
| **Caring** | Providing one on one care for a child |
| **Changing** | Changing Diapers |
| **Cleaning** | Activities including sweeping, tidying, wiping of surfaces |
| **Feeding** | Serving or aiding in feeding of snacks or meals to children |
| **Nap** | Putting children down to sleep or helping them to fall asleep. |
| **Other** | Any tasks which did not fit into another category |
| **Outdoor Prep** | Includes dressing our undressing children or themselves in outdoor clothing |
| **Playing** | Playing with toys or completing other non-educational activities |
| **Prep** | Preparation or setup for a task |
| **Supervision** | Observation without direct interaction with other workers or children |

Mean exposure times were additionally expressed as a percentage of total collection duration to determine the time spent in each high flexion posture based on child age category. Finally, an analysis of postural adoption by task was performed to identify the childcare related tasks which might present the greatest potential risk in each child age category as well as tasks or child age categories which might be considered knee sparing.

# 3.3 Results

## 3.3.1 Postures

Of the eighteen childcare workers included in this analysis, 6 worked with infants, 3 with toddlers, and 9 with preschool aged children. Ten postures involving varying degrees of knee flexion were identified as occurring during occupational childcare (Figure *3.1*): dorsiflexed kneeling (DK), plantarflexed kneeling (PK), single arm supported kneeling (SAK), double arm supported kneeling (DAK), flatfoot squatting (FS), heels up squatting (HS), floor sitting (FLRS), side sitting or leaning (SS), stool sitting (STLS, either on child sized or adult sized chairs), and stooping (STP, also referred to as bending and reaching). Brief descriptions of each of these postures have been provided in Table *3.2* Identified childcare postures with the potential to elicit high knee flexion angles performed by individuals caring for children of each age category. . Eight of the ten identified postures had third quartile knee flexion angle values exceeding 120° in at least one of the child age ranges (Figure *3.2*).

Table 3.2 Identified childcare postures with the potential to elicit high knee flexion angles performed by individuals caring for children of each age category.

| Posture | Description |
|---|---|
| **Heels-Up Squatting (HS)** | Forefeet are in contact with the ground, while the heels are raised. The knees are anterior to the feet while the buttocks rests as close to the heels as possible. |
| **Flatfoot Squatting (FS)** | Feet are flat on the ground, at shoulder width or greater distance apart. The knees are driving toward the shoulders, located superiorly yet in line with the feet, while the tailbone is typically pointed to the ground unless squatting to perform a lift from the ground. |
| **Dorsiflexed Kneeling (DK)** | Symmetrical or asymmetrical (where one knee is in contact with the ground while the opposite foot is planted in a posture similar to a lunge) kneeling, with flexed forefoot, so that the head of the metatarsals and the plantar aspect of the toes are in contact with the ground. The buttocks rests as close to the heels as possible. |

| | |
|---|---|
| **Plantarflexed Kneeling (PK)** | Symmetrical or asymmetrical kneeling, where the instep of the foot is in contact with the ground, and the buttocks rests as close to the heels as possible. |
| **Double Arm Supported Kneeling (DAK)** | Knees and hands are in contact with the ground, roughly inferior to the hips and shoulders respectively. Body weight is evenly distributed between all four contact points. This posture may also be observed as non-stationary when an individual is crawling on the ground. |
| **Single Arm Supported Kneeling (SAK)** | Similar pose to the double arm supported kneeling, where only a single hand is in contact with the ground, so that the body weight is evenly distributed between the three contact points. |
| **Stool Sitting (STLS)** | Buttocks is seated on a child- or adult-sized chair or on a stool wherein the seat pan height is at or below knee level. Both feet are typically planted on the ground inferior to the knees. |
| **Floor Sitting (FLRS)** | Buttocks is seated on the ground. Legs may be bent so that the feet are crossed in front of the body or extended anteriorly or laterally from the body. |
| **Side Sitting or Leaning (SS)** | Typically transitioned to from a symmetrical kneeling posture, knees are bent however buttocks has moved laterally from the heels so that one hip rests on the ground. This posture can be adopted with or within a single hand in contact with the ground for additional support |
| **Stooping (STP)** | Movement primarily involving a hinge about the hips, could also be referred to as bending and reaching, to lift a child or object from an estimated height of 0.5 m or greater above the floor. Knee flexion angle typically does not exceed 90°. |

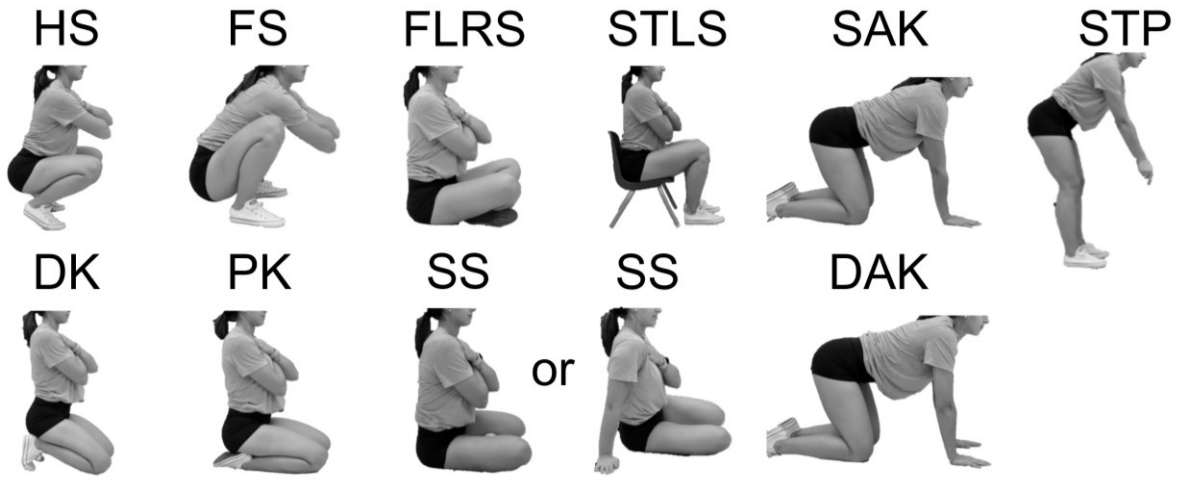


Figure 3.1 Simulation of 10 postures identified as frequently adopted in occupational childcare including (clockwise from top left): heels up squatting (HS), flatfoot squatting (FS), floor sitting (FLRS), stool sitting (STLS), single arm supported kneeling (SAK), stooping (STP), double arm supported kneeling (DAK), side sitting or leaning (SS), plantarflexed kneeling (PK), and dorsiflexed kneeling (DK)

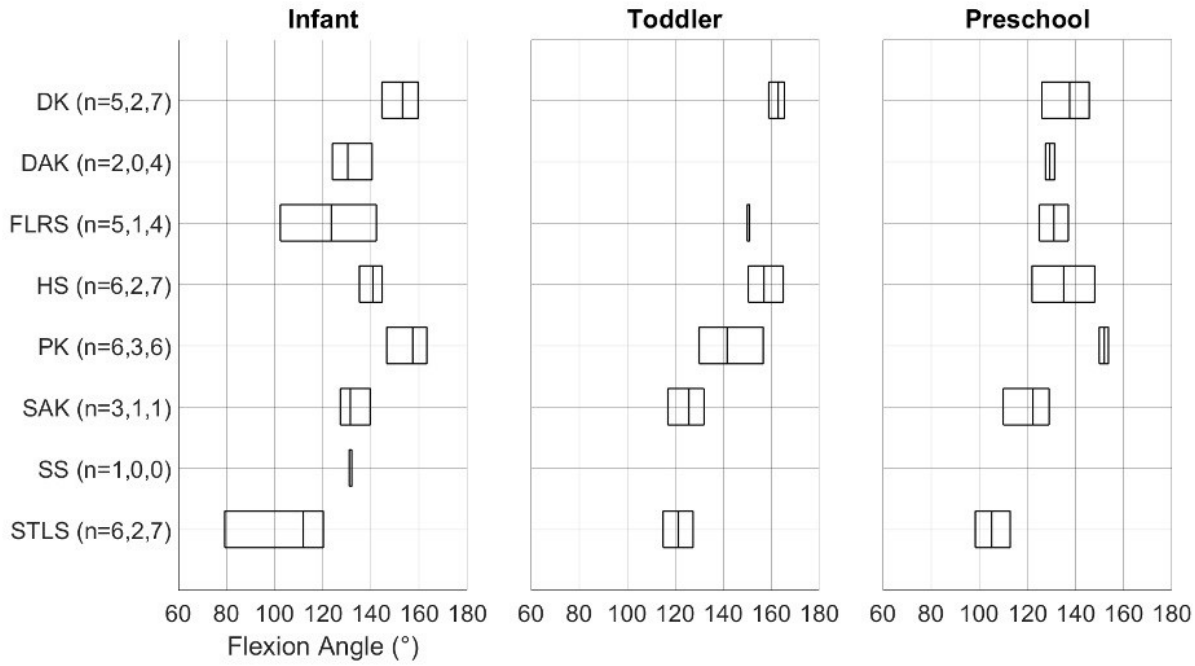


Figure 3.2 Average range of peak flexion angles achieved for each identified high knee flexion posture. The number of participants included per category are indicated next to each posture (n= infant, toddler, preschool).

## 3.3.2 Time Spent in High Flexion Exposures

Cumulative exposure time and exposure cycle time analyses were subsequently calculated for each high knee flexion posture (Figure *3.3* and Figure *3.4*).

Task related exposure analysis revealed that childcare workers spent the greatest duration of time sitting on the floor, sitting on child sized furniture, or plantarflexed kneeling (Figure *3.3*). For individual instances of high flexion postures, single exposures to floor sitting were found to be longest for childcare workers, across all child age categories (mean duration 37.61 ± 24.34 s, Figure *3.4*). Childcare workers assumed high knee flexion postures for greater than one third of the collection time (Figure *3.5*), regardless of the age of child being cared for. For childcare workers working with infant, toddler, and preschool aged children, 1.57 hours, 1.55 hours, and 1.24 hours were spent in high flexion respectively.

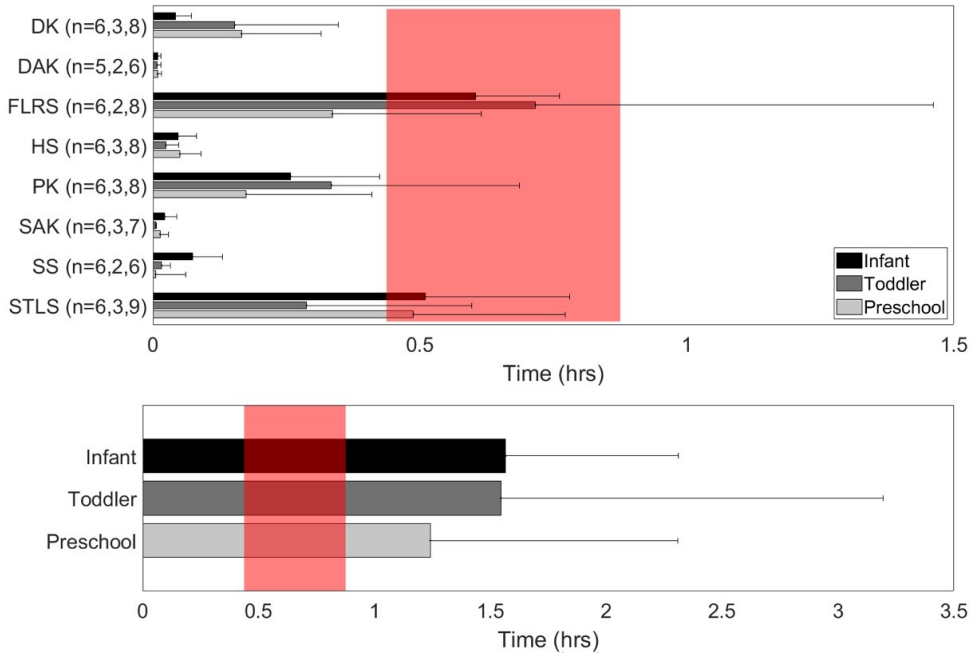


Figure 3.3 Mean cumulative time (hours) spent in high knee flexion postures for each child age category. Top: Time spent in each posture. The number of participants per category are indicated next to each posture (n= infant, toddler, preschool). Bottom: Total exposure duration (sum of all high flexion postures) performed by childcare workers caring for children of each age category. The previously reported daily exposure thresholds believed to be associated with increased risk of OA development have been scaled to the mean collection duration (shaded region).

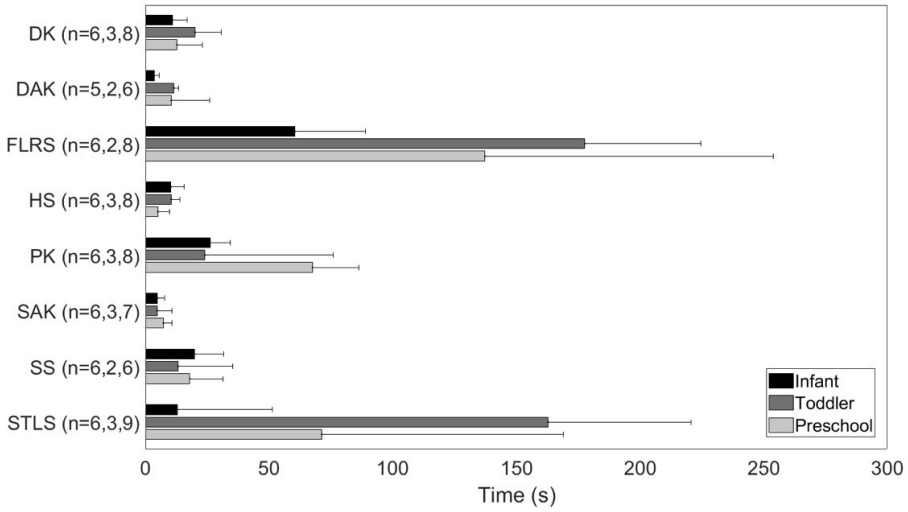


Figure 3.4 Mean time (s) per exposure instance spent in high knee flexion postures for each child age category. The number of participants per category are indicated next to each posture (n= infant, toddler, preschool).

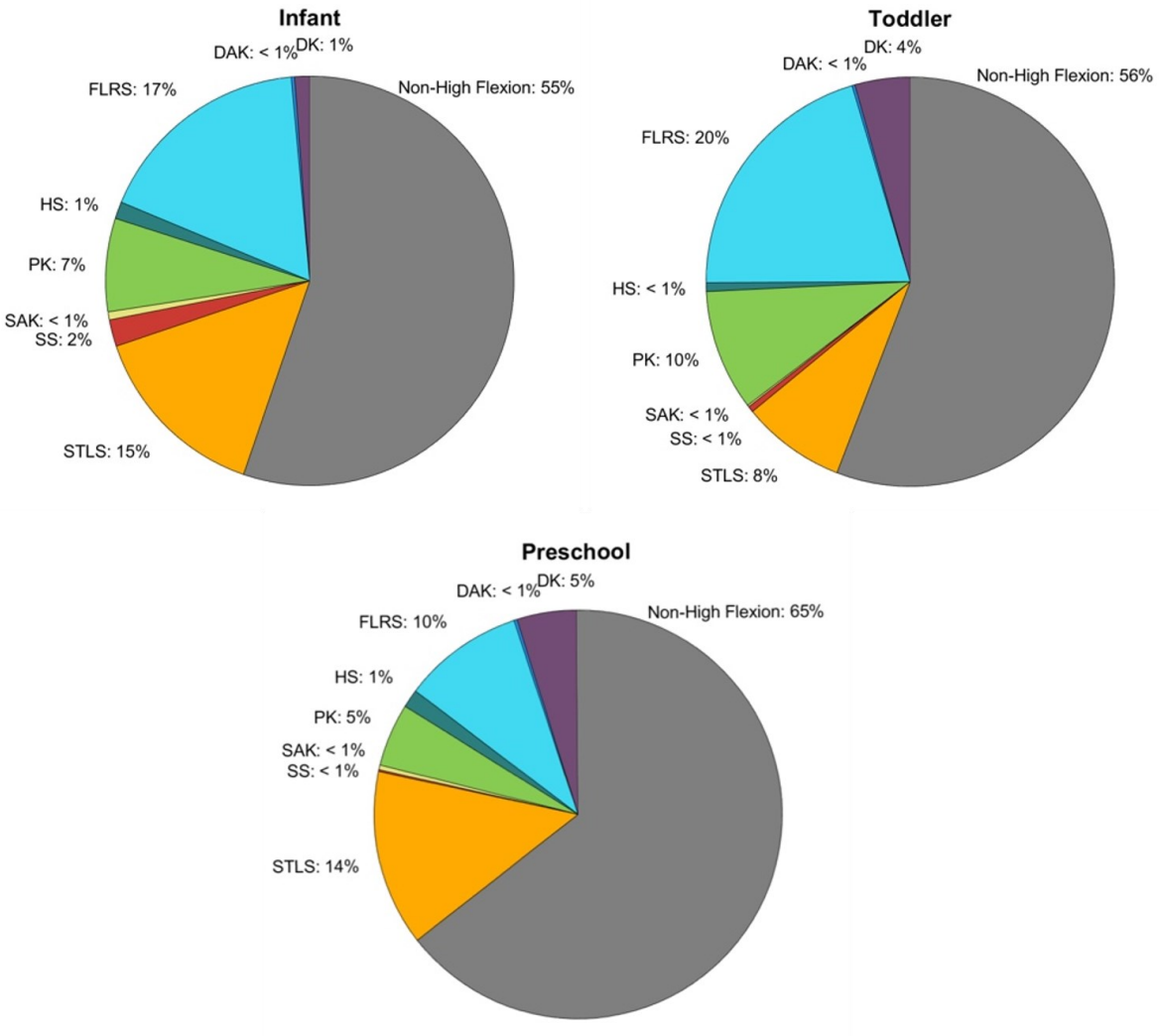


Figure 3.5 Postural division as a percent of collection duration averaged for each child age category.

## 3.3.3 Frequency of High Flexion Exposures

Frequency of adoption analysis revealed an average of 159, 113, and 114 instances of high knee flexion postures in childcare workers caring for infant, toddler, and preschool aged children respectively (Figure *3.6*). Instances of kneeling and seated postures were found to occur at the highest frequencies when caring for children of all ages.

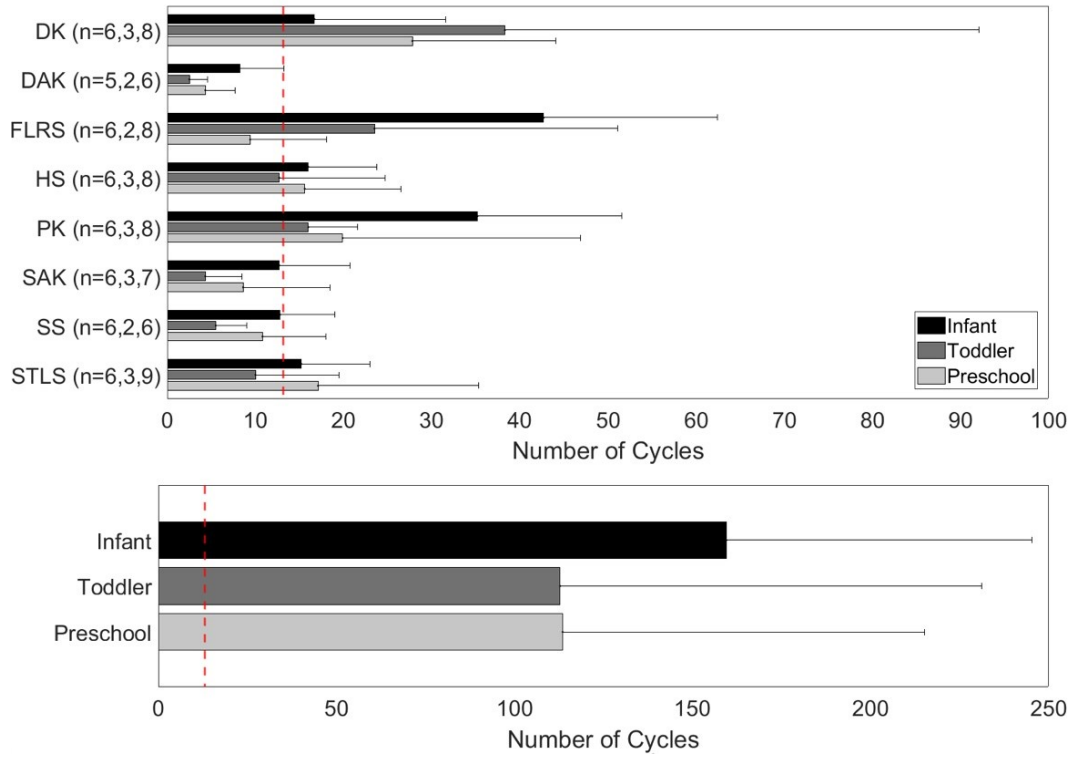


Figure 3.6 Frequency of adoption of high knee flexion postures by child age category. Top: Number of each high flexion posture. The number of participants per category are indicated next to each posture (n= infant, toddler, preschool). Bottom: Total number of cycles (sum of all high flexion postures) performed by childcare workers caring for children of each age category. The previously reported daily number of cycles believed to be associated with increased risk of OA development has been scaled to the mean collection duration (dotted vertical line).

## 3.3.4 Postural Division by Task

Postures adopted while completing each childcare related task have been presented in Figure *3.7*. Childcare workers caring for infants were found to preferentially adopt seated postures for most tasks, with less postural variability when compared with those caring for toddler and preschool aged children. Additionally, the adoption of high flexion postures by task changed with the age of children being cared for, where time spent playing in high flexion was highest with infants, time spent napping and feeding in high flexion were highest with toddlers, and feeding, activity, and playing in high flexion were highest with preschoolers. This analysis also revealed that changing, bathroom, prep, and supervision tasks across all child ages required childcare workers to adopt high knee flexion postures the least.

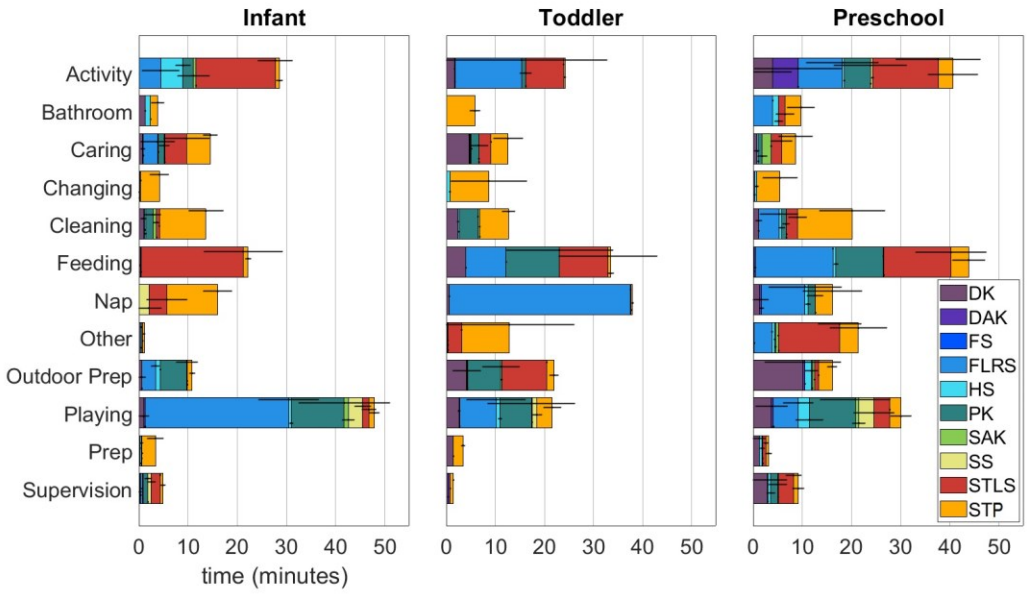


Figure 3.7 Average time (minutes) spent in flexed knee postures for each childcare task by child age category. Each bar is composed of only postures which were adopted for a specific task, presented in the order in which they appear in the legend. Please refer to the online article for color legend.

Note. Standard deviations for each posture during each task are displayed from top to bottom in decreasing order of time. For example, when working with infants, structured activities were performed for an average of 28 minutes. Of this time, 16 ± 3.5 minutes (mean ± standard deviation) were spent sitting on a child sized stool, 4.5 ± 1.5 minutes in heels up squatting, 4.4 ± 3.9 minutes sitting on the floor, 2.2 ± 3.2 minutes in plantarflexed kneeling, 0.81 ± 0.72 minutes stooping, and 0.5 ± 0 minutes in single arm supported kneeling.

## 3.4 Discussion

This study constitutes the first attempt at quantitatively and objectively evaluating the adoption of high knee flexion postures assumed when caring for children of varying age categories during a typical working childcare shift in Canada to evaluate the potential for postural related increases in the incidence levels of OA development in this occupation. Through video analysis, a series of eight high knee flexion postures were identified as occurring in occupational childcare while caring for infant, toddler, and preschool aged children. While recent studies have evaluated the cumulative exposure times childcare workers spend in knee straining postures, to our knowledge, this study is the first to provide these data in combination with an analysis of frequency of transitions into and out of such postures. Additionally, this study presents the first characterization of childcare related tasks through the high flexion postures adopted during their execution when caring for children of different ages.

Despite uncertainty in the literature surrounding the occupational determinants of knee OA, it is believed that cumulative exposures to high knee flexion postures of 1-2 hours or high flexion exposure frequencies of greater than 30 cycles over the course of a typical working shift in an occupational context may increase the risk of micro-traumas of the musculoskeletal system (Coggon et al., 2000; C. Cooper et al., 1994; D'Souza et al., 2008; Jensen, 2008). Additionally, percentages of time as low as 6% of work shifts spent in knee straining postures have been suggested to result in elevated risks of musculoskeletal diseases such as knee OA (C. Cooper et al., 1994). While the individual instances of each high flexion posture were quite short (mean of 37.61 ± 24.34 s), the cumulative duration of time spent in high knee flexion postures within the 3.25 hour period observed in this study was found to exceed one hour, regardless of the age of children being cared for. The only comparative results to our cumulative postural exposure are those of Holtermann et al. (Holtermann et al., 2020) and Burford et al. (Burford et al., 2017) where knee straining exposures (kneeling and squatting) in childcare were studied based on wearable data classification. Our cumulative exposures to kneeling and squatting postures (DK, PK, SAK, DAK, and HS), when expressed as a percentage of work hours, were found to be higher than those previously reported. Assuming a standard 8-hour shift, the duration of daily knee straining postures in our study were found to be 11.54 ± 7.96%, 16.04 ± 17.68%, and 12.60 ± 13.72% for infant, toddler, and preschool aged care givers respectively. This discrepancy may be due to differences in daycare furnishings, choice of technique employed for postural classification, the pedagogical focus of the childcare centre (which may influence the independence of the children being cared for), or overestimations in the current results due to the extrapolation of partial-day video data to a representative working shift. It is noted that each daycare center will allocate childcare responsibilities and workload differently throughout the day, therefore it is possible that in some locations, greater adoption of high flexion exposures might occur in the mornings compared to the afternoons.

The frequencies of high knee flexion postures reported in this study were found to be between 3 and 5 times the suggested levels associated with increased incidences of OA. The frequency of adoption of multiple postures, including dorsiflexed and plantarflexed kneeling, heels up squatting, as well as floor and stool sitting, independently exceed the guideline for daily high knee flexion posture adoption frequency when scaled to the study duration. When

comparing the frequency results here presented to those reported for other occupations, the number of transitions assumed by childcare workers caring for infants (159) in the studied 3.25 hour period are similar to those performed by pavers (155) and tilers (164) over an entire working day, while exposures when caring for toddlers and preschool aged children (113 and 114 respectively) are similar to those in screed layers and painters (125 and 126 respectively) (Ditchen, 2012). These findings are of particular importance given the recognized association between postural adoption in construction and manual labour based occupations and increased risk of knee OA development (Coggon et al., 2000; C. Cooper et al., 1994; Ditchen, 2012; Jensen et al., 2010; Sandmark et al., 2000; Schiphof et al., 2008). It is particularly important to study the transitions between standing and high flexion postures, given that muscular demands in transitional movements have been shown to be significantly higher than in static high flexion postures (Tennant et al., 2014). Increased muscular activations about the knee could result in increased loading within the joint, ultimately resulting in an elevated risk of cartilage degeneration (C. Cooper et al., 1994; Kingston et al., 2016). Findings of this study therefore suggest that childcare workers are likely at increased risk of OA development given both the frequency and duration of high knee flexion postural adoption throughout their working day.

While postural analysis is critical in the assessment of OA risk, relating the observed postures to specific occupational tasks is necessary for the contextual understanding of childcare related exposures. Task specific postural analysis may provide the foundation for workplace improvements which could in turn reduce the risk of OA development in childcare workers. Childcare workers caring for infants adopted seated postures for greater periods of time than those caring for toddlers and preschoolers, yet it's noted that these infant educators also had the highest number of transitions. These findings may be attributable to the independence of the children being cared for, wherein infants were observed to require a greater level of interaction from their care givers during most activities. Based on our analysis, while it appeared that the choice of high knee flexion postures adopted to complete a task varied by child age, the variability between individuals was also quite high, and therefore no preferential patterns for high knee flexion adoption associated with childcare tasks emerged consistently between workers caring for children of a particular age. It was shown however that high knee flexion postures were adopted most frequently during structured activities, while playing, and while

feeding children. It is interesting to note that when analyzing the lifting and postural demands of the spine, Labaj et al (2019) also concluded that structured activities and playing were among the most demanding tasks for childcare workers. These tasks may therefore be of particular interest when seeking to provide recommendations or guidelines to reduce musculoskeletal exposures in occupational childcare.

The U.S. Bureau of Labor Statistics reported that in 2017-2018 over half of all injuries reported in childcare resulted in days away from work or job restrictions (US Bureau of Labor Statistics, 2018). This report indicated that incidences of injuries to the knee were second only to injuries to the spine and occurred in similar frequencies to those at the shoulder (US Bureau of Labor Statistics, 2018), while between 2010 and 2019 the WSIB in Ontario reported that 8% of all childcare related approved lost time claims involved acute injuries to the knee (WSIB Ontario, 2020). Given the frequency of high knee flexion adoption across all childcare related tasks, none could be reported as knee sparing based on the current analysis, leaving workers susceptible to injury or cumulative trauma to the joint. Four tasks were identified however as requiring the least knee flexion, including changing, bathroom, prep, and supervision, and thus could be seen as the least detrimental to the knee should job modification be possible to ease the burden on the joint. While not reported in this study, Labaj et al. reported an increased incidence of awkward postures while lifting in childcare workers caring for infants and toddlers (where lifting of children was often performed from a seated or kneeling posture) (Labaj et al., 2016). Awkward postures (with and without the presence of lifting) could be associated with increased risk of pain and musculoskeletal impairments for childcare workers(Corlett & Bishop, 2007; Gratz et al., 2002) and might also be linked to the increased incidences of injuries due to bodily reactions and exertions reported by the WSIB Ontario (WSIB Ontario, 2019). These findings echo those previously presented by Grant et al. who further reported that childcare workers were uninformed as to the potential risks associated with postures involving high knee flexion (Grant et al., 1995). Therefore, improvements to both the working environments and guidelines provided to childcare workers are necessary in order to prevent musculoskeletal injuries.

The work here presented has the following limitations. The dataset presented in this study is quite unique given the privacy concerns associated with collecting video data within childcare settings. The sample of knee flexion angles measurable from the video data was limited due to

lack of visibility of the required landmarks or poor recording quality given that this data was collected with the purpose of analyzing spinal loading and lifting in childcare workers. While those studies utilizing sensor-based measures alone may provide an opportunity to capture larger anonymous data sets, we believe that the data presented in this study offer a comprehensive analysis of all childcare related tasks and the high flexion postures which are adopted during their execution. Another potential limitation of the current study is that the analyzed childcare centers were all from Kingston, Ontario. While we do not believe that there would be large differences in childcare related tasks and postural adoption in childcare centres located in other regions, we acknowledge that differences in cultural philosophies or physical environments may create variations in data from different centres. This local data would be most applicable therefore to childcare workers in areas with similar statistics to Ontario where 1 in 132 childcare workers reported an injury severe enough to require time away from their position over the past 10 years, based on the 2016 Canadian census data (Statistics Canada, 2016; WSIB Ontario, 2020); and where the number of reported lost time claims in childcare and home support workers from 2011 to 2019 increased by 119% and accounted for 3.3% of all claims in the province and 11% of claims in businesses in which the employers do not operate under the collective liability insurance principle (WSIB Ontario, 2019). It is additionally noted that exposures in this study were scaled based on exposure data collected only in the mornings, which might not be representative of childcare tasks and postures performed over an 8-hour working period. However, we have no reason to believe that the postures and activities performed in the afternoon would be different from those performed in the mornings, and further, our findings suggest that both the frequency and duration full day thresholds for increased likelihood of OA development are already exceeded within the 3.25-hour period studied. Finally, we acknowledge that in order to identify risk factors relating to OA development, a longitudinal- and population-based analysis would be required. We have therefore chosen instead to use published risk thresholds for increased incidences of OA development (conservatively scaled to our data collection duration) to determine if childcare workers could be considered an at-risk population. Exposures beyond these frequency and duration based thresholds have been identified to elevate the risk of knee OA by multiple studies (Coggon et al., 2000; C. Cooper et al., 1994; D'Souza et al., 2008; Jensen, 2008; Tennant et al., 2018; X. Wang et al., 2020), however we acknowledge

that this approach considers the loading effects of all high flexion postures to be equal even though different high flexion postures would have at least some variation in their contribution to daily cumulative joint loading (A. Horng et al., 2015).

## 3.5 Conclusions

The results presented in this study for the frequency of adoption and cumulative duration analyses conducted on eighteen childcare workers working with infant, toddler, and preschool aged children suggest that it is likely that childcare workers exceed thresholds associated with increased incidences of knee OA development. It was found that childcare workers adopted kneeling and seated postures most regularly for extended durations and at elevated frequencies. When comparing tasks which elicited high flexion postures, structured activities, playing, and feeding were found to be performed for the longest durations. Results of this study may therefore serve as a foundation to guide efforts in reducing the exposure to high flexion postures, which have been identified to increase the incidence of knee OA, in occupational childcare settings.

# Chapter 4

# Evaluating the Robustness of Automatic IMU Calibration for Lower Extremity Motion Analysis in High Knee Flexion Postures

## 4.1. Introduction

Inertial measurement units, composed of 3D accelerometers, gyroscopes, and magnetometers, present a commercially available low-cost and minimally intrusive means of objectively measuring 3D body segment kinematics in settings beyond traditional motion capture laboratories. In an idealized scenario, by placing an IMU on each joint segment of interest, orientations and angles for each segment and joint could be measured. In reality, these calculations involve complex computational sensor fusion processes in order to combine the raw inertial measures (Kok, Hol, & Schön, 2017; Laidig, Schauer, & Seel, 2017; Weygers et al., 2021). Measures of accelerations and angular velocities obtained through MEMS based sensors may suffer from distortions due to the accumulation of systematic errors and biases (Woodman, 2007) which must be corrected or compensated for prior to any further processing of these data. Advances in MEMS-based sensor development however have proven effective in minimizing accrued errors, with recent studies suggesting that the differences in optical and inertial based estimates of joint angles attributable to drift errors might now be on the same magnitude as those

caused by the malalignment of anatomical frames (Teufl, Miezal, Taetz, & Fröhlich, 2018; Vitali & Perkins, 2020). Therefore, accurate alignment of these anatomical frames based on inertial data is critical in order to advance the use of these sensors outside of laboratory and clinical settings (Laidig, Lehmann, Begin, & Seel, 2019; Olsson, Kok, Seel, & Halvorsen, 2020; Seel, Schauer, & Raisch, 2012).

A fundamental problem in the application of IMUs to the measure of human kinematics lies in the lack of a global system by which the measures of each sensor can be related, either to one another, or to the physiological structures onto which they are attached. To this end, several methods for aligning sensor-based coordinate systems (CSs) with established anatomical CSs (Wu & Cavanagh, 1995b; Wu et al., 2002, 2005) have been proposed (Vitali & Perkins, 2020). The first proposed method depends on the precise alignment of the IMU mountings with the anatomical axes, thereby omitting the need for computational-based alignments entirely, an example of which was presented by Favre et al. (2006). This method however requires expert placement of the sensors, and at best will yield a rough approximation of the segmental axes of interest. The alternative to perfectly aligned sensors requires that the user calculate the sensor to segment mounting orientation which, while computationally more difficult, allows for the arbitrary mounting of the IMUs to the body, thereby increasing the likelihood of their use in research-based environments. The calibration vectors required for sensor to segment alignment have frequently been calculated by means of calibration postures and/or movements (Vitali & Perkins, 2020). The simplest form of this calibration requires participants to stand in a static "neutral" posture (with their legs straight, feet perpendicular and located directly inferior to the hips, looking ahead, with arms relaxed straight by their sides, hands pointing in) from which the gravitational acceleration as measured by the accelerometers can be used to define the longitudinal axes of each segment (Favre et al., 2008; Reenalda et al., 2016). While the use of magnetometer measures has been proposed for the reduction of angular drift in the horizontal plane, and therefore the definition of a frontal anatomical axis (Vitali et al., 2017), these sensors are prone to magnetic drift, making their use in real world settings problematic (G. Cooper et al., 2009; Seel et al., 2014). Therefore, in addition to a static posture, functional approaches to calibration have been proposed, wherein a series of movements are performed about a joint to isolate a single axis of rotation (Favre et al., 2008; Alberto Ferrari et al., 2010; Luinge et al.,

2007). While these functional methods for sensor to segment calibration are quite simple in implementation, their applicability to broad populations is low given that the calibration's success depends on the wearers ability to execute the functional postures or movements, which might not be possible in impaired or obese populations (Weygers et al., 2021). Recent studies have sought to relate inertial measures with the anatomical axes of the segment on which they are mounted through model-based approaches (Muller et al., 2017; Seel et al., 2014; Weygers et al., 2021) and their results show high levels of agreement with optical-based joint angle estimates without requiring precise sensor alignment techniques or the execution of specific calibration motions.

The method proposed by Seel et al. (2014), which will be referred to as the Seel joint axis (SJA) algorithm, utilizes the kinematic constraints of joints of the lower limbs in order to align IMUs with the body, thus enabling the calculation of joint center positions and joint axes in any setting. Their proposed method allows for these calculations free from assumptions as to sensor placement, the use of prescribed postures or movements, and reliance on magnetometers. Therefore, they propose that the knee be modeled as a hinge joint while the ankle and hip be modeled as spherical joints, and exploit the constraints of these models to locate the position of each joint's center of rotation as well as the direction of each joint's flexion-extension axis in local sensor-based coordinates through least squares optimization using measurements of arbitrary motions exciting all degrees of freedom of the joint in question (Seel et al., 2014). Subsequently, the angular accelerations from each IMU can be rotated into the joint coordinate system and integrated about the joint axis, which yields a highly accurate yet slowly drifting estimate of flexion-extension. This drift however can be compensated for through sensor fusion in order to take advantage of the drift-free characteristics of acceleration-based angle estimates while discarding the significant noise inherent to these measures. Küderle et al. (2018) proposed an extension to this implementation in order to mitigate the risk of achieving erroneous calibrations during optimization for the knee when non-ideal calibration data is available. This extension is referred to as the constrained Seel knee axis (CSKA) algorithm and has been found to improve the accuracy of sensor to segment calibrations about the knee without requiring specific calibration motions. Both the SJA and CSKA will be presented in greater detail to follow in Subsection 4.2.

Given the frequent adoption of high knee flexion postures in occupational settings (Coggon et al., 2000; Jensen, 2008; Laudanski, Buchman-Pearle, & Acker, 2022); as well as the relation between the adoption of high knee flexion postures and the risk of OA development (Anderson & Felson, 1988; Felson, 2013; Wallace et al., 2017), the ability to measure these postures as they occur naturally in non-laboratory settings is critical for the development of effective guidelines for postural adoption in occupational settings. The proposed SJA and CSKA algorithms offer promise towards the goal of human motion measurement outside of laboratory settings however experimental validation in previous studies has almost exclusively involved robotically constrained motions or gait activities (Küderle et al., 2018; Nguyen et al., 2019; Nowka, Kok, & Seel, 2019; Olsson, Seel, Lehmann, & Halvorsen, 2019; Seel et al., 2014). High knee flexion postures tend to illicit increased soft tissue artefact and a much wider range of joint angles than experienced during walking (Buchman-Pearle & Acker, 2021; T. Tsai, Lu, Kuo, & Lin, 2011), it is important therefore to investigate the accuracy of flexion-extension angle estimates in the lower limbs during these postures using the SJA and CSKA algorithms prior to their implementation in real world settings.

Therefore, the purpose of this study was to evaluate the performance of the SJA and CSKA algorithms, following simple calibration motions, in multiple high knee flexion postures inspired by childcare workers. The results of this first attempt, which are further described in Subsection 4.8, suggested that the proposed sensor fusion equations were insufficient to correct for drift pollution in the estimated angles during the high flexion postures of interest. Therefore, a possible modification is proposed in Subsection 4.5 to improve the stability of the final angle estimates, and results of this modification were validated through comparison with flexion angles calculated based on simultaneously collected optical-motion capture data during multiple high knee flexion postures.

## 4.2. Description of the CSKA Algorithm for Sensor to Segment Alignment

The proposed algorithms by Seel et al. and Küderle et al. require that one IMU be affixed to the proximal and distal segments of each joint from which angles can be calculated (Küderle et al., 2018; Seel et al., 2014, 2012). For generalizability, the location and orientation of each sensor

relative to the joint in question need not be known. This mounting strategy however requires that a definition of the joint axis and center of rotation be obtained in both of the local sensor frames prior to the calculation of joint angles.

Seel et al. (2012) proposed modeling the knee joint as a 1 DoF hinge type model in order to simplify the biomechanical model of this joint. This approximation is reasonable for two reasons; First, the greatest degree of motion occurring at this joint is measured in in the sagittal plane. Second, there is a tendency for deviations in estimated axes relating to secondary kinematics leading to inaccuracies in the calculations of abduction-adduction and internal-external rotation angles based on inertial sensors (Weygers et al., 2021). This 1 DoF hinge type model additionally simplifies the calculations of joint angles given that the center of rotation of the joint need not be defined in order to solve for the joint axis in each sensor frame. When solving for the joint axis (about which the flexion-extension occurs), the measured gyroscope rotations for each sensor alone can be used in the case of a hinge-type joint, given that the constraints of this model ensure that the angular velocities measured by the proximal and distal sensors be equal, save the contribution of the joint angle velocity and a time-variant rotation matrix within each signal (Seel et al., 2012). Taking into account the arbitrary mounting of the sensors, the measures will differ by some rotation matrix ${}^{S_2}_{S_1}\boldsymbol{R}$ describing the rotation from the local frame of the second sensor into the local frame of the first.

$$ {}^{S_1}\omega_{leg}(t) = {}^{S_2}_{S_1}\boldsymbol{R} \ * \ {}^{S_2}\omega_{leg}(t), \tag{4.1} $$

where ${}^{S_i}\omega_{leg}$ represents the measured angular velocity expressed about the coordinate system axes of sensor *i,* attributable to the movement of the leg as a whole. The equality imposed by the model can therefore be formulated as follows:

$$ \left\| {}^{S_1}\omega_{leg} \right\|_2 - \left\| {}^{S_2}\omega_{leg} \right\|_2 = 0, \quad \forall t \tag{4.2} $$

where $\| \bullet \|_2$ represents the Euclidean norm and $\forall t$ indicating 'for all instances of time *t*'. This equation can be further broken down by expressing the movement of the leg as a projection of the angular velocity into the joint plane:

$$ {}^{S_i}\omega_{leg} = {}^{S_i}\omega(t) \times {}^{S_i}\hat{\jmath}, \tag{4.3} $$

where ${}^{S_i}\hat{j}$ is a representation of the joint axis expressed about the coordinate system axes of sensor *i*. To simplify the notation from here on, the following variables will be used: ${}^{S_i}\omega = \omega_i$ and ${}^{S_i}\hat{j} = \hat{j}_i$. Thus, combining eq. (4.2) into eq. (4.3):

$$\Phi\left(t;\, \hat{j}_1, \hat{j}_2\right) := \left\|\omega_1(t) \times \hat{j}_1\right\|_2 - \left\|\omega_2(t) \times \hat{j}_2\right\|_2 = 0, \quad \forall t \tag{4.4}$$

where $\omega_1$ and $\omega_2$ represent the angular velocity expressed about the coordinate system axes of each sensor and $\hat{j}_1$ and $\hat{j}_2$ represent the joint axis in each sensor coordinate frame. This constraint holds for all time instants regardless of the relative orientation of each sensor. The orientation of a joint axis unit vector within each sensor's local coordinate system can thus be obtained through a least-squares optimization to minimize eq. (4.4) given any gyroscopic signals measured during arbitrary motions of each sensor. The orientation of the joint axis unit vector in each sensor's coordinate system is therefore the solution of the following:

$$\min_{\hat{j}_1, \hat{j}_2} f(\hat{j}_1, \hat{j}_2) \tag{4.5}$$

with

$$f(\hat{j}_1, \hat{j}_2) = \sum_{i=1}^{N} \Phi(t_i;\, \hat{j}_1, \hat{j}_2)^2, \tag{4.6}$$

where $t_{1,\ldots,N}$ are the time points of the randomized motions used in the calculation for calibration.

The unit vectors $\hat{j}_1$ and $\hat{j}_2$ can then be expressed in spherical coordinates so as to decrease the number of optimization parameters from 6 to 4.

$$\hat{j}_i = \left[\cos(\varphi_i)\sin(\theta_i), \sin(\varphi_i)\sin(\theta_i), \cos(\theta_i)\right]^T \tag{4.7}$$

where $\varphi_1, \varphi_2 \in \left[-\frac{\pi}{2}, \frac{\pi}{2}\right]$ represent the inclinations and $\theta_1, \theta_2 \in [0, 2\pi]$ represent the azimuths in sensor frame *i* (*i* = 1,2).

It is here that the CSKA algorithm extension proposed by Küderle et al. is implemented (Küderle et al., 2018). By determining the direction of the gravitational axes through the accelerometer readings during a brief static period, a global vector can be defined in both of the local sensor frames (Küderle et al., 2018). Through this vector, a geometric constraint can be imposed during calibration by aligning both sensor CSs' z-axes with the direction of gravity, thus creating an equality in the angles measured between the joint axes and the z-axis in each sensor frame and reducing the parameters of the optimization problem. In order to achieve this

alignment, the local CSs must be converted into the global reference system, and given that the two local representations of the knee joint axes $\hat{j}_1$ and $\hat{j}_2$ must be aligned in the global CS, this equality can be expressed as follows:

$$ {}^{S_1}_{G}\hat{q}(t) \times {}^{S_1}\hat{j} \times {}^{S_1}_{G}\hat{q}^*(t) = {}^{S_2}_{G}\hat{q}(t) \times {}^{S_2}\hat{j} \times {}^{S_2}_{G}\hat{q}^*(t) \quad \forall t \tag{4.8} $$

where ${}^{S_i}_{G}\hat{q}(t)$ represents the orientation of sensor *i* within the global CS in a quaternion form and ${}^{S_i}_{G}\hat{q}^*(t)$ represents the transpose of this orientation quaternion. This same equation can be re-written to represent the gravitational vector as measured by each accelerometer:

$$ {}^{S_1}_{G}\hat{q}(t) \times {}^{S_1}\hat{a}_g(t) \times {}^{S_1}_{G}\hat{q}^*(t) = {}^{S_2}_{G}\hat{q}(t) \times {}^{S_2}\hat{a}_g(t) \times {}^{S_2}_{G}\hat{q}^*(t) \quad \forall t \tag{4.9} $$

where ${}^{S_i}\hat{a}_g(t)$ represents the direction of the gravitational vector in sensor frame *i*. Knowing that these gravitational vectors must also be aligned in each sensor CS, a quaternion transforming the gravitational vector into the joint axes in both local CSs can be expressed as:

$$ {}^{a}_{j}\hat{q}_g(t) \times {}^{S_i}\hat{a}_g \times {}^{a}_{j}\hat{q}^*_g(t) = {}^{S_i}\hat{\jmath}, \quad \forall i. \tag{4.10} $$

Note here that the quaternions are responsible for rotations between unit vectors (representing the accelerometer-based estimate of gravity and the knee joint axis) rather than rotations between coordinate systems. These quaternions, for non-parallel vectors, are defined as follows:

$$ {}^{a}_{b}\hat{q} = \left[\cos\left(\frac{\alpha}{2}\right), -r_x \sin\left(\frac{\alpha}{2}\right), -r_y \sin\left(\frac{\alpha}{2}\right), -r_z \sin\left(\frac{\alpha}{2}\right)\right], \tag{4.11} $$

with

$$ \hat{r} = \hat{a} \times \hat{b}, \tag{4.12} $$

$$ \alpha = \measuredangle_{3D}(\hat{a}, \hat{b}), \tag{4.13} $$

where ${}^{a}_{b}\hat{q}$ represents the quaternion which rotates the unit vector $\hat{a}$ into the unit vector $\hat{b}$. Therefore from eq. (4.10) and eq. (4.11), it becomes evident that the angle $\alpha_i(t)$ between the gravitational vectors and the respective joint axis must be identical when expressed in each sensor frame *i*:

$$ \alpha(t) = \alpha_1(t) = \alpha_2(t) = \measuredangle_{3D}\left({}^{S_1}\hat{a}_g(t), {}^{S_1}\hat{\jmath}\right) = \measuredangle_{3D}\left({}^{S_2}\hat{a}_g(t), {}^{S_2}\hat{\jmath}\right). \tag{4.14} $$

As long as the calibration data collected includes a short period of static ($t_0$) from which the direction of the gravitational vector can be determined, the orientations of the joint axes in each sensor frame can be aligned using eq. (4.14). In order to use this alignment to simplify the

optimization problem posed in eq. (4.4) the sensor CSs are rotated such that $\alpha(t_0)$ aligns with one of the angles of the defined spherical coordinate systems. Küderle et al. (2018) therefore recommend rotating both CSs such that ${}^{S_i}\hat{a}_g(t_0)$ aligns with the local z-axes and, in spherical coordinates, the angle between each representation of gravity and the local z-axis would be equal ($\alpha(t_0) = \theta = \theta_1 = \theta_2$). This equality enables the optimization parameters to be further reduced to a set of three:

$$[\varphi_1 \quad \varphi_2 \quad \theta], \tag{4.15}$$

where $\theta$ now represents the angle between the gravitational vector and the joint flexion-extension axis.

Küderle et al. (2018) proposed the use of the Levenberg-Marquardt (LM) algorithm to solve the least squares optimization of eq.(4.5). The LM algorithm is a trust region method based on a quadratic approximation of the objective function which replaces the second order derivative of the objective function (the Hessian) with an approximation based on the Jacobian matrices. This algorithm yields a faster convergence to a minimum value than the simple Gradient Descent method however can be similarly vulnerable to local minima as the Gaus-Neuton algorithm originally proposed by Seel et al. (Kuderle, 2017; Nocedal & Wright, 2000; Seel et al., 2012). Therefore, an explicit solution of the Jacobian should be derived prior to optimization to aid in the computation. Based on the derivation of eq. (4.4) provided by Seel et al. (2016) and constrained by Küderle et al. (2018), the Jacobian matrix in the newly rotated coordinate systems is given by:

$$J = \left[\frac{d\omega_{1,leg}(t)}{d\hat{\jmath}_1}\frac{d\hat{\jmath}_1}{d\varphi_1} \quad -\frac{d\omega_{2,leg}(t)}{d\hat{\jmath}_2}\frac{d\hat{\jmath}_2}{d\varphi_2} \quad \left(\frac{d\omega_{1,leg}(t)}{d\hat{\jmath}_1}\frac{d\hat{\jmath}_1}{d\theta} - \frac{d\omega_{2,leg}(t)}{d\hat{\jmath}_2}\frac{d\hat{\jmath}_2}{d\theta}\right)\right], \tag{4.16}$$

where:

$$\frac{d\hat{j}_i}{d\theta} = \left[\cos(\varphi_i)\cos(\theta_i) \quad \sin(\varphi_i)\cos(\theta_i) \quad -\sin(\theta_i)\right]^T \tag{4.17}$$

$$\frac{d\hat{j}_i}{d\varphi} = \left[-\sin(\varphi_i)\sin(\theta_i) \quad \cos(\varphi_i)\sin(\theta_i) \quad 0\right]^T. \tag{4.18}$$

Using these new equations (eqs. (4.16), (4.17), and (4.19)), the minimization problem presented in eq. (4.5) can be solved, and finally the derived joint axis vectors must be rotated back into their respective sensor frames.

It should be noted that the CSKA algorithm's calibration may fail in cases where θ is close to 90°, which might occur should the segment movements not be sufficiently different so as to facilitate distinguishing between them, in which case the optimization may yield a local minimum in the parameter space representing misaligned joint axes. In these cases, the minimization should be rerun, with the axis vector of one of the sensors having been rotated 180°, however, should the optimization also yield no aligned vector pair, calibration is deemed unsuccessful. It is noted that, in all performed validation experiments for this thesis work, successful calibration of the joint axes in the local sensor CSs were achieved either through the initial or the rerun (one axis rotated 180°) optimization.

## 4.3. IMU-Based Knee Flexion Angle Measurement

Following the sensor to segment calibration of all IMUs in order to define the anatomical axes of each joint relative to the local sensor frames, the identified values for $j_1$, and $j_2$ can be used to calculate the flexion-extension angles of the knee joint. By utilizing these vectors, the gyroscope signals can be integrated only around the joint axis, yielding a slowly drifting yet otherwise highly accurate measure of joint flexion-extension (Seel et al., 2012). This angle can then be combined through sensor fusion with a noisy yet driftless angle estimate calculated from the measured accelerations projected into the joint plane, so as to generate a stable, drift free angle estimate for any motion.

The gyroscope-based flexion-extension angle can be calculated by integrating the measured angular velocities from each sensor around the previously calculated joint axis, as follows (Seel et al., 2012):

$$\alpha_{gyro} = \int_0^T (\omega_u(t) \cdot \hat{j}_u - \omega_l(t) \cdot \hat{j}_l) dt + \alpha_0, \tag{4.19}$$

where the subscript *u* denotes the sensor attached to the limb superior to the joint and the subscript *l* denotes the sensor attached to the inferior limb. Additionally, the integration is only capable of providing a relative angle between these upper and lower segments, therefore some initial angle, $\alpha_0$, previously determined by alternate means, must be added to the estimation. Most commonly, if participants begin a trial in a standing position, these initial angles can all be assigned a value of 0°.

For the accelerometer-based flexion-extension angle estimate, we must first shift the measured accelerations into the joint plane and discard the gravitational component along the known z-axis. To do this, we must first define an arbitrary vector which is located in the joint plane:

$$^{S_i}\hat{e}_z = {}^{S_i}\hat{a}_g(t_o), \tag{4.20}$$

$$^{S_i}\hat{e}_x = {}^{S_i}\hat{a}_g(t_o) \times {}^{S_i}\hat{j}, \tag{4.21}$$

$$^{S_i}\hat{e}_y = {}^{S_i}\hat{a}_g(t_o) \times {}^{S_i}\hat{e}_x, \tag{4.22}$$

where $^{S_i}\hat{e}_{x,y,z}$ are representations of unit vectors of the global coordinate system in the respective sensor frame $i$, and $^{S_i}\hat{a}_g(t_o)$ represents the direction of the gravitational vector at time 0. These unit vectors can be combined to create a rotation quaternion ${}^{j}_{e_z}\hat{\boldsymbol{q}}$ from which the acceleration can be projected into the joint plane as follows:

$$\hat{a}'_{proj} = {}^{j}_{e_z}\hat{q} \times \hat{a} \times {}^{j}_{e_z}\hat{q}^{*} \cdot \left(\hat{e}'_x + \hat{e}'_y\right), \tag{4.23}$$

where $'$ denotes values already rotated into the joint coordinate system and $\hat{a}$ denotes the normalized acceleration vector. Subsequently, the inclination of each segment can be calculated as the angle between the projected acceleration and an arbitrary vector in the joint plane (either $\hat{e}'_x$ or $\hat{e}'_y$ can be used), and these inclinations can be combined to determine a relative joint angle as follows:

$$\alpha_{acc} = \alpha_{acc,u} - \alpha_{acc,l} + (\alpha_0 - \alpha_{acc,0}), \tag{4.24}$$

with

$$\alpha_{acc,i} = \measuredangle_{3D}\left(\hat{a}'_{proj,i}, \hat{e}'_j\right), \tag{4.25}$$

where $\alpha_{acc,0}$ denotes the initial angle estimate based on the accelerometer measures, which will be removed from the final accelerometer angle, $i$ represents the sensor frame ($i = l, u$), and $j$ represents the reference vector (either $x$ or $y$).

These angle estimates can then be combined using a simple complementary filter, as suggested by Seel et al. (2014):

$$\alpha(t)_{comp,i} = \lambda\alpha_{acc,i}(t) + (1-\lambda)\big(\alpha_{comp,i}(t-\Delta t) + \alpha_{gyr,i}(t) - \alpha_{gyr,i}(t-\Delta t)\big), \tag{4.26}$$

where $\lambda$ is a weighting factor, assigned a value of 0.01, and $\Delta t$ is the sampling step size. Finally, the angles estimated using the IMUs superior and inferior to the joint were combined such that:

$$\alpha_{knee}(t) = \alpha_{comp,l}(t) - \alpha_{comp,u}(t). \tag{4.27}$$

# 4.4. Sensor to Segment Alignment for Spherical Joint Axis Estimation by Seel et al.

For the ankle and hip joints, the application of a hinge-type model would be inappropriate; as such Seel et al. (2012) proposed a 3 DoF spherical joint model as an alternative. The angular velocities of segments connected by a 3 DoF joint are not generally relatable as they are in a 1 DoF joint, therefore while the calculation of joint axes based on gyroscope signals alone is sufficient in a hinge-type model, the resultant vectors $j_1$ and $j_2$ in a spherical joint will not be aligned. The position of the joint center of rotation estimated in each sensor frame must be obtained in order to exploit the kinematic constraints of the model. Thus, two joint position vectors, $o_1$ and $o_2$, must be defined as vectors pointing from the origin of each local sensor frame to the joint center. To solve for these joint position vectors, a combination of the accelerometer and gyroscope readings are required, and as such we denote the accelerations of each sensor as $a_1(t)$ and $a_2(t)$. The accelerations of each measured segment must be attributable to the rotation and movement of the leg about the joint centre, also known as the radial and tangential accelerations about the joint, represented by the term $\Gamma(\omega_i(t),\ o_i)$, as well as to the acceleration of the joint centre itself, denoted by the term $(a_i(t) - \Gamma(\omega_i(t),\ o_i))$. The acceleration of the joint centre must be measured equally by both the proximal and distal sensors to the given joint, and as such the following constraint was proposed (Seel et al., 2012):

$$\Psi(t;\ o_1, o_2) := \|a_1(t) - \Gamma(\omega_1(t), o_1)\|_2 - \|a_2(t) - \Gamma(\omega_2(t), o_2)\|_2 = 0 \quad \forall t,. \tag{4.28}$$

$$\Gamma(\omega_i(t), o_i) := \omega_i(t) \times o_i \times \omega_i(t) + o_i \times \frac{d\omega_i(t)}{dt}, \tag{4.29}$$

$$\frac{d\omega_i(t)}{dt} \approx \frac{\omega(t-2\Delta t) - 8\omega(t-\Delta t) + 8\omega(t+\Delta t) + \omega(t+2\Delta t)}{12\Delta t}, \tag{4.30}$$

where eq. (4.30) represents a symmetric third-order approximation for the time derivative of the angular velocity, $\Delta t$ represents the sampling step size of the sensor, and $i$ represents the sensor frame ($i$ = 1,2).

Estimates of each joint offset vector ($\hat{o}_1$and $\hat{o}_2$) can then be determined by minimizing eq. (4.28) in a least squares optimization as follows

$$\min_{o_1,o_2} h(o_1, o_2). \tag{4.31}$$

with

$$h(o_1, o_2) = \sum_{i=1}^{N} \Psi(t;\ o_1, o_2)^2. \tag{4.32}$$

For this optimization, the Jacobian implemented is again based on the derivation by Seel et al. (Seel, 2016), the $k^{\text{th}}$ row of which follows:

$$J_{pos,k} = \begin{bmatrix} -\dfrac{\Gamma\left(-\omega_1(t),\ a_1(t) - \Gamma(\omega_1(t), o_1)\right)}{\|a_1(t) - \Gamma(\omega_1(t), o_1)\|_2} \\ \dfrac{\Gamma\left(-\omega_2(t),\ a_2(t) - \Gamma(\omega_2(t), o_2)\right)}{\|a_2(t) - \Gamma(\omega_2(t), o_2)\|_2} \end{bmatrix}^T. \tag{4.33}$$

It is important to note that the optimized offset vectors, $\hat{o}_1$and $\hat{o}_2$, do not necessarily point directly from the origin of the sensor frame to the joint center of rotation but rather from any point along the joint axis vector which originates at the origin of the sensor frame. Therefore, the joint axis vectors ($j_1$ and $j_2$) and the joint offset vector estimates can be combined in order to solve for the vectors which minimize the distance between each sensor and the joint center of rotation in each sensor frame ($o_1$ and $o_2$)

$$o_1 = \hat{o}_1 - j_1 \frac{\hat{o}_1 \cdot j_1 + \hat{o}_2 \cdot j_2}{2}, \quad o_2 = \hat{o}_2 - j_2 \frac{\hat{o}_1 \cdot j_1 + \hat{o}_2 \cdot j_2}{2} \tag{4.34}$$

## 4.5. Iterative Sensor to Segment Alignment for Spherical Joint Axis Estimation by Seel et al.

When seeking to apply the proposed SJA algorithm (presented in Subsections 4.2 and 4.4) for the definition of the joint axis and center of rotation in each sensor frame about a spherical joint,

preliminary validations using the data collected for this thesis (Subsection 4.8) could not confirm the reported accuracies by Seel et al. (2014, 2012). These discrepancies may have resulted from the type of sensor used, the calibration postures performed, the duration of trials analyzed, or the ranges of motion elicited during the postures performed in this study. Regardless of their sources, the iterative Seel spherical axis (ISSA) algorithm was developed as part of this work to provide more stable and repeatable estimates of the joint axis and center of rotation based on the data herein collected.

Given the vulnerability of the Levenberg-Marquardt algorithm to local minima during least squares optimizations, 1000 iterations of the optimization were performed, each from a randomized initialization point. The initialization value which yielded the smallest square root of the sum of squares of the gradient values was then selected and input into a Trust Region Reflective (TRF) algorithm to solve the least squares optimization of eq. (4.15). The TRF, as its name suggests, is a trust region method wherein the algorithm iteratively performs minimization on trust region subproblems, such that these subspaces are shaped by the distance to the bounds and the direction of the gradient to avoid making steps directly into the constraining bounds while also exploring the whole variable space (Branch, Coleman, & Li, 1999). This algorithm allows users to define the cost-function by which the variable space will be searched. To accelerate convergence, this method reflects the search directions from the bounds, and in each iteration, the cost function is used to modify the residual vector and the Jacobian for a robust convergence with the true gradient (Triggs, Mclauchlan, Hartley, & Fitzgibbon, 2000). A smooth approximation of the absolute value loss was selected as the cost function, with a scaling factor of 0.1 and the Jacobian given by eq. (4.16) to solve for $j_l$, and $j_u$. Solving for the joint positions in each sensor frame, $o_l$, and $o_u$, was performed as proposed by Seel et al. (2012) and explained in Subsection 4.4, and subsequently, a verification phase was implemented to ensure that an opposite signed solution or failure to converge upon the joint centre during optimization had not occurred.

### 4.5.1.Sensor to Segment Alignment Iteration for the Ankle

For the ankle, verification was performed during a posture in which a large range of motion would be observed (a plantarflexed kneeling trial was utilized in this study). The sign of the first

and second components of $j_l$, the joint axis expressed in the lower sensor's CS, were flipped, and an estimate of the gyroscope-based flexion angle during the motion trial was calculated using eq. (4.19). If the minimum and maximum values of this angle estimate were found to be between 100° and -100° respectively (these values were chosen such that any estimated angle within their range might be physiologically possible following drift compensation (Brockett & Chapman, 2016)), the rotation of $j_l$ was kept, otherwise the rotation was rejected. Subsequently, the ankle angle was estimated using a complementary fusion equation including both the accelerometer and gyroscope measures (explained in detail below in Subsection 4.6). The minimum and maximum values of this new angle were then calculated, if they were not found to be within -80° to 80°, respectively, the signs of the x and y accelerations and angular velocity signals within the calibration trials were flipped as were the x and y components of the gravitational vector for the foot.

It was assumed that if the angles calculated using the joint axis and center of rotation vectors were non-physiological, an opposite signed solution may have been reached given the orientation of the sensor during collection. Provided the sensors were always mounted with the local z-axis pointing away from the body, only the x and y components of each measurement should be rotated. These newly rotated calibration data were then input to the optimization problem posed in eq. (4.4) to solve again for $j_l$, and $j_u$. These new values were again input to eq. (4.19), and flipped if the estimated angle had minimums or maximums beyond the range of -100° to 100°. Finally, new values for $o_l$, and $o_u$ were found by optimizing eq. (4.31) using the un-rotated calibration data and combining these results with the newly solved for $j_l$, and $j_u$ using eq. (4.34).

### 4.5.2.Sensor to Segment Alignment Iteration for the Hip

For the hip, verification was again performed during a posture which would elicit a large range of motion (a supported kneeling trial was utilized in this study). The hip angle for this motion trial was estimated using a complementary fusion equation including both the accelerometer and gyroscope measures (explained in detail below in Subsection 4.6) and mean values were calculated across the entire trial as well as during the central 2 s of the trial (when the participant was known to be static and in maximum hip flexion). If either of the mean values were found to be less than 0° the signs of the x and y accelerations and angular velocity signals within the

calibration trials were flipped as were the x and y components of the gravitational vector for the thigh. Subsequently these data were input to the optimization problem posed in eq. (4.4) to solve for new values of $j_l$, and $j_u$. These joint axis vectors along with the un-rotated calibration gyroscope data were then used to estimate the flexion angle using eq. (4.19) and the overall mean and static mean values for this angle were calculated. Should either of these mean values be found to be less than 0°, the sign of the x and y components of $j_l$ were changed. For the hip, the original $o_l$, and $o_u$ vectors are not recalculated.

## 4.6. IMU-Based Flexion Angle Measurements for the Ankle and Hip

Similarly to the angle calculations at the knee, the gyroscope-based flexion-extension angle for the ankle and hip can be calculated using eq. (4.19). In the case of the spherical joints, the acceleration vectors can be divided by their components using eq. (4.29) where the radial and tangential acceleration can be calculated using the gyroscope signal and respective $o_i$, and subsequently subtracted from the acceleration signals to yield only the acceleration of the joint center, $a_{jc}$, as follows:

$$a_{jc,i} = a_i - \left(\omega_i(t) \times o_i \times \omega_i(t) + o_i \times \frac{d\omega_i(t)}{dt}\right), \tag{4.35}$$

for each joint frame $i$ ($i$ =1,2). This joint center acceleration can then be shifted from the local CS into the joint plane using two vectors located within this plane defined as follows:

$$x_i = \hat{j}_i \times C, \tag{4.36}$$

$$y_i = \hat{j}_i \times x_i, \tag{4.37}$$

where $C$ represents a reference vector in the joint plane (the vector $[-1,0,0]^T$ was used in this study). Therefore, the shifted accelerations for each sensor, $u$ and $l$ can be calculated as follows:

$$a_{proj,i} = \left[\left[a_{jc,i} \cdot x_i\right]^T, \left[a_{jc,i} \cdot y_i\right]^T, 1\right]^T. \tag{4.38}$$

The angle between these two projected acceleration vectors is then calculated as follows:

$$\alpha_{acc} = \measuredangle_{3D}(a_{proj,l}, a_{proj,u}) - \alpha_{acc,0}. \tag{4.39}$$

Given the noisy signal characteristics of the acceleration-based flexion-extension angle, a Savitsky-Golay filter is subsequently applied with a 15-sample window size in order to smooth the data and eliminate any large, non-physiological spikes. A representative example of this accelerometer-based joint angle estimation calculated with accelerations in both the sensor and joint coordinate systems can be found in Figure B.1 and Figure B.4 for the Ankle and Hip respectively. Representative examples of gyroscope-based angle estimates calculated with angular velocities in each sensor axis as well as about the joint flexion-extension axis can additionally be found in Figure B.2 and Figure B.5 for the Ankle and Hip respectively.

Seel et al. (2012) propose using the same complementary filter proposed for the knee as presented in eq. (4.26) and eq. (4.27) when calculating ankle flexion-extension. Validation of these equations for the current data however could not confirm the reported accuracies, potentially indicating the need for application-specific filters. Therefore flexion-extension angles were additionally calculated using the following proposed alternative complementary filters.

In order to combine the accelerometer- and gyroscope-based angle estimates to calculate the ankle flexion-extension angle, a weighted constraint was applied, similar to that introduced by Olsson et al. (2019) for fast and slow motions, wherein the accelerometer-based angle would be given a higher weighting and therefore have a greater influence on the overall angle estimate during static periods than during periods of detected motion when the gyroscope-based estimates would be more heavily weighted. The ankle angle would therefore be calculated as:

$$\alpha_{ankle}(t) = \alpha_{ankle}(t-1) + \big(\alpha_{acc}(t) - \alpha_{acc}(t-1)\big) + 0.2 * \Big(\alpha_{gyro}(t) - \alpha_{gyro}(t-1)\Big) \quad \text{for } |\alpha_{acc}(t) - \alpha_{acc}(t-1)| < 0.15 \text{ and } \big|\alpha_{gyro}(t) - \alpha_{gyro}(t-1)\big| < 0.3 \tag{4.40}$$

and for all other instances:

$$\alpha_{ankle}(t) = \alpha_{ankle}(t-1) + 0.2 * \big(\alpha_{acc}(t) - \alpha_{acc}(t-1)\big) + 0.8 * \Big(\alpha_{gyro}(t) - \alpha_{gyro}(t-1)\Big) \tag{4.41}$$

The flexion-extension angle for the hip was calculated using the following complementary fusion equation:

$$\alpha_{hip}(t) = 0.65 * \Big(\alpha_{acc}(t) - \alpha_{gyro}(t-1)\Big) + \alpha_{gyro}(t). \tag{4.42}$$

Representative examples of ankle and hip joint angles calculated using these ISSA complementary filters alongside the $\alpha_{acc}$ and $\alpha_{gyro}$ can be found in Figure B.3 and Figure B.6 respectively.

# 4.7. Experimental Validation

In order to validate the algorithm performance and therefore the feasibility of estimating lower limb joint angles of the ankle, knee, and hip based on IMU signals during high flexion movements, a sample of 52 participants were recruited. Fifty participants from which complete datasets were collected were included in this analysis (Table *4.1*). Individuals were asked to self report any history of knee joint disease, current knee pain or leg injury. These prior injuries did not preclude them from participating in the study unless the participant indicated that they were incapable of kneeling or squatting without difficulty or pain. Participants were not required to have any prior history of interacting with or caring for children in order to participate. This study was approved by the University of Waterloo Research Ethics Board and informed consent was obtained prior to each collection.

Table 4.1 Mean (SD) descriptive and anthropometric participant information. Daily squatting regularity was rated on a 3-point scale where scores from 1 to 3 equated to rarely, occasionally, and regularly squatting. While all participants were currently living in Canada, heritage was self reported as relating to their ancestry as ethnicity has been suggested as a potential influencing factor in the development of knee OA (Chong, 2016; Leszko, Hovinga, Lerner, Komistek, & Mahfouz, 2011).

| Parameter | Female ($n$ = 32) | Male ($n$ =18) | Total ($n$ = 50) |
|---|---|---|---|
| Age (years) | 20.84 (3.36) | 21.75 (4.51) | 21.15 (3.76) |
| Height (m) | 1.67 (0.06) | 1.80 (0.07) | 1.71 (0.09) |
| Mass (kg) | 68.57 (16.88) | 83.08 (15.81) | 73.71 (17.78) |
| Squat Regularity | 1.97 (0.69) | 1.94 (0.64) | 1.96 (0.67) |
| Dominant Leg (R/L) | 27/5 | 16/2 | 43/7 |
| Heritage (Western/ non-Western) | 27/5 | 10/8 | 37/13 |

Seven wireless IMUs (Xsens MTw Awinda, Xsens Technology B.V., Netherlands, Gyro.: 2000 deg/s, Acc.: 16 G, sampling frequency: 60 Hz) were attached bilaterally to the superior aspect of participant's feet, the lateral aspects of the participant's shanks and thighs, and over the base of the participant's sacrum. The foot sensors were attached to the participant's footwear, roughly above the superior aspect of the mid-foot, mid-distance between the medial malleolus and the head of the first metatarsal. The shank and thigh sensors were attached roughly one third the distance from the lateral malleoli to the lateral epicondyle of the tibia and roughly midway between the greater trochanter and the lateral epicondyle of the femur respectively. All sensors,

save for those on the feet, were attached using foam backed, anti-slip fabric wraps (fabrifoam®, Fabrifoam Products, United States of America). With the exception of placing sensors in the general regions described above, no specific orientations or positions were enforced.

Clusters of four non-collinear infrared emitting diodes were attached to the lateral surface of each IMU with the exception of the foot, where the cluster was mounted to the lateral aspect of the participant's footwear (as can be seen in Figure 4.1). These clusters were tracked using an 18-camera optoelectronic motion capture system (NDI Certus/3020, Northern Digital Inc., Waterloo, ON, Canada, sampling frequency: 50Hz).

Figure 4.1 Participant instrumentation , where the shank, thigh, and pelvis marker clusters have been affixed to the lateral aspect of the IMUs while the foot cluster can be seen mounted to the posterior aspect of the shoe while the IMUs are located on the superior aspect of the shoe.

Prior to beginning the high flexion trials, participants completed a 5s standing trial in addition to functional hip (isolated upper leg motion through a star-arc hip circumduction (Camomilla, Cereatti, Vannozzi, & Cappozzo, 2006)) and functional knee (isolated cyclic flexion/extension motion of the lower leg while the upper leg was held parallel to the ground) motion trials. Following these calibration trials, participants completed three 10 m walking trials at a self-selected pace. Subsequently, participants were asked to complete three repetitions in

randomized order of the following movements commonly adopted in occupational childcare and previously described in Table *3.2*: heels-up squatting (HS), flatfoot squatting (FS), dorsiflexed kneeling (DK), plantarflexed kneeling (PK), single arm supported kneeling (SAK), double arm supported kneeling (DAK), sitting on an adult sized chair (ACS), sitting on a child sized chair (CCS), and stooping (STP) (Figure *4.2*). Based on the analysis performed in Chapter 3, stool sitting (STLS) had been identified as a frequently adopted posture by the childcare workers studied, however none of the centers included appeared to have adult-sized furniture available for these individuals. Therefore, this identified posture was divided into two movements, ACS and CCS to capture the differences in joint angles occurring when sitting on adult- and child-sized chairs. Each trial consisted of participants stepping forward with their non-dominant leg prior to transitioning from standing into each pose, holding the fully flexed pose for 5 seconds, and transitioning back to standing based on verbal cues. Kneeling transitions were performed asymmetrically through a lunging posture, where the dominant knee made contact with the ground prior to the non-dominant knee. For supported kneeling trials, the supporting hand was placed on the ground below the shoulder only once individuals had achieved a kneeling posture. Participants were free to take any length of rest period between trials as they deemed necessary. Data were collected simultaneously for both systems during all motion trials


Figure 4.2 Childcare-inspired postures performed in this study (clockwise from top left): heels up squatting (HS), flatfoot squatting (FS), dorsiflexed kneeling (DK), plantarflexed kneeling (PK), stooping (STP), sitting on a child sized chair (CCS), sitting on an adult sized chair (ACS), double arm supported kneeling (DAK), and single arm supported kneeling (SAK).

## 4.7.1.Data Analysis

All optical motion capture data were filtered using a dual pass, second order Butterworth filter with a cutoff frequency of 6Hz (Longpré, Acker, & Maly, 2015; Winter, 2009). Missing data resulting from marker occlusion (where no more than 0.5 seconds of data were missing) were interpolated using cubic spline interpolation (Visual3D, v.6, C-Motion, Inc., Germantown, MD, USA) and any trial with periods of marker occlusion >25 frames were excluded from further analysis. Subsequently, segmental coordinate systems were constructed with axial definitions as outlined in Table A.1 and ankle, knee, and hip joint angles were calculated following Cardan Z-X-Y sequences corresponding to flexion-extension, ab/adduction, and internal/external rotation anatomical axes about each joint (Winter, 2009; Wu & Cavanagh, 1995b; Wu et al., 2002). All angles were calculated with the coordinates of the distal segment and resolved into the proximal segments' coordinate systems. The virtual pelvis and foot segments were selected when calculating the hip and ankle angles respectively (Table A.1). Flexion/extension angles calculated for all joints across all trials were exported to be compared offline to those estimated based on the inertial sensor data (Matlab 9.9, The Mathworks, Release R2020b, Natick, MA, USA).

The CSKA and ISSA algorithms were implemented in Python (Python 3.6, Python Software Foundation, https://www.python.org/). Gravitational vectors were defined based on the 5s static standing trial while the joint position and joint center of rotation vectors for each sensor and each joint were calculated based on a combination of the functional knee and hip movements as well as data from a single 10m gait trial. For the ankle and hip, sensor data from a stooping trial was added to the calibration data. These movements ensured motion about all degrees of freedom of the joint, however could not be considered completely random as those included by Seel et al. (Seel et al., 2012). For the ankle, a plantarflexed kneeling trial was selected for verification during the iterative process of solving for the joint axis and center of rotation, while for the hip a double arm supported kneeling trial was selected. Once the *j* and *o* vectors, representing the joint axis and center of rotation, had been calculated, they were then used to rotate each sensor's gyroscope and accelerometer data into the joint CSs in order to solve for joint flexion-extension at the ankle, knee, and hip for each motion trial. For the knee, angle estimates were calculated based on the methods detailed in Subsection 4.3. For the ankle and hip, flexion-extension angles obtained using the complementary filter proposed by Seel et al. (2012) as presented in eq. (4.26) and eq. (4.27) were calculated for initial validation, and subsequently these angles were calculated based on the methods detailed in Subsection 4.6, using the complementary filters here proposed through eq. (4.40) and eq. (4.41) for the ankle, and eq. (4.42) for the hip. Ankle, knee, and hip flexion-extension angles were subsequently exported for comparison with the optical-based joint angle estimates.

Joint angle data from both the IMU- and optical-based systems were zeroed to the first frame of data for each trial, during which the participant stood upright prior to commencing the motion, and subsequently normalized to 101 points prior to comparison. For each motion and each joint, the IMU-based flexion-extension angles were evaluated through the following parameters: the mean (mean of the absolute value of optical signal – IMU signal), standard deviation (SD), and the standard error of the mean (SEM; $SD/\sqrt{number\ of\ IMU\ samples}$) for (i) the difference in range of motion (RoM; maximal – minimal joint angle) and (ii) the error between protocols (the grand mean error), both expressed in degrees, over all participants. Root mean squared error (RMSE) as well as percent mean error (PME, *grand mean error/ Optical RoM)* were also calculated for all motion trials in order to compare results with those previously reported.

Participant means across the 3 trials per motion were calculated for all analysis values prior to calculating group means for each posture and joint.

Additionally, Pearson correlation coefficients (R) were computed between the time normalized joint angles estimated through the CSKA and ISSA algorithms and the optical motion capture protocols by joint and by trial and averaged across trials per participant for each of the nine movements and three joints separately prior to calculating group means for each posture and joint. Correlation coefficient strengths were interpreted using the following criteria: 0.00-0.09 (none), 0.10-0.29 (weak), 0.30-0.59 (moderate), and 0.60-1.00 (strong) (Cohen, Cohen, West, & Aiken, 2003).

### 4.7.2.Statistical Analyses

In order to assess the presence of any potential differences in joint angle accuracies between the right and left ankle, knee, and hip joints as well as between postures, statistical analyses were performed using two-way mixed model analyses of variance (ANOVAs) (pose (9) × side (2)) on the participant mean Pearson's correlation coefficients and RMSE values (a total of 6 ANOVAs were therefore run: 3 joints x 2 measures). An alpha level of 0.016 (0.05/3) was used to determine statistical significance for main effects and interactions following a Bonferroni *p*-value significance correction adjusting for the tests conducted on the three joints of each leg. In cases where a significant main effect was detected, a post-hoc Tukey test was performed in order to determine significant differences. All statistical analyses were completed using Matlab 9.9 (The Mathworks, Release R2020b, Natick, MA, USA).

## 4.8. Results

All results here presented represent a comparison of flexion-extension kinematics estimated for the right leg only, while results for the left leg can be found in Appendix C. Statistical analyses between legs revealed no significant differences between the left and right side for the hip and knee, however significant differences were found in the Pearson's correlation coefficient and RMSE values at the ankle, signifying stronger correlations between the IMU and optical methods for the right side than the left, and higher RMSE values on the left side than the right. While these results were found to be significantly different, the mean differences between left and right

RMSEs were found to be 4.49°, a difference which when interpreted within the accuracy of the methods presented is not believed to be clinically meaningful in the analysis of high flexion postures.

Representative kinematic results estimated using the SJA and ISSA algorithms with IMU data as well as traditional optical-based measures for each of the nine childcare-inspired postures for one participant are shown for the ankle in Figure 4.3 and Figure 4.4 respectively and for the hip in Figure 4.6 and Figure 4.7 respectively. Representative kinematic results for the knee estimated using the CSKA algorithm as well as optical-based motion capture measures for each of the nine childcare-inspired postures can be seen in Figure 4.5. Additionally, given that the CSKA algorithm has previously been validated in gait by Küderle et al. (2018), the performance of the current implementation is also demonstrated in gait across these figures as well as in the tabular results presented later in this Subsection.

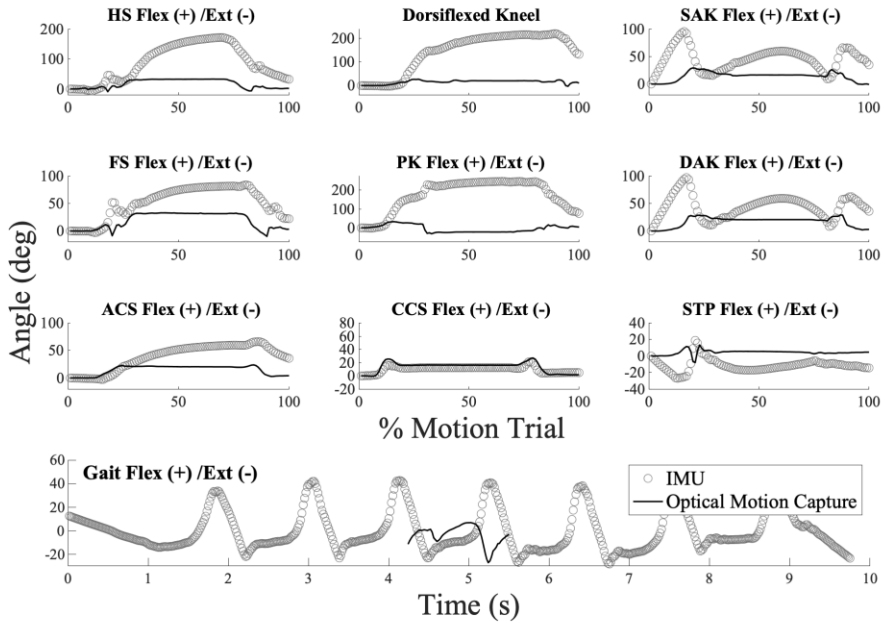


Figure 4.3 Estimated right ankle joint angle data for a representative participant based on IMU and optical motion capture data. IMU estimates were obtained using the SJA algorithm. Each of the nine childcare-inspired postures are represented as a percentage of the motion trial, while the gait trial is displayed over time, given that the optical system could only capture a portion of the strides completed.

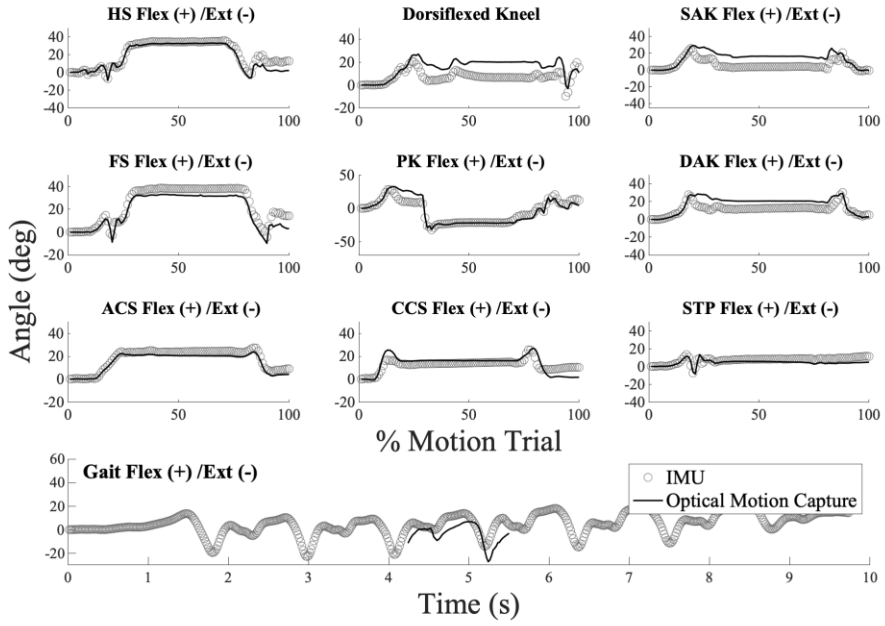


Figure 4.4 Estimated right ankle joint angle data for a representative participant based on IMU and optical motion capture data. IMU estimates were obtained using the ISSA algorithm. Each of the nine childcare-inspired postures are represented as a percentage of the motion trial, while the gait trial is displayed over time, given the optical system could only capture a portion of the strides completed.

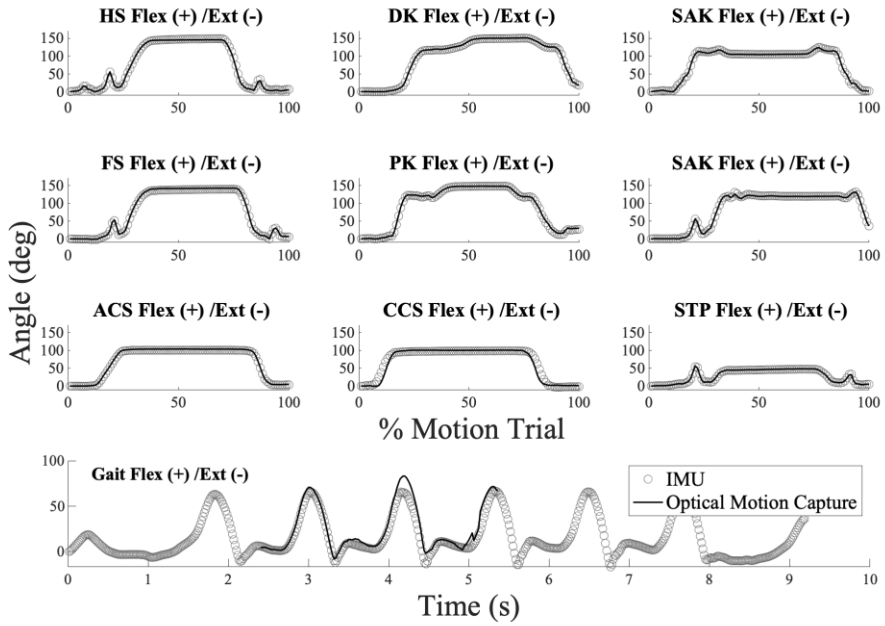


Figure 4.5 Estimated right knee joint angle data for a representative participant based on IMU and optical motion capture data. IMU estimates were obtained using the CSKA algorithm. Each of the nine childcare-inspired postures are represented as a percentage of the motion trial, while the gait trial is displayed over time, given the optical system could only capture a portion of the strides completed.

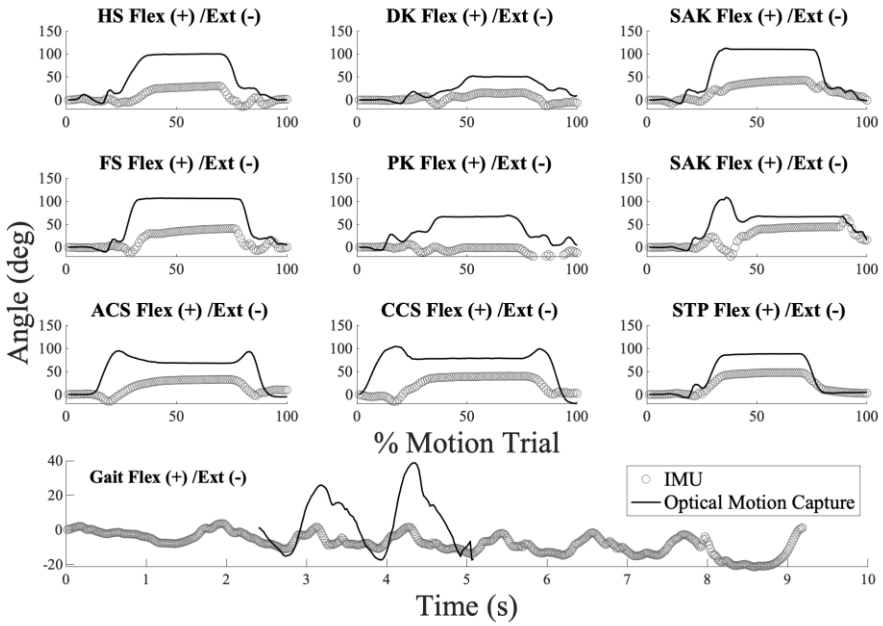


Figure 4.6 Estimated right hip joint angle data for a representative participant based on IMU and optical motion capture data. IMU estimates were obtained using the SJA algorithm. Each of the nine childcare-inspired postures are represented as a percentage of the motion trial, while the gait trial is displayed over time, given the optical system could only capture a portion of the strides completed.

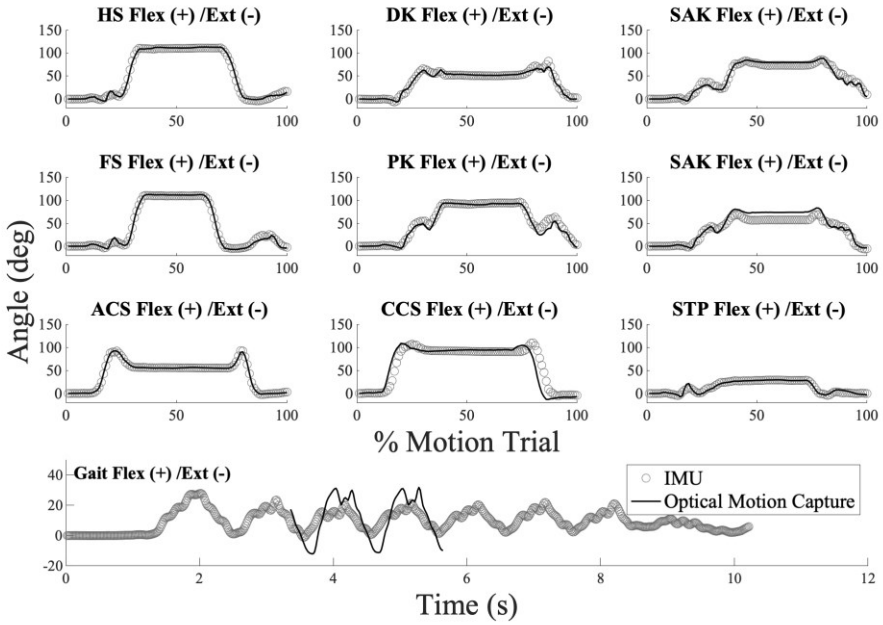


Figure 4.7 Estimated right hip joint angle data for a representative participant based on IMU and optical motion capture data. IMU estimates were obtained using the ISSA algorithm. Each of the nine childcare-inspired postures are represented as a percentage of the motion trial, while the gait trial is displayed over time, given the optical system could only capture a portion of the strides completed.

Pearson's correlation coefficients describing the strength of the linear relationship between the flexion-extension kinematics calculated through conventional laboratory-based optical motion capture and CSKA (knee) and ISSA (hip and ankle) algorithms based on IMU data for all participants can be seen in a box-and-whisker plot (Figure 4.8) for all childcare-inspired postures. Any trial in which occlusion of the optical motion capture markers occurred for greater than 25 frames was excluded from comparisons, resulting in a varying number of participants being included in the comparisons for each motion and each joint. For the ankle, 27, 28, 39, 38, 40, 36, 42, 39, 31, and 42 participants were compared; for the knee, 38, 39, 47, 47, 45, 46, 47, 46, 39, and 43 participants were compared; and for the hip, 36, 19, 48, 47, 45, 45, 47, 45, 40, and 46 participants were compared, all for ACS, CCS, DK, PK, FS, HS, DAK, SAK, STP and Gait respectively. The particularly low number of participants included in the analysis of the CCS posture resulted from significant occlusion of the pelvis marker cluster due to the back of the child sized chair. It is additionally believed that the limited capture volume of the optical motion capture system may have caused many of the occlusions which resulted in participants being excluded from comparisons.

For the childcare-inspired postures analyzed, all median R values represented strong correlations across all joints, save the median value for the ankle angle during CCS which represented moderate correlations. All values falling within 3 times the interquartile range of the 25$^{th}$ percentile (captured within the whiskers of the plot, Figure *4.8*) represented moderate (ankle CCS, DK, DAK, and SAK $\geq 0.36$ and hip CCS and HS $\geq 0.55$) or strong correlations. The mean, SD, and SEM of these Pearson correlation coefficients across all participants can be seen in Table 4.2.

Table 4.2 Relationship between IMU- and optical motion capture-based right lower limb joint angles through Pearson's correlation coefficients. IMU-based joint angles were estimated using the CSKA and ISSA algorithm. Correlation coefficients have been presented for the 9 childcare-inspired postures (ACS, CCS, DK, PK, FS, HS, DAK, SAK, and STP) as well as in gait.

| | | **ACS** | **CCS** | **DK** | **PK** | **FS** | **HS** | **DAK** | **SAK** | **STP** | **Gait** |
|---|---|---|---|---|---|---|---|---|---|---|---|
| Ankle | Mean | 0.935 | 0.545 | 0.756 | 0.976 | 0.885 | 0.896 | 0.801 | 0.751 | 0.881 | 0.523 |
| | SD | 0.135 | 0.296 | 0.163 | 0.040 | 0.266 | 0.111 | 0.333 | 0.227 | 0.099 | 0.468 |
| | SEM | 0.026 | 0.056 | 0.026 | 0.006 | 0.042 | 0.019 | 0.051 | 0.036 | 0.018 | 0.072 |
| Knee | Mean | 0.998 | 0.867 | 0.986 | 0.995 | 0.985 | 0.915 | 0.987 | 0.991 | 0.810 | 0.807 |
| | SD | 0.004 | 0.084 | 0.033 | 0.012 | 0.040 | 0.179 | 0.018 | 0.030 | 0.386 | 0.306 |
| | SEM | 0.001 | 0.013 | 0.005 | 0.002 | 0.006 | 0.026 | 0.003 | 0.004 | 0.062 | 0.047 |
| Hip | Mean | 0.931 | 0.753 | 0.872 | 0.925 | 0.960 | 0.893 | 0.703 | 0.797 | 0.834 | 0.522 |
| | SD | 0.163 | 0.203 | 0.200 | 0.089 | 0.099 | 0.196 | 0.534 | 0.435 | 0.361 | 0.254 |
| | SEM | 0.027 | 0.047 | 0.029 | 0.013 | 0.015 | 0.029 | 0.078 | 0.065 | 0.057 | 0.037 |

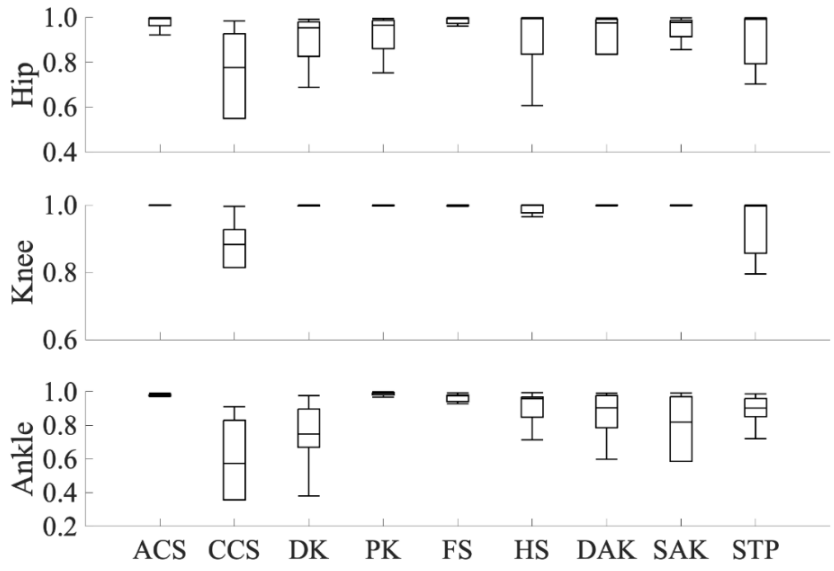


Figure 4.8 Box-and-whiskers plots for the Pearson's correlation coefficients (R) for the right ankle, knee, and hip flexion-extension angles representing the linear correlation between the IMU- and optical motion capture-based protocols.

Differences in RoM and grand mean error between the joint flexion-extension angles calculated through both protocols expressed through the mean, SD, and SEM, as well as RMSE and PME can be seen in Table 4.3 for all childcare-inspired postures as well as in gait. Comparing results across the nine childcare-inspired postures and gait, the mean differences in RoM values between protocols were found to be 2.90° ± 8.74° for the ankle, 2.36° ± 5.56° for the knee, and 5.59° ± 15.60° for the hip. Mean RMSE between protocols were found to be 6.61° ± 2.96° for the ankle, 7.55° ± 5.82° for the knee, and 14.64° ± 6.73° for the hip. The greatest errors were observed in gait, followed by child chair sitting and both supported and unsupported kneeling. Given the magnitudes of the flexion-extension angles observed in the studied postures, these errors represent 18.48 ± 13.99%, 5.55 ± 4.45%, and 15.03 ± 5.87% differences between protocols across all postures for the ankle, knee, and hip respectively.

Statistical analyses revealed main effects for pose at all joints. Child chair sitting was found to have the lowest R values at the ankle and knee and the highest RMSE values for the knee and hip. For the hip, both the single and double arm supported kneeling postures had the lowest R values. For the ankle, the highest RMSE values were observed in plantarflexed kneeling and in child chair sitting.

Table 4.3 Differences between IMU- and optical motion capture-based right lower limb joint angles. IMU-based joint angles were estimated using the CSKA and ISSA algorithms. Differences between IMU- and optical-based angles were quantified through the difference in the range of motion, the grand mean error, the Root Mean Squared error, and the percent mean error. The differences are presented for 9 childcare-inspired postures (ACS, CCS, DK, PK, FS, HS, DAK, SAK, and STP). All values are expressed in degrees unless otherwise stated.

| | | | ACS | CCS | DK | PK | FS | HS | DAK | SAK | STP | Gait |
|---|---|---|---|---|---|---|---|---|---|---|---|---|
| **Ankle** | **Difference in RoM** | Error Mean | 2.202 | 2.847 | 0.385 | 4.811 | 0.308 | 0.528 | 2.882 | 1.442 | 0.283 | 13.310 |
| | | Error SD | 3.032 | 6.180 | 4.280 | 9.391 | 4.667 | 2.878 | 10.416 | 4.699 | 4.120 | 37.754 |
| | | Error SEM | 0.584 | 1.168 | 0.685 | 1.523 | 0.738 | 0.480 | 1.607 | 0.752 | 0.740 | 5.826 |
| | **Grand Mean Error** | Error Mean | 2.186 | 6.709 | 5.395 | 6.853 | 4.035 | 3.664 | 4.978 | 6.224 | 3.302 | 10.685 |
| | | Error SD | 1.417 | 4.493 | 3.503 | 4.280 | 2.854 | 2.617 | 3.313 | 3.791 | 2.196 | 8.455 |
| | | Error SEM | 0.141 | 0.447 | 0.349 | 0.426 | 0.284 | 0.260 | 0.330 | 0.377 | 0.219 | 0.841 |
| | **Root Mean Squared Error** | | 2.628 | 8.140 | 6.479 | 8.140 | 4.976 | 4.530 | 6.009 | 7.338 | 3.987 | 13.860 |
| | **Percent Mean Error** | | 9% | 22% | 15% | 8% | 10% | 9% | 57% | 18% | 11% | 25% |
| **Knee** | **Difference in RoM** | Error Mean | 1.447 | 3.683 | 0.751 | 0.518 | 0.779 | 8.086 | 0.221 | 0.331 | 2.295 | 5.448 |
| | | Error SD | 3.201 | 5.533 | 2.901 | 4.416 | 2.292 | 16.967 | 3.794 | 2.851 | 7.935 | 5.692 |
| | | Error SEM | 0.519 | 0.886 | 0.423 | 0.644 | 0.342 | 2.502 | 0.553 | 0.420 | 1.271 | 0.868 |
| | **Grand Mean Error** | Error Mean | 1.975 | 14.046 | 4.453 | 3.348 | 3.431 | 6.973 | 2.701 | 2.892 | 4.024 | 11.290 |
| | | Error SD | 1.202 | 17.297 | 4.292 | 2.900 | 3.020 | 6.232 | 2.216 | 2.416 | 3.317 | 6.546 |
| | | Error SEM | 0.120 | 1.721 | 0.427 | 0.289 | 0.301 | 0.620 | 0.220 | 0.240 | 0.330 | 0.651 |
| | **Root Mean Squared Error** | | 2.339 | 22.394 | 6.343 | 4.476 | 4.636 | 9.377 | 3.552 | 3.799 | 5.231 | 13.332 |
| | **Percent Mean Error** | | 2% | 13% | 3% | 2% | 3% | 6% | 2% | 2% | 7% | 15% |
| **Hip** | **Difference in RoM** | Error Mean | 1.774 | 0.334 | 9.497 | 6.414 | 4.996 | 6.170 | 2.319 | 1.837 | 10.444 | 12.115 |
| | | Error SD | 13.178 | 31.543 | 15.912 | 22.743 | 9.760 | 12.678 | 9.199 | 9.074 | 24.008 | 7.932 |
| | | Error SEM | 2.196 | 7.236 | 2.297 | 3.317 | 1.455 | 1.890 | 1.342 | 1.353 | 3.796 | 1.169 |
| | **Grand Mean Error** | Error Mean | 6.997 | 24.891 | 8.428 | 9.040 | 7.671 | 8.035 | 17.071 | 12.958 | 11.212 | 10.020 |
| | | Error SD | 5.687 | 19.283 | 6.025 | 7.128 | 5.735 | 6.390 | 12.449 | 9.429 | 9.084 | 6.255 |
| | | Error SEM | 0.566 | 1.919 | 0.599 | 0.709 | 0.571 | 0.636 | 1.239 | 0.938 | 0.904 | 0.622 |
| | **Root Mean Squared Error** | | 9.098 | 31.862 | 10.408 | 11.548 | 9.626 | 10.287 | 21.260 | 16.056 | 14.455 | 11.821 |
| | **Percent Mean Error** | | 7% | 24% | 15% | 12% | 8% | 9% | 20% | 16% | 16% | 24% |

## 4.9. Discussion

In this study, joint angles for the ankle, knee, and hip were estimated based on IMU data using the CSKA and ISSA algorithms. For each joint, the joint axis and center of rotation were found based on calibration motions involving individual isolated movements of the hip and knee as well as a brief static pose and a walking bout. When compared to the gold-standard laboratory-based methods of measuring joint angles, the results here presented demonstrate strong similarities when estimating joint angles during postures of high knee flexion which are frequently adopted in occupational childcare.

The strongest agreement in our results were seen consistently in the angles calculated for the knee joint. This is no surprise given that the motion of the knee occurs primarily about the flexion-extension and thus the biomechanical model applied best matched the ground-truth for this joint. For the ankle and hip, previous results have demonstrated strong agreement between the algorithm proposed by Seel et al.(2014) and optical motion capture when using a series of functional calibration motions. Seel et al (2014) reported RMSE values < 2.61° at the ankle during gait while Lebleu et al (2020) reported RMSE values between 2.0°± 1.3° and 2.9°± 1.4° for the ankle and between 2.1°± 1.3° and 2.5°± 1.7° for the hip and differences in RoM between 0.9°± 0.8° and 1.6°± 1.1° at the ankle and 1.0°± 1.0° and 1.1°± 0.7° at the hip during overground and stair gait. However it is noted that few validations of the proposed algorithm in spherical joints exist, and these often compare angles during gait alone (Lebleu et al., 2020; Olsson et al., 2019; Seel et al., 2014). When walking, healthy human ankle and hip joints move primarily in flexion-extension, and therefore perform most similarly to a hinge joint. It is possible that in testing the performance of this algorithm in high flexion movements, the accuracy of estimates decreased given that a greater portion of the motion measured by the sensors now occurred about either the abduction-adduction or internal-external rotation axes. Furthermore, it is possible that in developing the proposed ISSA complementary filters for the high knee flexion postures, the accuracy of angle estimates during gait, when the majority of motion does occur about the flexion-extension axis, might suffer. It is additionally observed that for the ankle and hip, greater errors occurred in postures which elicited the highest ranges of motion (notably plantarflexed kneeling for the ankle and the supported kneeling postures for the hip). Future work should seek

to better understand why postures with increased ranges of motion result in greater inaccuracies between inertial- and optical-based methods.

While successful sensor to segment calibrations and definitions of the joint axis and joint center of rotation in the local sensor CS was achieved for all joints across all participants, it must be noted that opposite signed solutions were at times observed in the subsequent calculations of joint angles for the ankle and hip. Particularly, these opposite signed solutions were observed to occur during the supported kneeling trials. These trials were not omitted from the presented means and therefore are likely to be partially responsible for the increased errors observed in these spherical joints. Future work should therefore focus on determining why successfully defined *j* and *o* vectors might yield opposite signed joint angles and how this might be mitigated moving forward.

Using the introduced iterative processes and complementary filters, it could be shown that the proposed modification to the algorithm by Seel et al. (2014) for spherical joints reduced the likelihood of failed optimizations, resulting in the incorrect calculation of the joint axis and center of rotation. As explained above, this method does continue to show issues with computational stability for certain movements, however these issues appeared to occur less frequently when compared to the implementation of the SJA algorithm for the childcare-inspired postures performed in this study. It must be noted that the ISSA method does introduce significant computational overhead when compared to the SJA given the iterative optimization process. However, provided the calculation of joint angles using either the SJA or ISSA algorithms occurs offline rather than in real time, it is believed that the additional time for computation is justified due to the improved accuracy and consistency in defining the joint axis and center of rotations. Future work could include a mathematical analysis of the algorithm seeking to quantify the speed of convergence and the numerical stability between methods. Given the strong correlation between the joint flexion-extension angles calculated using the CSKA and ISSA for the knee, ankle, and hip joints respectively, these algorithms appear the most suited for the analysis of high flexion postures.

The calibration motions performed in this study must also here be discussed. Seel et al. initially proposed the use of arbitrary motions about each joint, and recently have proposed

methods for the autocalibration of the SJA algorithm (Graurock, Schauer, & Seel, 2016; Molnar et al., 2018; Seel et al., 2012). In order for any inertial-based motion capture system to be successful in real-world settings, the calibration method must be simple and easy to perform, even for individuals with movement impairments. The calibration movements employed in this study included isolated flexion-extension about the knee and rotations in all directions about the hip. These motions, while not hard to perform, do require an individual performing them to balance on one leg, and therefor may prove impractical for all populations. However, the calibration based on simpler movements, such as walking for example, may not prove sufficient when seeking to calibrate a system for measurements in high flexion postures. It may be possible to perform similar motions to those employed in this study in seated or reclined postures, and to subsequently replace the postures used during the iterative optimization with postures that mimic the same ranges of motion yet do not require participants to descend onto the ground, perhaps including a toe touch and raising onto one's toes as alternatives. Future investigations could therefore investigate the use of alternative calibration movements and their effects on the accuracy of sensor to segment calibrations. It is noted that the total duration of the calibration postures required by the ISSA algorithm in its current implementation was no more than two to three minutes, and these calibration motions could be performed in any environment by an able-bodied individual. Therefore, it is believed that the proposed calibration motions would not pose a roadblock for implementation given the intended application for this system lies in the measurement of high flexion postures within occupational settings, and that the intended population therefore are capable and familiar with the required motions.

Based on previously published findings, raw IMU data were filtered in an effort to reduce high frequency noise and isolated motions of the upper and lower legs were collected as calibration trials prior to input to the CSKA and ISSA algorithms (Küderle et al., 2018). Compared to the literature, the RMSE values reported for gait in this study are higher than those previously reported (between 3.3$^{o}$ and 8$^{o}$) (Küderle et al., 2018; Seel et al., 2012) however the mean RMSE values for the ankle and knee for the nine childcare-inspired postures fall within this previously reported range. It is believed that multiple factors, which will here be discussed, may have influenced the quality of the optical and inertial motion data, and resulted in reduced accuracies. The limited capture volume of the optical motion capture system, which given the 18

cameras utilized in this study was in fact quite large compared to some motion-capture spaces, resulted in only a brief portion of gait trials being recorded by the optical system. The capture volume additionally led to difficulty in participants performing the seated motions while maintaining full visibility of the marker clusters, particularly those on the feet and the pelvis. A balance must be struck when working with optical motion capture systems between ensuring a sufficiently large capture volume and increasing the visibility of a marker cluster by multiple cameras (Aristidou & Lasenby, 2013). However, even with a large number of cameras, instances of marker occlusion leading to missing data are inevitable when introducing other objects such as chairs into the collection volume, and therefore it is believed that the number of trials lost to occlusion may have affected the accuracy of results by decreasing the ultimate sample size analyzed, especially in the case of the child chair sitting trials. Secondly, while mounting the optical motion capture clusters to the lateral aspects of the IMUs creates an equality in the soft-tissue artefact experienced by both systems, it may also have introduced noise into the optical measurements. However, in order to mitigate this potential noise, optical clusters were attached to the IMUs with double sided tape and also secured to the segment using elasticated Velcro® straps. Additionally, all data were filtered to eliminate any high frequency noise contamination. High knee flexion postures are known to result in unique soft tissue deformation in comparison to postures of low-to-moderate flexion given the contact which occurs between the thigh and calf in this range (Kingston & Acker, 2018). While the quantification of this soft tissue artefact is not within the scope of this study, it is noted that the differences in RoMs between methods were consistently $< 10°$ with mean values $< 5°$ for all joints, leading to the conclusion that the IMU based joint angle calculations are no more affected by soft tissue artefact than the optical-based motion capture system.

Finally, the comparison of flexion-extension angle estimates based on inertial motion capture to those measured by optical motion capture as a ground truth must be addressed. While optical-based motion capture methods have been the gold-standard for the kinematic measurement of human motion for over 40 years, caution must be exercised in such comparisons given the fundamental differences in the definition of anatomical frames based on positions vs. motion (in the cases of optical vs. inertial measures). While standard practices have been established for the definition of anatomical coordinate systems based on identifiable bony prominences on the body

(Wu & Cavanagh, 1995b; Wu et al., 2002, 2005), differences in the definitions of anatomical frames have been shown to occur based on the method used for the localization of anatomical landmarks as well as the use of landmarks alone or approaches which include functional calibration movements (Robinson & Vanrenterghem, 2012). Given these differences which can occur within optical motion capture for which detailed collection methods have been established, it is no surprise that the manner in which these anatomical frames are defined between optical and inertial systems may lead to misalignment in the anatomical frames, resulting in perceived errors within estimated joint angles. It is additionally noted that despite best practices, optical motion capture in no way can be believed to yield ground truth data such as that which might be obtained through stereoradiography or dual-plane fluoroscopy (Fiorentino et al., 2017).

# 4.10.Conclusions

In summary, the estimation of joint kinematics through the IMU-based CSKA and ISSA algorithms present a viable means of measuring ankle, knee, and hip flexion-extension angles and may be applied to their measurement within occupational and home settings. The proposed ISSA modifications to the SJA algorithm appear to improve the stability of the sensor to segment calibration for spherical joints. This study demonstrates algorithm performance to be similar in estimating lower-limb joint flexion-extension angles when compared with optical-motion capture-based methods to those previous reported during gait when estimating these angles in high knee flexion trials. The calibration movements used in this study are believed to be movements which could easily be performed by individuals accustomed to performing high flexion movements.

The methods here presented will support the measurement of high flexion postural adoption within occupational settings. Given the association between postures of high knee flexion and the initiation and progression of knee OA, the ability to measure these postures as they occur naturally will enable the development of guidelines driven by objective exposure data. As described, the computational requirements of the proposed system may be a limitation to its implementation in remote settings, however, so long as the data can be processed off-line following collections, this should not present a barrier to its implementation. Further testing under real-world conditions should be performed prior to collections within home and

occupational settings, along with the development of alternative calibration procedures should the system be used to analyze individuals with limited or altered mobility.

# Chapter 5

# A Multi-Dimensional Dynamic Time Warping Distance-Based Framework for the Recognition of High Knee Flexion Postures in Inertial Sensor Data

## 5.1. Introduction

Osteoarthritis of the knee is a debilitating disorder of increasing prevalence, with repetitive cyclic or prolonged joint loading having been associated with the initiation and progression of knee joint tissue degradation leading to OA (Anderson & Felson, 1988; Felson, 2013; Parry, Ogollah, & Peat, 2019; Yucesoy, Charles, Baker, & Burchfiel, 2015). These loading patterns are often observed during high knee flexion activities (such as kneeling and squatting), where the knee flexion angle exceeds $120^{o}$. Despite their association with increased risk of musculoskeletal injuries, workers across many occupations are often required to perform repetitive and sustained high knee flexion motions for a significant portion of their working hours. These occupations further require their employees to lift and carry heavy or awkward loads which, when combined with high knee flexion postures, have been associated with a five-fold increase in risk of OA development (C. Cooper et al., 1994). While much attention has been paid to the direct costs of

healthcare associated with OA, work-related musculoskeletal disorders are commonly reported in connection with work-restrictions, time loss, and leaves which result in substantial indirect costs, often ignored when considering the burden of OA on society and on those living with the disease (Forde et al., 2002; Gupta, Hawker, Laporte, Croxford, & Coyte, 2005; W. Zhang, Gignac, Beaton, Tang, & Anis, 2010; X. Zhang, Xia, Dai, Sun, & Fu, 2018).

Despite the growing incidence of knee OA worldwide and the financial burdens associated with this disease, methods employed for the evaluation of acute and chronic injuries resulting from high knee flexion exposures in occupational settings have until recently involved either observational or questionnaire based qualification of movement types or the use of full body motion capture systems within research laboratories in lieu of objective real world measures (Grant et al., 1995; Jensen et al., 2010; Klussmann et al., 2010; Schiphof et al., 2008; Seidler et al., 2008). While questionnaires present the most unobtrusive means of obtaining exposure related data from occupational workers, their results generally suffer from bias and show no criterion validity when compared to objective measures (Kwak, Proper, Hagströmer, & Sjöström, 2011). Motion analysis laboratories in contrast offer accurate and reliable means of measuring kinematic variables associated with the development and progression of knee OA; however, their application in the study of occupation-based exposures has been limited due to their high costs, the time associated with setup and post-processing, and the visibility requirements of these optical-based systems. The increasing popularity of wearable sensors, however, provides a potential means of objective human mobility measurement as individuals interact with their surroundings in both occupational and home settings (Bauer et al., 2016; Crema et al., 2017; Kluge et al., 2017; Schall, Fethke, Chen, & Gerr, 2015). These wearable sensors, often composed of accelerometers and gyroscopes, offer a minimally intrusive means of measuring occupational kinematics over multiple workdays, however, the interpretation of their data as they relate to occupational exposures is non-trivial. Therefore, recent studies have sought to apply pattern recognition and machine learning algorithms in order to interpret the raw sensor data for activity identification and monitoring (Ditchen et al., 2015; Holtermann et al., 2020; Song et al., 2016; D. Yang et al., 2019; Zubair, Song, & Yoon, 2017).

Activity classification generally involves a two-stage process wherein representative features are extracted from a series of sequential or overlapping time windows of sensor data and

subsequently input to a classification algorithm to associate each window with a specific movement or activity (Preece, Goulermas, Kenney, Howard, et al., 2009). The goal in deriving classification features from sensor-based signals is to reduce the dimensionality of the signal while ensuring maximum class separability, through feature complexity and robustness to variations over time (Phinyomark et al., 2012). Within the last fifteen years however, researchers have begun to investigated the potential for direct classification of time-series data (Barth et al., 2015; Chang et al., 2016; Kaya & Gündüz-Öğüdücü, 2015; M. Kim et al., 2019; Kluge et al., 2017). The classification of these time-series data can be performed similarly to any traditional classification problem, wherein the distance between two samples (now time-series curves) are computed and input into classification algorithm for identification.

One challenge which must be overcome in the classification of time series data lies in the variability of these signals. The scale of time-domain waveforms obtained from wearable sensors can differ greatly depending on the signal being processed as well as on the segment to which the sensor is affixed. Traditionally, when classification features are calculated, these differences in scale are exploited as a means of group separation, such that larger scale differences would provide greater separability; therefore, when classifying time-domain data, amplitude normalization is often performed to avoid attributing a greater importance to any one signal while determining the distance between samples (Kaya & Gündüz-Öğüdücü, 2015; Matsuda, Morikuni, Imakura, Ye, & Sakurai, 2020). Additionally, recognition accuracy may be affected by temporal variations in movements within and between individuals, therefore, non-linear corrections can be applied to one or both of the signals in order to compensate for these variations. This process, often referred to as alignment, can be performed prior to calculating the distance between samples or can serve as an alternative distance metric by which the classification can be performed (Barth et al., 2013; Kaya & Gündüz-Öğüdücü, 2015).

Alignment-based distance metrics for classification are typically calculated between some unknown signal and a previously identified signal template (Veltink et al., 1996). Examples of template-based Dynamic Time Warping (DTW) for classification have utilized either raw accelerometer or gyroscope data in applications of stride segmentation within free walking bouts in both healthy and clinical populations as well as in the recognition of hand gestures during activities of daily living. (Chang et al., 2016; Mekruksavanich et al., 2020; Qiu, Liu, et al., 2018).

As an expansion to this application, distance metrics can be combined across sensor axes or sensor types in a process known as multi-dimensional Dynamic Time Warping in order to increase the separability of samples thereby increasing the accuracy of calibration (Barth et al., 2013, 2015). While these approaches have been used for the identification of activities of daily living such as sitting, standing, lying down, and walking (both on level ground and on stairs) (Mekruksavanich et al., 2020; Muscillo, Conforto, Schmid, Caselli, & D'Alessio, 2007; Paiyarom, Tungamchit, Keinprasit, & Kayasith, 2009), to date, no studies have sought to apply these template-based DTW techniques to the identification of high knee flexion postures.

The childcare industry in particular has been shown to require its employees to adopt a wide variety of high knee flexion postures for significant portions of their working hours in addition to the frequent lifting and carrying of children, yet to our knowledge, only two studies have sought to apply sensor-based approaches to the analysis of knee straining postures in these individuals (Burford et al., 2017; Holtermann et al., 2020). Further, both Holtermann et al. (2020) and Burford et al. (2017) applied tools developed for the study of high knee flexion postures across multiple occupations and therefore neither considered high flexion postures beyond kneeling, squatting, and sitting, despite the variety of poses adopted when caring for children (Laudanski et al., 2022). Therefore, the objective of this study was to develop a sensor-based framework for the detection and measurement of childcare-specific postures. In order to accomplish this, we propose the use of a multi-dimensional Dynamic Time Warping distance-based machine learning algorithm, insensitive to any postural variability which might accompany the presence of load, such that it might ultimately be used for the continuous identification of high flexion exposures in childcare settings.

## 5.2. Participants and Experimental Protocol

Details surrounding participant recruitment, instrumentation, and a portion of the experimental protocol have previously been described at length in Chapter 4 however will briefly be reviewed here. Fifty participants (18 males/32 females, height: 1.11 ± 0.83 m, mass: 73.70 ± 17.78 kg, age: 21.14 ± 3.76 years) were recruited and instrumented with 7 wireless IMUs (Xsens MTw Awinda, Xsens Technology B.V., Netherlands, Gyro.: 2000 deg/s, Acc.: 16 G, sampling frequency: 60 Hz) attached bilaterally to the superior aspect of the feet, the lateral aspect of the shanks and

thighs, as well as over the base of the sacrum. Following instrumentation, each participant was asked to completed a 5 s standing trial in addition to functional hip (isolated upper leg motion through a star-arc hip circumduction (Camomilla et al., 2006)) and functional knee (isolated cyclic flexion/extension motion of the lower leg while the upper leg was held parallel to the ground) motion trials. Following these calibration trials, participants completed three 10 m walking trials at a self-selected pace and subsequently completed three repetitions of the following movements commonly adopted in occupational childcare in randomized order: heels-up squatting (HS), flatfoot squat (FS), dorsiflexed kneeling (DK), plantarflexed kneeling (PK), single arm supported kneeling (SAK), double arm supported kneeling (DAK), sitting on an adult sized chair (ACS), sitting on a child sized chair (CCS), stooping (STP), and standing (STD). Following the completion of these motions, participants performed a series of floor level motions including crossed leg sitting (CLS), and side sitting (SS) and side leaning (SL) to both the left and right. Examples of all childcare-inspired motions performed in this study can be seen in Figure 5.1.

All motions save stooping and supported kneeling (SAK and DAK) were performed under unloaded and loaded conditions such that any altered movement mechanics associated with holding a load would be captured and therefore incorporated into the classification algorithm. Loaded conditions were designed so as to simulate the effects of carrying or interacting with a 50th percentile child of 24 months (WHO Multicentre Growth Reference Study Group, 2006). It must additionally be noted that this weight exceeds previously reported lifting thresholds associated with the potential for increased likelihood of OA development and progression if lifted regularly or over extended periods of time (E. C. Lau et al., 2000). For these loaded trials, participants were outfitted with a sling wrap baby carrier (worn across the shoulder of the participant's choosing) into which the 12 kg load was placed. A representative participant wearing the sling wrap baby carrier can be seen in Figure *5.2*. The baby carrier was used in order to ensure the weight was held close to the body as one would hold a child rather than being held away from the body as one might hold an object to be lifted. Participants were instructed to hold the weight in the sling as though they were holding a child rather than allowing the weight to be supported by the sling.

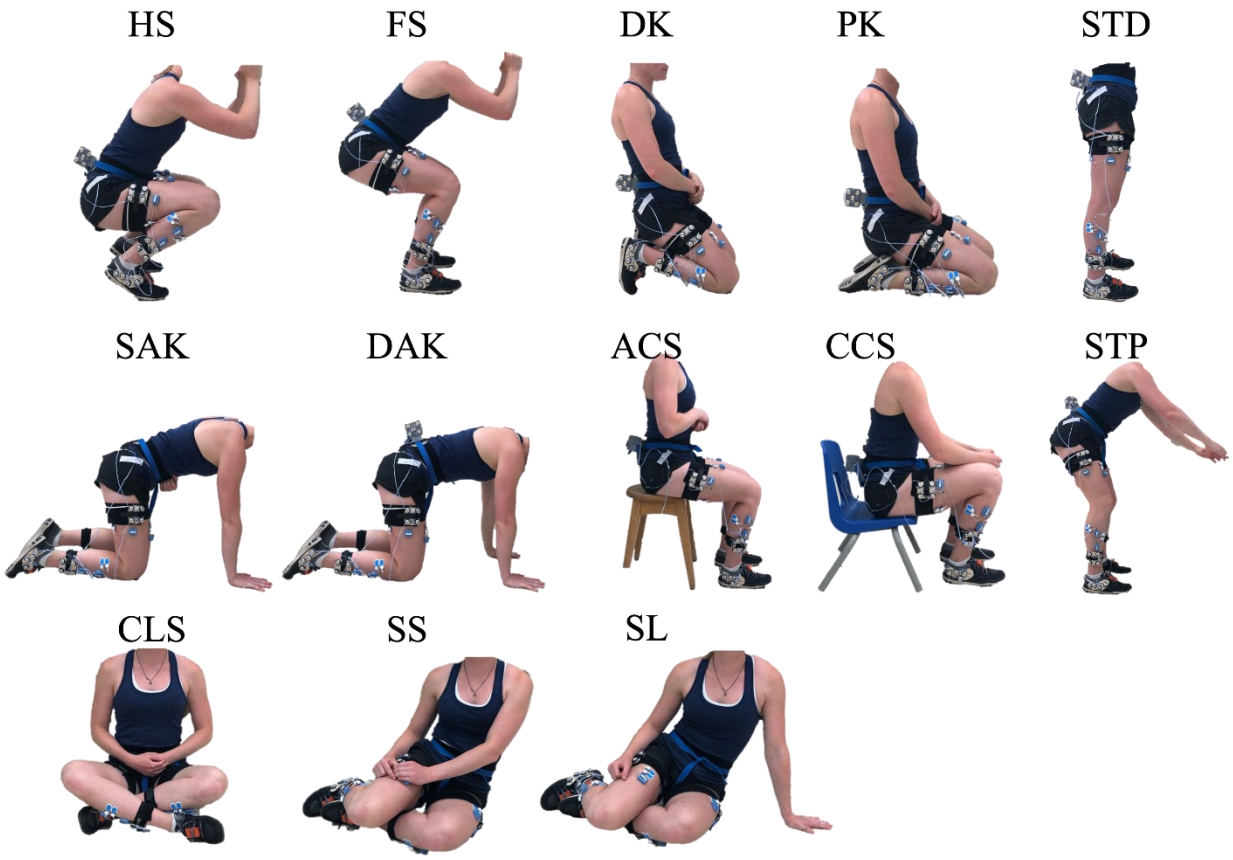


Figure 5.1 Childcare-inspired motions performed in this study (by row): heels-up squatting (HS), flatfoot squatting (FS), dorsiflexed kneeling (DK), plantarflexed kneeling (PK), standing (STD), single arm supported kneeling (SAK), double arm supported kneeling (DAK), sitting on an adult sized chair (ACS), sitting on a child sized chair (CCS), stooping (STP),crossed leg sitting (CLS), side sitting (SS, displayed to the left), and side leaning (SL, displayed to the left). SS and SL were additionally performed to the participant's right.

Unloaded and loaded trials were block randomized in order to minimize the number of transitions into and out of the sling wrap baby carrier. A minimum of three blocks of each condition were performed, and participants were free to take any length of rest period between trials as they deemed necessary or at any time to request an end to the current loaded lifting block. The unloaded and loaded blocks were repeated until a minimum of 3 successful trials per motion and condition had been completed. For all experimental protocol here described, approval from the University of Waterloo Research Ethics Board and participants' informed consent were obtained.

Figure 5.2 Participant instrumented with the sling wrap baby carrier and the 12 kg load. Participants were given the choice across which shoulder the baby carrier would be worn and instructed to hold the weight as if they were holding a child rather than allowing it to be supported by the carrier.

## 5.3. Sensor Signal Processing and Data Labelling

Raw IMU data were processed using the CSKA and ISSA algorithms presented in Chapter 4 in order to calculate flexion-extension angles for the ankle, knee, and hip for all motions and load conditions. Representative angles for one participant during a heels-up squat prior to any data segmentation can be seen in Figure 5.3. It is noted that the angle estimates from the right and left joints are oppositely signed given that each sensor was mounted in the same orientation, regardless of the leg to which it was attached. Therefore, if the local $y$ axis was most closely aligned with gravity and pointed superiorly when positive, the local $+x$ and $+z$ axes would be oppositely signed between the left and right legs. The start and end point of each motion were identified manually based on the right knee flexion-extension angles and applied to all joints. Given that each trial started and ended with a static standing period, the start of each motion was identified as closely as possible to the last frame of standing prior to any motion commencing. Similarly, the end of each motion was identified as closely as possible to the first frame of standing following the completion of any motion associated with the trial. For the squatting trials, participants were instructed to take a step forward before beginning their squat and

similarly to take a step backward following the completion of ascent from the squat. These steps were excluded when segmenting the trials.

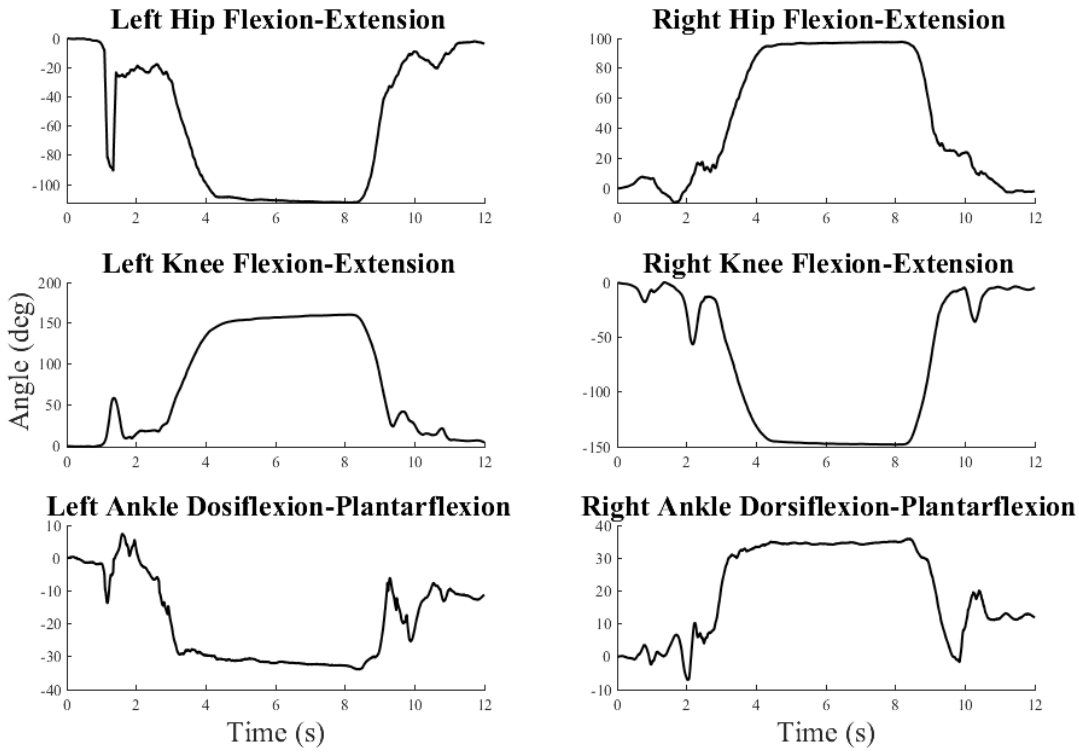


Figure 5.3 Typical joint angle signals for one heels-up squatting motion for the left and right hips, knees, and ankles. Flexion/ dorsiflexion is positive for the right ankle, the left knee, and the right hip, and negative for the opposite limb.

For each walking trial, three separate step-cycles were manually identified, again based on the angles for the right knee. The start of each step-cycle was identified as closely as possible to the moment of maximum knee extension while the end of the step-cycle was identified as the next instance of maximum knee extension given the cyclic nature of walking.

Each trial was labeled according to the motion performed. Loaded and unloaded trials were not labeled differently in order to create a classifier which would correctly identify postures regardless of if they were performed with or without a load. DAK and SAK trials were combined for classification and simply labeled as supported kneeling (SK) while all SS and SL motions were labeled as side sitting (SS) given the similarity in lower limb joint kinematics observed between movements.

## 5.4. Multi-Dimensional Dynamic Time Warping Distance-Based *k*-Nearest Neighbour Classifier

The following section will describe how different aspects of Dynamic Time Warping can be combined and serve as the basis for a *k*-Nearest Neighbour classification model for the robust identification of several childcare-inspired motions.

### 5.4.1. Multi-Dimensional Dynamic Time Warping as a Distance Metric for Movement Classification

*k*NN classification algorithms have been used in many previous activity classification studies based on wearable sensor signals (Altun & Barshan, 2010; Bao & Intille, 2004; Lin et al., 2016; Preece, Goulermas, Kenney, Howard, et al., 2009; Sinha et al., 2021) due to their computational simplicity. They utilize specific distance metrics by which the distances between samples can be calculated in order to determine the closest motion to an unknown sample within the multidimensional feature space. This feature space must therefore be populated with a series of labeled datapoints (often referred to as model building or training datapoints) each corresponding to a specific motion. Most commonly, Euclidian distances are used for human motion classification due to the similarity of scales of all input feature sets (Von Tscharner & Goepfert, 2003); however, this metric is best suited for a feature based classification rather than time-series approaches. Unlike Euclidean distances, Dynamic Time Warping is well suited to the comparison and distinction between time-series data as it considers the entire trajectory of signals while compensating for temporal variations (Barth et al., 2013; Kaya & Gündüz-Öğüdücü, 2015). Multi-dimensional Dynamic Time Warping (mDTW), an extension of the traditional DTW approach, allows for the combination of DTW based distances across multiple inputs. We therefore propose the use of mDTW distances as inputs to a *k*-Nearest Neighbour classifier in order to identify childcare-inspired motions using a combination of lower limb flexion-extension angles calculated based on inertial sensor data. The workflow for this proposed mDTW *k*NN algorithm can be found in Figure 5.4.

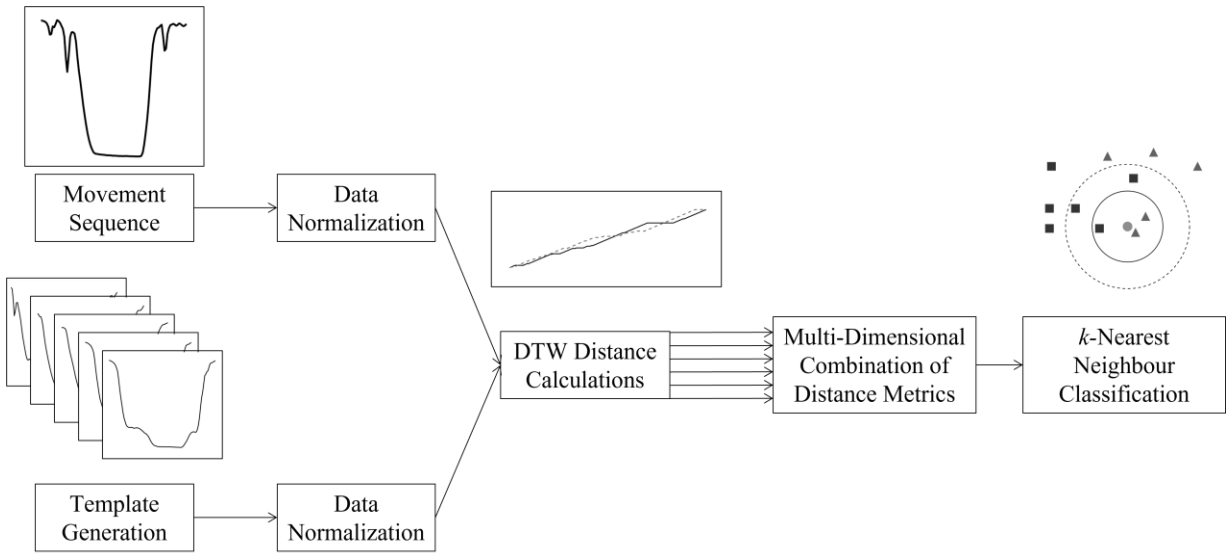


Figure 5.4 Signal processing workflow for the mDTW kNN algorithm, related to Subsections 5.4.3 – 5.4.5. The DTW distances for each joint were calculated between a single normalized trial (referred to as a movement sequence) and the normalized templates included in the developed model. A smaller distance between the sequence and template would represent greater similarity between waveforms. Once each movement sequence had been compared to all templates for the corresponding joint, the DTW distances were combined across joints using custom weighting factors such that the movement class would ultimately be determined based on the mDTW distance.

## 5.4.2. Division of Data for Model Development, Testing, and Validation

Movement trials from a subset of 35 randomly selected participants were combined to create the algorithm building dataset (for development and testing) while the remaining 15 participants' data were withheld for model validation.

## 5.4.3. Movement Sequences and Template Generation

A series of movement sequences $S_{trial}$ were created such that each contained data from a single trial from which the childcare-inspired motion would be segmented. Given that each motion was collected in isolation, each $S_{trial}$ represents only one motion type, and consists of left and right ankle, knee, and hip flexion-extension angle data, each of length *N*.

$$S_{trial} = (s_0 \dots s_{N-1}) = \begin{pmatrix} s_{RKnee,0} & s_{RKnee,1} & \cdots & s_{RKnee,N-1} \\ s_{LKnee,0} & s_{LKnee,1} & \cdots & s_{LKnee,N-1} \\ s_{RAnkle,0} & s_{RAnkle,1} & \cdots & s_{RAnkle,N-1} \\ \vdots & \vdots & \ddots & \vdots \\ s_{LHip,0} & s_{LHip,1} & \cdots & s_{LHip,N-1} \end{pmatrix} \quad (5.1)$$

A series of templates *T* could then be generated from the 35 participants' motion data through the manual segmentation explained in Subsection 5.3 in order to populate the *k*NN labeled feature space. The dataset here analyzed provided 1911 templates across the 11 childcare-inspired movements (reduced from the 13 movements presented in Subsection 5.2 following grouping of the supported kneeling movements together and side-sitting and side-leaning movements together) and gait trials, with each template consisting of the left and right ankle, knee, and hip flexion-extension angle data. All segmented trials were subsequently linearly interpolated to a length of 101 samples for each joint angle separately. All movement sequences which were not used for templating were additionally normalized through linear interpolation to a length of 101 samples, however no segmentation was performed on these data. All segmented and unsegmented data were scale normalized to a range of [-1, 1]. A representative movement sequence and template based on the right knee angle during HS can be seen in Figure 5.5. The variability between templates for a representative movement class can be seen in Figure 5.6. The movement sequences and templates for all joints for a heels-up squatting trial can be found in Figure D.1 - Figure D.6 as well as those for a walking bout which can be found in Figure E.1 - Figure E.6.

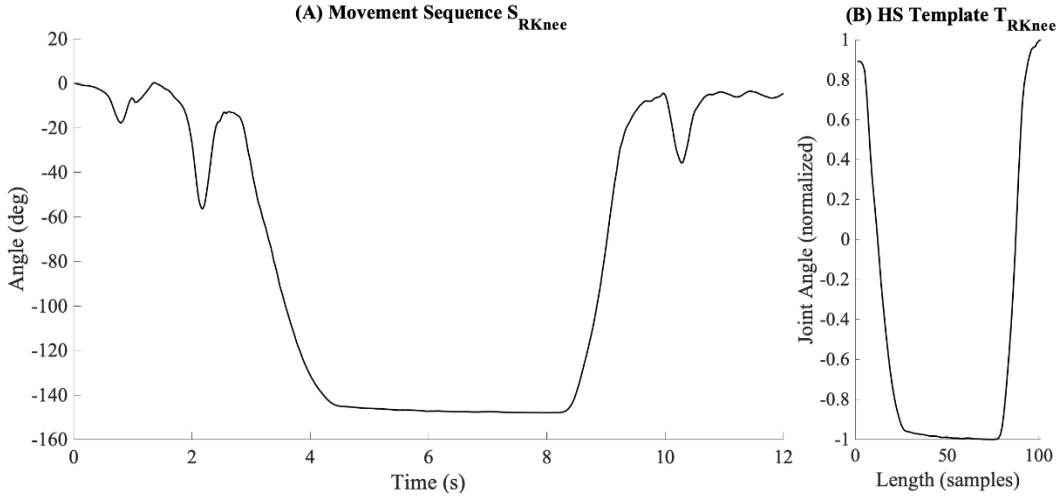


Figure 5.5 A representative unnormalized movement sequence $S_{RKnee}$ for the flexion angle of the right knee during a heels-up squatting motion trial (**A**) along with the corresponding heels-up squat template $T_{RKnee}$ generated from this sequence for the right knee (**B**).

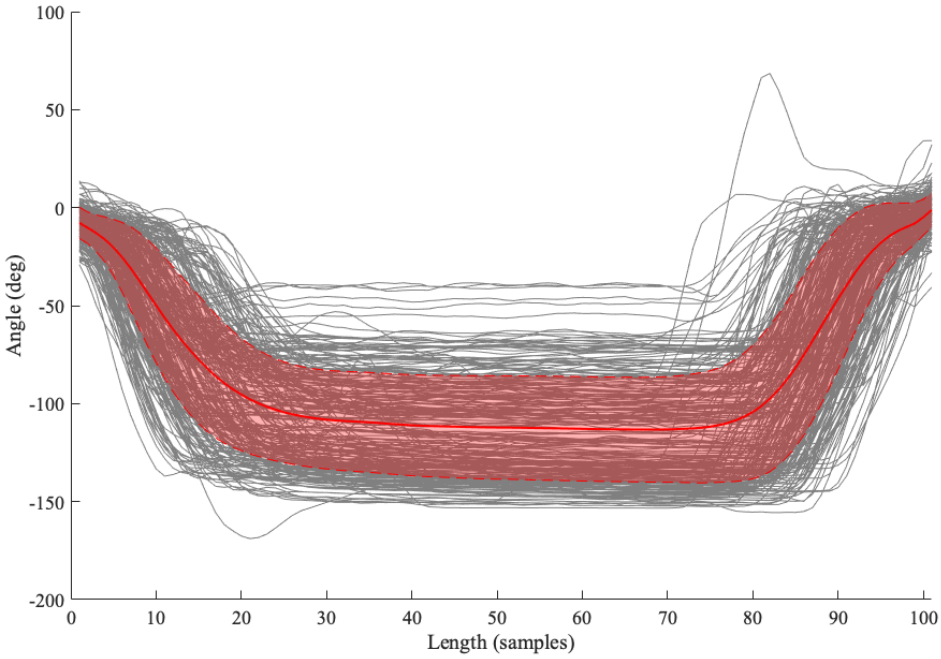


Figure 5.6 Templates generated for heels-up squatting based on the right knee across all trials and participants. Mean and standard deviation curves have been overlayed in red, demonstrating the variability within templates representing the speed of ascent and descent as well as the depth of posture achieved by participants within a single movement for this study's population.

## 5.4.4. Calculation of the Multi-Dimensional Dynamic Time Warping Distance

For each comparison between a given movement sequence *S* and a template *T* based on data from a single joint, a measure of distance, *D,* was calculated based on similarities between the waveforms (Paliwal, Agarwal, & Sinha, 1982; Sakoe & Chiba, 1978; Theodoridis & Koutroumbas, 2003). *D* is therefore calculated as a $M \times N$ matrix, where *M* is the length of the template *T* (representing the rows), and *N* is the length of the movement sequence *S* (representing the columns). Given that both the templates and the sequences were normalized to 101 points, each *D* is therefore calculated as a $101 \times 101$ matrix. Each element of *D* is calculated as the distance between each combination of elements from *T* and *S* using the Euclidean norm such that:

$$D(m,n) = \sqrt{(t_m - s_n)^2}\ \forall\ m \in \{0, \dots, M-1\}, n \in \{0, \dots, N-1\}, \tag{5.2}$$

$$D = \begin{bmatrix} d_{11} & d_{21} & \dots & d_{M1} \\ d_{12} & & & \\ \vdots & & d_{mn} & \vdots \\ & & & \\ d_{1N} & & \dots & d_{MN} \end{bmatrix}.$$

When $t_m$ and $s_n$ are similar, the local value of $d$ would be small, representing a strong similarity between measures, while large values of $d$ represent less similarity between measures. The top row of $D$ represents the distance between the beginning of the template $T$ and the complete sequence $S$ while the bottom row represents the distance between the end of the template and $S$. The ultimate DTW distance can then be calculated based on a path through the matrix $D$ which is parameterized by two isometric sequences, $ix$ and $iy$, representing the warped paths of $S$ and $T$ which minimize the following:

$$D = \sum_{\substack{m \in ix \\ n \in iy}} d_{mn}(MN). \tag{5.3}$$

The warped paths, $ix$ and $iy$, are calculated from $d_{11}$ to $d_{MN}$ and advance through the matrix in a series of moves described by the following constraints:

$$(m,n) \rightarrow (m+1,n)\ if\ d_{m+1,n} < \left(d_{m,n+1}\ and\ d_{m+1,n+1}\right), \tag{5.4}$$

$$(m,n) \rightarrow (m,n+1)\ if\ d_{m,n+1} < \left(d_{m+1,n}\ and\ d_{m+1,n+1}\right), \tag{5.5}$$

$$(m,n) \rightarrow (m+1,n+1)\ if\ d_{m+1,n+1} < \left(d_{m+1,n}\ and\ d_{m,n+1}\right), \tag{5.6}$$

such that the final distance, $d_{MN}$, represents the DTW distance between the waveforms $S$ and $T$. For this study, warping paths were constrained to be within 50 samples of a straight line fit between waveforms, which for templates and sequences of 101 points, represents a maximum warping of 49.5%. This warping path constraint was selected as it was found to maximize classification accuracy when iterating in intervals of 10 from 0 to 100. An example of the warping path calculated between a given movement sequence and template for the right knee is shown in Figure 5.7.

A DTW distance was calculated for each of the six joints and subsequently a weighted sum of these distances was calculated in order to generate a new multi-dimensional distance metric. Weightings for each distance element were initially selected through manual iteration, when iterating in intervals of 0.05 from 0.25 to 0.75 and prescribing a value of 1.00 to $D_{RKnee}$, as follows:

$$D_{mDTW} = 0.25 \cdot D_{LAnkle} + 0.25 \cdot D_{RAnkle} + 0.75 \cdot D_{LKnee} + D_{RKnee} + 0.75 \cdot D_{LAHip} + 0.75 \cdot D_{RHip}. \quad (5.7)$$

This distance metric could be treated the same as any distance measure input to a *k*-Nearest Neighbour algorithm for the classification of derived features (rather than continuous time domain data used here) would be, and thus would allow for the identification of childcare-inspired motions based on inertial estimates of lower limb flexion-extension angles.

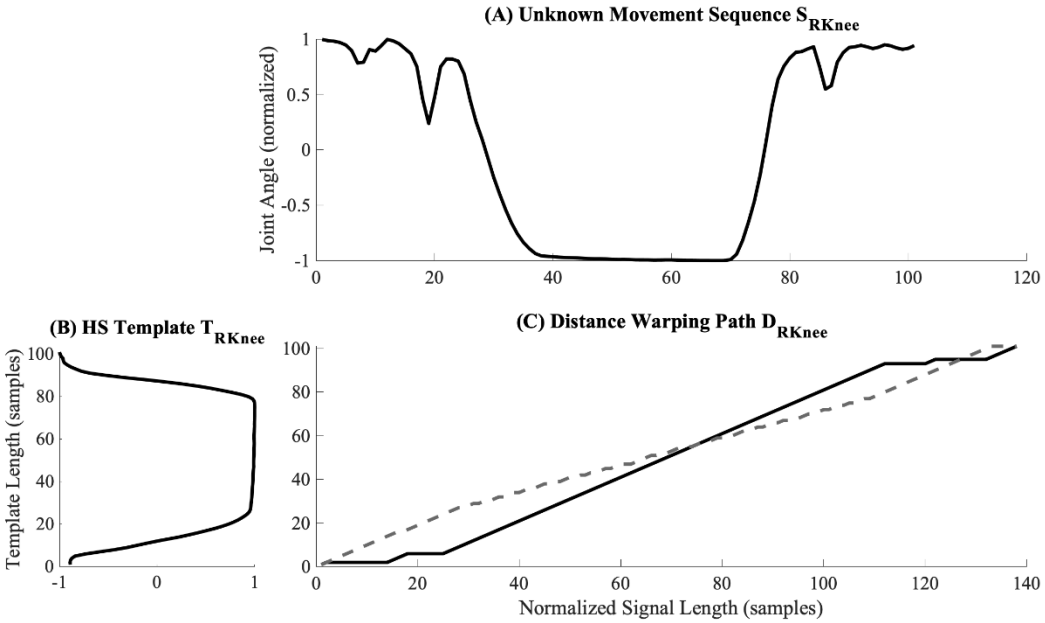


Figure 5.7 Representative warping paths ix and iy derived during the calculation of $D_{RKnee}$ (**C**) based on only the right knee between the movement sequence $S_{RKnee}$ (**A**) and the template $T_{RKnee}$ (**B**) for a heels-up squatting motion trial. Each signal is warped such that the highest level of similarity between waveforms can be achieved. Note that in warping the signals, the length of the final sample may be longer than either original waveform. The dotted line and solid line represent the warped recreations of the movement sequence and template respectively.

## 5.4.5. *k*-Nearest Neighbour Classification Algorithm Development and Testing

Templates built from the randomly selected 35 participants' data were combined with their appropriate motion labels to create the algorithm building dataset for the development and testing of a *k*NN cross-validated classifier. This dataset was relied upon for iterative parameter tuning and ultimately populated the labeled feature space from which classifications would be made. The following motion groupings were therefore included: HS (heels-up squatting), FS (flatfoot squatting), DK (dorsiflexed kneeling), PK (plantarflexed kneeling), ACS (sitting on an

adult sized chair), CCS (sitting on a child sized chair), SK (single arm supported kneeling and double arm supported kneeling), CLS (crossed leg sitting), SS (side sitting and side leaning to the left or the right), STP (stooping), STD (standing), and WLK (walking). Therefore, for our twelve-activity classification problem, each motion would be identified as a different class, $\alpha$, such that $\alpha_i = 0, 1, 2, ..., 11$. It is advised that each movement class should be equally represented within the algorithm building dataset so as to ensure the final parameters that the iterative algorithm building process selected were non-biased towards any class or condition (Madhu-Das & Srichand, 2006). Due to the grouping of similar movements, the number of templates included in this dataset for SS was significantly greater than those included for the other motions (471 individual templates were included for the SS motion while 150 ± 13 templates were included for the other childcare-inspired motions). Given that neither supported kneeling trial was performed under loaded conditions, the combination of these trials into one class, SK, resulted in a similar yet slightly higher number of trials of this class being included in this dataset when compared to those of the other classes (166 individual templates were included for SK). Finally, it is noted that STP and WLK were also only performed without load and therefore were the least represented movement classes with only 83 and 84 templates included respectively.

A holdout validation method was employed to develop and test the classifier, such that 80% of the templates from each motion were randomly allocated as development data (often referred to as training data) while the remaining 20% were withheld for testing (Webb & Copsey, 2011). The development data were then partitioned into five equal parts, or folds, in order to use five-fold cross-validation to develop the *k*NN classifier and obtain an initial estimate of classification accuracy. Permutations of four folds were therefore used to populate the feature space of labeled datapoints, while the fifth fold was reserved for testing. In this way, the accuracy of the initial classifications through the *k*NN classifier were obtained from the average of the five permutations when using a value of $k = 1$ and distances between samples calculated based on eq. (5.7).

Following the initial classifier development, the model performance was evaluated across multiple values of *k*, logarithmically spaced between 1 and the length of the building dataset, 1911, in order to determine the optimal number of nearest neighbours for this classification problem. The five-fold classification errors associated with each *k* value were then plotted and

the value of $k$ which minimized the cross-validated losses was selected as optimal. The model was found to classify most accurately when a value of 1 was attributed to $k$.

Subsequently, the weighting parameters used in the mDTW distance metric calculation were also optimized using this cross-validated model. Each weighting coefficient was varied within ±0.045 of the initial values presented in eq. (5.7) with a step size of 0.015 for the left ankle, knee, and hip, and the right ankle and hip, while for the right knee the weighting coefficient was varied between 0.7 and 1. These permutations were tested simultaneously such that the combination of coefficients which best minimized the five-fold classification losses was selected, thereby increasing the predictivity of the model. The final mDTW distance was calculated as follows:

$$D_{mDTW} = 0.26 \cdot D_{LAnkle} + 0.20 \cdot D_{RAnkle} + 0.72 \cdot D_{LKnee} + D_{RKnee} + 0.67 \cdot D_{LAHip} + 0.76 \cdot D_{RHip}. \quad (5.8)$$

Once these parameters had been tuned, a final $k$NN model was developed using all development data and subsequently evaluated using the test samples (the 20% of templates held-back from the algorithm building dataset, which will be referred to as segmented trials) as well as using the corresponding movement sequences which had not undergone segmentation, in order to determine the model's performance when identifying unknown waveforms from individuals on which the classifier was trained.

Finally, movement sequences for all motions and loading conditions from each of the 15 participants withheld for validation were classified in order to evaluate the classification accuracy when the model was provided with novel data.

## 5.4.6.Classification Error Measurement

The classification performance of all models was quantified as the ratio of correct classifications to the total number of classifications. While the rate of successfully identifying each motion based on chance would be 7.7% (100% / the number of motions to be classified), the goal of the developed classification framework was to identify each motion as accurately as possible. To this end, sensitivity and specificity were calculated for each motion in order to determine whether any motions suffered from greater risk of classification errors within the development, testing, and validation models (Webb & Copsey, 2011).

Sensitivity, a measure of the true positive classifications which can also be referred to as recall, was calculated as the proportion of waveforms of a certain motion correctly identified, as in eq. (5.9):

$$Sensitivity = \frac{TP}{TP + FN}, \tag{5.9}$$

where TP, or true positive, are the number of sequences within a given motion correctly identified as such, and FN, or false negative, are the number of sequences within a given motion incorrectly identified as other motions. Therefore the term (TP + FN) represents the total number of sequences for the given motion (Webb & Copsey, 2011). A high sensitivity value would represent the ability to classify a motion with few false negatives but does not consider the number of false positives.

Specificity, a measure of true negative classifications, was calculated as the proportion of feature sets not belonging to a specific motion correctly identified as other motions, as in eq. (5.10):

$$Specificity = \frac{TN}{TN + FP}, \tag{5.10}$$

where TN, or true negative, are the number of sequences not belonging to a given motion correctly classified as belonging to the other motions, and FP, or false positive, are the number of sequences not belonging to a given motion which are incorrectly classified as the motion in question. Therefore the term (TN + FP) represents the total number of sequences belonging to all other motions (Webb & Copsey, 2011). A high specificity value would represent the ability to classify a motion with few false positives, however, does not consider the number of false negatives.

Given the presence of imbalanced templates across motions, balanced accuracy, $Acc_{Bal}$, was also calculated, as in eq. (5.11):

$$Acc_{Bal} = \frac{1}{2} \cdot \frac{TP}{TP + FN} + \frac{1}{2} \cdot \frac{TN}{TN + FP}, \tag{5.11}$$

This metric combines both the sensitivity and specificity of a given model and limits inflated accuracy scores by combining the number of true positives (TP), true negatives (TN), false positives (FP), and false negatives (FN) into a single representative value (Lin et al., 2018). All

classifications and analyses of error were completed using Matlab 9.13 (The Mathworks, Release R2022b, Natick, MA, USA).

### 5.4.7.Statistical Analyses

In order to assess the presence of any potential differences in classification accuracies of the novel participant movement sequences under unloaded and loaded conditions, a statistical analysis was performed using a one-way ANOVA on the classification accuracy values for each of the 9 motions performed under both load conditions (noting that SK, STP, and WLK were not performed while holding the load). An alpha level of 0.05 was used to determine significance.

## 5.5. Results

Through five-fold cross-validation, the initial mDTW *k*NN algorithm was developed based on movement templates of lower limb flexion-extension angles calculated from inertial sensor data across twelve motions from 35 participants. Initial classification accuracy following cross-validation of the templates included in the algorithm building dataset was found to be 82.2%. Sensitivity, specificity, and balanced accuracy values for all classifiers have been presented in Table 5.1, Table 5.2, and Table 5.3 respectively. Despite imbalances in the number of templates included for each motion, consistent specificity values were reported across classes based on this model (mean specificity was found to be 98.1% ± 1.3%); however, when balancing for the sample sizes using eq. (5.11), the balanced accuracy of the model was found to be 89.5%. In this initial model, the highest levels of misclassification were observed between flatfoot and heels-up squatting.

The parameters selected for *k* and for the weightings used in the mDTW distance metric calculation were subsequently tuned in order to reduce the cross-validated classification errors of this initial model. Subsequently, a new *k*NN model was developed using the entirety of the development data templates to populate the feature space of labeled datapoints, and this model was evaluated using the segmented trials withheld for testing. The classification accuracy of this new model increased to 84.1% overall, with a balanced accuracy of 88%, suggesting that untuned parameters contributed in part to confusion within the classifier.

The tuned classifier's performance was next evaluated using movement sequences corresponding to the 20% of data withheld for testing from the algorithm building dataset. The classification accuracy achieved for these data was 82.3%, with a mean balanced accuracy of 86% across all motions, suggesting that the classifier was capable of identifying novel movement sequences performed by individuals for which it was trained, with only minor decreases in overall accuracy achieved when classifying these movement sequences when compared to the classification of segmented motion trials (motion templates). Sensitivity and specificity values for each motion revealed that the greatest classification accuracies were achieved when identifying kneeling motions and crossed leg sitting, while the most common misclassifications occurred between flatfoot squatting, heels up squatting, and stooping, where the squatting motions were frequently identified as stooping, yet stooping was not misclassified as squatting. It is noted however that the classification specificities were consistent across all motions (98.1% ± 2.0%), representing the classifiers strong ability the reject false positives. This classification model also revealed that while walking was identified with 100% accuracy when classifying segmented data for individual steps, the templates were not sufficient for the identification of walking sequences which may include multiple steps.

Table 5.1 Sensitivity based confusion matrices for the classification of twelve childcare-inspired motions based on (A) the cross-validation of the algorithm building templates, (B) the testing of segmented data using a model based on tuned k and the mDTW weighting parameters, (C) the testing of movement sequences using the tuned parameter model, and (D) the validation of the tuned parameter model on novel participant movement sequences. All values are expressed as percentages relative to the total number of classifications for each childcare-inspired motion. Bolded cells denote correct classifications. The twelve motions analyzed were: heels-up squatting (HS), flatfoot squatting (FS), dorsiflexed kneeling (DK), plantarflexed kneeling (PK), sitting on an adult sized chair (ACS), sitting on a child sized chair (CCS), single arm supported kneeling and double arm supported kneeling (SS), crossed leg sitting (CLS), side sitting and side leaning to the left or the right (SS), stooping (STP), standing (STD), and walking (WLK). *Target Class represents the correct class of each template or sequence. **Output Class represents the class predicted by the classifier.

**A**

| | Cross-Validated *k*NN | | | | | | | | | | | |
|---|---|---|---|---|---|---|---|---|---|---|---|---|
| Target Class* | DK | **71.8** | 10.3 | 5.1 | 5.1 | 2.6 | 0.0 | 5.1 | 0.0 | 0.0 | 0.0 | 0.0 |
| | PK | 0.0 | **100** | 0.0 | 0.0 | 0.0 | 0.0 | 0.0 | 0.0 | 0.0 | 0.0 | 0.0 |
| | FS | 0.0 | 0.0 | **81.6** | 10.5 | 5.3 | 2.6 | 0.0 | 0.0 | 0.0 | 0.0 | 0.0 |
| | HS | 0.0 | 0.0 | 27.0 | **64.9** | 5.4 | 2.7 | 0.0 | 0.0 | 0.0 | 0.0 | 0.0 |
| | CCS | 2.6 | 0.0 | 0.0 | 0.0 | **68.4** | 26.3 | 0.0 | 0.0 | 0.0 | 0.0 | 2.6 | 0.0 |
| | ACS | 0.0 | 0.0 | 0.0 | 2.6 | 5.3 | **92.1** | 0.0 | 0.0 | 0.0 | 0.0 | 0.0 | 0.0 |
| | SK | 7.3 | 2.4 | 2.4 | 0.0 | 2.4 | 0.0 | **82.9** | 0.0 | 0.0 | 0.0 | 2.4 | 0.0 |
| | STP | 4.8 | 0.0 | 4.8 | 19.0 | 0.0 | 0.0 | 0.0 | **71.4** | 0.0 | 0.0 | 0.0 | 0.0 |
| | STD | 0.0 | 0.0 | 0.0 | 5.6 | 0.0 | 5.6 | 0.0 | 11.1 | **77.8** | 0.0 | 0.0 | 0.0 |
| | CLS | 3.4 | 3.4 | 0.0 | 3.4 | 0.0 | 0.0 | 3.4 | 0.0 | 0.0 | **72.4** | 13.8 | 0.0 |
| | SS | 1.7 | 0.8 | 0.0 | 0.0 | 1.7 | 0.8 | 1.7 | 0.0 | 0.0 | 5.0 | **88.2** | 0.0 |
| | WLK | 0.0 | 0.0 | 0.0 | 0.0 | 0.0 | 0.0 | 0.0 | 0.0 | 0.0 | 0.0 | 0.0 | **100** |
| | | DK | PK | FS | HS | CCS | ACS | SK | STP | STD | CLS | SS | WLK |
| | Output Class** | | | | | | | | | | | | |

**B**

| | Tuned Parameter *k*NN on Segmented Testing Data | | | | | | | | | | | |
|---|---|---|---|---|---|---|---|---|---|---|---|---|
| Target Class | DK | **76.9** | 5.1 | 5.1 | 2.6 | 5.1 | 0.0 | 5.1 | 0.0 | 0.0 | 0.0 | 0.0 | 0.0 |
| | PK | 0.0 | **100** | 0.0 | 0.0 | 0.0 | 0.0 | 0.0 | 0.0 | 0.0 | 0.0 | 0.0 | 0.0 |
| | FS | 0.0 | 0.0 | **81.6** | 13.2 | 2.6 | 2.6 | 0.0 | 0.0 | 0.0 | 0.0 | 0.0 | 0.0 |
| | HS | 0.0 | 0.0 | 24.3 | **73.0** | 2.7 | 0.0 | 0.0 | 0.0 | 0.0 | 0.0 | 0.0 | 0.0 |
| | CCS | 2.6 | 0.0 | 0.0 | 0.0 | **68.4** | 26.3 | 0.0 | 0.0 | 0.0 | 0.0 | 2.6 | 0.0 |
| | ACS | 0.0 | 2.6 | 0.0 | 2.6 | 2.6 | **92.1** | 0.0 | 0.0 | 0.0 | 0.0 | 0.0 | 0.0 |
| | SK | 7.3 | 0.0 | 2.4 | 0.0 | 2.4 | 0.0 | **85.4** | 0.0 | 0.0 | 0.0 | 2.4 | 0.0 |
| | STP | 4.8 | 0.0 | 9.5 | 9.5 | 0.0 | 0.0 | 0.0 | **76.2** | 0.0 | 0.0 | 0.0 | 0.0 |
| | STD | 0.0 | 0.0 | 0.0 | 0.0 | 5.6 | 0.0 | 0.0 | 5.6 | **61.1** | 5.6 | 22.2 | 0.0 |
| | CLS | 0.0 | 3.4 | 0.0 | 3.4 | 0.0 | 0.0 | 3.4 | 0.0 | 0.0 | **75.9** | 13.8 | 0.0 |
| | SS | 1.7 | 0.8 | 0.0 | 0.0 | 0.0 | 0.0 | 0.0 | 0.0 | 0.0 | 5.9 | **91.6** | 0.0 |
| | WLK | 0.0 | 0.0 | 0.0 | 0.0 | 0.0 | 0.0 | 0.0 | 0.0 | 0.0 | 0.0 | 0.0 | **100** |
| | | DK | PK | FS | HS | CCS | ACS | SK | STP | STD | CLS | SS | WLK |
| | Output Class | | | | | | | | | | | | |

**C**

| Tuned Parameter kNN on Testing Movement Sequences | | | | | | | | | | | | | |
|---|---|---|---|---|---|---|---|---|---|---|---|---|---|
| Target Class | DK | **100** | 0.0 | 0.0 | 0.0 | 0.0 | 0.0 | 0.0 | 0.0 | 0.0 | 0.0 | 0.0 | 0.0 |
| | PK | 0.0 | **87.2** | 0.0 | 2.6 | 2.6 | 0.0 | 0.0 | 2.6 | 2.6 | 0.0 | 2.6 | 0.0 |
| | FS | 2.6 | 0.0 | **57.9** | 7.9 | 0.0 | 0.0 | 2.6 | 28.9 | 0.0 | 0.0 | 0.0 | 0.0 |
| | HS | 2.6 | 0.0 | 18.4 | **52.6** | 0.0 | 0.0 | 0.0 | 26.3 | 0.0 | 0.0 | 0.0 | 0.0 |
| | CCS | 2.7 | 0.0 | 0.0 | 2.7 | **89.2** | 5.4 | 0.0 | 0.0 | 0.0 | 0.0 | 0.0 | 0.0 |
| | ACS | 0.0 | 0.0 | 0.0 | 2.6 | 10.5 | **84.2** | 0.0 | 2.6 | 0.0 | 0.0 | 0.0 | 0.0 |
| | SK | 2.4 | 2.4 | 0.0 | 0.0 | 0.0 | 0.0 | **95.1** | 0.0 | 0.0 | 0.0 | 0.0 | 0.0 |
| | STP | 4.8 | 0.0 | 0.0 | 4.8 | 0.0 | 0.0 | 0.0 | **90.5** | 0.0 | 0.0 | 0.0 | 0.0 |
| | STD | 0.0 | 0.0 | 0.0 | 0.0 | 0.0 | 0.0 | 0.0 | 0.0 | **89.5** | 0.0 | 10.5 | 0.0 |
| | CLS | 0.0 | 0.0 | 0.0 | 0.0 | 0.0 | 0.0 | 0.0 | 0.0 | 0.0 | **96.6** | 3.4 | 0.0 |
| | SS | 0.8 | 0.8 | 0.0 | 0.0 | 0.8 | 2.5 | 0.0 | 0.0 | 0.0 | 2.5 | **92.4** | 0.0 |
| | WLK | 14.3 | 0.0 | 0.0 | 0.0 | 0.0 | 4.8 | 4.8 | 47.6 | 14.3 | 0.0 | 14.3 | **0.0** |
| | | DK | PK | FS | HS | CCS | ACS | SK | STP | STD | CLS | SS | WLK |

Output Class

**D**

| Tuned Parameter *k*NN on Novel Participant Movement Sequences | | | | | | | | | | | | | |
|---|---|---|---|---|---|---|---|---|---|---|---|---|---|
| Target Class | DK | **63.2** | 6.9 | 0.0 | 1.1 | 9.2 | 9.2 | 4.6 | 0.0 | 0.0 | 0.0 | 5.7 | 0.0 |
| | PK | 1.1 | **79.3** | 0.0 | 0.0 | 0.0 | 0.0 | 8.0 | 0.0 | 0.0 | 0.0 | 11.5 | 0.0 |
| | FS | 6.9 | 1.1 | **35.6** | 25.3 | 2.3 | 1.1 | 0.0 | 27.6 | 0.0 | 0.0 | 0.0 | 0.0 |
| | HS | 3.4 | 2.3 | 32.2 | **39.1** | 4.6 | 0.0 | 0.0 | 18.4 | 0.0 | 0.0 | 0.0 | 0.0 |
| | CCS | 0.0 | 0.0 | 1.2 | 6.0 | **67.9** | 22.6 | 1.2 | 1.2 | 0.0 | 0.0 | 0.0 | 0.0 |
| | ACS | 0.0 | 0.0 | 1.2 | 1.2 | 30.5 | **65.9** | 0.0 | 0.0 | 0.0 | 0.0 | 1.2 | 0.0 |
| | SK | 20.0 | 9.4 | 0.0 | 1.2 | 4.7 | 3.5 | **48.2** | 0.0 | 0.0 | 0.0 | 12.9 | 0.0 |
| | STP | 0.0 | 0.0 | 9.3 | 4.7 | 0.0 | 4.7 | 4.7 | **76.7** | 0.0 | 0.0 | 0.0 | 0.0 |
| | STD | 0.0 | 0.0 | 1.2 | 3.5 | 2.4 | 2.4 | 1.2 | 4.7 | **76.5** | 0.0 | 4.7 | 3.5 |
| | CLS | 1.3 | 4.3 | 3.9 | 0.0 | 3.9 | 1.3 | 0.0 | 0.0 | 0.0 | **61.8** | 26.3 | 0.0 |
| | SS | 5.6 | 7.3 | 3.1 | 3.5 | 5.9 | 4.2 | 3.8 | 0.3 | 0.0 | 12.6 | **53.5** | 0.0 |
| | WLK | 0.0 | 0.0 | 0.0 | 0.0 | 6.7 | 4.4 | 2.2 | 75.6 | 2.2 | 0.0 | 8.9 | **0.0** |
| | | DK | PK | FS | HS | CCS | ACS | SK | STP | STD | CLS | SS | WLK |

Output Class

Table 5.2 Specificity values achieved in the classification of twelve childcare-inspired motions. All values are expressed as percentages relative to the total number of classified waveforms belonging to other motions. The twelve motions analyzed were: heels-up squatting (HS), flatfoot squatting (FS), dorsiflexed kneeling (DK), plantarflexed kneeling (PK), sitting on an adult sized chair(ACS), sitting on a child sized chair (CCS), single arm supported kneeling and double arm supported kneeling (SS), crossed leg sitting (CLS), side sitting and side leaning to the left or the right (SS), stooping (STP), standing (STD), and walking (WLK).

| Motion Classifier Type | DK | PK | FS | HS | CCS | ACS | SK | STP | STD | CLS | SS | WLK |
|---|---|---|---|---|---|---|---|---|---|---|---|---|
| Cross-Validated *kNN* | 97.8 | 98.1 | 96.3 | 96.6 | 97.3 | 96.2 | 98.6 | 99.5 | 100 | 98.4 | 98 | 100 |
| Tuned Parameter *k*NN on Segmented Data | 98.1 | 98.6 | 96.4 | 97.4 | 98.2 | 97.1 | 99.2 | 99.7 | 100 | 97.9 | 97.0 | 99.7 |
| Tuned Parameter *k*NN on Movement Sequences | 97.6 | 99.5 | 98.2 | 98.2 | 98.4 | 98.4 | 99.5 | 92.2 | 98.9 | 99.2 | 97.1 | 100 |
| Novel Participant Movement Sequences | 93.0 | 93.6 | 92.8 | 93.1 | 89.5 | 92.1 | 95.7 | 88.3 | 99.8 | 94.3 | 89.8 | 99.5 |

Table 5.3 Balanced accuracy values achieved in the classification of twelve childcare-inspired motions. All values are expressed as percentages. The twelve motions analyzed were: heels-up squatting (HS), flatfoot squatting (FS), dorsiflexed kneeling (DK), plantarflexed kneeling (PK), sitting on an adult sized chair(ACS), sitting on a child sized chair (CCS), single arm supported kneeling and double arm supported kneeling (SS), crossed leg sitting (CLS), side sitting and side leaning to the left or the right (SS), stooping (STP), standing (STD), and walking (WLK).

| Motion Classifier Type | DK | PK | FS | HS | CCS | ACS | SK | STP | STD | CLS | SS | WLK |
|---|---|---|---|---|---|---|---|---|---|---|---|---|
| Cross-Validated kNN | 84.7 | 99.0 | 88.9 | 80.7 | 82.9 | 94.2 | 90.8 | 85.5 | 88.9 | 85.4 | 93.1 | 100 |
| Tuned Parameter kNN on Segmented Data | 87.5 | 99.3 | 89.0 | 85.2 | 83.3 | 94.6 | 92.3 | 88.0 | 80.6 | 86.9 | 94.3 | 99.9 |
| Tuned Parameter kNN on Movement Sequences | 98.8 | 93.3 | 78.1 | 75.4 | 93.8 | 91.3 | 97.3 | 91.3 | 94.2 | 97.9 | 94.8 | 50.0 |
| Novel Participant Movement Sequences | 78.1 | 86.5 | 64.2 | 66.1 | 78.7 | 79.0 | 92.0 | 82.5 | 88.1 | 78.1 | 71.7 | 49.8 |

Finally, the tuned and tested classification model was used to predict the childcare-inspired motions for movement sequences from fifteen novel participants (withheld from the algorithm building dataset). The classifier was found to be 55.6% accurate when identifying childcare-inspired motions from novel participants, however when considering the balanced accuracy, this value increased to 74.6%. Specificity values were slightly diminished when classifying novel participant waveforms (93.5% ± 3.6%), however the greatest changes were observed in sensitivity with a mean value of 55.6% ± 23% found when including gait, or if gait trials were excluded, mean sensitivity was found to be 60.7 % ± 15%. In this model, elevated levels of misclassifications were observed between motions of similar types (i.e., between dorsiflexed, plantarflexed, and supported kneeling; flatfoot and heels-up squatting; sitting on adult or child sized chairs; and crossed leg or side sitting). By grouping these motions by similarities,

classification accuracy was increased to 75.7%, with sensitivity, specificity, and balanced accuracy values for these groupings shown in Table *5.4*.

Statistical differences between loading conditions were evaluated based on the performance of the tuned and tested classification model's predictions of all movement sequences from the fifteen novel participants, revealing no significant differences between the classification of unloaded and loaded trials. The sensitivity-based confusion matrices for the classifications based on each of these loading conditions can be found in Table F.1. It was therefore concluded that the developed model is insensitive to any potential movement variability resulting from the presence of a load while performing these motions.

Table 5.4 Sensitivity, specificity, and balanced accuracy values achieved in the classification of childcare-inspired motions when grouped based on similarity of motions such that kneeling encompasses dorsiflexed, plantarflexed, and supported kneeling, squatting encompasses flatfoot and heels-up squatting, chair sitting encompasses sitting on adult- and child-sized chairs, and floor sitting encompasses crossed leg and side sitting. All values are expressed as percentages.

| Motion Classifier Type | Kneeling | Squatting | Chair Sitting | Stooping | Standing | Floor Sitting | WLK |
|---|---|---|---|---|---|---|---|
| Sensitivity | 80.3 | 66.1 | 93.4 | 76.7 | 76.5 | 70.7 | 0.0 |
| Specificity | 81.3 | 86.2 | 81.7 | 88.3 | 99.8 | 82.8 | 99.5 |
| Balanced Accuracy | 81.0 | 76.0 | 88.0 | 83.0 | 88.0 | 77.0 | 49.8 |

## 5.6. Discussion

In this study, a multi-dimensional Dynamic Time Warping distance-based *k*NN algorithm for the recognition of motions frequently adopted in occupational childcare based on inertial sensor data was developed. Joint angles of the left and right ankles, knees, and hips were segmented into motion templates to populate the classification feature space and subsequently these templates were compared, using DTW, to continuous movement sequences representing heels-up and flatfoot squatting, dorsiflexed and plantarflexed kneeling, single and double arm supported kneeling, sitting on adult- and child-sized chairs, crossed leg sitting, side sitting and side leaning to the left or the right, stooping, standing, and walking. The weighted sum of these DTW-based distances between waveforms was then calculated and a nearest neighbour to the unknown movement sequence would be determined based on the minimum mDTW distance, calculated between all templates. Experimental results demonstrate that the model was capable of classifying eleven of the twelve childcare-inspired motions with 55.6% accuracy when classified

independently, or, when grouping motions based on their similarities, with an accuracy of 75.7%. The developed model was not capable of classifying sequences of walking data based on a single step template.

The mDTW distance-based classification approach developed in this study has previously been adopted for the segmentation of strides and the identification of activities of daily living such as sitting, standing, lying down, and walking (both on level ground and on stairs) (Barth et al., 2015; Kluge et al., 2017; Muscillo et al., 2007; Paiyarom et al., 2009), to our knowledge this paper constitutes the first study to apply this technique to the identification of high knee flexion postures typically adopted by childcare workers. The ability to measure and interpret motions which elicit high knee flexion and are specific to an occupation without the presence of a researcher is essential for the assessment of high knee flexion postures within occupational settings. Based on classified wearable sensor data, quantitative measures of the frequency and duration of high knee flexion postural adoption can be obtained, by which the demands of a given workplace or occupation can be determined. Ultimately this data may lead to the development of workplace specific guidelines for minimizing the continued or prolonged adoption of postures associated with an increased risk of knee OA development. While two studies have previously sought to classify high flexion postures within childcare settings, each used models developed for the identification of high flexion postures across many occupations, resulting in broadly defined posture classes such as squatting and kneeling. As such, these models were incapable of quantifying the many high flexion postures observed to be uniquely adopted when caring for children, which were included in the current study (Burford et al., 2017; Holtermann et al., 2020; Laudanski et al., 2022).

The accuracy of the developed model to classify movement sequences based on predefined templates was evaluated both on data from participants who were and were not included in the labeled classification feature space. The highest accuracies were achieved when a portion of a given participant's data had been included in this feature space, thus, if possible, a brief collection of supervised movement trials from novel participants could be added to the algorithm building dataset prior to the measurement of unsupervised exposure data in workplace settings. Alternatively, the movements of novel participants could be classified using the developed tuned and tested model, and the classification accuracies could then be interpreted within the reported

sensitivity and specificity levels here provided, as well as within the sensitivity and specificity levels presented when grouping motions based on similarities.

The classification framework presented in this study utilizes previously estimated joint angles rather than raw IMU data in order to ensure an interpretable association between the classification inputs and the output motion classes. While many machine learning-based approaches can be applied to the classification of human motion, several of these utilize deep learning to map connections between inputs and outputs through what is colloquially referred to as a "black box" (Roscher, Bohn, Duarte, & Garcke, 2020). Despite the demonstrated success of these approaches across a broad array of applications (Cho & Kim, 2012; A. Choi et al., 2019; Hsu & Lin, 2002; F.-C. Wang et al., 2021; Zimmermann et al., 2018), recent efforts in the development of explainable or interpretable machine learning have sought to create "white box" algorithms from which the link between inputs and results are transparent, interpretable, and explainable (Doshi-Velez & Kim, 2017; Roscher et al., 2020; Vilone & Longo, 2021). Given the evaluation of high knee flexion postures adopted in occupational settings goes beyond simply identifying their occurrence, it was important to develop a classification framework based on kinematic values which could be easily understood, interpreted, and further analyzed by users within both academic and occupational communities. We therefore believe that the use of a computationally simple *k*NN classification model based on mDTW distances satisfies these objectives and will serve to advance the research and knowledge surrounding exposures of high knee flexion beyond laboratory-based settings.

Classification accuracies of all childcare-inspired motions, with the exception of walking, using the tuned and tested classification model were found to be well above the rate of chance (7.7%) based on movement sequences performed by participants both included and novel to the labeled classification feature space. The decrease in classification accuracy between these individuals is likely attributable to inter-subject variability in joint ranges of motion and movement patterns leading to confusion in the classification of kinematically similar motion. The highest rates of misclassifications in novel participant data were observed in flatfoot and heels-up squatting, where movement sequences were frequently identified as belonging to one of these two squatting motions or as a stoop rather than a squat. These misclassifications may be attributable to the variability of movement strategies adopted during the stoop motion, given that

the instructions provided to participants for this motion were to bend over as if they were picking up a child. The individuals recruited for this study were primarily young adults currently enrolled in a kinesiology undergraduate or graduate program. Given these participant demographics, it is unlikely that the majority of these individuals interact with young children on a regular basis, however unlike a generic sampling of students from across a university population, it is likely that these participants would have received advanced training in injury preventative lifting strategies. Therefore, there is an increased probability that the stooping motions adopted by many would not be described as an isolated flexion about the hips but rather be akin to a squatting motion with increased hip flexion. If we continue with this hypothesized description of a stooping motion, it is highly likely that a squatting motion performed by an individual who was unable to achieve high knee flexion during squatting yet exhibited a greater degree of hip flexion to move their torso forward and increase their balance might have been most similar to a stooping motion rather than the labeled squatting motion templates in which a greater range of knee flexion angles are achieved while the trunk is held relatively perpendicular to the ground resulting in decreased hip flexion. Similarly, for the supported kneeling motions, participants were not directed as to how to place their feet, and as such may have adopted either dorsiflexion or plantarflexion at their ankles. Therefore, it is likely that the greatest difference between these supported kneeling motions for individuals incapable of achieving high knee flexion in either the dorsiflexed or plantarflexed kneeling motions would occur in the hip flexion angles. Given the mDTW distance metric weighting similarities between knee joint angles more heavily than those measured at the hip, these differences in hip angle may not have been sufficiently large so as to differentiate between the supported and unsupported kneeling motions.

While the proposed algorithm was demonstrated to be capable of classifying motions frequently adopted by childcare workers in the dataset here presented, there are several limitations to this classifier which must be considered. The current classification model was developed using simulated occupational data which was collected in a laboratory-based setting. Despite encouraging participants to perform each movement as naturally as possible, motion timings were controlled in order to ensure that participant remained in maximum flexion for 5 seconds, which likely affected the manner in which participants moved. Therefore, moving forward the classifier should be provided with a series of templates based on unconstrained

movements in order to minimize the risk of miscalculations based on the prescribed motions adopted in this study.

Similarly, it must be noted that the dataset used in this study was composed of movement sequences which were recorded in isolation, such that no sequence contained transitions from one motion class to another. While the data included in the model sufficiently captured both the descent and ascent phases of each motion, in occupational settings it is likely that individuals might transition between motions (i.e., transition from kneeling to sitting, or descend into a flatfoot squat but ascend through a heels-up squat). The developed algorithm would likely be unable to classify such postural transitions. Therefore, future work should explore the possibility of extending the classification ability of the model in order to distinguish between different phases of motion including descent, static holding, and ascent of each movement, ultimately enabling the classifier to successfully detect consecutive phases as different motion types based on the existing dataset here provided. Additional data would be required however in order for the classifier to be capable of identifying the transitional movements themselves. One must additionally be aware that the proposed linear weightings of DTW distances in the mDTW approach might not be the most robust when seeking to applying the developed classifier to the identification of transitions in continuous datasets. Given the subtle differences between many of the high knee flexion movements simulated in the current study, it might be appropriate to explore a non-linear approach when combining the DTW distances to best distinguish between postures.

Finally, in this study a supervised learning algorithm was utilized which requires each sample within the classification feature space to be labeled. Given that data here presented were collected in a laboratory setting, manual labels were applied to each motion at the time of collection. Should additional data be collected and added to the classification feature space in the future, this data would additionally require labeling, and therefore the collection of movement trials to be added would require the presence of a researcher or the use of filming equipment in order to manually identify each motion performed prior to adding their templates to the classification building dataset.

## 5.7. Conclusion

Successful classification of eleven movements (heels-up and flatfoot squatting, dorsiflexed and plantarflexed kneeling, supported kneeling, sitting on adult- and child-sized chairs, crossed leg sitting, side sitting and leaning, stooping, and standing) was achieved using a multi-dimensional Dynamic Time Warping distance-based Nearest Neighbour classification algorithm. A combination of weighted DTW distances calculated between motion templates and continuous movement sequences representing joint angles for the ankles, knees, and hips was found to be effective for the classification of these movements frequently performed in occupational childcare. The generally high classification rates achieved when classifying data from participants both included and precluded from the algorithm building dataset indicate strong potential for the proposed model's application to the quantitative measurement of postural requirements in childcare settings. Future work should therefore seek to expand this classifier in order to identify separate phases for each motion rather than motions in their entirety in order to be successfully applied to the measurement and identification of high knee flexion postures in real world settings. While the movements analyzed in this study replicated those observed in childcare settings, the proposed model could be applied across numerous occupations to inform future musculoskeletal injury prevention initiatives.

# Chapter 6

# Evaluating the Feasibility of Applying the Developed Multi-Dimensional Dynamic Time Warping Distance-Based Framework to the Measurement and Recognition of High Knee Flexion Postures in a Simulated Childcare Environment

## 6.1. Introduction

The ability to automatically and robustly detect specific postures from continuously collected inertial data is essential for the monitoring and measurement of occupational exposures. The analysis of movements as they are naturally occurring in occupational settings is particularly important in cases where the frequent and repetitive adoption of high knee flexion postures is required, as these postures have been associated with increased incidences of knee OA. Childcare workers specifically have been shown to exceed the published duration and frequency thresholds associated with the OA development (Burford et al., 2017; Holtermann et al., 2020;

Laudanski et al., 2022) yet to date no study has quantified these exposures in North American childcare settings in order to inform guidelines for risk mitigation.

Previous applications of activity classification based on inertial sensor data vary greatly in: i) the type and number of sensors used in a given study, ii) the signal characteristics selected from which to build classification models tasked with activity recognition, and iii) the type of machine learning techniques selected (Allahbakhshi, Hinrichs, Huang, & Weibel, 2019; Altun et al., 2010; Anna Ferrari, Micucci, Mobilio, & Napoletano, 2020).

Selecting the optimal number of sensors to use for a given classification problem is a non-trivial decision. It has been suggested that an increased number of sensors may result in an increased number of activities which can be classified, yet a higher number of sensors will also result in greater complexity in terms of setup, calibration, and computation (Allahbakhshi et al., 2019; Maurer, Smailagic, Siewiorek, & Deisher, 2006). Studies seeking to analyze gait characteristics have typically shown that a single inertial sensor mounted on either the foot or shank is sufficient for step or stride segmentation (Barth et al., 2015; Bejarano et al., 2015; Chang et al., 2016; Kluge et al., 2017). When seeking to expand the classification beyond a single activity however, it has been suggested that a single sensor may not be sufficient in differentiating between motions (Bao & Intille, 2004; De Vries, Garre, Engbers, Hildebrandt, & Van Buuren, 2011; Gyllensten & Bonomi, 2011). De Vries et al. (2011) demonstrated that a combination of sensors mounted on the ankle and hip outperformed a single hip-worn sensor when distinguishing between activities such as sitting, standing, walking, cycling, and stair ambulating. Similarly, Altun et al. (2010) and Barshan et al. (2013) proposed the use of five sensors, attached to participants thighs, wrists, and pelvis, for the classification of 19 activities including a mixture of daily and sports activities. Therefore, there is currently no standard approach to selecting the optimal number or configuration of sensors when seeking to classify human movement, however it is evident that the complexity of the classification problem must be considered when determining the number of sensors to use and where these should be placed.

Much like the variation observed across studies in the configuration of sensors to be included in a classification problem, there are significant differences in the types of signals, the segmentation (or windowing) of these signals, and the selection of representative data or features

from which to classify each activity of interest. The use of different sensors or signals can provide a variety of information about the movement being performed (Fu, Damer, Kirchbuchner, & Kuijper, 2020; Muscillo et al., 2007), therefore features from accelerometers (Muscillo et al., 2007; Paiyarom et al., 2009), gyroscopes (Barth et al., 2013), processed joint kinematic data (Bejarano et al., 2015), and combinations of these signals (Altun et al., 2010; Barshan & Yüksek, 2013; Barth et al., 2015; Chang et al., 2016; Kluge et al., 2017; Mekruksavanich et al., 2020) have been employed for activity classification problems. Similarly, segmentation of sensor data into smaller time increments, commonly referred to as windowing, is often undertaken prior to activity classification (Preece, Goulermas, Kenney, Howard, et al., 2009). Data windowing can be derived based on a fixed time duration (Altun et al., 2010; Barshan & Yüksek, 2013; Mekruksavanich et al., 2020) or on the calculated activity duration (Bejarano et al., 2015; Chang et al., 2016; Muscillo et al., 2007) however, no standards exist to dictate the appropriate length of window for activity classification and as such significant discrepancies exist between studies. Finally, the choice of data from which to build an activity classifier differs greatly across the currently available literature. Successful classification depends heavily on this choice in order to ensure maximum separability between postures or activities. Feature-based classification algorithms have traditionally relied on the extraction of representative features from both the time and frequency domain including but not limited to the mean, variance, number of zero crossings, or dominant frequencies of a signal (Altun et al., 2010; Barshan & Yüksek, 2013; Laudanski et al., 2015). More recently, the application of template-based classification schemes has been proposed in order to classify activities directly from inertial time series waveforms (Barth et al., 2015; Kluge et al., 2017; Muscillo et al., 2007; Paiyarom et al., 2009). This approach has been shown to be effective when seeking to classify postures or activities commonly performed in daily living, however no standards exist to guide the selection of data from which a classification model should be built for any given application.

Finally, based on the choices made during data collection and pre-processing, an appropriate machine learning based classification model must be selected. The developed classifier must be capable of detecting differences between the features it is provided, regardless of signal variability without being overfit to any specific dataset (Asghari Oskoei & Hu, 2007). For each application therefore, the appropriate classification model must be selected.

The measurement of activities and postures adopted in real-world environments requires significantly different approaches than would be adopted in laboratory settings. Instrumentation and calibration procedures must be minimal and easily performed when seeking to measure exposures in domestic and occupational settings and care must be taken in order to avoid any disruptions or restrictions to the participants in order to capture movements as they would naturally occur. Beyond concerns surrounding instrumentation and data collections, care must be paid when seeking to apply a classification model developed solely on laboratory data to the identification of free-living motions. Gyllensten and Bonomi (2011) sought to evaluate the accuracy of four laboratory-trained classification algorithms at identifying six activities (lying down, sitting/standing, dynamic/transitions, walking, cycling, and running) based on data collected from free-living participants and found a significant decrease in their performance when classifying real-world data. Similarly, Bastian et al. (2015) evaluated the performance of a laboratory-calibrated classification algorithm when identifying a series of activities such as walking, running, cycling, and taking the bus, based on what they coined semi-free-living data. They found significant decreases in classification accuracy compared to cross-validation results using laboratory-based data, but noted the accuracy was improved when free-living data were added to the algorithm training dataset (Bastian et al., 2015). While most classification models for human activity recognition are developed based on predefined postures and activities performed in controlled laboratory-based environments (van Hees, Golubic, Ekelund, & Brage, 2013), movements performed in non-controlled environments tend to exhibit a high degree of variability and overlap between features which are not captured by these laboratory trained models (Bastian et al., 2015; Gyllensten & Bonomi, 2011). Therefore, despite every attempt to increase variability in laboratory-based data by encouraging participants to move as they naturally would, the extent to which classification algorithms developed in laboratory settings can be applied to real-world data remains unclear.

In the present study, we sought to explore the feasibility of extending the developed multi-dimensional Dynamic Time Warping distance-based Nearest Neighbour classification algorithm to identify and measure postures frequently adopted when performing childcare specific activities within a simulated childcare environment. Thus, two versions of the algorithm were developed and tested: the first version was developed using a combination of motion templates

generated from controlled laboratory-based collections (Chapter 5) and continuous motion windows from activities performed in the pseudo-childcare-environment, whereas the second version was developed using only the continuous motion windows from the pseudo-childcare dataset. The outcome of each classification model was compared to the ground truth reference for movement classes obtained by manual labeling of each motion in order to identify successes and potential barriers to applying the proposed approach to the classification of postures in childcare settings.

## 6.2. Participants and Experimental Protocol

Twelve parent and child pairs were recruited from the University of Waterloo faculty and staff as well as from the community through online advertisements, flyers, and word of mouth. Any current injury which prevented an individual from independently caring for their child would result in study exclusion. People of all genders were invited to participate. Additionally, children were required to be capable of sitting independently and to have not yet started kindergarten. While both the parent and their child were present for all data trials, the term *participant* will be used only to refer to the adult, from which measurements were obtained. The all-female participant pool were 33.09 ± 5.34 years of age; 1.65 ± 0.04 m in height; and had a child of age 1.38 ± 0.61 years and height 0.81 ± 0.07 m. Nine participants were right leg dominant while three were left leg dominant. This study was approved by the University of Waterloo Research Ethics Board and informed consent was obtained prior to each collection.

The laboratory in which all collections were conducted was transformed in order to mimic a childcare environment. Therefore, a collection space was established by surrounding the center of the laboratory with child gates, and soft floor coverings were laid down in the center of the collection space. The space was filled with child toys, a small table and two child-sized chairs, a highchair, and a changing table on which were stored books and additional toys. Child cots were stacked above the child gates just outside the collection space. The changing table was anchored to the floor to prevent tipping. This laboratory layout can be seen in Figure *6.1*.

A B

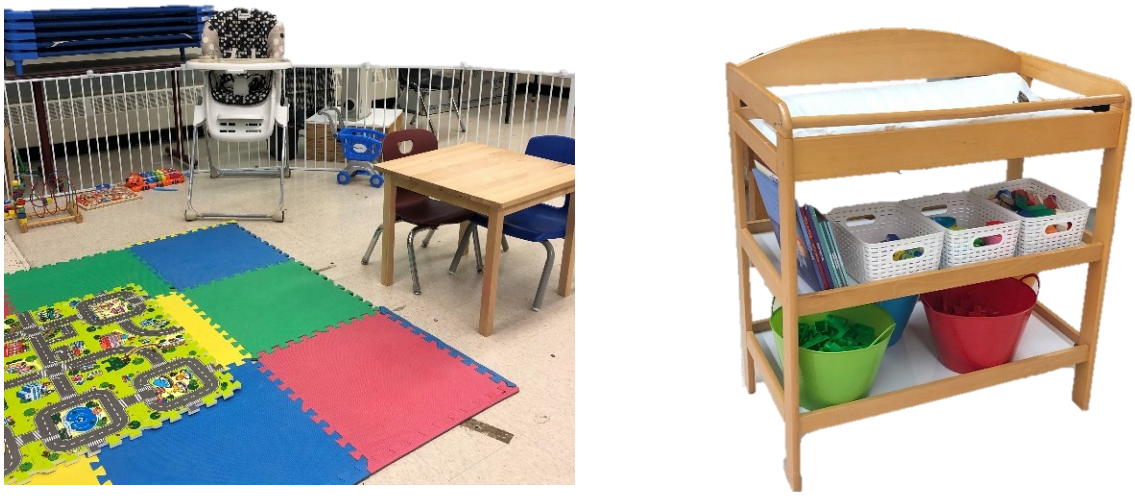

Figure 6.1 Laboratory space configuration mimicking a childcare environment wherein A. the child gates, soft floor coverings, and child furnishings can be seen, and in B. the changing table with additional toys and books is depicted.

Seven wireless IMUs (Cometa WaveTrack Inertial System, Cometa Systems srl., Italy, Gyro.: 1000 deg/s, Acc.: 8 G, sampling frequency: 284 Hz) were attached bilaterally to the superior aspect of participant's feet, the lateral aspects of the participant's shanks and thighs, and over the base of the participant's sacrum. The foot sensors were attached to the participant's footwear, roughly above the superior aspect of the mid-foot, mid-distance between the medial malleolus and the head of the first metatarsal. The shank and thigh sensors were attached roughly one third the distance from the lateral malleoli to the lateral epicondyle of the tibia and roughly midway between the greater trochanter and the lateral epicondyle of the femur respectively. All sensors, save for those on the feet, were affixed, via Velcro®, within foam backed, anti-slip fabric wraps (fabrifoam®, Fabrifoam Products, United States of America) in order to minimize relative movement between the sensors and the segments to which they were attached while eliminating the risk that a sensor could be removed by the child during collections. No specific orientations or positions were enforced when placing the sensors beyond what has been described above.

Following instrumentation, participants were asked to complete a series of calibration postures including 5s of quiet standing, functional hip (isolated upper leg motion through a star-arc hip circumduction (Camomilla et al., 2006)) and functional knee (isolated cyclic flexion/extension motion of the lower leg while the upper leg was held parallel to the ground)

motion trials, a toe touch trial (primarily accomplished through hip flexion while keeping the knees as extended as possible), a heel raise trial (accomplished through ankle plantarflexion, where the raised heel posture was held for one count prior to returning to standing), and a 10 m walking trial at a self-selected pace. Subsequently, participants were asked to engage in different activities (each recorded as a separate movement trial) with their child in randomized order, e.g., building a block castle or reading a book. (A full list of activities can be found in Table 6.1). The children were free to help in the setup of any activity and engage as much or as little with the activity as they wanted. Should the child not want to participate in the activity, the participant was given the choice to either end the activity or to engage with their child in a similar activity in which they would be more interested. Upon the completion of any activity, if their child wanted to continue engaging with the items being used, the participant was instructed to mimic returning them to their place of origin rather than taking them away from their child. Participants were at liberty to indicate when they felt their child was no longer interested in continuing collections, each completing between 5 and 9 activities. A mean of 6.67 ± 0.94 activities were performed across all twelve participants with trial durations ranging between 30 seconds and 11 minutes.

Table 6.1 List of activities performed within the simulated childcare environment.

| Activities | Details |
|---|---|
| Block Castle Building | The participant was instructed to retrieve a box of blocks located on the changing table's higher shelf, and to bring them to the center of the collection space. Participants were then free to engage in playing with the blocks and their child for roughly 5 minutes, then were encouraged to return the blocks to the box and return the box to the changing table shelf where it was originally stored. |
| Floor Level Playing | The participant was instructed to retrieve a box of toy cars from the changing table's higher shelf and to bring this box to the center of the collection space where a series of foam tiles printed with houses and roads had been placed. They were then encouraged to engage in playing with their child and the toy cars for roughly 5 minutes. In this time, if their child preferred to play with wooden puzzles or other floor level toys, they were free to do so. Following the completion of this activity, the participant was asked to return the cars to the box and replace the box on the changing table shelf where it was originally stored. |
| Lego® Block Building and Sorting | The participant was instructed to select a minimum of two baskets from the changing table's lower shelf containing large Lego® blocks of different colours, and to carry these blocks to the center of the collection space. They were then asked to dump out the blocks and play with them and their child for roughly 5 minutes. Subsequently, the participant was asked to engage their child in returning the blocks to the appropriately coloured basket and finally to return the baskets to the changing table shelf. |
| Book Reading | The participant was instructed to select one or two books from the changing table and to carry the book(s) to the center of the collection space. They were given the |

| | |
|---|---|
| | choice whether to sit on the ground or at the child-sized table in order to read to their child. In this time their child was free to sit anywhere they liked (either on the floor, on a child-sized chair, or on their parent's lap). Once they had finished reading or roughly 5 minutes had passed, the participant was asked to return the book(s) to the changing table shelf from which it (they) came. |
| Child Changing | The participant was asked to lift their child onto the changing table and mimic the motions they would perform if they were to change a diaper on their child. Once complete, the participant was asked to return their child to the ground. While not directed, it must be noted that no child was left unattended while on the changing table, and the participant was free to use the changing table safety belt if they so chose. |
| Child Feeding | The participant was asked to retrieve a box from the higher changing table shelf which contained plastic cups, bowls, plates, and cutlery and bring it to the child-sized table in the center of the collection space. Depending on the age of the child, they were then asked to either play with these dishes with their child while seated at the child-sized table, or to lift their child into the highchair provided and play with their child and the dishes on the highchair table. Participants were free to provide a snack for their child at this time if they wished, or simply to pretend to eat using the dishes provided. Following their snack or a period of roughly 5 minutes, the participant was asked to return the dishes to the box, and to wipe down their child and the eating surface with a cloth before taking their child out of the highchair if appropriate and returning the box to the changing table shelf. |
| Child Napping | The participant was asked to pick up a series of four sleeping cots which were stacked on a table just outside the child gates and to arrange them in the center of the collection space. They were then asked to pick up their child and to lay them onto a cot and to interact with them as they lay down. The children were not required to stay laying down, and therefore the participant was free to interact with their child on and around the cots. After a period of approximately 5 minutes, the participant was asked to return the cots to the table from which they were taken. |
| Cleaning Tasks | Participants were asked to take a cloth from the higher shelf of the changing table and wipe down the surface of the changing table and the child-sized table. They were then asked to take a broom and dustpan located behind the changing table and sweep the collection space, then to dispose of the contents of the dustpan into a garbage pail also located behind the changing table before returning both the broom and dustpan to where they were found. (Note that the laboratory floors and soft floor coverings were cleaned prior to every collection and this task was merely performed as a simulation rather than truly cleaning the space.) |

Video recordings were synchronously captured using a Logitech C270 HD webcam for all activities. Recordings were used for data labeling, against which the performance of the classification algorithms would be evaluated.

## 6.3. Sensor Signal Processing and Manual Data Labeling

To match the units of measure of the Xsens MTw Awinda inertial sensors used previously in the development of the measurement and classification algorithms in Chapter 4 and Chapter 5, the raw acceleration signals from the Cometa WaveTrack inertial sensors used in this study were

converted from G (the gravitational force equivalent) to $m/s^2$, and the raw Cometa gyroscopic signals were converted from deg/s to rad/s. These data were subsequently processed using the CSKA and ISSA algorithms presented in Chapter 4 in order to define the joint position and joint center of rotation vectors by which each sensor could be aligned to the segment on which it was attached. The calibration data for the knee consisted of a combination of sensor signals from the 10 m walking trial and the functional knee and hip movements. For the ankle and hip, these same data were additionally combined with sensor signals from the toe-touching movement. For the ankle, the heel raise trial was selected for verification during the iterative process of solving for the joint axis and center of rotation, while for the hip, the toe-touching trial was selected. Once the *j* and *o* vectors, representing the joint axis and center of rotation, had been calculated, they were then used to rotate each sensor's gyroscope and accelerometer signals into the joint CSs in order to solve for joint flexion-extension at the ankle, knee, and hip for each motion trial. For the knee, angle estimates were calculated based on the equations presented in Subsection 4.3 while the ankle and hip angles were calculated based on the equations presented in Subsection 4.6. Given the extended duration of each motion trial collected in this study, efforts to mitigate the errors associated with gyroscopic drift over time were implemented, such that each joint angle was calculated over 60 second increments, zeroed to the final value of the previous time increment, and concatenated across the duration of each trial. Finally, joint angle estimates for each trial were linearly detrended in order to mitigate any remaining effects of drift on these data.

Using the video recordings, each performed movement was labeled with one of eleven movement labels presented in Chapter 5: HS (heels-up squatting), FS (flatfoot squatting), DK (dorsiflexed kneeling), PK (plantarflexed kneeling), CCS (sitting on a child sized chair), SK (single arm supported kneeling and double arm supported kneeling), CLS (crossed leg sitting), SS (side sitting and side leaning to the left or the right), STP (stooping), STD (standing), and WLK (walking). The adult chair sitting label was not assigned in this dataset as no adult sized chairs were provided during collections. Due to the limited framerate resolution of the video data recorded, only one label per second could be attributed to the sensor data.

A sliding window technique was applied to segment the pseudo-childcare data into continuous movement windows; wherein 2 second windows (568 samples) with a consecutive

overlap of 1 second between each were derived. The decision to use this window length was motivated by the resolution of the labels and the frequency in which postural changes were observed within the dataset.

Based on the dynamic nature of caring for children and the variability in postures observed throughout this study, it became apparent that postures adopted in an occupational setting would likely not be performed in isolation (e.g., consistently descending and ascending using the same posture). Given that individuals were often observed to descend into a high flexion posture, change postures while in high flexion, and subsequently ascend from the posture employing a separate movement modality, phase of motion labels were added to the movement labels to distinguish each posture adopted during descent, static high flexion, and ascent motions. When two different knee straining movements occurred within a two second window, the movements were labeled in the order they occurred. When one knee straining movement was preceded or followed by walking or standing, the knee straining movement would be listed first in the label. All movement labels identified for this dataset can be found in Appendix H.

Similarly, the templates previously created for each of the movements in Chapter 5 save standing and walking, were further divided in order to create templates for each posture and phase of motion (e.g., the HS template was divided into three new templates: HS_Descent, HS_Static, and HS_Ascent). The start and end point of each template were segmented as described in Subsection 5.3. The end of descent and the start of ascent were both manually identified based on the right knee flexion-extension angle and served to distinguish the start and end of the static phase. Therefore, the start of the static phase was identified as the first frame indicating no perceivable change in joint angle following descent and end of the static phase was identified as the last frame of no perceivable change in joint angle preceding ascent. Combined movement templates were additionally created to represent every possible movement transition captured by these laboratory-based movements (e.g., standing followed by HS descent or HS descent followed by HS ascent). The combination of all movement labels created based on templates along with those created from the dataset herein collected can be found in Appendix G.

## 6.4. Multi-Dimensional Dynamic Time Warping Distance-Based *k*-Nearest Neighbour Classifier

The following section will describe the development and testing of four mDTW *k*NN models for the classification of postures adopted during the childcare specific activities within a simulated childcare environment. The signal processing framework for the testing and validation of these models can be seen in Figure *6.4*.

### 6.4.1. Division of Data for Model Development, Testing, and Validation

Continuous movement windows from a subset of 10 randomly selected participants were allocated to the algorithm building datasets (comprised of a larger dataset for development and a smaller dataset for testing) while the remaining 2 participants' data were withheld for model validation.

#### 6.4.1.1. Model *A* – Developed with a Combination of Laboratory-Based Templates and Continuous Windows of Pseudo-Childcare Movements

The first classification model developed used the template data previously generated for each childcare-inspired motion, now divided by phase, in addition to the continuous movement windows generated from the pseudo-childcare activity trials. Neither the templates nor the movement windows were scale normalized, however all data was time normalized to 101 points. The workflow for this mDTW *k*NN model can be found in Figure 6.2.

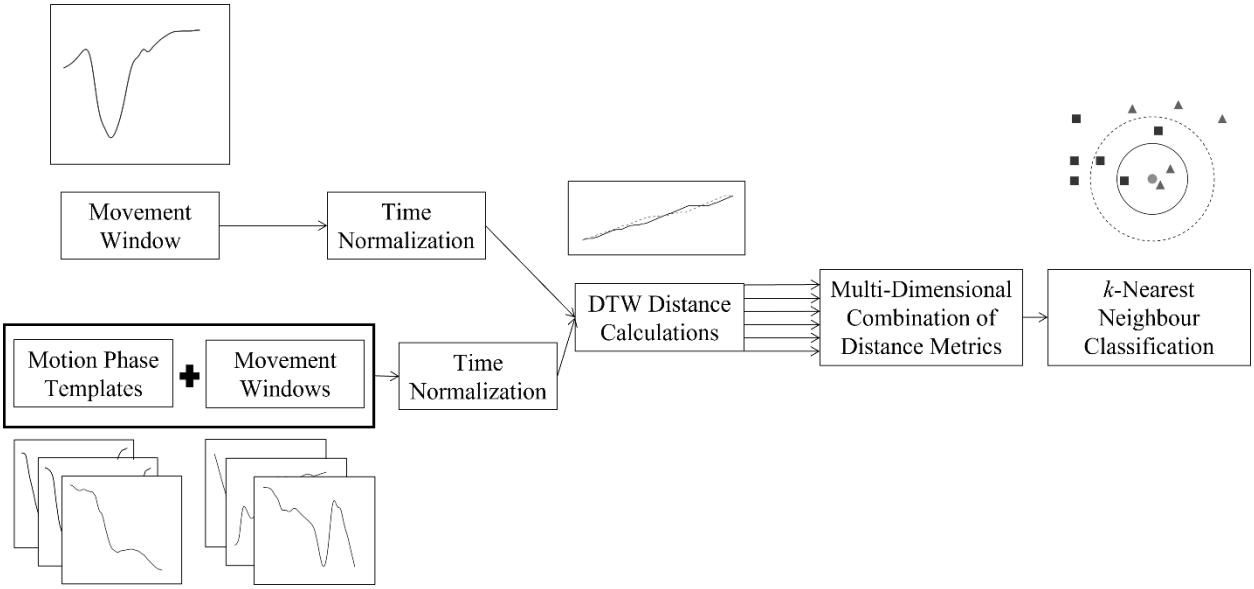


Figure 6.2 Signal processing workflow for the mDTW kNN classification model A. The development dataset for this model included both normalized templates for each posture and phase of motion generated from postures performed in isolation in a laboratory setting as well as continuous movement windows generated during childcare specific activities within a simulated childcare environment. The DTW distances for each joint were calculated between a single time normalized movement window and each template and window within the model development dataset. Once each movement window had been compared to all development data for the corresponding joint, the DTW distances were combined across joints using custom weighting factors to ultimately determine the movement class based on the mDTW distance.

### 6.4.1.2. Model *B* – Developed with only Continuous Windows of Pseudo-Childcare Movements

The second classification model developed utilized only the continuous movement windows generated from the pseudo-childcare activity trials collected in this study to populate the model development dataset. Again, no scale normalization was performed on these data windows however each window was normalized to 101 datapoints. The workflow for this mDTW *k*NN model can be found in Figure 6.3.

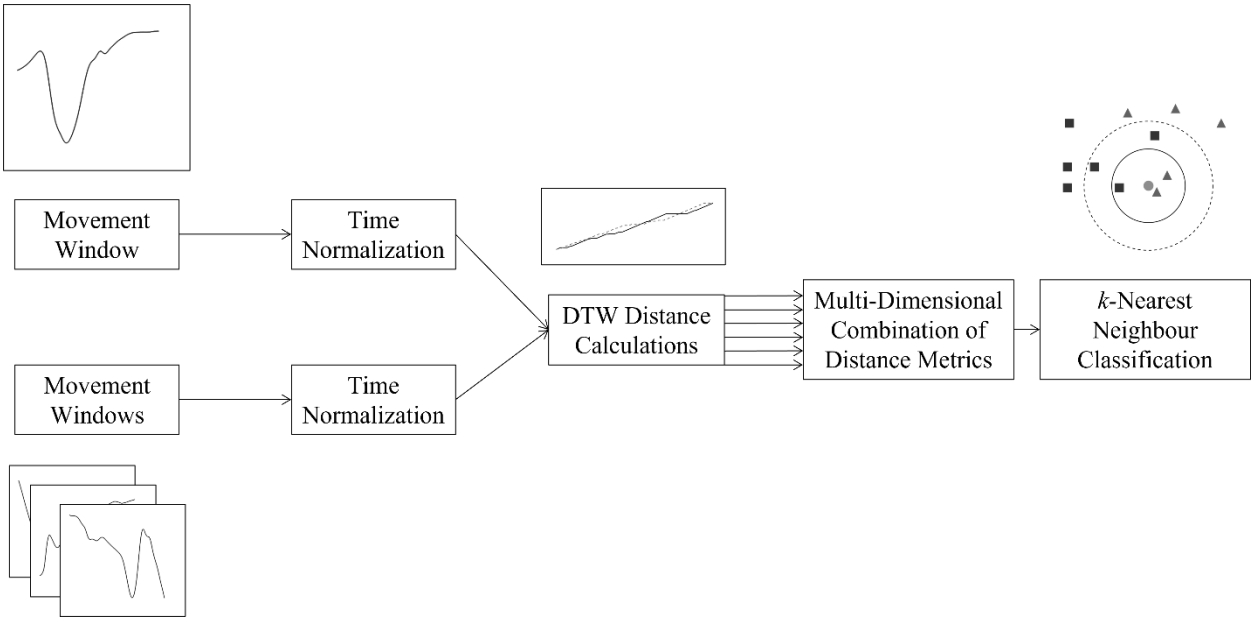


Figure 6.3 Signal processing workflow for the mDTW kNN classification model B. The development dataset for this model included only the continuous movement windows generated during childcare specific activities within a simulated childcare environment collected as part of this study. The DTW distances for each joint were calculated between a single time normalized movement window and each movement window within the model development dataset. Once each movement window had been compared to all development data for the corresponding joint, the DTW distances were combined across joints using custom weighting factors to ultimately determine the movement class based on the mDTW distance.

#### 6.4.1.3. Data Division Strategy *a* – Stratified Random Partitioning

A holdout validation method was employed to develop and test the classification models, such that stratified random partitioning was employed to divide the continuous movement windows from each trial. 80% of the data windows were randomly allocated as development data while the remaining 20% were withheld for testing. In the case of model *A*, all movement templates were combined with the 80% in order to form the development dataset.

#### 6.4.1.4. Data Division Strategy *b* – Partitioning of Continuous Windows from a Single Trial

In order to test the models on data which more closely resembled the datasets to be classified during model validation and ultimately the datasets which would be collected from true childcare environments, this second data division model involved the partitioning of all continuous movement windows from a single randomly selected childcare activity trial of a single participant for testing. The remaining movement windows, combined with all motion templates in the case of model *A*, were allocated for model development.

#### 6.4.1.5. Validation Dataset

All continuous movement windows from the two participants excluded from model development and testing were assigned to the model validation dataset. Validation of each model was performed on the first movement trial from this dataset, containing data from the Block Castle Building activity performed by one of the two participants, as well as on the dataset as a whole.

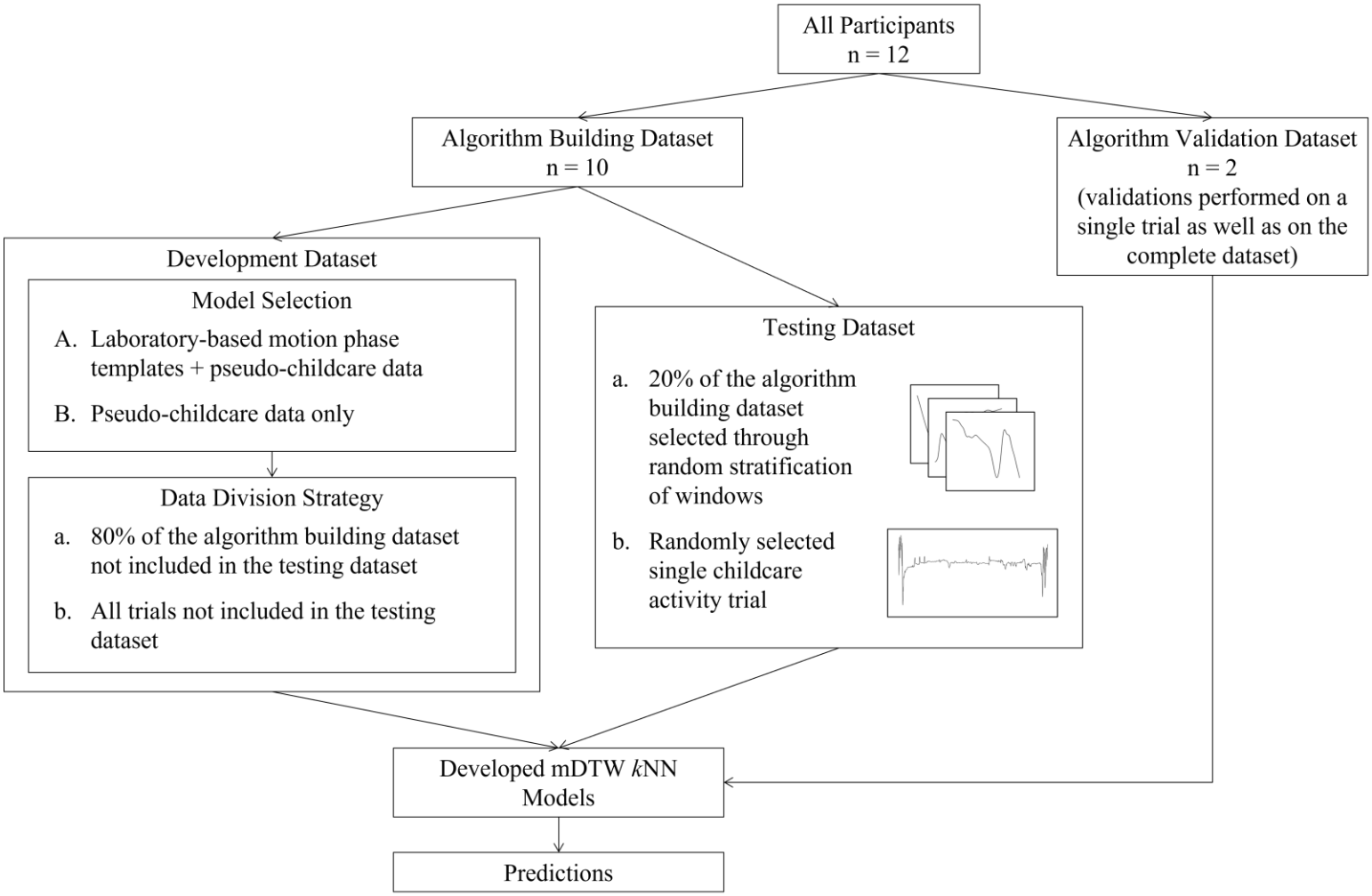


Figure 6.4 Signal processing workflow for the division of data collected during all pseudo-childcare activities into the algorithm development, testing, and validation datasets. The testing datasets for each model were determined based on the division strategy employed, such that in division strategy **a**) 20% of the windows, as selected through random data stratification, were assigned to the testing dataset, while in division strategy **b**) all windows from a single randomly selected childcare activity trial were assigned to the testing dataset. Each model was validated using both a single trial from the algorithm validation dataset as well as the complete validation dataset.

### 6.4.2. mDTW *k*-Nearest Neighbour Algorithm Development and Parameter Tuning

All appropriate templates and movement windows were combined with their respective motion labels in order to create the algorithm building datasets for the development of four *k*NN 5-fold cross-validated classification models (based on the combination of models *A* and *B* with data division strategies *a* and *b*). The labeled feature spaces from which classifications were made therefore included a total of 159 possible movement classes in model *A* and 149 possible classes in model *B* (due to the lack of adult chair sitting within the pseudo-childcare motion trials). All movement class labels for models *A* and *B* can be found in Appendix G and Appendix H.

The development and testing datasets were relied upon for iterative parameter tuning based on each data division strategy, acknowledging that this tuning might result in overfitting of the models to the testing data provided. Following the initial classifier development, values of *k* were varied between 1 and 21 with a step size of 2 to determine a value of *k* which would minimize the cross-validated losses. These permutations yielded a value of $k = 1$ for data division strategy *a* and a value of $k = 17$ for data division strategy *b*.

Subsequently, the weighting parameters used in the mDTW distance metric calculation were optimized using each cross-validated model. Each weighting coefficient was simultaneously varied in increments of 0.05 between 0.2 and 1. The final mDTW distance for data division strategy *a* was calculated using eq. (6.1), as follows:

$$D_{mDTW\_a} = 0.4 \cdot D_{LAnkle} + 0.35 \cdot D_{RAnkle} + 0.5 \cdot D_{LKnee} + 0.95 \cdot D_{RKnee} + 0.2 \cdot D_{LAHip} + 0.45 \cdot D_{RHip}. \quad (6.1)$$

while the mDTW distance for data division strategy *b* was calculated using eq. (6.2), as follows:

$$D_{mDTW\_b} = 0.4 \cdot D_{LAnkle} + 0.35 \cdot D_{RAnkle} + 0.4 \cdot D_{LKnee} + 0.95 \cdot D_{RKnee} + 0.6 \cdot D_{LAHip} + 0.8 \cdot D_{RHip}. \quad (6.2)$$

Finally, the size of the warping window was iterated by 5 between 5 and 100 frames of data in order to find the value which minimized classification losses. For all models, a value of 50 was found to be optimal based on these iterative tests.

Once all parameters had been tuned, the final classification models were developed and subsequently evaluated using the data reserved for testing and validation in order to determine each model's performance when identifying movements from individuals included in the model development (testing dataset) as well as from novel participants (validation dataset).

### 6.4.3. Classification Error Measurement

The performance of each classification model using each data division strategy was quantified as the ratio of correct classifications to the total number of classifications. Measures of sensitivity and specificity were additionally calculated for each movement class through eq. (5.9) and eq. (5.10).

It is noted that each movement class was not equally represented in the algorithm datasets given the disparity in movement adoption within the pseudo-childcare collections, therefore the balanced accuracy for each movement class was additionally calculated, using eq. (5.11). All classifications and analyses of error were completed using Matlab 9.13 (The Mathworks, Release R2022b, Natick, MA, USA).

## 6.5. Results

Classification accuracies achieved when identifying postures adopted during childcare specific activities performed within a simulated childcare environment on data from participants on which the four mDTW *k*NN models had (testing) and had not (validation) been developed are presented in Table 6.2. When evaluating the performance of each model using the movement windows withheld for testing, model *Bb* (which included only data windows herein collected and was tested on continuous movement windows corresponding to one trial from a participant included in the model development) was found to outperform all other models, with an overall classification accuracy of 80.79%. When analysing the predictions of this model (as can be seen in the confusion matrix provided in Appendix I), the high classification accuracy can primarily be attributed to the successful identification of static crossed leg sitting. All other movements, save one instance of descent to static crossed leg sitting were incorrectly identified. Therefore, it is believed that the classification accuracy of this model is highly volatile and would be highly dependent on the motions performed in the trial being similar to other data included in the *k*NN

feature space. This belief was further reinforced through the classification of a single trial performed by a novel participant (Table 6.2 Validation Data – Single Trial), where the accuracies of models *Ab* and *Bb* were nearly identical.

Table 6.2 Model specific accuracies achieved in the classification of motions adopted when caring for and interacting with a child within a simulated childcare environment. All values are expressed as percentages. All models relied upon a multi-dimensional Dynamic Time Warping distance-based k-Nearest Neighbour algorithm (mDTW kNN) algorithm for movement classification. Models Aa and Ab were developed using a combination of laboratory-based templates and continuous windows of pseudo-childcare movements. Models Ba and Bb were developed using only the continuous windows of pseudo-childcare movements. Models Aa and Ba were developed based on 80% of the continuous movement windows from 10 participants' data and tested on the remaining 20%, separated using stratified random partitioning. For models Ab and Bb, all continuous movement windows from a single trial of a single participant were partitioned for testing, while the remaining data windows were all employed in model development and therefore populated the NN feature space. Validation for all models was performed on a single trial of a single participant as well as on all windows of all trials performed by the novel two participants excluded from model development.

| Model & Data Division Strategy | Test Data - Single Trial | Validation Data - Single Trial | Validation Dataset |
|---|---|---|---|
| Model Aa | 42.22 | 16.53 | 26.63 |
| Model Ba | 42.50 | 16.25 | 26.66 |
| Model Ab | 35.37 | 4.20 | 23.89 |
| Model Bb | 80.79 | 4.48 | 23.99 |

Given the vast number of potential movement classes within both Models *A* and *B*, the summed sensitivity-based confusion matrices for each model obtained based on predictions made when classifying the appropriate testing data are shown in Table *6.3*, wherein the target and output classes have been reduced to the movements alone by combining all phases of a particular movement (for example dorsiflexed kneeling (DK) represents DK Ascent, DK Ascent to Standing, DK Ascent to Walking, DK Descent, DK Descent to Ascent, DK Descent to Side Sitting Static, DK Descent to Static, DK Static to Plantarflexed Kneeling Static, DK Static to Side Sitting Static, DK Static, DK Static to Ascent, DK Static to Supported Kneeling Ascent, DK Static to Supported Kneeling Static, Standing to DK Descent, Stoop to DK Descent, and Walking to DK Descent). The classification performance of these same models when identifying movement classes from the validation dataset (novel subject data) are shown in the sensitivity-based confusion matrices presented in Table 6.4. The specificity and balanced accuracy values for all models during testing and validation have been presented in Table 6.5 and Table 6.6 respectively.

Table 6.3 Sensitivity-based confusion matrices for the classification of continuous movement windows of testing data containing motions performed while completing pseudo-childcare activities in a simulated childcare environment. All values are expressed as percentages. All models relied upon a multi-dimensional Dynamic Time Warping distance-based k-Nearest Neighbour algorithm (mDTW kNN) algorithm for movement classification. Models Aa (Table **A**) and Ab (Table **C**) were developed using a combination of laboratory-based templates and continuous windows of pseudo-childcare movements. Models Ba (Table **B**) and Bb (Table **D**) were developed using only the continuous windows of pseudo-childcare movements. Models Aa and Ba were developed based on 80% of the continuous movement windows from 10 participants' data and tested on the remaining 20%, separated using stratified random partitioning. For models Ab and Bb, all continuous movement windows from a single trial of a single participant were partitioned for testing, while the remaining data windows were all employed in model development and therefore populated the NN feature space. Bolded cells denote correct classifications. All movement classes have been summed and expressed as only the motion performed in the first second of each window, as follow: heels-up squatting (HS), flatfoot squatting (FS), dorsiflexed kneeling (DK), plantarflexed kneeling (PK), sitting on an adult sized chair(ACS), sitting on a child sized chair (CCS), single arm supported kneeling and double arm supported kneeling (SS), crossed leg sitting (CLS), side sitting and side leaning to the left or the right (SS), stooping (STP), standing (STD), and walking (WLK). *Target Class represents the correct class of each template or sequence. **Output Class represents the class predicted by the classifier.

**A**

Model *Aa*

*Templates: Laboratory based motion phase templates and pseudo-childcare data*
*Test data: 20% of pseudo-childcare data selected through random stratification*

| Target Class* | CLS | STD | HS | WLK | SK | PK | SS | STP | DK | CCS | FS |
|---|---|---|---|---|---|---|---|---|---|---|---|
| CLS | **48.2** | 2.3 | 0.0 | 1.0 | 2.3 | 4.0 | 25.4 | 1.9 | 6.8 | 7.8 | 0.5 |
| STD | 2.8 | **35.0** | 0.7 | 8.3 | 0.0 | 11.1 | 11.8 | 19.4 | 5.6 | 4.2 | 1.4 |
| HS | 26.7 | 1.7 | **30.0** | 10.0 | 1.7 | 8.3 | 18.3 | 1.7 | 0.0 | 1.7 | 0.0 |
| WLK | 9.0 | 11.4 | 1.2 | **28.6** | 2.0 | 4.5 | 6.9 | 26.5 | 5.7 | 1.6 | 2.4 |
| SK | 15.5 | 1.5 | 0.6 | 5.9 | **32.5** | 7.7 | 14.2 | 8.7 | 6.5 | 5.9 | 0.9 |
| PK | 12.8 | 0.3 | 0.0 | 0.6 | 7.1 | **42.4** | 11.6 | 2.7 | 7.7 | 13.4 | 1.5 |
| SS | 11.7 | 0.8 | 0.1 | 0.9 | 3.0 | 3.8 | **72.2** | 1.5 | 2.3 | 3.0 | 0.6 |
| STP | 4.5 | 5.3 | 3.3 | 16.0 | 1.6 | 9.4 | 7.0 | **41.0** | 5.7 | 2.9 | 3.3 |
| DK | 4.6 | 0.0 | 0.0 | 1.2 | 4.6 | 7.0 | 6.7 | 12.5 | **56.3** | 4.9 | 2.1 |
| CCS | 27.8 | 1.2 | 0.0 | 0.6 | 3.0 | 0.6 | 5.9 | 11.8 | 3.0 | **46.2** | 0.0 |
| FS | 1.8 | 1.8 | 7.0 | 1.8 | 0.0 | 7.0 | 10.5 | 10.5 | 14.0 | 1.8 | **43.9** |

Output Class**

**B**

Model *Ba*
*Templates: Pseudo-childcare data*
*Test data: 20% of pseudo-childcare data selected through random stratification*

| Target Class | Output Class: CLS | STD | HS | WLK | SK | PK | SS | STP | DK | CCS | FS |
|---|---|---|---|---|---|---|---|---|---|---|---|
| CLS | **48.4** | 2.3 | 0.0 | 1.0 | 2.3 | 4.0 | 25.3 | 1.8 | 6.8 | 7.8 | 0.5 |
| STD | 2.8 | **35.0** | 0.7 | 8.3 | 0.0 | 11.1 | 11.8 | 19.4 | 5.6 | 4.2 | 1.4 |
| HS | 26.7 | 1.7 | **31.7** | 10.0 | 1.7 | 8.3 | 18.3 | 1.7 | 0.0 | 0.0 | 0.0 |
| WLK | 9.0 | 11.4 | 1.2 | **28.6** | 2.0 | 4.5 | 6.9 | 26.5 | 5.7 | 1.6 | 2.4 |
| SK | 16.1 | 1.5 | 1.2 | 5.9 | **33.1** | 8.0 | 15.2 | 5.3 | 6.8 | 5.9 | 0.9 |
| PK | 13.1 | 0.3 | 0.0 | 0.6 | 7.1 | **43.3** | 11.6 | 1.8 | 7.7 | 13.4 | 1.2 |
| SS | 11.8 | 0.8 | 0.3 | 1.0 | 3.2 | 4.1 | **71.9** | 1.1 | 2.2 | 3.3 | 0.5 |
| STP | 4.5 | 5.3 | 3.3 | 16.0 | 1.6 | 9.4 | 7.0 | **41.0** | 5.7 | 2.9 | 3.3 |
| DK | 4.6 | 0.0 | 0.0 | 1.2 | 4.6 | 7.0 | 7.0 | 6.4 | **56.9** | 10.1 | 2.1 |
| CCS | 27.8 | 1.2 | 0.0 | 0.6 | 3.0 | 0.6 | 10.1 | 3.6 | 7.1 | **46.2** | 0.0 |
| FS | 1.8 | 1.8 | 7.0 | 1.8 | 0.0 | 7.0 | 10.5 | 10.5 | 14.0 | 1.8 | **43.9** |

**C**

Model *Ab*
*Templates: Laboratory based motion phase templates and pseudo-childcare data*
*Test data: Randomly selected single continuous trial from pseudo-childcare data*

| Target Class | Output Class: FS | CLS | WLK | STD | DK | SS | ACS | HS | SK | CCS | STP |
|---|---|---|---|---|---|---|---|---|---|---|---|
| FS | **0.0** | 57.1 | 28.6 | 0.0 | 14.3 | 0.0 | 0.0 | 0.0 | 0.0 | 0.0 | 0.0 |
| CLS | 0.0 | **38.7** | 0.0 | 49.8 | 0.0 | 5.1 | 0.9 | 0.5 | 0.5 | 4.1 | 0.5 |
| WLK | 0.0 | 0.0 | **0.0** | 25.0 | 50.0 | 25.0 | 0.0 | 0.0 | 0.0 | 0.0 | 0.0 |
| STD | 0.0 | 100.0 | 0.0 | **0.0** | 0.0 | 0.0 | 0.0 | 0.0 | 0.0 | 0.0 | 0.0 |
| DK | 0.0 | 0.0 | 0.0 | 0.0 | **0.0** | 0.0 | 0.0 | 0.0 | 0.0 | 0.0 | 0.0 |
| SS | 0.0 | 0.0 | 0.0 | 0.0 | 0.0 | **0.0** | 0.0 | 0.0 | 0.0 | 0.0 | 0.0 |
| ACS | 0.0 | 0.0 | 0.0 | 0.0 | 0.0 | 0.0 | **0.0** | 0.0 | 0.0 | 0.0 | 0.0 |
| HS | 0.0 | 0.0 | 0.0 | 0.0 | 0.0 | 0.0 | 0.0 | **0.0** | 0.0 | 0.0 | 0.0 |
| SK | 0.0 | 0.0 | 0.0 | 0.0 | 0.0 | 0.0 | 0.0 | 0.0 | **0.0** | 0.0 | 0.0 |
| CCS | 0.0 | 0.0 | 0.0 | 0.0 | 0.0 | 0.0 | 0.0 | 0.0 | 0.0 | **0.0** | 0.0 |
| STP | 0.0 | 0.0 | 0.0 | 0.0 | 0.0 | 0.0 | 0.0 | 0.0 | 0.0 | 0.0 | **0.0** |

**D**

Model *Bb*

*Templates: Pseudo-childcare data*

*Test data: Randomly selected single continuous trial from pseudo-childcare data*

| Target Class | FS | CLS | WLK | STD | DK | SS | SK | CCS |
|---|---|---|---|---|---|---|---|---|
| FS | **0.0** | 57.1 | 14.3 | 0.0 | 14.3 | 14.3 | 0.0 | 0.0 |
| CLS | 0.0 | **87.0** | 0.0 | 0.0 | 0.0 | 6.0 | 1.8 | 5.5 |
| WLK | 0.0 | 0.0 | **0.0** | 0.0 | 50.0 | 50.0 | 0.0 | 0.0 |
| STD | 0.0 | 100.0 | 0.0 | **0.0** | 0.0 | 0.0 | 0.0 | 0.0 |
| DK | 0.0 | 0.0 | 0.0 | 0.0 | **0.0** | 0.0 | 0.0 | 0.0 |
| SS | 0.0 | 0.0 | 0.0 | 0.0 | 0.0 | **0.0** | 0.0 | 0.0 |
| SK | 0.0 | 0.0 | 0.0 | 0.0 | 0.0 | 0.0 | **0.0** | 0.0 |
| CCS | 0.0 | 0.0 | 0.0 | 0.0 | 0.0 | 0.0 | 0.0 | **0.0** |

Output Class

Table 6.4 Sensitivity-based confusion matrices for the classification of continuous movement windows of validation data containing motions performed while completing pseudo-childcare activities in a simulated childcare environment. All values are expressed as percentages. All four models relied upon a multi-dimensional Dynamic Time Warping distance-based k-Nearest Neighbour algorithm (mDTW kNN) algorithm for movement classification. Bolded cells denote correct classifications. All movement classes have been summed and expressed as only the motion performed in the first second of each window, as follow: heels-up squatting (HS), flatfoot squatting (FS), dorsiflexed kneeling (DK), plantarflexed kneeling (PK), sitting on an adult sized chair(ACS), sitting on a child sized chair (CCS), single arm supported kneeling and double arm supported kneeling (SS), crossed leg sitting (CLS), side sitting and side leaning to the left or the right (SS), stooping (STP), standing (STD), and walking (WLK). *Target Class represents the correct class of each template or sequence. **Output Class represents the class predicted by the classifier.

**A**

Model *Aa*

*Validation on all movement windows from two participants withheld from the algorithm building dataset*

| Target Class* | STD | WLK | HS | CLS | SS | STP | FS | DK | PK | SK | CCS |
|---|---|---|---|---|---|---|---|---|---|---|---|
| STD | **3.9** | 25.5 | 1.0 | 25.5 | 21.6 | 19.6 | 0.0 | 0.0 | 0.0 | 2.9 | 0.0 |
| WLK | 6.3 | **21.0** | 2.5 | 9.4 | 19.4 | 19.4 | 5.6 | 3.1 | 3.1 | 3.8 | 6.9 |
| HS | 1.0 | 2.9 | **25.4** | 6.3 | 9.3 | 0.5 | 6.8 | 7.8 | 14.6 | 21.0 | 4.4 |
| CLS | 5.9 | 2.4 | 0.4 | **33.2** | 32.9 | 6.5 | 0.3 | 0.4 | 0.4 | 2.1 | 15.4 |
| SS | 12.9 | 9.4 | 1.3 | 18.5 | **34.3** | 14.6 | 0.4 | 3.0 | 2.1 | 0.4 | 3.0 |
| STP | 11.6 | 14.7 | 1.9 | 8.4 | 15.9 | **25.9** | 3.4 | 0.9 | 7.2 | 4.1 | 5.9 |
| FS | 0.0 | 6.6 | 14.8 | 4.9 | 14.8 | 0.0 | **24.6** | 0.0 | 4.9 | 29.5 | 0.0 |
| DK | 0.8 | 0.0 | 7.2 | 0.8 | 9.6 | 0.8 | 0.0 | **42.4** | 5.6 | 24.0 | 8.8 |
| PK | 1.4 | 1.4 | 0.0 | 27.8 | 16.7 | 4.2 | 4.2 | 6.9 | **15.3** | 4.2 | 18.1 |
| SK | 0.0 | 0.0 | 0.3 | 17.6 | 10.1 | 7.8 | 7.8 | 2.0 | 14.3 | **26.1** | 14.0 |
| CCS | 0.9 | 0.9 | 0.0 | 21.5 | 15.2 | 0.9 | 0.0 | 0.0 | 9.7 | 5.7 | **45.3** |

Output Class**

**B**

Model *Ba*

*Validation on all movement windows from two participants withheld from the algorithm building dataset*

| Target Class | | | | | | | | | | | | |
|---|---|---|---|---|---|---|---|---|---|---|---|---|
| | STD | **3.9** | 25.5 | 1.0 | 25.5 | 21.6 | 19.6 | 0.0 | 0.0 | 0.0 | 2.9 | 0.0 |
| | WLK | 6.3 | **21.0** | 1.9 | 10.0 | 19.4 | 19.4 | 5.6 | 3.1 | 3.1 | 4.4 | 6.3 |
| | HS | 1.0 | 2.9 | **23.9** | 4.4 | 9.3 | 0.5 | 7.8 | 10.2 | 15.6 | 18.0 | 6.3 |
| | CLS | 5.7 | 2.5 | 0.4 | **33.4** | 32.8 | 6.2 | 0.3 | 0.5 | 0.6 | 1.8 | 15.8 |
| | SS | 12.9 | 9.4 | 1.3 | 18.5 | **34.3** | 14.6 | 0.4 | 3.0 | 2.1 | 0.4 | 3.0 |
| | STP | 11.9 | 14.7 | 1.3 | 8.4 | 16.3 | **25.6** | 3.8 | 0.9 | 7.2 | 4.1 | 5.9 |
| | FS | 0.0 | 6.6 | 26.2 | 4.9 | 14.8 | 0.0 | **31.1** | 0.0 | 4.9 | 11.5 | 0.0 |
| | DK | 0.8 | 0.0 | 12.8 | 1.6 | 0.8 | 0.8 | 4.0 | **42.4** | 9.6 | 18.4 | 8.8 |
| | PK | 1.4 | 1.4 | 6.9 | 18.1 | 16.7 | 4.2 | 0.0 | 6.9 | **15.3** | 11.1 | 18.1 |
| | SK | 0.0 | 0.0 | 5.0 | 15.7 | 12.3 | 0.3 | 4.2 | 2.0 | 14.8 | **28.0** | 17.6 |
| | CCS | 0.9 | 0.9 | 0.0 | 21.5 | 15.2 | 0.9 | 0.0 | 0.0 | 9.7 | 5.7 | **45.3** |
| | | STD | WLK | HS | CLS | SS | STP | FS | DK | PK | SK | CCS |

Output Class

**C**

Model *Ab*

*Validation on all movement windows from two participants withheld from the algorithm building dataset*

| Target Class | | | | | | | | | | | | | |
|---|---|---|---|---|---|---|---|---|---|---|---|---|---|
| | STD | **6.9** | 28.4 | 0.0 | 25.5 | 21.6 | 9.8 | 0.0 | 2.0 | 0.0 | 2.9 | 2.9 | 0.0 |
| | WLK | 7.5 | **29.0** | 1.3 | 16.9 | 18.8 | 8.1 | 0.6 | 1.3 | 3.8 | 1.9 | 10.6 | 0.6 |
| | HS | 1.5 | 4.9 | **16.6** | 2.4 | 13.2 | 1.0 | 0.5 | 1.5 | 39.5 | 13.2 | 3.4 | 2.4 |
| | CLS | 3.5 | 2.5 | 0.3 | **24.5** | 35.7 | 2.4 | 0.4 | 1.0 | 1.0 | 0.3 | 28.1 | 0.1 |
| | SS | 13.3 | 3.9 | 0.0 | 17.2 | **48.5** | 3.0 | 0.0 | 0.0 | 1.3 | 5.6 | 7.3 | 0.0 |
| | STP | 6.9 | 17.8 | 0.9 | 12.8 | 18.8 | **13.1** | 0.3 | 8.1 | 9.7 | 1.9 | 9.1 | 0.6 |
| | FS | 1.6 | 4.9 | 4.9 | 1.6 | 18.0 | 0.0 | **0.0** | 8.2 | 19.7 | 27.9 | 3.3 | 9.8 |
| | DK | 0.0 | 1.6 | 3.2 | 1.6 | 0.8 | 0.0 | 0.0 | **19.2** | 39.2 | 7.2 | 14.4 | 12.8 |
| | PK | 2.8 | 0.0 | 8.3 | 22.2 | 20.8 | 1.4 | 0.0 | 5.6 | **9.7** | 1.4 | 23.6 | 4.2 |
| | SK | 0.3 | 0.0 | 2.0 | 19.9 | 6.7 | 0.6 | 3.9 | 0.3 | 17.9 | **1.1** | 47.3 | 0.0 |
| | CCS | 0.0 | 2.9 | 0.0 | 10.6 | 9.5 | 0.0 | 0.0 | 0.0 | 5.4 | 3.4 | **68.2** | 0.0 |
| | ACS | 0.0 | 0.0 | 0.0 | 0.0 | 0.0 | 0.0 | 0.0 | 0.0 | 0.0 | 0.0 | 0.0 | **0.0** |
| | | STD | WLK | HS | CLS | SS | STP | FS | DK | PK | SK | CCS | ACS |

Output Class

**D**

Model *Bb*

*Validation on all movement windows from two participants withheld from the algorithm building dataset*

| Target Class | STD | WLK | HS | CLS | SS | STP | FS | DK | PK | SK | CCS |
|---|---|---|---|---|---|---|---|---|---|---|---|
| STD | **8.8** | 27.5 | 0.0 | 24.5 | 21.6 | 9.8 | 0.0 | 2.0 | 0.0 | 2.9 | 2.9 |
| WLK | 8.8 | **27.0** | 0.0 | 16.9 | 21.3 | 8.1 | 0.0 | 1.3 | 4.4 | 1.9 | 10.6 |
| HS | 1.5 | 4.4 | **15.1** | 2.4 | 13.2 | 1.5 | 1.5 | 0.5 | 42.4 | 13.7 | 3.9 |
| CLS | 2.5 | 2.3 | 0.5 | **25.2** | 35.8 | 2.1 | 0.4 | 0.9 | 0.9 | 0.5 | 28.7 |
| SS | 13.7 | 3.4 | 0.0 | 18.5 | **47.6** | 2.6 | 0.0 | 0.0 | 1.3 | 5.6 | 7.3 |
| STP | 6.6 | 17.2 | 0.9 | 13.1 | 19.4 | **12.2** | 0.3 | 8.4 | 10.6 | 1.6 | 9.7 |
| FS | 0.0 | 6.6 | 18.0 | 1.6 | 18.0 | 0.0 | **0.0** | 3.3 | 19.7 | 29.5 | 3.3 |
| DK | 0.0 | 1.6 | 16.8 | 1.6 | 0.8 | 0.0 | 0.0 | **19.2** | 40.0 | 5.6 | 14.4 |
| PK | 2.8 | 0.0 | 6.9 | 20.8 | 26.4 | 0.0 | 0.0 | 5.6 | **9.7** | 2.8 | 25.0 |
| SK | 0.3 | 0.0 | 2.8 | 20.2 | 6.7 | 0.3 | 3.1 | 0.3 | 17.4 | **1.1** | 47.9 |
| CCS | 0.0 | 2.9 | 0.0 | 10.6 | 9.5 | 0.0 | 0.0 | 0.0 | 5.4 | 3.4 | **68.2** |

Output Class

Table 6.5 Specificity values achieved in the classification of continuous movement windows of testing and validation data containing motions performed while completing pseudo-childcare activities in a simulated childcare environment. All values are expressed as percentages relative to the total number of classified windows belonging to other motions. All movement classes have been summed and expressed as only the motion performed in the first second of each window, as follow: heels-up squatting (HS), flatfoot squatting (FS), dorsiflexed kneeling (DK), plantarflexed kneeling (PK), sitting on an adult sized chair(ACS), sitting on a child sized chair (CCS), single arm supported kneeling and double arm supported kneeling (SS), crossed leg sitting (CLS), side sitting and side leaning to the left or the right (SS), stooping (STP), standing (STD), and walking (WLK). (When a class was not present within the target or output classes, that class is marked as NA).

| Data Type | Posture Classifier Type | DK | PK | FS | HS | CCS | ACS | SK | STP | STD | CLS | SS | WLK |
|---|---|---|---|---|---|---|---|---|---|---|---|---|---|
| Testing | Model *Aa* | 90.2 | 90.3 | 97.7 | 98.9 | 89.9 | NA | 94.4 | 87.9 | 95.7 | 81.7 | 74.9 | 94.4 |
| | Model *Ba* | 89.8 | 90.2 | 97.8 | 98.7 | 89.1 | NA | 94.4 | 90.4 | 95.7 | 81.5 | 74.6 | 94.3 |
| | Model *Ab* | 96.6 | NA | 100.0 | 98.8 | 90.3 | 97.7 | 98.8 | 98.8 | 43.5 | 0.0 | 87.5 | 97.7 |
| | Model *Bb* | 98.4 | NA | 100.0 | NA | 94.0 | NA | 97.9 | NA | 100.0 | 0.0 | 92.2 | 99.5 |
| Validation | Model *Aa* | 95.0 | 85.4 | 93.2 | 96.0 | 73.0 | NA | 84.4 | 81.9 | 86.4 | 67.1 | 58.6 | 87.2 |
| | Model *Ba* | 94.5 | 84.7 | 94.0 | 92.9 | 71.9 | NA | 86.2 | 84.3 | 86.6 | 68.6 | 59.0 | 87.2 |
| | Model *Ab* | 93.4 | 74.1 | 97.3 | 96.3 | 48.1 | 95.9 | 89.3 | 92.3 | 87.6 | 65.9 | 51.9 | 83.5 |
| | Model *Bb* | 93.9 | 73.5 | 97.6 | 93.2 | 47.5 | NA | 89.1 | 93.0 | 88.6 | 65.3 | 51.5 | 84.1 |

Table 6.6 Balanced accuracy values achieved in the classification of continuous movement windows of testing and validation data containing motions performed while completing pseudo-childcare activities in a simulated childcare environment. All values are expressed as percentages. All movement classes have been summed and expressed as only the motion performed in the first second of each window, as follow: heels-up squatting (HS), flatfoot squatting (FS), dorsiflexed kneeling (DK), plantarflexed kneeling (PK), sitting on an adult sized chair(ACS), sitting on a child sized chair (CCS), single arm supported kneeling and double arm supported kneeling (SS), crossed leg sitting (CLS), side sitting and side leaning to the left or the right (SS), stooping (STP), standing (STD), and walking (WLK). (When a class was not present within the target or output classes, that class is marked as NA).

| Data Type | Posture Classifier Type | DK | PK | FS | HS | CCS | ACS | SK | STP | STD | CLS | SS | WLK |
|---|---|---|---|---|---|---|---|---|---|---|---|---|---|
| Testing | Model *Aa* | 73.0 | 66.0 | 71.0 | 64.0 | 68.0 | NA | 63.0 | 64.0 | 65.0 | 65.0 | 74.0 | 61.0 |
| | Model *Ba* | 73.0 | 67.0 | 71.0 | 65.0 | 68.0 | NA | 64.0 | 66.0 | 65.0 | 65.0 | 73.0 | 61.0 |
| | Model *Ab* | 48.0 | NA | 50.0 | 49.0 | 45.0 | 49.0 | 49.0 | 49.0 | 22.0 | 19.0 | 44.0 | 49.0 |
| | Model *Bb* | 49.0 | NA | 50.0 | NA | 47.0 | NA | 49.0 | NA | 50.0 | 43.0 | 46.0 | 50.0 |
| Validation | Model *Aa* | 69.0 | 50.0 | 59.0 | 61.0 | 59.0 | NA | 55.0 | 54.0 | 45.0 | 50.0 | 46.0 | 54.0 |
| | Model *Ba* | 68.0 | 50.0 | 63.0 | 58.0 | 59.0 | NA | 57.0 | 55.0 | 45.0 | 51.0 | 47.0 | 54.0 |
| | Model *Ab* | 56.0 | 42.0 | 49.0 | 56.0 | 58.0 | 48.0 | 45.0 | 53.0 | 47.0 | 45.0 | 50.0 | 56.0 |
| | Model *Bb* | 57.0 | 42.0 | 49.0 | 54.0 | 58.0 | NA | 45.0 | 53.0 | 49.0 | 45.0 | 50.0 | 55.0 |

While the overall performance of all models was quite similar when identifying movement classes from continuous pseudo-childcare activities completed within a simulated childcare environment, the sensitivity values reveal subtle differences between the data division strategies. Models developed using strategy *b*, where all movement windows save those from a single trial were used in development, were most accurate at identifying child chair sitting and side sitting (models *Ab* and *Bb* both achieving 68.2% accuracy for CCS and 48.5% and 47.6% accuracy for SS respectively). Models developed using strategy *a,* where 20% of the continuous movement windows were withheld for testing, had a higher number of postures which were identified correctly at accuracies greater than 30% (model *Aa* succeeding in identifying CLS, SS, DK, and CCS with > 30% accuracy, model *Ba* identifying these postures as well as FS with >30% accuracy). It appears this distribution of minor classification success may have led to the models developed using data division strategy *a* slightly outperforming those developed using a greater proportion of the continuous motion windows. However, there appears to be no marked benefit to including the movement templates generated in Chapter 5 when classifying the windows of continuous data collected during pseudo childcare activities.

## 6.6. Discussion

In this study, four multi-dimensional Dynamic Time Warping distance-based *k*NN algorithms for movement classification were applied to data acquired during pseudo-childcare activities in a simulated childcare environment. The proposed modifications to the developed quantification framework proved effective in calculating flexion-extension angles for the ankles, knees, and hips in continuous childcare tasks however the performance of the classification models, developed using a framework previously validated using laboratory-based simulations of childcare-inspired postures, was markedly decreased when identifying these same postures from continuous motion trials. Classification results of the present work support the previously presented theory that classification models developed within controlled environments, such as in laboratory settings, with or without the addition of real-world data within the model development, may underperform when applied to real-world data (Bastian et al., 2015; Gyllensten & Bonomi, 2011; van Hees et al., 2013). The dataset here presented for classification was collected within a laboratory environment, however it is believed that the study design and simulated childcare environment, in combination with the presence of a child, who was likely immune to the Hawthorne effect (McCambridge, Witton, & Elbourne, 2014), elicited movements akin to those which would be adopted in the real-world.

The accuracy of the models developed using data division strategy *a*, wherein a stratified random partitioning holdout validation method was employed to create the development and testing datasets, consistently outperformed those developed using data division strategy *b*, where all continuous data windows, with the exception of those belonging to a single activity trial for one participant, were included in the development dataset. With stratified random partitioning, the initial dataset is divided into subgroups known as strata. These strata typically reflect the same movement classes found within the initial dataset with the caveat that representation of all classes should be present within each stratum. Given that the number of windows in the dataset here collected representing static postures far exceeded those of all transitions, the percentage of transitions included in the development strata far exceeded that found in the initial dataset. It is likely due to this new distribution in data that a higher classification accuracy was achieved when classifying the stratified data in comparison to the classification of continuous movement

windows (as observed in the distribution of classification sensitivities presented in Table *6.3* A and B when compared to those in Table *6.3* C and D). This assumption was further supported when considering the balanced accuracies achieved during classification of the validation dataset, where overall classification accuracies of 54.7%, 55.2%, 50.6% and 50.6% for models *Aa*, *Ba*, *Ab*, and *Bb* respectively were attained. The differences in the achieved accuracies compared to the balanced accuracies (26.63%, 26.66%, 23.89%, and 23.99% for models *Aa*, *Ba*, *Ab*, and *Bb* respectively) suggest that the disparities in class sizes within the model development data played a marked role in misclassifications of each model. The identification of transitions from real-world data was also shown to be problematic in work by Gyllensten and Bonomi (2011). Therefore, future efforts to apply these models to the classification of movements adopted in childcare settings should pay particular attention to the equality of representation of each movement class within the model development data in order to increase the accuracy of successfully identifying movement transitions.

When classifying windows of continuous motion, each movement class predicted should be a possible logical progression from the class predicted in the prior window. A first attempt at correcting the predictions made when classifying the validation data was implemented through a prior knowledge correction module, wherein illogical transitions (e.g., from HS descent to walking), were replaced based on the prediction of the previous and subsequent window. This approach was not found to improve the classification accuracies of any of the developed models given that the correction was dependent on the motion estimate of the first window being correct. Therefore, future efforts should investigate the application of probabilistic weightings during movement classification in order to successfully identify the postures performed however, this development was beyond the scope of the current study.

The losses of performance observed in the four classification models presented are likely attributable to variations in movements not present within the initial laboratory trials. In particular, the floor sitting movements performed for template generation involved the adoption of very specific postures (either sitting with legs crossed in front of the body or sitting with both knees bent and feet tucked posteriorly towards either hip) while in the pseudo-childcare trials, floor sitting took on a wide variety of postures (often characterized by one or both legs being extended further than had been prescribed in the controlled trials). It is noted also that at times,

postures identified as side leaning during labeling of the pseudo-childcare trials were more akin to lying on one's side rather than simply using an arm to support the seated posture. Given the limited number of movement labels assigned to all motions observed in these trials it is likely that the variations in angular kinematics within each movement class resulted in confusion within the models. It is possible that additional templates generated during variations of these postures or an increased number of movement classes which better described the seated postures observed may have improved the classification accuracies related to floor sitting movements.

Similarly, when caring for and interacting with their child, participants were often observed to adopt a stooped posture when standing or walking. This increase in hip flexion observed across postures but absent from the laboratory-based movement templates may have contributed to increased misclassifications; given an increase in similarities between joint angles during standing, stooping, the stance phase of walking, and even during seated postures in cases where the participant's legs were outstretched before them. Gyllensten and Bonomi (2011) similarly reported a tendency for participants to assume a posture characterized by increased forward leaning in daily life when compared to laboratory settings, therefore this postural characterization must be considered when adapting models for movement classifications in the real-world. The addition of a metric, such as the sensor-based accelerations or the expression of the gravitational vector in local sensor coordinates, might allow for better representation of the differences between dynamic and static postures as well as between standing and seated postures within the distance calculation and therefore better distinction between postures overall.

Perhaps the main limitations of applying the developed classification framework to the identification of movements during pseudo-childcare activities however lies in the high variability observed in postural adoption in real-world settings, leading to a lack of symmetry between the lower-limbs and therefore an increase in kinematic overlap between movements. Given the combination of angular kinematics from both legs in the calculation of distance metrics by which the classification was performed, any instance where the posture adopted by one leg was different than that of the opposite leg, as would be observed in the case of a lunging posture, where one leg might be said to be squatting while the other would be kneeling, would lead to confusion within the classifier. Instances such as this should be considered in future model development wherein a greater number of trials representing these motions could be

collected and added to the templates of existing motions or labeled as new motions for classification. Further, the methods used in template generation for model *A* must here be discussed. It was previously explained in Subsections 5.3 that each motion template was generated through manual segmentation of the movement sequence of the right knee. This segmentation proved effective in the classification of laboratory-based data in Chapter 5 regardless of participants' leg dominance (therefore regardless of the leg with which they commenced each trial). When further dividing these templates into phases of motion (as explained in Subsection 6.3) however, this segmentation method may have led to confusion within the model given that seven participants included in the dataset from Chapter 5 were left leg dominant. Templates for these participants may not have represented the full range of motion experienced by the left leg during each movement which may have resulted in increased misclassifications when postures were initiated with the left leg in the current analysis. Thus, in future development, the templates for the left and right legs could be mirrored in order to increase the sample for each joint and reduce the risk of misclassification due to right knee-based segmentation. By focusing future development on these identified potential sources of error, a more thorough report on postural adoption and high flexion exposures at the knee can be obtained from data collected in occupational settings.

It is clear based on the data collected in this study that postures adopted in real-world settings are not as easily distinguishable as they might be when performed under controlled conditions. More refined movement templates or shorter windows of continuous movement might be created based on data similar to those measured in this study which would encompass the variability of real-world movement while providing further refinement to the class labels, however, this was impossible to address in the present study. The length of the movement windows generated herein was dictated by the time-based resolution and the visual quality of the videos from which each movement label was extracted. Therefore, to address the issue of precision in real-time annotations, future validation studies should seek to utilize high resolution video recordings from which additional precision during the a posteriori annotation of labels can be obtained. The issue of lack of representativeness of real-world data in laboratory-derived classifiers has previously been discussed by van Hees et al. (2013). In their study, they simulated an underrepresentation of movement classes through eight models seeking to quantify daily walking time to analyze the

effects of study design on model performance. Ultimately, van Hees et al. (2013) highlighted the limitations associated with classifying real-world data using models which are not effectively developed for the complex data they seek to classify. Bastian et al. (2015) presented a possible means of overcoming some of the limitations of a laboratory-derived classifier by recalibrating the model to include a portion of the real-world data in its training dataset. While this recalibration method led to improvements in the classification of certain movement classes, it was also found to decrease the accuracy of others (Bastian et al., 2015). The present work is complementary to these two studies in that the laboratory-based templates generated for model development were directly inspired by the postures to be classified within childcare environments, and that the developed models included windows of continuous pseudo-childcare movements in an attempt to improve the accuracy of postural identification. However, the results here presented also similarly suggest that the complexity of real-world data may preclude these movements from being classified using any model developed for laboratory-based movement classification.

## 6.7. Conclusion

In this study, the feasibility of extending the developed multi-dimensional Dynamic Time Warping distance-based Nearest Neighbour classification algorithm to identify and measure postures frequently adopted when performing childcare specific activities within a simulated childcare environment was explored. The sensor to segment calibration and proposed modifications to the complementary filters proved provided an effective means by which lower-limb flexion-extension joint kinematics could be measured in continuous data. Subsequently, four multi-dimensional Dynamic Time Warping distance-based *k*-Nearest Neighbour classification algorithms were developed using a combination of controlled laboratory-based movements and windows of continuous movements performed in a simulated childcare environment. Their performances were compared when classifying continuous windows of pseudo-childcare activities. While the framework used in the development of these models was found to be stable in the classification of controlled movements, their performance was markedly lower when identifying postures performed in real-world mimicking trials. It is believed that this decrease in classification accuracy may be due to the variability in postural adoption which

cannot be replicated during laboratory-based movement simulations and as such it is likely that laboratory-derived classification algorithms are not well suited to the classification of motions in occupational settings. This study further demonstrated that combining laboratory and real-world data in the development of the mDTW *k*NN model was not sufficient to mitigate these issues. Future work should therefore seek to expand upon the algorithm development dataset by increasing the number of templates representing dynamic transitions into and out of high knee flexion postures and well as those representing a greater range of postural variability based on data collected in non-controlled motion trials.

# Chapter 7

# Conclusions

## 7.1. Problem Restatement

Knee osteoarthritis (OA) has been characterized as a heterogeneous disease which may arise from a molecular, anatomic, and physiologic mechanistic pathways, all leading to joint disfunction and damage. Several studies have sought to understand the mechanical factors arising from the repetitive and prolonged adoption of high flexion postures in occupational settings as potential contributors to disease progression across a plethora of occupations, yet to date only a handful of studies have explored the potential for OA initiation and progression due to childcare related exposures at the knee. Therefore, this thesis aimed to characterize the adoption of high knee flexion postures in childcare and to develop a means by which these postures could be identified and measured in occupational settings using non-laboratory-based wearable sensing technologies.

## 7.2. Specific Thesis Objectives: Revisited

This thesis explored three specific objectives in order to accomplish its overarching global objectives. The first of these specific objectives involved the characterization of the postural requirements of childcare as they relate to high knee flexion and was accomplished through the

observational analysis of video recordings performed in **Study 1** (Chapter 3). Findings of this study constitute the first attempt to quantitatively and objectively evaluate exposures of high knee flexion in childcare workers in North America. It was revealed that both the exposure- and frequency-based thresholds associated with increased incidences of knee OA development were exceeded within a typical working day when caring for children of all ages. Further, this investigation led to a characterization of the childcare specific tasks which commonly elicited the adoption of high knee flexion postures.

The second specific objective involved the application, extension, and validation of sensor to segment alignment algorithms through which inertial sensor data collected from the lower limbs could be calibrated and used to measure ankle, knee, and hip flexion-extension kinematics in multiple high flexion postures. This objective relates specifically to the measurement component of the second global objective and was accomplished through **Study 2** (Chapter 4). Through modifications to the Seel joint axis algorithm for spherical joints, inertial based estimates of flexion-extension angles for all joints were found to be strongly correlated with those obtained through a "gold-standard" optical-based motion capture system. The results of this study therefore suggest that the constrained Seel knee axis and the iterative Seel spherical axis algorithms present an effective solution for the sensor to segment alignment necessary for the measurement of joint kinematics across multiple high knee flexion postures frequently adopted in childcare settings.

The third and final specific objective of this thesis involved the development of a machine learning based classification model capable of identifying the high knee flexion postures frequently adopted by childcare workers. In order to address this objective, a multi-dimensional Dynamic Time Warping distance-based framework for the classification of these postures was developed based on *in vivo* simulations of these postures in a controlled laboratory-based environment (**Study 3**, Chapter 5). Results of this study suggested that isolated high knee flexion postures performed within a controlled environment could be effectively identified based on a combination of Dynamic Time Warping distances between single trials of high flexion motions and previously identified movement sequences. The performance of this framework was then evaluated through four classification models tasked with identifying high flexion postures adopted during the completion of pseudo-childcare activities within a simulated childcare

environment, conditions which were believed to mimic real-world measures (**Study 4**, Chapter 6). The models evaluated in this study were found to be incapable of accurately identifying the motions performed to a level which would be considered satisfactory to accurately report on postural adoption within a childcare setting. This investigation led to the conclusion that real-world data is characterized by increased postural variability which cannot be replicated during controlled movement simulations in laboratory settings and as such further development of the movement templates representing a greater range of postural variability is required. Nevertheless, these models provide a foundation for the identification of high knee flexion postures frequently adopted in childcare settings based solely on wearable sensor data.

## 7.3. Global Thesis Objectives: Revisited

The research presented in this thesis was driven by two global objectives. The first was to explore the adoption of high knee flexion postures within occupational childcare environments in order to further our understanding of the associations, if any, between childcare related exposures and the potential for knee joint degeneration and the initiation and progression of knee OA. Findings presented in **Study 1** (Chapter 3) affirm the belief that childcare workers adopt high knee flexion postures in excess of both the frequency- and duration-based thresholds for increased risk of knee OA development. The secondary overarching objective lay in the development of a framework through which these knee straining postures could be identified and measured using solely the measures obtained from inertial-based wearable sensors. The results from **Study 2** (Chapter 4) demonstrate the possibility of measuring occupational joint kinematics using only arbitrarily mounted inertial sensors calibrated based on a series of brief calibration movements which can be performed in any environment. Based on these angle estimates, a classification framework was developed in **Study 3** (Chapter 5) by which each knee straining posture simulated in a controlled laboratory-based environment could be identified. This framework was ultimately applied to the classification of pseudo-real-world data, wherein results suggest that the laboratory-derived model was insufficient in identifying postures performed in non-controlled environments (**Study 4**, Chapter 6). Ultimately, the second global objective was satisfied within controlled environments however future development is required prior to applying the developed models to the measurement of exposures in childcare settings.

## 7.4. Conclusions

The observational analysis of eighteen childcare workers caring for infant, toddler, and preschool-aged children revealed ten frequently adopted postures with varying degrees of knee flexion. Of those postures, eight were found to elicit knee flexion angles surpassing 120°: dorsiflexed kneeling, plantarflexed kneeling, single and double arm supported kneeling, heels-up squatting, sitting on the floor, side sitting or side leaning, and sitting on child-sized furniture. The mean frequency of postural adoption and mean cumulative times spent in high flexion postures were each found to exceed the previously reported thresholds for OA development. These knee straining postures were observed to be adopted for the longest durations within periods of structured activities, playing, and feeding. These results therefore confirm the likelihood that risk of knee OA development is higher in childcare workers given the exposure related demands of this occupation.

A selection of ten postures, inspired by those observed the video-based analysis, were subsequently simulated within a controlled laboratory environment, and from these simulations, joint flexion-extension angles for the ankle, knee, and hip were estimated using inertial data. These kinematic estimates were obtained following sensor to segment calibration using both the constrained Seel knee axis algorithm as well as the iterative Seel spherical axis algorithm, developed herein, using custom complementary filters and subsequently compared to gold-standard optical motion capture-based kinematic measures. This study represents the first attempt at applying the sensor to segment calibration methods towards the measurement of high knee flexion postures. Findings revealed the accuracies of the estimated lower-limb joint flexion-extension angles in high knee flexion postures, when compared to optical motion capture-based methods, to be similar to those previously reported during gait. These algorithms developed for sensor calibration and kinematic analyses will ultimately support the objective measurement of high flexion postural adoption within occupational settings.

The flexion-extension angle estimates obtained from each childcare-inspired motion then served as the basis for the development of a multi-dimensional Dynamic Time Warping distance-based *k*-Nearest Neighbour classification algorithm. A series of movement templates were generated from all high flexion trials and subsequently compared against the complete movement

sequences in order to obtain measures of waveform similarities for each joint through Dynamic Time Warping. These measures were subsequently combined in order to calculate the multi-dimensional Dynamic Time Warping distance with which postural classifications were determined. This is the first known attempt to classify specific variations of high knee flexion postures and generally high classification rates were achieved when identifying childcare-inspired postures in data from participants both included and precluded from the algorithm development.

Finally, the feasibility of applying the developed classification framework to the recognition of high knee flexion postures adopted during continuous pseudo-childcare activities within a simulated childcare environment was evaluated. While acceptable classification rates were achieved when identifying childcare-inspired postures performed in a controlled laboratory environment with the developed framework, the performance of four developed models in identifying movements from continuous real-world data was markedly lower. While these laboratory-derived classification models are therefore not well suited for the classification of motions in occupational settings, the results of this feasibility study revealed key differences between laboratory and real-world data which will be essential in the future refinement of these models towards being applied to the qualification and quantification of high knee flexion exposures in childcare environments.

In summary, the work presented within this thesis points to the possibility of an association between the frequency and duration of adopted high knee flexion postures in occupational childcare and a potential for increased risk of knee OA initiation and progression given the similarity of exposure levels in childcare to those observed in other industries in which this association exists. Based on these findings, a wearable and computational solution towards measuring these postures and closing the gap between the mechanistic and occupational literature relating to high knee flexion postural adoption in childcare was offered. The validated approach to automatic IMU calibration and lower extremity motion analysis presented herein provides a means by which quantitative exposure data can be captured in occupational settings; while the proposed classification framework provides a necessary foundation for the identification of occupational postures based on inertial data. Additionally, potential shortfalls of building such a classification model primarily on laboratory-based data were provided in order to

support future development towards successful movement classification in real-world settings. This work therefore satisfies the original objectives of this thesis while providing guidance for further work, which has the potential to provide valid exposure assessments in fields beyond the scope of this project.

# Bibliography


Ahmad, S. A. (2009). *Moving approximate entropy and its application to the electromyographic control of an artificial hand*. University of Southampton.

Akagi, M. (2005). Deep knee flexion in the Asian population. In J. Bellemans, M. D. Ries, & J. M. Victor (Eds.), *Total Knee Arthroplasty* (pp. 311–316). Berlin, Heidelberg: Springer.

Akhavian, R., & Behzadan, A. H. (2016). Smartphone-based construction workers' activity recognition and classification. *Automation in Construction*, *71*(Part 2), 198–209.

Allahbakhshi, H., Hinrichs, T., Huang, H., & Weibel, R. (2019). The key factors in physical activity type detection using real-life data: A systematic review. *Frontiers in Physiology*, *10*(FEB), 1–20.

Altun, K., & Barshan, B. (2010). Human activity recognition using inertial / magnetic sensor units. *Human Behavior Understanding*, *6219*, 38–51.

Altun, K., Barshan, B., & Tunçel, O. (2010). Comparative study on classifying human activities with miniature inertial and magnetic sensors. *Pattern Recognition*, *43*(10), 3605–3620.

Amsuss, S., Goebel, P. M., Jiang, N., Graimann, B., Paredes, L., & Farina, D. (2014). Self-correcting pattern recognition system of surface EMG signals for upper limb prosthesis control. *IEEE Transactions on Biomedical Engineering*, *61*(4), 1167–1176.

Anderson, J. J., & Felson, D. T. (1988). Factors associated with osteoarthritis of the knee in the first national health and nutrition examination survey (Hanes 1). *American Journal of Epidemiology*, *128*(1), 179–189.

Andriacchi, T. P., & Favre, J. (2014). The nature of in vivo mechanical signals that influence cartilage health and progression to knee osteoarthritis. *Current Rheumatology Reports*, *16*(11), 1–8.

Andriacchi, T. P., Mundermann, A., Smith, R. L., Alexander, E. J., Dyrby, C. O., & Koo, S. (2004). A framework for the in vivo pathomechanics of osteoarthritis at the knee. *Annals of Biomedical Engineering Biomed Eng*, *32*(3), 447–457.

Aristidou, A., & Lasenby, J. (2013). Real-time marker prediction and CoR estimation in optical motion capture. *The Visual Computer*, *29*(1), 7–26.

Arokoski, J. P. A., Hyttinen, M. M., Helminen, H. J., & Jurvelin, J. S. (1999). Biomechanical and structural characteristics of canine femoral and tibial cartilage. *Journal of Biomedical Materials Research*, *48*(2), 99–107.

Arokoski, J. P. A., Hyttinen, M. M., Lapveteläinen, T., Takács, P., Kosztáczky, B., Módis, L., … Helminen, H. J. (1996). Decreased birefringence of the superficial zone collagen network in the canine knee (stifle) articular cartilage after long distance running training, detected by quantitative polarised light microscopy. *Annals of the Rheumatic Diseases*, *55*(4), 253–264.

Arokoski, J. P. A., Jurvelin, J. S., Väätäinen, U., & Helminen, H. J. (2000). Normal and

pathological adaptations of articular cartilage to joint loading. *Scandinavian Journal of Medicine and Science in Sports*, *10*(4), 186–198.

Arokoski, J. P. A., Kiviranta, I., Jurvelin, J., Tammi, M., & Helminen, H. J. (1993). Long-distance running causes site-dependent decrease of cartilage glycosaminoglycan content in the knee joints of beagle dogs. *Arthritis & Rheumatism*, *36*(10), 1451–1459.

Asghari Oskoei, M., & Hu, H. (2007). Myoelectric control systems-A survey. *Biomedical Signal Processing and Control*, *2*(4), 275–294.

Aziz, O., Russell, C. M., Park, E. J., & Robinovitch, S. N. (2014). The effect of window size and lead time on pre-impact fall detection accuracy using support vector machine analysis of waist mounted inertial sensor data. *2014 36th Annual International Conference of the IEEE Engineering in Medicine and Biology Society, EMBC 2014*, (i), 30–33.

Bao, L., & Intille, S. S. (2004). Activity recognition from user-annotated acceleration data. *Pervasive Computing*, *3001*, 1–17.

Barshan, B., & Yüksek, M. C. (2013). Recognizing daily and sports activities in two open source machine learning environments using body-worn sensor units. *Computer Journal*, *57*(11), 1649–1667.

Barth, J., Oberndorfer, C., Kugler, P., Schuldhaus, D., Winkler, J., Klucken, J., & Eskofier, B. (2013). Subsequence dynamic time warping as a method for robust step segmentation using gyroscope signals of daily life activities. *Proceedings of the 35th Annual International Conference of the IEEE Engineering in Medicine and Biology Society, EMBS*, 6744–6747.

Barth, J., Oberndorfer, C., Pasluosta, C., Schülein, S., Gassner, H., Reinfelder, S., … Eskofier, B. M. (2015). Stride segmentation during free walk movements using multi-dimensional subsequence dynamic time warping on inertial sensor data. *Sensors*, *15*(March), 6419–6440.

Bastian, T., Maire, A., Dugas, J., Ataya, A., Villars, C., Gris, F., … Simon, C. (2015). Automatic identification of physical activity types and sedentary behaviors from triaxial accelerometer: Laboratory-based calibrations are not enough. *Journal of Applied Physiology*, *118*(6), 716–722.

Bauer, C. M., Heimgartner, M., Rast, F. M., Ernst, M. J., Oetiker, S., & Kool, J. (2016). Reliability of lumbar movement dysfunction tests for chronic low back pain patients. *Manual Therapy*, *24*, 81–84.

Bejarano, N. C., Ambrosini, E., Pedrocchi, A., Ferrigno, G., Monticone, M., & Ferrante, S. (2015). A novel adaptive, real-time algorithm to detect gait events from wearable sensors. *IEEE Transactions on Neural Systems and Rehabilitation Engineering*, *23*(3), 413–422.

Benser, E. T. (2015). Trends in inertial sensors and applications. *2nd IEEE International Symposium on Inertial Sensors and Systems, IEEE ISISS 2015 - Proceedings*, 2–5.

Bleser, G., Taetz, B., Miezal, M., Christmann, C., Steffen, D., & Regenspurger, K. (2017). Development of an inertial motion capture system for kinematic analysis of ski jumping. *I-Com*, *16*(2), 113–129.

Boissy, P., Choquette, S., Hamel, M., & Noury, N. (2007). User-based motion sensing and fuzzy logic for automated fall detection in older adults. *Telemedicine and E-Health*, *13*(6), 683–694.

Boyle, J., Karunanithi, M., Wark, T., Chan, W., & Colavitti, C. (2006). Quantifying functional mobility progress for chronic disease management. *Annual International Conference of the IEEE Engineering in Medicine and Biology - Proceedings*, 5916–5919.

Branch, M. A., Coleman, T. F., & Li, Y. (1999). A subspace, interior, and conjugate gradient method for large-scale bound-constrained minimization problems. *Society for Industrial and Applied Mathematics Journal on Scientific Computing*, *21*(1), 1–23.

Bright, K. A., & Calabro, K. (1999). Child care workers and workplace hazards in the United States: Overview of research and implications for occupational health professionals. *Occupational Medicine*, *49*(7), 427–437.

Brockett, C. L., & Chapman, G. M. (2016). Biomechanics of the ankle. *Orthopaedics and Trauma*, *30*(3), 232–238.

Brown, M. Z., & Gerberich, S. G. (1993). Disabling Injuries to Childcare Workers in Minnesota, 1985 to 1990. *Journal of Occupational and Environmental Medicine*, *35*(12), 1236–1243.

Buchman-Pearle, J. M., & Acker, S. M. (2021). Estimating soft tissue artifact of the thigh in high knee flexion tasks using optical motion Capture : Implications for marker cluster placement. *Journal of Biomechanics*, *127*(July), 110659.

Bureau of Labor Statistics. (2016). Occupational outlook handbook - childcare workers.

Burford, E. M., Ellegast, R., Weber, B., Brehmen, M., Groneberg, D., Sinn-Behrendt, A., & Bruder, R. (2017). The comparative analysis of postural and biomechanical parameters of preschool teachers pre- and post-intervention within the ErgoKiTa study. *Ergonomics*, *60*(12), 1718–1729.

Bussmann, J. B., Martens, W. L., Tulen, J. H., Schasfoort, F. C., van den Berg-Emons, H. J., & Stam, H. J. (2001). Measuring daily behavior using ambulatory accelerometry: the Activity Monitor. *Behavior Research Methods, Instruments, & Computers : A Journal of the Psychonomic Society, Inc*, *33*(3), 349–356.

Calder, J. (1994). Occupational health and safety issues for child-care providers. *Pediatrics*, *94*(6), 1072–1074.

Camomilla, V., Bergamini, E., Fantozzi, S., & Vannozzi, G. (2018). Trends supporting the in-field use of wearable inertial sensors for sport performance evaluation : A systematic review. *Sensors*, *18*(873), 1–50.

Camomilla, V., Cereatti, A., Vannozzi, G., & Cappozzo, A. (2006). An optimized protocol for hip joint centre determination using the functional method. *Journal of Biomechanics*, *39*(6), 1096–1106.

Canetti, E. F. D., Schram, B., Orr, R. M., Knapik, J., & Pope, R. (2020). Risk factors for development of lower limb osteoarthritis in physically demanding occupations: A

systematic review and meta-analysis. *Applied Ergonomics*, *86*, 103097.

Casamassima, F., Ferrari, A., Milosevic, B., Ginis, P., Farella, E., & Rocchi, L. (2014). A wearable system for gait training in subjects with Parkinson's disease. *Sensors*, *14*(4), 6229–6246.

Cervantes, J., Garcia-Lamont, F., Rodríguez-Mazahua, L., & Lopez, A. (2020). A comprehensive survey on support vector machine classification: Applications, challenges and trends. *Neurocomputing*, *408*, 189–215.

Chang, H. C., Hsu, Y. L., Yang, S. C., Lin, J. C., & Wu, Z. H. (2016). A wearable inertial measurement system with complementary filter for gait analysis of patients with stroke or Parkinson's disease. *IEEE Access*, *4*, 8442–8453.

Cheng, H. Y. K., Cheng, C. Y., & Ju, Y. Y. (2013). Work-related musculoskeletal disorders and ergonomic risk factors in early intervention educators. *Applied Ergonomics*, *44*(1), 134–141.

Cho, Y. J., & Kim, J. Y. (2012). The effects of load, flexion, twisting and window size on the stationarity of trunk muscle EMG signals. *International Journal of Industrial Ergonomics*, *42*(3), 287–292.

Choi, A., Jung, H., & Mun, J. H. (2019). Single inertial sensor-based neural networks to estimate COM-COP inclination angle during walking. *Sensors*, *19*(2974), 1–12.

Choi, C., Micera, S., Carpaneto, J., & Kim, J. (2009). Development and quantitative performance evaluation of a noninvasive EMG computer interface. *IEEE Transactions on Biomedical Engineering*, *56*(1), 188–191.

Chong, H. (2016). *Do East Asians Achieve Greater Knee Flexion than Caucasian North Americans, and are East Asian Kneeling and Squatting Styles Kinetically Different from North American Norms?* University of Waterloo.

CIHI. (2021). *Canadian Joint Replacement Registry: 2019–2020 Full Annual Report*. Ottawa.

CIHI. (2022). *Hip and Knee Replacements in Canada: CJRR Annual Report, 2020–2021*. Ottawa.

Coggon, D., Croft, P., Kellingray, S., Barrett, D., McLaren, M., & Cooper, C. (2000). Occupational physical activities and osteoarthritis of the knee. *Arthritis and Rheumatism*, *43*(7), 1443–1449.

Cohen, J., Cohen, P., West, S. G., & Aiken, L. S. (2003). *Applied multiple regression/correlation analysis for the behavioral sciences* (3rd ed.). Mahwah, NJ, US: Lawrence Erlbaum Associates Publishers.

Cooper, C., McAlindon, T., Coggon, D., Egger, P., & Dieppe, P. (1994). Occupational activity and osteoarthritis of the knee. *Annals of the Rheumatic Diseases*, *53*(2), 90–93.

Cooper, G., Sheret, I., McMillian, L., Siliverdis, K., Sha, N., Hodgins, D., … Howard, D. (2009). Inertial sensor-based knee flexion/extension angle estimation. *Journal of Biomechanics*,

*42*(16), 2678–2685.

Corlett, E. N., & Bishop, R. P. (2007). A technique for assessing postural discomfort. *Ergonomics*, *19*(2), 175–182.

Crema, C., Depari, A., Flammini, A., Sisinni, E., Haslwanter, T., & Salzmann, S. (2017). IMU-based solution for automatic detection and classification of exercises in the fitness scenario. *SAS 2017 - 2017 IEEE Sensors Applications Symposium, Proceedings*.

D'Souza, J. C., Werner, R. A., Keyserling, W. M., Gillespie, B., Rabourn, R., Ulin, S., & Franzblau, A. (2008). Analysis of the third national health and nutrition examination survey (NHANES III) using export ratings of job categories. *American Journal of Industrial Medicine*, *51*, 37–46.

De Vries, S. I., Garre, F. G., Engbers, L. H., Hildebrandt, V. H., & Van Buuren, S. (2011). Evaluation of neural networks to identify types of activity using accelerometers. *Medicine and Science in Sports and Exercise*, *43*(1), 101–107.

DeFrances, C. J., Lucas, C., & Golosinskiy, A. (2008). *2006 National Hospital Discharge Survey. national health statistics reports*.

Ditchen, D. M. (2012). *Erfassung arbeitsbedingter Kniebelastungen an ausgewählten . (ENGL: Recording work-related knee loads at selected workplaces)*. Berlin.

Ditchen, D. M., Ellegast, R. P., Gawliczek, T., Hartmann, B., & Rieger, M. A. (2015). Occupational kneeling and squatting: development and validation of an assessment method combining measurements and diaries. *International Archives of Occupational and Environmental Health*, *88*(2), 153–165.

Doshi-Velez, F., & Kim, B. (2017). Towards a rigorous science of interpretable machine learning. *ArXiv*, 1–13.

Duda, R. O., Hart, P. E., & Stork, D. G. (2000). *Pattern Classification* (2nd Editio).

Englehart, K., & Hudgins, B. (2003). A robust, real-time control scheme for multifunction myoelectric control. *IEEE Trans Biomed Eng*, *50*(7), 848–854.

Englund, M., & Lohmander, L. S. (2004). Risk factors for symptomatic knee osteoarthritis fifteen to twenty-two years after meniscectomy. *Arthritis and Rheumatism*, *50*(9), 2811–2819.

Erick, P. N., & Smith, D. R. (2011). A systematic review of musculoskeletal disorders among school teachers. *BMC Musculoskeletal Disorders*, *12*, 13–17.

Fasel, B., Spörri, J., Schütz, P., Lorenzetti, S., & Aminian, K. (2017). An inertial sensor-based method for estimating the athlete's relative joint center positions and center of mass kinematics in alpine ski racing. *Frontiers in Physiology*, *8*(NOV), 1–11.

Favre, J., Jolles, B. M., Aissaoui, R., & Aminian, K. (2008). Ambulatory measurement of 3D knee joint angle. *Journal of Biomechanics*, *41*, 1029–1035.

Favre, J., Luthi, F., Jolles, B. M., Siegrist, O., Najafi, B., & Aminian, K. (2006). A new

ambulatory system for comparative evaluation of the three-dimensional knee kinematics , applied to anterior cruciate ligament injuries. *Knee Surgery, Sports Traumatology, Arthroscopy*, *14*, 592–604.

Felson, D. T. (1988). Epidemiology of hip and knee osteoarthritis. *Epidemiologic Reviews*, *10*, 1–28.

Felson, D. T. (1994). Do occupation-related physical factors contribute to arthritis? *Bailliere's Clinical Rheumatology*, *8*(1), 63–77.

Felson, D. T. (2006). Osteoarthritis of the knee. *The New England Journal of Medicine*, *354*, 841–848.

Felson, D. T. (2013). Osteoarthritis as a disease of mechanics. *Osteoarthritis and Cartilage*, *21*(1), 10–15.

Felson, D. T., Nevitt, M. C., Zhang, Y., Aliabadi, P., Baumer, B., Gale, D., … Xu, L. (2002). High prevalence of lateral knee osteoarthritis in Beijing Chinese compared with Framingham Caucasian subjects. *Arthritis and Rheumatism*, *46*(5), 1217–1222.

Felson, D. T., & Zhang, Y. (1998). Osteoarthritis with a view to prevention. *Arthritis & Rheumatism*, *41*(8), 1343–1355.

Fernández-González, P., Koutsou, A., Cuesta-Gómez, A., Carratalá-Tejada, M., Miangolarra-Page, J. C., & Molina-Rueda, F. (2020). Reliability of kinovea® software and agreement with a three-dimensional motion system for gait analysis in healthy subjects. *Sensors (Switzerland)*, *20*(11).

Ferrari, Alberto, Cutti, A. G., Garofalo, P., Raggi, M., Heijboer, M., Cappello, A., & Davalli, A. (2010). First in vivo assessment of "Outwalk": a novel protocol for clinical gait analysis based on inertial and magnetic sensors. *Medical & Biological Engineering & Computing*, *48*(1), 1–15.

Ferrari, Anna, Micucci, D., Mobilio, M., & Napoletano, P. (2020). On the personalization of classification models for human activity recognition. *IEEE Access*, *8*, 32066–32079.

Fiorentino, N. M., Atkins, P. R., Kutschke, M. J., Goebel, J. M., Foreman, K. B., & Anderson, A. E. (2017). Soft tissue artifact causes significant errors in the calculation of joint angles and range of motion at the hip. *Gait and Posture*, *55*(December 2016), 184–190.

Foerster, F., & Fahrenberg, J. (2000). Motion pattern and posture: correctly assessed by calibrated accelerometers. *Behavior Research Methods, Instruments, & Computers*, *32*, 450–457. Retrieved from http://www.ncbi.nlm.nih.gov/pubmed/11029819

Foerster, F., Smeja, M., & Fahrenberg, J. (1999). Detection of posture and motion by accelerometry: a validation study in ambulatory monitoring. *Computers in Human Behavior*, *15*(5), 571–583.

Forde, M. S., Punnett, L., & Wegman, D. H. (2002). Pathomechanisms of work-related musculoskeletal disorders: Conceptual issues. *Ergonomics*, *45*(9), 619–630.

Fu, B., Damer, N., Kirchbuchner, F., & Kuijper, A. (2020). Sensing technology for human activity recognition: A comprehensive survey. *IEEE Access*, *8*, 83791–83820.

Gaudreault, N., Hagemeister, N., Poitras, S., & de Guise, J. A. (2013). Comparison of knee gait kinematics of workers exposed to knee straining posture to those of non-knee straining workers. *Gait & Posture*, *38*, 187–191.

Grant, K. A., Habes, D. J., & Tepper, A. L. (1995). Work activities and musculoskeletal complaints among preschool workers. *Applied Ergonomics*, *26*(6), 405–410.

Gratz, R. R., Claffey, A., King, P., & Scheuer, G. (2002). The physical demands and ergonomics of working with young children. *Early Child Development and Care*, *172*(6), 531–537.

Graupe, D., Salahi, J., & Kohn, K. H. (1982). Multifunctional prosthesis and orthosis control via microcomputer identification of temporal pattern differences in single-site myoelectric signals. *Journal of Biomedical Engineering*, *4*(1), 17–22.

Graurock, D., Schauer, T., & Seel, T. (2016). Automatic pairing of inertial sensors to lower limb segments – a plug-and-play approach. *Current Directions in Biomedical Engineering*, *2*(1), 715–718.

Griffin, T. M., & Guilak, F. (2005). The role of mechanical loading in the onset and progression of osteoarthritis. *Exercise and Sport Science Reviews*, *33*(4), 195–200.

Grood, E. S., & Suntay, W. J. (1983). A joint coordinate system for the clinical description of three-dimensional motions: Application to the knee. *Journal of Biomechanical Engineering*, *105*(2), 136–144.

Gupta, S., Hawker, G. A., Laporte, A., Croxford, R., & Coyte, P. C. (2005). The economic burden of disabling hip and knee osteoarthritis (OA) from the perspective of individuals living with this condition. *Rheumatology*, *44*(12), 1531–1537.

Gyllensten, I. C., & Bonomi, A. G. (2011). Identifying types of physical activity with a single accelerometer: Evaluating laboratory-trained algorithms in daily life. *IEEE Transactions on Biomedical Engineering*, *58*(9), 2656–2663.

Hendriksen, P. F., Korshøj, M., Skotte, J., & Holtermann, A. (2020). Detection of kneeling and squatting during work using wireless triaxial accelerometers. *Ergonomics*, *63*(5), 607–617.

Henriksen, M., Creaby, M. W., Lund, H., Juhl, C., & Christensen, R. (2014). Is there a causal link between knee loading and knee osteoarthritis progression? A systematic review and meta-analysis of cohort studies and randomised trials. *BMJ Open*, *4*(7), 1–9.

Henriksen, M., Graven-Nielsen, T., Aaboe, J., Andriacchi, T. P., & Bliddal, H. (2010). Gait changes in patients with knee osteoarthritis are replicated by experimental knee pain. *Arthritis Care and Research*, *62*(4), 501–509.

Hollander, A. P., Heathfield, T. F., Webber, C., Iwata, Y., Bourne, R., Rorabeck, C., & Poole, A. R. (1994). Increased damage to type II collagen in osteoarthritic articular cartilage detected by a new immunoassay. *Journal of Clinical Investigation*, *93*(4), 1722–1732.

Holtermann, A., Hendriksen, P. F., Schmidt, K. G., Svendsen, M. J., & Rasmussen, C. D. N. (2020). Physical work demands of childcare workers in denmark: device-based measurements and workplace observations among 199 childcare workers from 16 day nurseries. *Annals of Work Exposures and Health*, *64*(6), 586–595.

Horng, A., Raya, J. G., Stockinger, M., Notohamiprodjo, M., Pietschmann, M., Hoehne-Hueckstaedt, U., … Glaser, C. (2015). Topographic deformation patterns of knee cartilage after exercises with high knee flexion: an in vivo 3D MRI study using voxel-based analysis at 3T. *European Radiology*, *25*(6), 1731–1741.

Horng, Y., Hsieh, S., Wu, H., Feng, C., & Lin, M. (2007). Work-related Musculoskeletal Disorders of the Workers in a Child Care Institution. *Tw J Phys Med Rehabil*, *36*(1), 15–21.

Hoshino, A., & Wallace, W. A. (1987). Impact-absorbing properties of the human knee. *Journal of Bone & Joint Surgery, British Volume*, *69*(5), 807–811.

Hsu, C.-W., & Lin, C.-J. (2002). A comparison of model selection methods for multi-class support vector machines. *IEEE Transactions on Neural Networks*, *13*(2), 415–425.

Hu, L. Y., Huang, M. W., Ke, S. W., & Tsai, C. F. (2016). The distance function effect on k-nearest neighbor classification for medical datasets. *SpringerPlus*, *5*(1304), 1–9.

Huang, H., Zhang, F., Hargrove, L. J., Dou, Z., Rogers, D. R., & Englehart, K. B. (2011). Continuous locomotion-mode identification for prosthetic legs based on neuromuscular - Mechanical fusion. *IEEE Transactions on Biomedical Engineering*, *58*(10 PART 1), 2867–2875.

Hurley, M. (1999). The role of muscle weakness in the pathogenesis of osteoarthritis. *Rheumatic Diseases Clinics of North America*, *25*, 283–298.

Huynh, T., & Schiele, B. (2005). Analyzing features for activity recognition. *Proceedings of the 2005 Joint Conference on Smart Objects and Ambient Intelligence Innovative Context-Aware Services: Usages and Technologies - SOc-EUSAI '05*, (October), 159–164.

Jackson, B. D., Wluka, A. E., Teichtahl, A. J., Morris, M. E., & Cicuttini, F. M. (2004). Reviewing knee osteoarthritis - A biomechanical perspective. *Journal of Science and Medicine in Sport*, *7*(3), 347–357.

Jensen, L. K. (2008). Knee osteoarthritis: Influence of work involving heavy lifting, kneeling, climbing stairs or ladders, or kneeling/squatting combined with heavy lifting. *Occupational and Environmental Medicine*, *65*(2), 72–89.

Jensen, L. K., Rytter, S., & Bonde, J. P. (2010). Exposure assessment of kneeling work activities among floor layers. *Applied Ergonomics*, *41*(2), 319–325.

Joshi, D., Nakamura, B. H., & Hahn, M. E. (2015). High energy spectrogram with integrated prior knowledge for EMG-based locomotion classification. *Medical Engineering and Physics*, *37*(5), 518–524.

Kajaks, T., & Costigan, P. (2015). The effect of sustained static kneeling on kinetic and kinematic knee joint gait parameters. *Applied Ergonomics*, *46*(Part A), 224–230.

Kaya, H., & Gündüz-Öğüdücü, Ş. (2015). A distance based time series classification framework. *Information Systems*, *51*, 27–42.

Kellgren, J. H., & Lawrence, J. S. (1952). Rheumatism in miners. Part II: X-Ray study. *Br J Industr Med*, *9*(3), 197–207.

Kellgren, J. H., & Lawrence, J. S. (1958). Osteo-arthrosis and disk degeneration in an urban population. *Annals of the Rheumatic Diseases*, *17*(4), 388–397.

Kempson, G. E., Spivey, C. J., Swanson, S. A. V, & Freeman, M. A. R. (1971). Patterns of cartilage stiffness on normal and degenerate human femoral heads. *Journal of Biomechanics*, *4*(6), 597–609.

Kiguchi, K., Imada, Y., & Liyanage, M. (2007). EMG-based neuro-fuzzy control of a 4DOF upper-limb power-assist exoskeleton. *Annual International Conference of the IEEE Engineering in Medicine and Biology - Proceedings*, 3040–3043.

Kim, K. S., Choi, H. H., Moon, C. S., & Mun, C. W. (2010). Comparison of k-nearest neighbor, quadratic discriminant and linear discriminant analysis in classification of electromyogram signals based on the wrist-motion directions. *Current Applied Physics*, *11*(3), 740–745.

Kim, M., Cho, J., Lee, S., & Jung, Y. (2019). Imu sensor-based hand gesture recognition for human-machine interfaces. *Sensors*, *19*(18), 1–13.

King, P. M., Gratz, R., & Kleiner, K. (2006). Ergonomic recommendations and their impact on child care workers' health. *Work*, *26*(1), 13–17.

King, P. M., Gratz, R., Scheuer, G., & Claffey, A. (1996). The ergonomics of child care: conducting worksite analyses. *Work*, *6*(1), 25–32.

Kingston, D. C., & Acker, S. M. (2018). Thigh-calf contact parameters for six high knee flexion postures : Onset , maximum angle , total force , contact area , and center of force. *Journal of Biomechanics*, *67*, 46–54.

Kingston, D. C., Tennant, L. M., Chong, H. C., & Acker, S. M. (2016). Peak activation of lower limb musculature during high flexion kneeling and transitional movements. *Ergonomics*, *59*(9), 1215–1223.

Kinney, A. L., Besier, T. F., Silder, A., Delp, S. L., D'Lima, D. D., & Fregly, B. J. (2013). Changes in in vivo knee contact forces through gait modification. *Journal of Orthopaedic Research*, *31*(3), 434–440.

Kivimaki, J., Riihimaki, H., & Hanninen, K. (1992). Knee disorders in carpet and floor layers and painters. *Scandinavian Journal of Work, Environment and Health*, *18*(5), 310–316.

Kluge, F., Gaßner, H., Hannink, J., Pasluosta, C., Klucken, J., & Eskofier, B. M. (2017). Towards mobile gait analysis: Concurrent validity and test-retest reliability of an inertial measurement system for the assessment of spatio-temporal gait parameters. *Sensors*, *17*(7), 1–14.

Klussmann, A., Gebhardt, H., Nübling, M., Liebers, F., Quirós Perea, E., Cordier, W., … Rieger,

M. A. (2010). Individual and occupational risk factors for knee osteoarthritis: results of a case-control study in Germany. *Arthritis Research & Therapy*, *12*(R88), 1–15.

Kok, M., Hol, J. D., & Schön, T. B. (2017). Using inertial sensors for position and orientation estimation. *Foundations and Trends in Signal Processing*, *11*(1–2), 1–153.

Kramer, O. (2013). K-Nearest Neighbors. In H. Springer, Berlin (Ed.), *Dimensionality Reduction with Unsupervised Nearest Neighbors* (Vol. 51, pp. 13–23).

Kraus, V. B., Blanco, F. J., Englund, M., Karsdal, M. A., & Lohmander, L. S. (2015). Call for standardized definitions of osteoarthritis and risk stratification for clinical trials and clinical use. *Osteoarthritis and Cartilage*, *23*(8), 1233–1241.

Kuderle, A. (2017). *Development of a wireless unit for longterm monitoring of the knee joint kinematics in arthrosis patients*. RWTH Aachen University.

Küderle, A., Becker, S., & Disselhorst-Klug, C. (2018). Increasing the robustness of the automatic IMU calibration for lower extremity motion analysis. *Current Directions in Biomedical Engineering*, *4*(1), 439–442.

Kumar, S. (2001). Theories of musculoskeletal injury causation. *Ergonomics*, *44*(1), 17–47.

Kwak, L., Proper, K. I., Hagströmer, M., & Sjöström, M. (2011). The repeatability and validity of questionnaires assessing occupational physical activity - a systematic review. *Scandinavian Journal of Work, Environment and Health*, *37*(1), 6–29.

Laasanen, M. S., Töyräs, J., Korhonen, R. K., Rieppo, J., Saarakkala, S., Nieminen, M. T., … Jurvelin, J. S. (2003). Biomechanical properties of knee articular cartilage. *Biorheology*, *40*(1–3), 133–140.

Labaj, A. (2014). *Posture and lifting exposure of daycare workers: a pilot field study*. Queen's University.

Labaj, A., Diesbourg, T., Dumas, G., Plamondon, A., Mercheri, H., & Larue, C. (2016). Posture and lifting exposures for daycare workers. *International Journal of Industrial Ergonomics*, *54*, 83–92.

Labaj, A., Diesbourg, T. L., Dumas, G. A., Plamondon, A., & Mecheri, H. (2019). Comparison of lifting and bending demands of the various tasks performed by daycare workers. *International Journal of Industrial Ergonomics*, *69*, 96–103.

Laidig, D., Lehmann, D., Begin, M.-A., & Seel, T. (2019). Magnetometer-free realtime inertial motion tracking by exploitation of kinematic constraints in 2-DoF joints. In *IEEE Engineering in Medicine and Biology Conference* (pp. 1233–1238).

Laidig, D., Schauer, T., & Seel, T. (2017). Exploiting kinematic constraints to compensate magnetic disturbances when calculating joint angles of approximate hinge joints from orientation estimates of inertial sensors*. In *2017 International Conference on Rehabilitation Robotics (ICORR)* (pp. 971–976). London: IEEE.

Lau, E. C., Cooper, C., Lam, D., Chan, V. N. H., Tsang, K. K., & Sham, A. (2000). Factors

associated with osteoarthritis of the hip and knee in Hong Kong Chinese: Obesity, joint injury, and occupational activities. *American Journal of Epidemiology*, *152*(9), 855–862.

Lau, H., Tong, K., & Zhu, H. (2009). Support vector machine for classification of walking conditions of persons after stroke with dropped foot. *Human Movement Science*, *28*(4), 504–514.

Laudanski, A. F., Brouwer, B., & Li, Q. (2013). Measurement of lower limb joint kinematics using inertial sensors during stair ascent and descent in healthy older adults and stroke survivors. *Journal of Healthcare Engineering*, *4*(4).

Laudanski, A. F., Brouwer, B., & Li, Q. (2015). Activity classification in persons with stroke based on frequency features. *Medical Engineering and Physics*, *37*(2).

Laudanski, A. F., Buchman-Pearle, J. M., & Acker, S. M. (2022). Quantifying high flexion postures in occupational childcare as they relate to the potential for increased risk of knee osteoarthritis. *Ergonomics*, *65*(2), 253–264.

Lebleu, J., Gosseye, T., Detrembleur, C., Mahaudens, P., Cartiaux, O., & Penta, M. (2020). Lower limb kinematics using inertial sensors during locomotion: Accuracy and reproducibility of joint angle calculations with different sensor-to-segment calibrations. *Sensors (Switzerland)*, *20*(3), 1–17.

Lee, S. H., Park, H. D., Hong, S. Y., Lee, K. J., & Kim, Y. H. (2003). A study on the activity classification using a triaxial accelerometer. In *25th Annual International Conference of the IEEE Engineering in Medicine and Biology Society* (pp. 2941–2943). Cancun: Ieee.

Leszko, F., Hovinga, K. R., Lerner, A. L., Komistek, R. D., & Mahfouz, M. R. (2011). In vivo normal knee kinematics: Is ethnicity or gender an influencing factor? *Clinical Orthopaedics and Related Research*, *469*(1), 95–106.

Leuenberger, K., Gonzenbach, R., Wiedmer, E., Luft, A., & Gassert, R. (2014). Classification of stair ascent and descent in stroke patients. In *11th International Conference on Wearable and Implantable Body Sensor Networks Workshops* (pp. 11–16).

Li, G., Zayontz, S., DeFrate, L. E., Most, E., Suggs, J. F., & Rubash, H. E. (2004). Kinematics of the knee at high flexion angles: an in vitro investigation. *Journal of Orthopaedic Research*, *22*(1), 90–95.

Lima, W. S., Souto, E., El-khatib, K., Jalali, R., & Gama, J. (2019). Human activity recognition using inertial sensors in a smartphone : An overview. *Sensors*, *19*(3213), 1–28.

Lin, J. F.-S., Joukov, V., & Kulić, D. (2018). Classification-based Segmentation for Rehabilitation Exercise Monitoring. *Journal of Rehabilitation and Assistive Technologies Engineering*, *5*, 1–12.

Lin, J. F.-S., Samadani, A.-A., & Kulić, D. (2016). *Segmentation by data point classification applied to forearm surface EMG. In: Leon-Gargica A. et al. (eds) Smart City 360. First EAI International Summit, Smart City 360*. Springer, Cham.

Lindberg, H., Roos, H., & Gärdsell, P. (1993). Prevalence of coxarthrosis in former soccer

players: 286 players compared with matched controls. *Acta Orthopaedica*, *64*(2), 165–167.

Linnan, L., Arandia, G., Bateman, L. A., Vaughn, A., Smith, N., & Ward, D. (2017). The health and working conditions of women employed in child care. *International Journal of Environmental Research and Public Health*, *14*(3), 1–14.

Longpré, H. S., Acker, S. M., & Maly, M. R. (2015). Muscle activation and knee biomechanics during squatting and lunging after lower extremity fatigue in healthy young women. *Journal of Electromyography and Kinesiology*, *25*(1), 40–46.

Lovejoy, C. O. (2007). The natural history of human gait and posture. Part 3. The knee. *Gait and Posture*, *25*(3), 325–341.

Luinge, H. J., Veltink, P. H., & Baten, C. T. M. (2007). Ambulatory measurement of arm orientation. *Journal of Biomechanics*, *40*, 78–85.

Madhu-Das, C., & Srichand, P. (2006). Maternal mortality and morbidity due to induced abortion in Hyderabad. *Journal of the Liaquat University of Medical and Health Sciences*, *5*(2), 62–65.

Maldonado, M., & Nam, J. (2013). The role of changes in extracellular matrix of cartilage in the presence of inflammation on the pathology of osteoarthritis. *BioMed Research International*, *2013*, 1–10.

Markon, P., & Le Beau, D. (1994). *Health and safety at work for day-care educators*. *Université du Québec à Chicoutimi*.

Massé, F., Gonzenbach, R. R., Arami, A., Paraschiv-Ionescu, A., Luft, A. R., & Aminian, K. (2015). Improving activity recognition using a wearable barometric pressure sensor in mobility-impaired stroke patients. *Journal of NeuroEngineering and Rehabilitation*, *12*(1), 1–15.

Matsuda, M., Morikuni, K., Imakura, A., Ye, X., & Sakurai, T. (2020). Multiclass spectral feature scaling method for dimensionality reduction. *Intelligent Data Analysis2*, *24*(6), 1273–1287.

Maurer, U., Smailagic, A., Siewiorek, D. P., & Deisher, M. (2006). Activity recognition and monitoring using multiple sensors on different body positions. *Proceedings - BSN 2006: International Workshop on Wearable and Implantable Body Sensor Networks*, *2006*, 113–116.

McCambridge, J., Witton, J., & Elbourne, D. R. (2014). Systematic review of the Hawthorne effect: New concepts are needed to study research participation effects. *Journal of Clinical Epidemiology*, *67*(3), 267–277.

McDermott, I. D., Masouros, S. D., & Amis, A. A. (2008). Biomechanics of the menisci of the knee. *Current Orthopaedics*, *22*(3), 193–201.

McKean, K. A., Landry, S. C., Hubley-Kozey, C. L., Dunbar, M. J., Stanish, W. D., & Deluzio, K. J. (2007). Gender differences exist in osteoarthritic gait. *Clinical Biomechanics*, *22*(4), 400–409.

Medina, M. Á. L., Espinilla, M., Paggeti, C., & Quero, J. M. (2019). Activity recognition for IoT devices using fuzzy spatio-temporal features as environmental sensor fusion. *Sensors*, *19*, 1–20.

Mekruksavanich, S., Jitpattanakul, A., Youplao, P., & Yupapin, P. (2020). Enhanced hand-oriented activity recognition based on smartwatch sensor data using LSTMs. *Symmetry*, *12*(9), 1–19.

Miller, J. D., Beazer, M. S., & Hahn, M. E. (2013). Myoelectric walking mode classification for transtibial amputees. *IEEE Transactions on Biomedical Engineering*, *60*(10), 2745–2750.

Molnar, M., Kok, M., Engel, T., Kaplick, H., Mayer, F., & Seel, T. (2018). A method for lower back motion assessment using wearable 6D inertial sensors. In *21st International Conference on Information Fusion (FUSION)* (pp. 799–806). ISIF.

Moore, K. ., Dalley, A. F., & Agur, A. M. R. (2010). *Clinically Oriented Anatomy*. (K. . Moore, A. F. Dalley, & A. M. R. Agur, Eds.) (6th editio). Wolters Kluwer.

Muller, P., Begin, M. A., Schauer, T., & Seel, T. (2017). Alignment-free, self-calibrating elbow angles measurement using inertial sensors. *IEEE Journal of Biomedical and Health Informatics*, *21*(2), 312–319.

Mundt, M., Johnson, W. R., Potthast, W., Markert, B., Mian, A., & Alderson, J. (2021). A comparison of three neural network approaches for measurement units. *Sensors*, *21*(4535), 1–14.

Muscillo, R., Conforto, S., Schmid, M., Caselli, P., & D'Alessio, T. (2007). Classification of motor activities through derivative dynamic time warping applied on accelerometer data. In *29th Annual International conference of the IEEE Engineering in Medicine and Biology Society* (pp. 4930–4933). Lyon.

Myers, C. S., & Rabiner, L. R. (1981). A comparative study of several dynamic time-warping algorithms for connected-word recognition. *Bell System Technical Journal*, *60*(7), 1389–1409.

Nagura, T., Dyrby, C. O., Alexander, E. J., & Andriacchi, T. P. (2002). Mechanical loads at the knee joint during deep flexion. *Journal of Orthopaedic Research*, *20*(4), 881–886.

Najafi, B., Aminian, K., Loew, F., Blanc, Y., & Robert, P. A. (2002). Measurement of stand-sit and sit-stand transitions using a miniature gyroscope and its application in fall risk evaluation in the elderly. *IEEE Transactions on Biomedical Engineering*, *49*(8), 843–851.

Najafi, B., Aminian, K., Paraschiv-Ionescu, A., Loew, F., Büla, C. J., & Robert, P. (2003). Ambulatory system for human motion analysis using a kinematic sensor: Monitoring of daily physical activity in the elderly. *IEEE Transactions on Biomedical Engineering*, *50*(6), 711–723.

Nayak, S., & Das, R. (2020). Application of artificial intelligence (AI) in prosthetic and orthotic rehabilitation. In V. Sezer, S. Öncü, & P. B. Baykas (Eds.), *Service Robotics*.

Nazmi, N., Abdul Rahman, M., Yamamoto, S.-I., Ahmad, S., Zamzuri, H., & Mazlan, S. (2016).

A review of classification techniques of EMG signals during isotonic and isometric contractions. *Sensors*, *16*(8), 1–28.

Neshteruk, C. D., Willis, E., Smith, F., Vaughn, A. E., Grummon, A. H., Vu, M. B., … Linnan, L. (2021). Implementation of a workplace physical activity intervention in child care: process evaluation results from the Care2BWell trial. *Translational Behavioral Medicine*, *11*(7), 1430–1440.

Nguyen, A., Roth, N., Ghassemi, N. H., Hannink, J., Seel, T., Klucken, J., … Eskofier, B. M. (2019). Development and clinical validation of inertial sensor-based gait-clustering methods in Parkinson's disease. *Journal of NeuroEngineering and Rehabilitation*, *16*(77), 1–14.

Nissen, N., Holm, P. M., Bricca, A., Dideriksen, M., Tang, L. H., & Skou, S. T. (2022). Clinicians' beliefs and attitudes to physical activity and exercise therapy as treatment for knee and/or hip osteoarthritis: a scoping review. *Osteoarthritis and Cartilage*, *30*(2), 260–269.

Nocedal, J., & Wright, S. J. (2000). *Numerical Optimization*. (T. V. Mikosch, S. M. Robinson, & S. I. Resnick, Eds.) (Second Edi). Springer.

Nowka, D., Kok, M., & Seel, T. (2019). On motions that allow for identification of hinge joint axes from kinematic constraints and 6D IMU data. In *18th European Control Conference* (pp. 1–7). Naples.

Nurhanim, K., Elamvazuthi, I., Izhar, L. I., & Ganesan, T. (2017). Classification of human activity based on smartphone inertial sensor using support vector machine. *IEEE 3rd International Symposium in Robotics and Manufacturing Automation (2017)*, 1–5.

Oettmeier, R., Arokoski, J. P. A., Roth, A. J., Helminen, H. J., Tammi, M., & Abendroth, K. (1992). Quantitative study of articular cartilage and subchondral bone remodeling in the knee joint of dogs after strenuous running training. *Journal of Bone and Mineral Research*, *7*(2), S419–S424.

Okuno, M., Uketa, S. I., Nakaseko, M., & Tokunaga, R. (1997). Work and workload of nursing personnel in a nursery school and two institutions for handicapped children. *Industrial Health*, *35*(2), 202–211.

Olsson, F., Kok, M., Seel, T., & Halvorsen, K. (2020). Robust plug-and-play joint axis estimation using inertial sensors. *Sensors (Switzerland)*, *20*(12), 1.

Olsson, F., Seel, T., Lehmann, D., & Halvorsen, K. (2019). Joint axis estimation for fast and slow movements using weighted gyroscope and acceleration constraints. In *22nd International conference on Information Fusion* (pp. 1–8). Ottawa.

Osteoarthritis Research Society International. (2018). Osteoarthritis: A Serious Disease, Submitted to the U. S. Food and Drug Administration. *Oarsi*.

Paiyarom, S., Tungamchit, P., Keinprasit, R., & Kayasith, P. (2009). Activity monitoring system using dynamic time warping for the elderly and disabled people. In *2nd International conference on Computer, Control, and Communication IEEE* (pp. 1–4). IEEE.

Paliwal, K. K., Agarwal, A., & Sinha, S. S. (1982). A modification over Sakoe and Chiba's dynamic time warping algorithm for isolated word recognition. *Signal Processing1*, *4*, 329–333.

Parry, E., Ogollah, R., & Peat, G. (2019). 'Acute flare-ups' in patients with, or at high risk of, knee osteoarthritis: a daily diary study with case-crossover analysis. *Osteoarthritis and Cartilage*, *27*(8), 1124–1128.

Perry, J., Garrett, M., Gronley, J. K., & Mulroy, S. J. (1995). Classification of walking handicap in the stroke population. *Stroke*, *26*(6), 982–989.

Phinyomark, A., Phukpattaranont, P., & Limsakul, C. (2012). Feature reduction and selection for EMG signal classification. *Expert Systems with Applications*, *39*(8), 7420–7431.

Picerno, P., Caliandro, P., Iacovelli, C., Simbolotti, C., Crabolu, M., Pani, D., … Cereatti, A. (2019). Upper limb joint kinematics using wearable magnetic and inertial measurement units: an anatomical calibration procedure based on bony landmark identification. *Scientific Reports*, *9*(1), 1–10.

Picerno, P., Cereatti, A., & Cappozzo, A. (2008). Joint kinematics estimate using wearable inertial and magnetic sensing modules. *Gait & Posture*, *28*(4), 588–595.

Picerno, P., Iosa, M., Souza, C. D., Grazia, M., Paolucci, S., & Morone, G. (2021). Wearable inertial sensors for human movement analysis : a five-year update. *Expert Review of Medical Devices*, *18*(1), 79–94.

Pirttikangas, S., Fujinami, K., & Nakajima, T. (2006). Feature selection and activity recognition from wearable sensors. In *Ubiquitous Computing Systems* (pp. 516–527).

Preece, S. J., Goulermas, J. Y., Kenney, L. P. J., & Howard, D. (2009). A comparison of feature extraction methods for the classification of dynamic activities from accelerometer data. *IEEE Transactions on Biomedical Engineering*, *56*(3), 871–879.

Preece, S. J., Goulermas, J. Y., Kenney, L. P. J., Howard, D., Meijer, K., & Crompton, R. (2009). Activity identification using body-mounted sensors - A review of classification techniques. *Physiological Measurement*, *30*(4).

Puig, A., Escalona, C., Padullés, J., Busquets, A., Padullés, X., & Marcos, D. (2019). Validity and reliability of the Kinovea program in obtaining angles and distances using coordinates in 4 perspectives. *Plos One*, *14*(6), 1–14.

Qi, W., Hosseini, A., Tsai, T. Y., Li, J. S., Rubash, H. E., & Li, G. (2013). In vivo kinematics of the knee during weight bearing high flexion. *Journal of Biomechanics*, *46*(9), 1576–1582.

Qiu, S., Liu, L., Zhao, H., Wang, Z., & Jiang, Y. (2018). MEMS inertial sensors based gait analysis for rehabilitation assessment via multi-sensor fusion. *Micromachines*, *9*(9), 1–17.

Qiu, S., Wang, Z., Zhao, H., Liu, L., & Jiang, Y. (2018). Using body-worn sensors for preliminary rehabilitation assessment in stroke victims with gait impairment. *IEEE Access*, *6*, 31249–31258.

Radin, E. L., Yang, K. H., Riegger, C., Kish, V. L., & O'Connor, J. J. (1991). Relationship between lower limb dynamics and knee joint pain. *Journal of Orthopaedic Research*, *9*(3), 398–405.

Rakhsha, M., Smith, C. R., Recuero, A. M., Brandon, S. C. E., Vignos, M. F., Thelen, D. G., & Negrut, D. (2018). Simulation of surface strain in tibiofemoral cartilage during walking for the prediction of collagen fibre orientation. *Computer Methods in Biomechanics and Biomedical Engineering: Imaging and Visualization*, *1163*, 1–10.

Rast, F. M., & Labruyère, R. (2020). Systematic review on the application of wearable inertial sensors to quantify everyday life motor activity in people with mobility impairments. *Journal of NeuroEngineering and Rehabilitation*, *17*(148), 1–19.

Rebula, J. R., Ojeda, L. V., Adamczyk, P. G., & Kuo, A. D. (2013). Measurement of foot placement and its variability with inertial sensors. *Gait and Posture*, *38*(4), 974–980.

Reenalda, J., Maartens, E., Homan, L., & Buurke, J. H. (Jaap). (2016). Continuous three dimensional analysis of running mechanics during a marathon by means of inertial magnetic measurement units to objectify changes in running mechanics. *Journal of Biomechanics*, *49*(14), 3362–3367.

Richmond, S. A., Fukuchi, R. K., Ezzat, A., Schneider, K., Schneider, G., & Emery, C. A. (2013). Are joint injury, sport activity, physical activity, obesity, or occupational activities rredictors for osteoarthritis? A systematic review. *Journal of Orthopaedic & Sports Physical Therapy*, *43*(8), 515-524 B1-B19.

Robinson, M. A., & Vanrenterghem, J. (2012). An evaluation of anatomical and functional knee axis definition in the context of side-cutting. *Journal of Biomechanics*, *45*(11), 1941–1946.

Roos, H., Lohmander, L. S., Wingstrand, H., Lindberg, H., & Gärdsell, P. (1994). The prevalence of gonarthrosis and its relation to meniscectomy in former soccer players. *The American Journal of Sports Medicine*, *22*(2), 219–222.

Roscher, R., Bohn, B., Duarte, M. F., & Garcke, J. (2020). Explainable machine learning for scientific insights and discoveries. *IEEE Access*, *8*, 42200–42216.

Rytter, S., Egund, N., Jensen, L. K., & Bonde, J. P. (2009). Occupational kneeling and radiographic tibiofemoral and patellofemoral osteoarthritis. *Journal of Occupational Medicine and Toxicology*, *4*(1), 1–9.

Sakoe, H., & Chiba, S. (1978). Dynamic programming algorithm optimization for spoken word recognition. *IEEE Transactions on Acoustics, Speech, and Signal Processing*, *26*(1), 43–49.

Samadani, A.-A., & Kulic, D. (2014). Hand gesture recognition based on surface electromyography. In *36th Annual International Conference of the IEEE Engineering in Medicine and Biology Society* (pp. 4196–4199).

Sandmark, H., Hogstedt, C., & Vingård, E. (2000). Primary osteoarthrosis of the knee in men and women as a result of lifelong physical load from work. *Scandinavian Journal of Work, Environment and Health*, *26*(1), 20–25.

Sapsanis, C., Georgoulas, G., & Tzes, A. (2013). EMG based classification of basic hand movements based on time frequency features. In *21st Mediterranean Conference on Control and Automation, MED 2013 - Conference Proceedings* (pp. 716–722). Crete.

Sarcevic, P., Kincses, Z., & Pletl, S. (2019). Online human movement classification using wrist-worn wireless sensors. *Journal of Ambient Intelligence and Humanized Computing*, *10*(1), 89–106.

Schall, M. C., Fethke, N. B., Chen, H., & Gerr, F. (2015). A comparison of instrumentation methods to estimate thoracolumbar motion in field-based occupational studies. *Applied Ergonomics*.

Schiphof, D., Boers, M., & Bierma-Zeinstra, S. M. A. (2008). Differences in descriptions of Kellgren and Lawrence grades of knee osteoarthritis. *Annals of the Rheumatic Diseases*, *67*(7), 1034–1036.

Schwartz, M. H., & Rozumalski, A. (2005). A new method for estimating joint parameters from motion data. *Journal of Biomechanics*, *38*(1), 107–116.

Seel, T. (2016). *Learning Control and Inertial Realtime Gait Analysis in Biomedical Applications*. Technical University of Berlin.

Seel, T., Raisch, J., & Schauer, T. (2014). IMU-based joint angle measurement for gait analysis. *Sensors*, *14*, 6891–6909.

Seel, T., Schauer, T., & Raisch, J. (2012). Joint axis and position estimation from inertial measurement data by exploiting kinematic constraints. In *IEEE International Conference on Control Applications* (pp. 45–49). Dubrovnik.

Seidler, A., Bolm-Audorff, U., Abolmaali, N., Elsner, G., Gül, A., Ridder, S., … Zichner, L. (2008). The role of cumulative physical work load in symptomatic knee osteoarthritis - A case-control study in Germany. *Journal of Occupational Medicine and Toxicology*, *3*(1), 1–8.

Shimaoka, M., Hiruta, S., Ono, Y., Nonaka, H., Wigaeus Hjelm, E., & Hagberg, M. (1997). A comparative study of physical work load in Japanese and Swedish nursery school teachers. *European Journal of Applied Physiology and Occupational Physiology*, *77*(1–2), 10–18.

Shrier, I. (2004). Muscle dysfunction versus wear and tear as a cause of exercise related osteoarthritis: An epidemiological update. *British Journal of Sports Medicine*, *38*(5), 526–535.

Silver, F. H., Bradica, G., & Tria, A. (2002). Elastic energy storage in human articular cartilage: Estimation of the elastic modulus for type II collagen and changes associated with osteoarthritis. *Matrix Biology*, *21*(2), 129–137.

Sinha, V. K., Patro, K. K., Plawiak, P., & Prakash, A. J. (2021). Smartphone-based human sitting behaviors recognition using inertial sensor. *Sensors*, *21*(6652), 1–14.

Snoeker, B. A. M., Bakker, E. W. P., Kegel, C. A. T., & Lucas, C. (2013). Risk factors for meniscal tears: A systematic review including meta-analysis. *Journal of Orthopaedic &*

*Sports Physical Therapy*, *43*(6), 352–367.

Song, J. B., Lee, C., Lee, W. J., Bahn, S., Jung, C. J., & Yun, M. H. (2016). Development of a job rotation scheduling algorithm for minimizing accumulated work load per body parts. *Work*, *53*(3), 511–521.

Statistics Canada. (2016). *2016 Census*. *2016 Census of Canada*. Ottawa.

Stockwell, W. (2003). *Angle Random Walk*. *Crossbow*.

Swarnakar, S. K., Agrawal, H., & Goel, A. (2021). *Smartphone Inertial Sensors-Based Human Activity Detection Using Support Vector Machine*. Springer Singapore.

Tak, S., Paquet, V., Woskie, S., Buchholz, B., & Punnett, L. (2009). Variability in risk factors for knee injury in construction. *Journal of Occupational and Environmental Hygiene*, *6*(2), 113–120.

Tennant, L. M., Chong, H. C., & Acker, S. M. (2018). The effects of a simulated occupational kneeling exposure on squat mechanics and knee joint load during gait. *Ergonomics*, *61*(6), 839–852.

Tennant, L. M., Maly, M. R., Callaghan, J. P., & Acker, S. M. (2014). Analysis of muscle activation patterns during transitions into and out of high knee flexion postures. *Journal of Electromyography and Kinesiology*, *24*(5), 711–717.

Teufl, W., Miezal, M., Taetz, B., & Fröhlich, M. (2018). Stability of magnetometer free inertial sensor based 3D joint kinematics. *Sensors*, *18*(1980), 1–22.

Teufl, W., Taetz, B., Miezal, M., Dindorf, C., Fröhlich, M., Trinler, U., … Bleser, G. (2021). Automated detection and explainability of pathological gait patterns using a one-class support vector machine trained on inertial measurement unit based gait data. *Clinical Biomechanics*, *89*, 1–7.

Tharwat, A., Gaber, T., Ibrahim, A., & Hassanien, A. E. (2017). Linear discriminant analysis: A detailed tutorial. *AI Communications*, *30*(2), 169–190.

The Social Research Centre. (2017). *2016 Early Childhood Education and Care Workforce Census*. Melbourne.

Theodoridis, S., & Koutroumbas, K. (2003). *Pattern Recognition* (2nd editio). Elsevier.

Triggs, B., Mclauchlan, P. F., Hartley, R. I., & Fitzgibbon, A. W. (2000). Bundle adjustment — A modern synthesis. In *Vision Algorithms: Theory and Practice* (Vol. 1883, pp. 298–372).

Trung, N. T., Makihara, Y., Nagahara, H., Mukaigawa, Y., & Yagi, Y. (2012). Inertial-sensor-based walking action recognition using robust step detection and inter-class relationships. *Proceedings - International Conference on Pattern Recognition*, (Icpr), 3811–3814.

Tsai, A. C., Hsieh, T. H., Luh, J. J., & Lin, T. Te. (2014). A comparison of upper-limb motion pattern recognition using EMG signals during dynamic and isometric muscle contractions. *Biomedical Signal Processing and Control*, *11*(1), 17–26.

Tsai, T., Lu, T., Kuo, M., & Lin, C. (2011). Effects of soft tissue artifacts on the calculated kinematics and kinetics of the knee during stair-ascent. *Journal of Biomechanics*, *44*(6), 1182–1188.

Um, T. T., Babakeshizadeh, V., & Kulić, D. (2017). Exercise motion classification from large-scale wearable sensor data using convolutional neural networks. In *IEEE/RSJ International Conference on Intelligent robots and systems* (pp. 2385–2390). Vancouver, BC.

US Bureau of Labor Statistics. (2018). *Injuries Illnesses and Fatalities*. *U.S. Department of Labor*.

Usharani, J., & Sakthivel, U. (2014). Human activity recognition using smartphone. In *1st International Conference on Innovations in Computing & Networking* (pp. 2012–2015).

van Hees, V. T., Golubic, R., Ekelund, U., & Brage, S. (2013). Impact of study design on development and evaluation of an activity-type classifier. *Journal of Applied Physiology*, *114*(8), 1042–1051.

Veltink, P. H., Bussmann, H. B. J., De Vries, W., Martens, W. L. J., & Van Lummel, R. C. (1996). Detection of static and dynamic activities using uniaxial accelerometers. *IEEE Transactions on Rehabilitation Engineering*, *4*(4), 375–385.

Venn, M., & Maroudas, A. (1977). Chemical composition and swelling of normal and osteoarthrotic femoral head cartilage. *Annals of the Rheumatic Diseases*, *36*, 121–129.

Vilone, G., & Longo, L. (2021). Classification of explainable artificial intelligence methods through their output formats. *Machine Learning & Knowledge Extraction*, *3*, 615–661.

Virayavanich, W., Alizai, H., Baum, T., Nardo, L., Nevitt, M. C., Lynch, J. A., … Link, T. M. (2013). Association of frequent knee bending activity with focal knee lesions detected with 3T magnetic resonance imaging: Data from the osteoarthritis initiative. *Arthritis Care and Research*, *65*(9), 1441–1448.

Vitali, R. V., Cain, S. M., McGinnis, R. S., Zaferiou, A. M., Ojeda, L. V., Davidson, S. P., & Perkins, N. C. (2017). Method for estimating three-dimensional knee rotations using two inertial measurement units: Validation with a coordinate measurement machine. *Sensors (Switzerland)*, *17*(9), 1–16.

Vitali, R. V., & Perkins, N. C. (2020). Determining anatomical frames via inertial motion capture: A survey of methods. *Journal of Biomechanics*, *106*, 1–10.

Von Tscharner, V., & Goepfert, B. (2003). Gender dependent EMGs of runners resolved by time/frequency and principal pattern analysis. *Journal of Electromyography and Kinesiology*, *13*(3), 253–272.

Wallace, I. J., Worthington, S., Felson, D. T., Jurmain, R. D., Wren, K. T., Maijanen, H., … Lieberman, D. E. (2017). Knee osteoarthritis has doubled in prevalence since the mid-20th century. *Proceedings of the National Academy of Sciences of the United States of America*, *114*(35), 9332–9336.

Wang, F.-C., Chen, S.-F., Lin, C.-H., Shih, C.-J., Lin, A.-C., Yuan, W., … Kuo, T. (2021).

Detection and classification of stroke gaits by deep neural networks employing inertial measurement units. *Sensors*, *21*(1864), 1–18.

Wang, L., Sun, Y., Li, Q., & Liu, T. (2018). Estimation of step length and gait asymmetry using wearable inertial sensors. *IEEE Sensors Journal*, *18*(9), 3844–3851.

Wang, N., Ambikairajah, E., Lovell, N. H., & Celler, B. G. (2007). Accelerometry based classification of walking patterns using time-frequency analysis. In *29th Annual International conference of the IEEE Engineering in Medicine and Biology Society* (pp. 4899–4902). Lyon.

Wang, X., Perry, T. A., Arden, N., Chen, L., Parsons, C. M., Cooper, C., … Hunter, D. J. (2020). Occupational risk in knee osteoarthritis: A systematic review and meta-analysis of observational studies. *Arthritis Care and Research*, *72*(9), 1213–1223.

Wang, Y., Nguyen, U. S. D. T., Lane, N. E., Lu, N., Wei, J., Lei, G., … Zhang, Y. (2021). Knee osteoarthritis, potential mediators, and risk of all-cause mortality: Data from the osteoarthritis initiative. *Arthritis Care and Research*, *73*(4), 566–573.

Webb, A. R. (2002). *Statistical Pattern Recognition* (2nd editio, Vol. 9). John Wiley & Sons, Ltd.

Webb, A. R., & Copsey, K. D. (2011). *Statistical Pattern Recognition* (3rd editio). Wiley.

Weygers, I., Kok, M., Seel, T., Shah, D., Taylan, O., Scheys, L., … Claeys, K. (2021). In-vitro validation of inertial-sensor-to-bone alignment. *Journal of Biomechanics*, *128*, 1–8.

Whitfield, B. H., Costigan, P. A., Stevenson, J. M., & Smallman, C. L. (2014). Effect of an on-body ergonomic aid on oxygen consumption during a repetitive lifting task. *International Journal of Industrial Ergonomics*, *44*, 39–44.

WHO Multicentre Growth Reference Study Group. (2006). WHO Child Growth Standards based on length/height, weight and age. *Acta Paediatrica, International Journal of Paediatrics*, *95*(SUPPL. 450), 76–85.

Winter, D. A. (2009). *Biomechanics and motor control of human movement*. (I. John Wiley & Sons, Ed.) (4th editio). Hoboken, NJ: Wiley.

Woodman, O. J. (2007). *An introduction to inertial navigation*. *University of Cambridge Computer Laboratory*. Cambridge.

Wortman, A. M. (1999). Preventing work-related musculoskeletal injuries. *Childcare Information Exchange*.

WSIB Ontario. (2019). *By the numbers 2019 WSIB statistical report*.

WSIB Ontario. (2020). *Allowed Lost Time Claims from Childcare Workers 2010-2019*.

Wu, G., & Cavanagh, P. R. (1995a). ISB recommendations for standardization in the reporting of kinematic data. *Journal of Biomechanics*.

Wu, G., & Cavanagh, P. R. (1995b). ISB recommendations in the reporting for standardization

of kinematic data. *Journal of Biomechanics*, *28*(10), 1257–1261.

Wu, G., Siegler, S., Allard, P., Kirtley, C., Leardini, A., Rosenbaum, D., … Stokes, I. (2002). ISB recommendation on definitions of joint coordinate system of various joints for the reporting of human joint motion—part I: ankle, hip, and spine. *Journal of Biomechanics*, *35*, 543–548.

Wu, G., Van Der Helm, F. C. T., Veeger, H. E. J., Makhsous, M., Van Roy, P., Anglin, C., … Buchholz, B. (2005). ISB recommendation on definitions of joint coordinate systems of various joints for the reporting of human joint motion - Part II: Shoulder, elbow, wrist and hand. *Journal of Biomechanics*, *38*(5), 981–992.

Yang, D., Huang, J., Tu, X., Ding, G., Shen, T., & Xiao, X. (2019). A wearable activity recognition device using air-pressure and IMU sensors. *IEEE Access*, *7*, 6611–6621.

Yang, W., Wang, K., & Zuo, W. (2012). Neighborhood component feature selection for high-dimensional data. *Journal of Computers*, *7*(1), 162–168.

Yao, J., Lancianese, S. L., Hovinga, K. R., Lee, J., & Lerner, A. L. (2008). Magnetic resonance image analysis of meniscal translation and tibio-menisco-femoral contact in deep knee flexion. *Journal of Orthopaedic Research*, *26*(5), 673–684.

Ying, H., Silex, C., Schnitzer, A., Leonhardt, S., & Schiek, M. (2007). Automatic step detection in the accelerometer signal. *4th International Workshop on Wearable and Implantable Body Sensor Networks (BSN 2007)*, 80–85.

Yoshikawa, M., Mikawa, M., & Tanaka, K. (2007). A myoelectric interface for robotic hand control using support vector machine. In *2007 IEEE/RSJ International Conference on Intelligent Robots and Systems* (pp. 2723–2728).

Young, A. J., Smith, L. H., Rouse, E. J., & Hargrove, L. J. (2013). Classification of simultaneous movements using surface EMG pattern recognition. *IEEE Transactions on Biomedical Engineering*, *60*(5), 1250–1258.

Yucesoy, B., Charles, L. E., Baker, B., & Burchfiel, C. M. (2015). Occupational and genetic risk factors for osteoarthritis: A review. *Work*, *50*(2), 261–273.

Zhang, J., Novak, A. C., Brouwer, B., & Li, Q. (2013). Concurrent validation of Xsens MVN measurement of lower limb joint angular kinematics. *Physiological Measurement*, *34*, 63–69.

Zhang, K., Sun, M., Lester, D. K., Pi-Sunyer, F. X., Boozer, C. N., & Longman, R. W. (2005). Assessment of human locomotion by using an insole measurement system and artificial neural networks. *Journal of Biomechanics*, *38*(11), 2276–2287.

Zhang, T., Wang, J., Xu, L., & Liu, P. (2006). Using wearable sensor and NMF algorithm to realize ambulatory fall detection. In *International Conference on Natural Computation 2006* (pp. 488–491).

Zhang, W., Gignac, M. A. M., Beaton, D., Tang, K., & Anis, A. H. (2010). Productivity loss due to presenteeism among patients with arthritis: Estimates from 4 instruments. *Journal of*

*Rheumatology*, *37*(9), 1805–1814.

Zhang, X., Xia, R., Dai, B., Sun, X., & Fu, W. (2018). Effects of exercise-induced fatigue on lower extremity joint mechanics, stiffness, and energy absorption during landings. *Journal of Sports Science and Medicine*, *17*(4), 640–649.

Zhang, Y., & Jordan, J. M. (2010). Epidemiology of osteoarthritis. *Clinical Geriatric Medicine*, *26*(3), 355–369.

Zimmermann, T., Taetz, B., & Bleser, G. (2018). IMU-to-segment assignment and orientation alignment for the lower body using deep learning. *Sensors*, *18*(302), 1–35.

Zubair, M., Song, K., & Yoon, C. (2017). Human activity recognition using wearable accelerometer sensors. In *2016 IEEE International Conference on Consumer Electronics-Asia, ICCE-Asia 2016* (pp. 1–5). IEEE.

# Appendices

# Appendix A
# Body Segment Coordinate System for the Lower Limbs

The following section will outline the segmental coordinate system definitions which were utilized for kinematic calculations in Chapter 4 based on optical motion capture data following ISB guidelines (Wu & Cavanagh, 1995a; Wu et al., 2002) with the addition of functional joint center calculations for the hip. These coordinate systems were implemented in Visual 3D (Visual 3D, C-Motion Inc., Germantown, MD). The standard pelvis system used in Visual 3D is the Coda pelvis, this segment was constructed prior to constructing a virtual pelvis which was used in hip joint angle calculations. Similarly, a standard foot segment was created in Visual 3D in addition to a virtual foot segment which was used in the ankle joint angle calculations.

Table A.1 Segmental coordinate system definitions utilized for the calculation of ankle, knee, and hip flexion-extension kinematics based on optical motion capture data.

| Segment | Description |
|---|---|
| Pelvis (Coda) | |
| Origin | Midpoint between the left and right anterior superior iliac spines |
| Z-axis | Vector passing from the origin towards the right anterior superior iliac spines |
| Y-axis | Cross product of the temporary vector from the Origin towards the midpoint of the left and right posterior superior iliac spines and the z-axis |
| X-axis | Cross product of the y- and z-axes |
| Pelvis segment | |
| Origin | Midpoint between the left and right iliac crests |
| YZ-plane | Plane created by the left to right iliac crests and the hip joint centers (established based on functional calibration trials). |
| Y-axis | Vector passing from the midpoint of the left and right hip joint centers towards the origin. |
| X-axis | Vector perpendicular to the YZ plane, oriented anteriorly |
| Z-axis | Vector perpendicular to the YZ plane, oriented anteriorly |

| | |
|---|---|
| Thigh segment | |
| Origin | Functional hip joint centre (Camomilla et al., 2006; Schwartz & Rozumalski, 2005) |
| Y-axis | Vector from the mid-point of the medial and lateral femoral epicondyles to the Origin |
| X-axis | Cross-product of the y-axis and a temporary vector from the Origin to the greater trochanter |
| Z-axis | Cross product of the x- and y-axes |
| Shank segment | |
| Origin | Midpoint between the medial and lateral tibial epicondyles |
| Y-axis | Vector from the midpoint of the medial and lateral malleoli to the Origin |
| X-axis | Cross-product of the y-axis and a temporary vector from the medial to the lateral tibial epicondyles |
| Z-axis | Cross product of the x- and y-axes |
| Foot segment | |
| Origin | Midpoint between the medial and lateral malleoli |
| Y-axis | Vector from the midpoint of the first and fifth metatarsal heads to the Origin |
| X-axis | Cross-product of the y-axis and a temporary vector from the first to the fifth metatarsal heads. |
| Z-axis | Cross product of the x- and y-axes |
| Foot segment (Virtual) – defined based on the coordinate system of the shank, tracked using the foot cluster | |

# Appendix B
# Sample Accelerometer- and Gyroscope-Based Estimates of Joint Angles

The following section contains representative curves for joint flexion-extension angles estimates based on accelerometer signals in the sensor-based coordinate system, accelerometer signals rotated into the joint coordinate system, gyroscope signals in the sensor-based coordinate system, gyroscope signals in the joint coordinate system, and finally a combination of the accelerometer- and gyroscope-based angles in the joint coordinate system compared to the final measured joint angle.

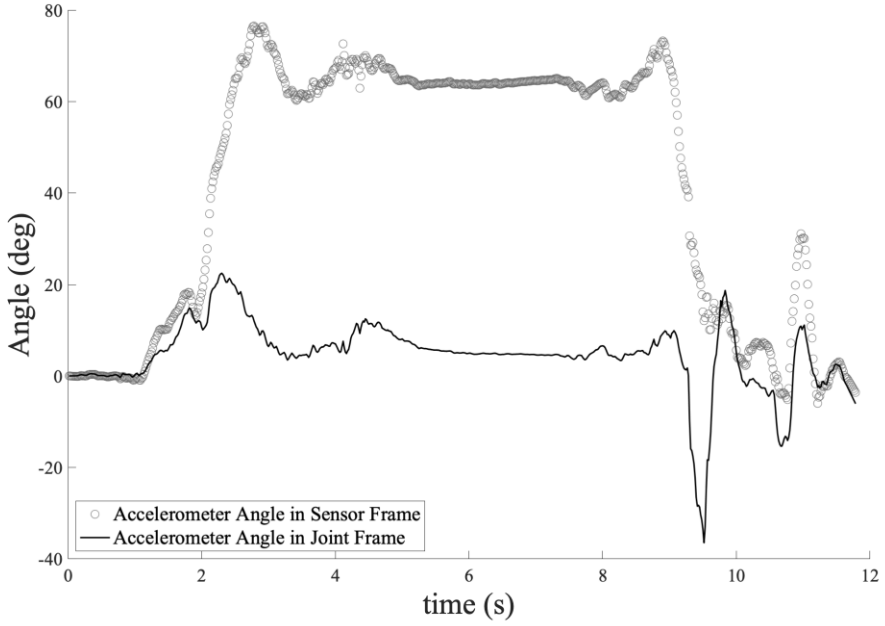


Figure B.1 Representative accelerometer-based ankle flexion-extension angles for a dorsiflexed kneeling trial calculated based on acceleration data in the sensor frame as well as on the portion of the acceleration data responsible for accelerating the joint centre as calculated through Eq. (4.35).

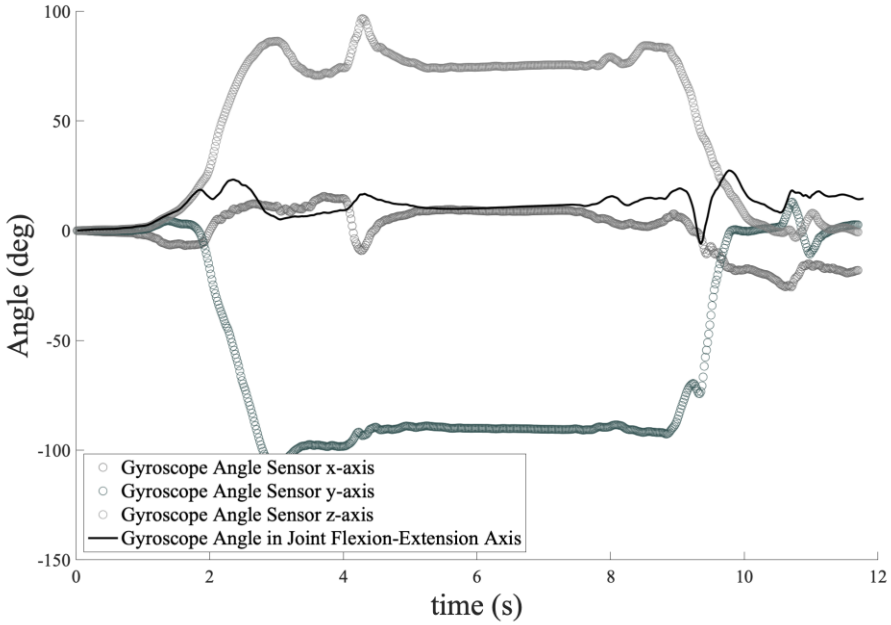


Figure B.2 Representative gyroscope-based ankle angles for a dorsiflexed kneeling trial calculated based on angular velocity data in the sensor frame (presented across all three axes of the gyroscope sensors) as well as angular velocity data which occurs about the ankle flexion-extension axis as calculated through eq. (4.19).

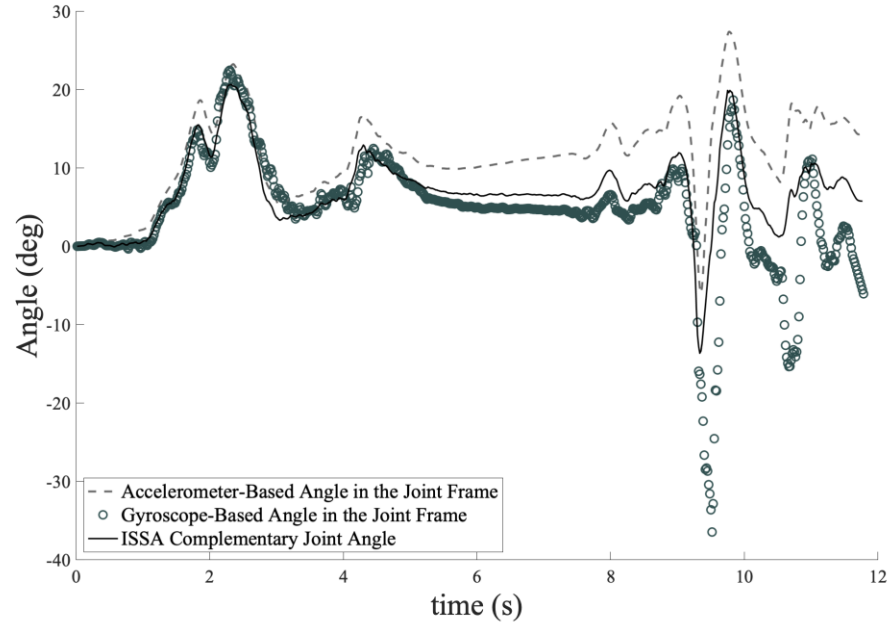


Figure B.3 Representative ankle angles for a dorsiflexed kneeling trial calculated using accelerometer and gyroscope data, rotated into the joint coordinate system, as well as the combination of these angles representing an estimate of the ankle angle as calculated using the ISSA complementary filter presented in eq. (4.40) and eq.(4.41).

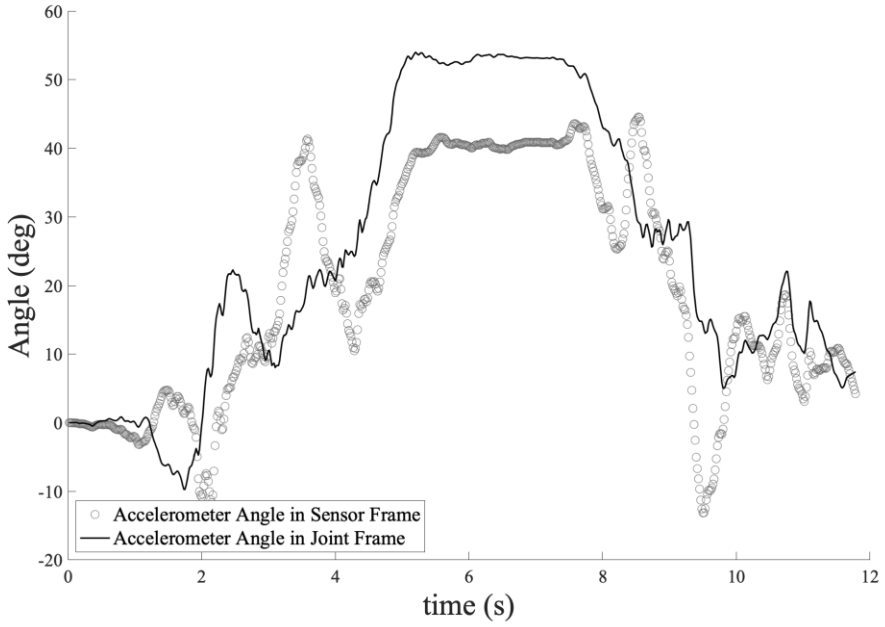


Figure B.4 Representative accelerometer-based hip flexion-extension angles for a dorsiflexed kneeling trial calculated based on acceleration data in the sensor frame as well as on the portion of the acceleration data responsible for accelerating the joint centre as calculated through Eq. (4.35).

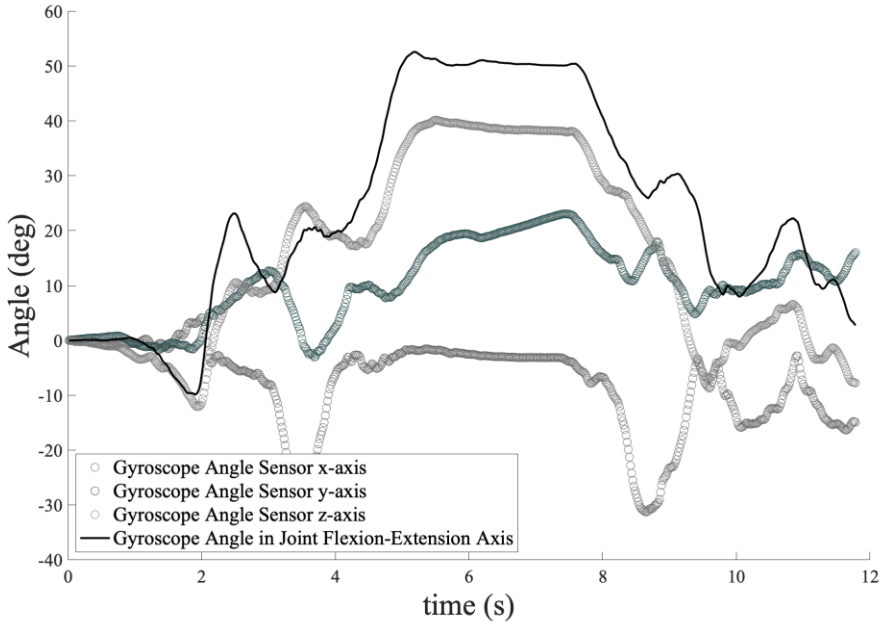


Figure B.5 Representative gyroscope-based hip angles for a dorsiflexed kneeling trial calculated based on angular velocity data in the sensor frame (presented across all three axes of the gyroscope sensors) as well as angular velocity data which occurs about the ankle flexion-extension axis as calculated through eq. (4.19).

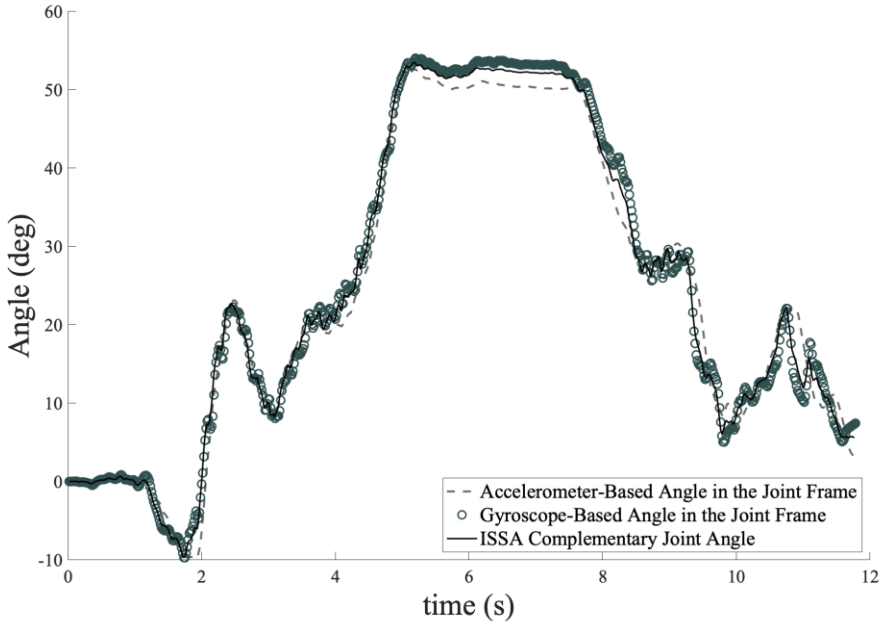


Figure B.6 Representative hip angles for a dorsiflexed kneeling trial calculated using accelerometer and gyroscope data, rotated into the joint coordinate system, as well as the combination of these angles representing an estimate of the hip angle as calculated using the ISSA complementary filter presented in eq. (4.42).

# Appendix C
# Comparison of Left Ankle, Knee, and Hip Flexion-Extension Kinematics Between Protocols

The comparison of ankle, knee, and hip flexion-extension kinematics estimated using the CSKA and ISSA algorithms with IMU data to traditional optical-based measures for each of the nine childcare-inspired postures for the left leg are here presented. Comparative values are also presented for Gait in Table C.1and Table C.2. Any trial in which occlusion of the optical motion capture markers occurred for greater than 25 frames were excluded from comparisons, resulting in 38, 32, 39, 37, 36, 39, 41, 36, 34, and 42 participants being compared for the ankle; 30, 32, 37, 37, 32, 42, 35, 33, 44, and 43 for the knee; and 31, 12, 40, 46, 31, 42, 42, 41, 44, and 46 for the hip, all for ACS, CCS, DK, PK, FS, HS, DAK, SAK, STP, and Gait respectively.

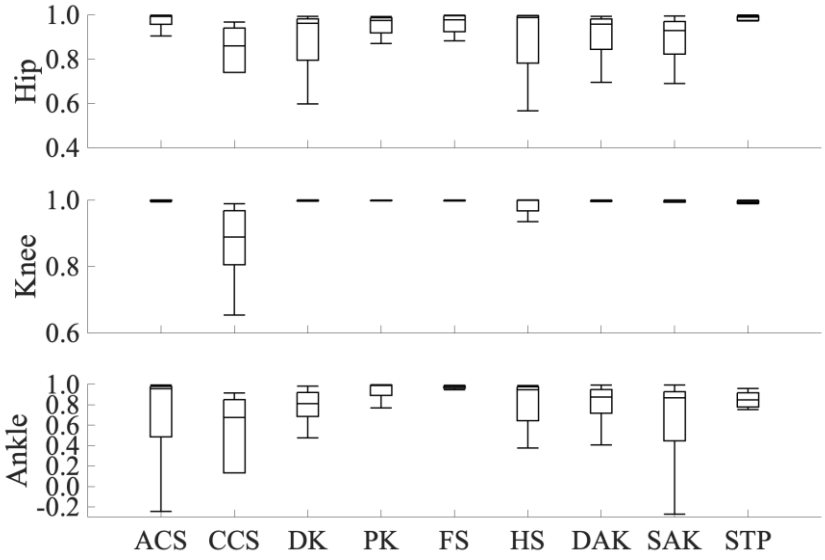


Figure C.1 Box-and-whiskers plots for the Pearson's correlation coefficients (R) for the left ankle, knee, and hip flexion-extension angles representing the linear correlation between the IMU and optical motion capture-based protocols.

Table C.1 Relationship between IMU- and optical motion capture-based left lower limb joint angles through Pearson's correlation coefficients. IMU-based joint angles were estimated using the CSKA and ISSA algorithm. Correlation coefficients have been presented for the 9 childcare-inspired postures (ACS, CCS, DK, PK, FS, HS, DAK, SAK, and STP) as well as in gait.

| | | **ACS** | **CCS** | **DK** | **PK** | **FS** | **HS** | **DAK** | **SAK** | **STP** | **Gait** |
|---|---|---|---|---|---|---|---|---|---|---|---|
| Ankle | Mean | 0.684 | 0.454 | 0.678 | 0.824 | 0.845 | 0.735 | 0.759 | 0.696 | 0.654 | 0.854 |
| | SD | 0.460 | 0.485 | 0.417 | 0.375 | 0.440 | 0.469 | 0.287 | 0.367 | 0.534 | 0.381 |
| | SEM | 0.075 | 0.086 | 0.067 | 0.062 | 0.073 | 0.075 | 0.045 | 0.061 | 0.091 | 0.059 |
| Knee | Mean | 0.926 | 0.824 | 0.934 | 0.993 | 0.979 | 0.918 | 0.993 | 0.944 | 0.918 | 0.862 |
| | SD | 0.364 | 0.341 | 0.320 | 0.018 | 0.047 | 0.195 | 0.018 | 0.137 | 0.263 | 0.324 |
| | SEM | 0.067 | 0.060 | 0.053 | 0.003 | 0.008 | 0.030 | 0.003 | 0.024 | 0.040 | 0.049 |
| Hip | Mean | 0.954 | 0.840 | 0.782 | 0.821 | 0.950 | 0.866 | 0.858 | 0.788 | 0.878 | 0.557 |
| | SD | 0.079 | 0.117 | 0.436 | 0.441 | 0.066 | 0.196 | 0.302 | 0.400 | 0.367 | 0.366 |
| | SEM | 0.014 | 0.034 | 0.069 | 0.065 | 0.012 | 0.030 | 0.047 | 0.062 | 0.055 | 0.054 |

Table C.2 Differences between IMU- and optical motion capture-based left lower limb joint angles. IMU-based joint angles were estimated using the CSKA and ISSA algorithms. Differences between IMU- and optical-based angles were quantified through the difference in the range of motion, the grand mean error, the Root Mean Squared error, and the percent mean error. The differences are presented for 9 childcare-inspired postures (ACS, CCS, DK, PK, FS, HS, DAK, SAK, and STP). All values are expressed in degrees unless otherwise stated.

| | | | ACS | CCS | DK | PK | FS | HS | DAK | SAK | STP | Gait |
|---|---|---|---|---|---|---|---|---|---|---|---|---|
| **Ankle** | **Difference in RoM** | Error Mean | 6.915 | 1.375 | 3.193 | 6.402 | 1.409 | 7.178 | 7.427 | 3.488 | 4.441 | 6.682 |
| | | Error SD | 13.041 | 14.548 | 9.267 | 17.531 | 5.537 | 29.821 | 7.791 | 10.256 | 8.774 | 15.601 |
| | | Error SEM | 2.116 | 2.572 | 1.484 | 2.882 | 0.923 | 4.775 | 1.217 | 1.709 | 1.505 | 2.407 |
| | **Grand Mean Error** | Error Mean | 7.052 | 11.080 | 8.017 | 13.253 | 6.044 | 7.503 | 7.389 | 9.563 | 6.021 | 9.780 |
| | | Error SD | 4.322 | 7.347 | 5.412 | 9.502 | 3.655 | 5.344 | 5.621 | 6.424 | 4.413 | 6.165 |
| | | Error SEM | 0.430 | 0.731 | 0.538 | 0.946 | 0.364 | 0.532 | 0.559 | 0.639 | 0.439 | 0.614 |
| | **Root Mean Squared Error** | | 8.345 | 13.459 | 9.718 | 16.374 | 7.088 | 9.220 | 9.339 | 11.611 | 7.525 | 11.619 |
| | **Percent Mean Error** | | 28% | 35% | 20% | 15% | 15% | 22% | 16% | 19% | 21% | 30% |
| **Knee** | **Difference in RoM** | Error Mean | 0.712 | 0.897 | 0.012 | 0.045 | 1.441 | 5.952 | 1.127 | 1.753 | 2.574 | 4.195 |
| | | Error SD | 3.216 | 6.866 | 1.435 | 4.657 | 6.134 | 17.298 | 5.264 | 4.563 | 10.202 | 6.042 |
| | | Error SEM | 0.587 | 1.214 | 0.236 | 0.766 | 1.084 | 2.669 | 0.890 | 0.794 | 1.538 | 0.921 |
| | **Grand Mean Error** | Error Mean | 6.360 | 17.267 | 9.044 | 3.766 | 5.502 | 6.470 | 3.065 | 4.316 | 3.317 | 9.654 |
| | | Error SD | 4.797 | 17.587 | 6.302 | 3.278 | 4.394 | 5.919 | 2.912 | 3.643 | 2.534 | 5.075 |
| | | Error SEM | 0.477 | 1.750 | 0.627 | 0.326 | 0.437 | 0.589 | 0.290 | 0.362 | 0.252 | 0.505 |
| | **Root Mean Squared Error** | | 8.132 | 24.937 | 11.151 | 5.024 | 7.166 | 8.833 | 4.252 | 5.657 | 4.218 | 11.22 |
| | **Percent Mean Error** | | 7% | 16% | 6% | 3% | 5% | 5% | 2% | 3% | 6% | 13% |
| **Hip** | **Difference in RoM** | Error Mean | 6.951 | 0.846 | 9.083 | 3.017 | 12.503 | 8.906 | 1.201 | 11.711 | 12.053 | 3.749 |
| | | Error SD | 7.143 | 15.050 | 18.595 | 22.711 | 18.649 | 23.626 | 20.814 | 32.428 | 22.994 | 41.895 |
| | | Error SEM | 1.283 | 4.345 | 2.940 | 3.349 | 3.350 | 3.646 | 3.212 | 5.064 | 3.466 | 6.177 |
| | **Grand Mean Error** | Error Mean | 5.821 | 16.085 | 15.209 | 13.474 | 10.431 | 14.095 | 11.904 | 15.387 | 8.396 | 13.011 |
| | | Error SD | 3.965 | 11.434 | 10.397 | 10.066 | 9.299 | 10.398 | 10.158 | 12.502 | 6.840 | 10.184 |
| | | Error SEM | 0.395 | 1.138 | 1.035 | 1.002 | 0.925 | 1.035 | 1.011 | 1.244 | 0.681 | 1.013 |
| | **Root Mean Squared Error** | | 7.062 | 19.710 | 18.566 | 16.884 | 14.194 | 17.820 | 15.813 | 19.984 | 10.875 | 16.558 |
| | **Percent Mean Error** | | 7% | 16% | 19% | 16% | 10% | 16% | 12% | 17% | 11% | 30% |

# Appendix D
# Sample Movement Sequences and Templates for Heels-Up Squatting

The following section contains representative movement sequence and template waveforms based on the joint angle estimates obtained from the right and left ankles, knees, and hips for a single trial of a heels-up squat.

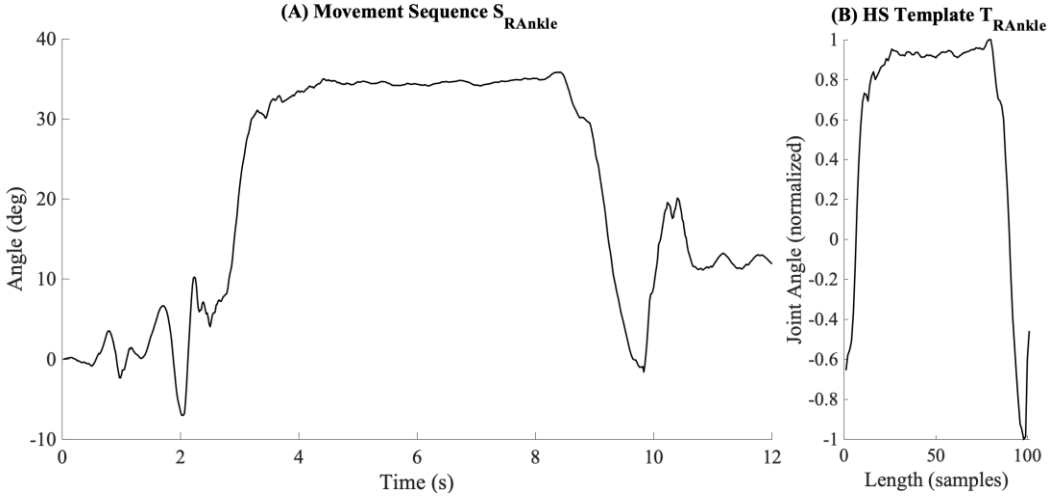


Figure D.1 A representative unnormalized movement sequence $S_{RAnkle}$ for the flexion angle of the right ankle during a heels-up squatting motion trial (**A**) along with the corresponding heels-up squat template $T_{RAnkle}$ generated from this sequence for the right ankle (**B**).

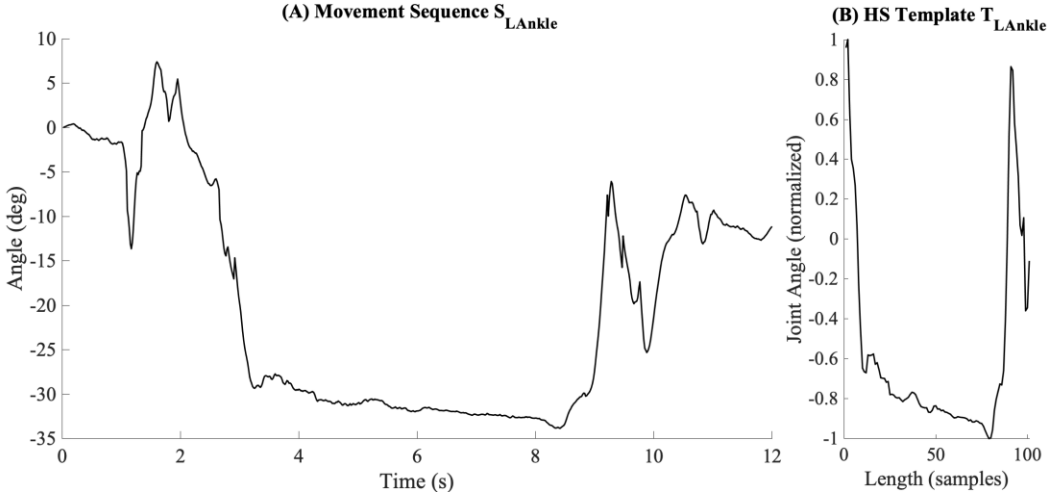


Figure D.2 A representative unnormalized movement sequence $S_{LAnkle}$ for the flexion angle of the left ankle during a heels-up squatting motion trial (**A**) along with the corresponding heels-up squat template $T_{LAnkle}$ generated from this sequence for the left ankle (**B**).

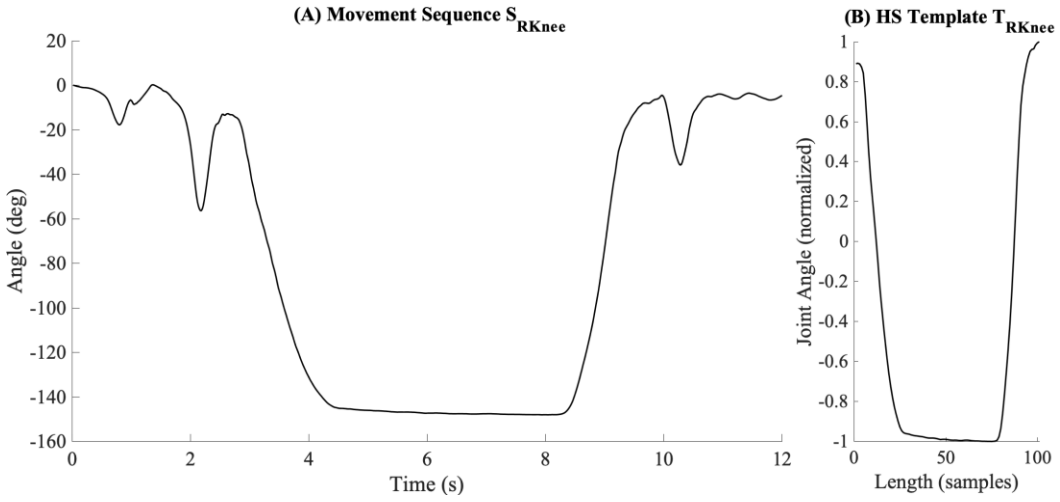


Figure D.3 A representative unnormalized movement sequence $S_{RKnee}$ for the flexion angle of the right knee during a heels-up squatting motion trial (**A**) along with the corresponding heels-up squat template $T_{RKnee}$ generated from this sequence for the right knee (**B**).

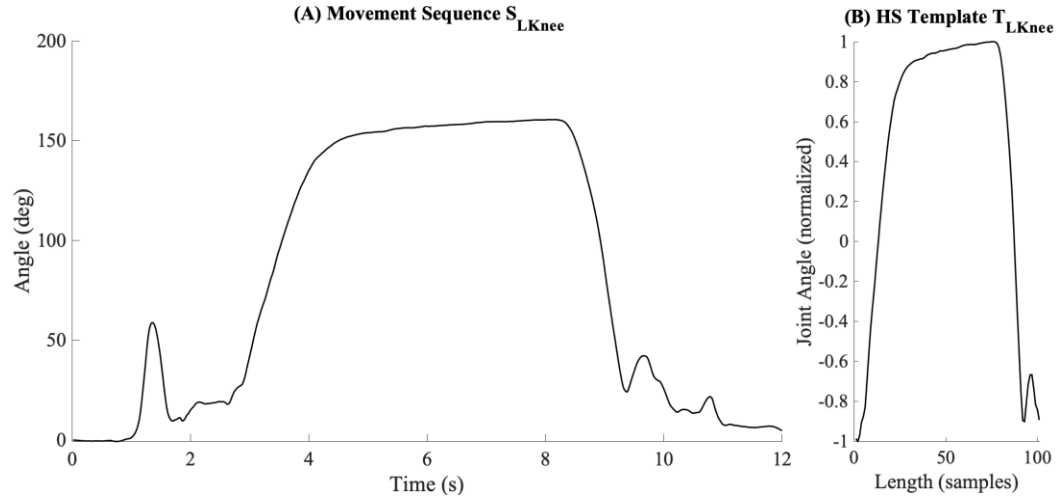


Figure D.4 A representative unnormalized movement sequence $S_{LKnee}$ for the flexion angle of the left knee during a heels-up squatting motion trial (**A**) along with the corresponding heels-up squat template $T_{LKnee}$ generated from this sequence for the left knee (**B**).

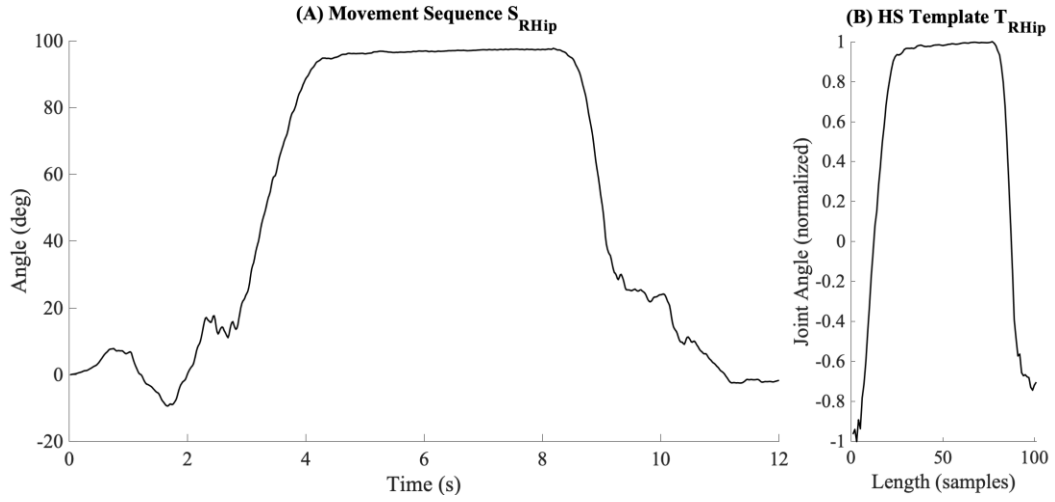


Figure D.5 A representative unnormalized movement sequence $S_{RHip}$ for the flexion angle of the right hip during a heels-up squatting motion trial (**A**) along with the corresponding heels-up squat template $T_{RHip}$ generated from this sequence for the right hip (**B**).

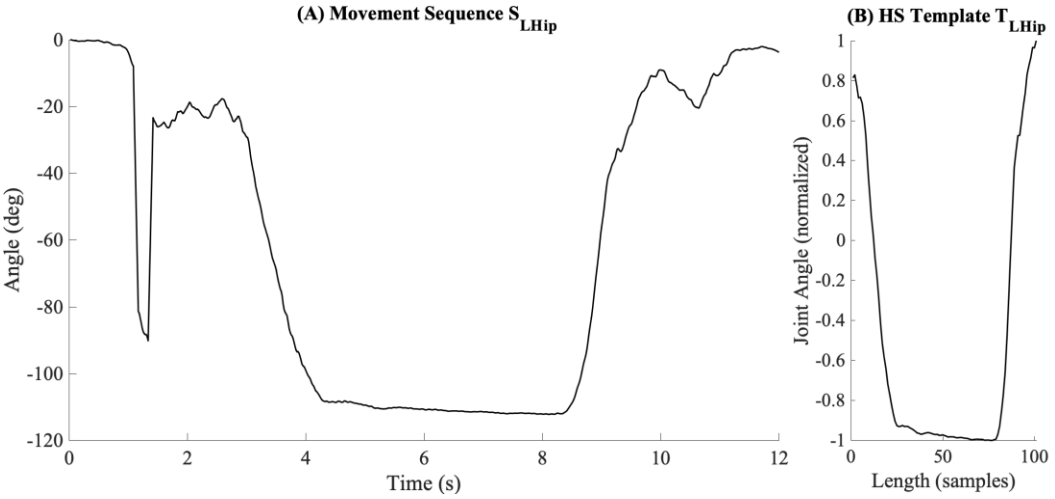


Figure D.6 A representative unnormalized movement sequence $S_{LHip}$ for the flexion angle of the left hip during a heels-up squatting motion trial (**A**) along with the corresponding heels-up squat template $T_{LHip}$ generated from this sequence for the left hip (**B**).

# Appendix E
# Sample Movement Sequences and Templates for a Walking Trial

The following section contains representative movement sequence and template waveforms based on the joint angle estimates obtained from the right and left ankles, knees, and hips for a single walking bout.

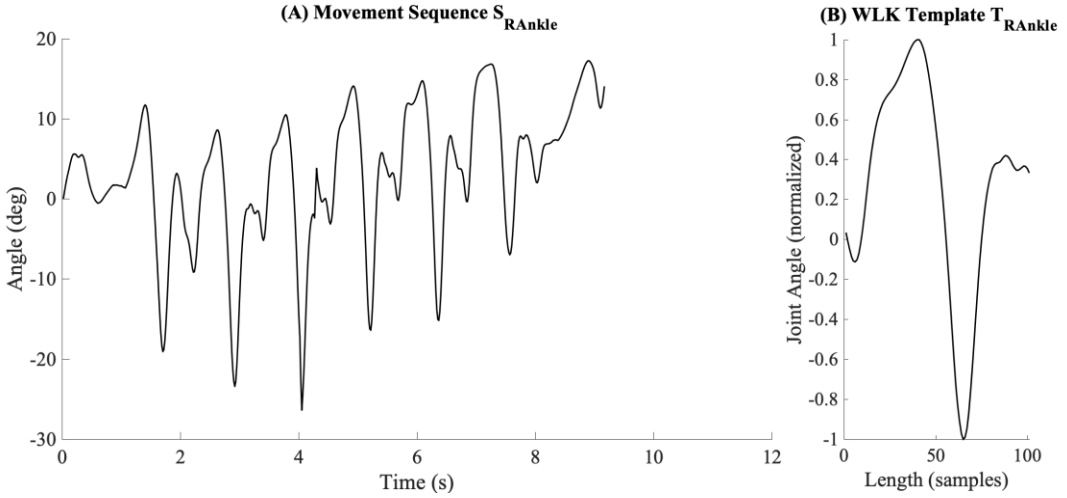


Figure E.1 A representative unnormalized movement sequence $S_{RAnkle}$ for the flexion angle of the right ankle during a walking bout (**A**) along with the corresponding step template $T_{RAnkle}$ generated from this sequence for the right ankle (**B**).

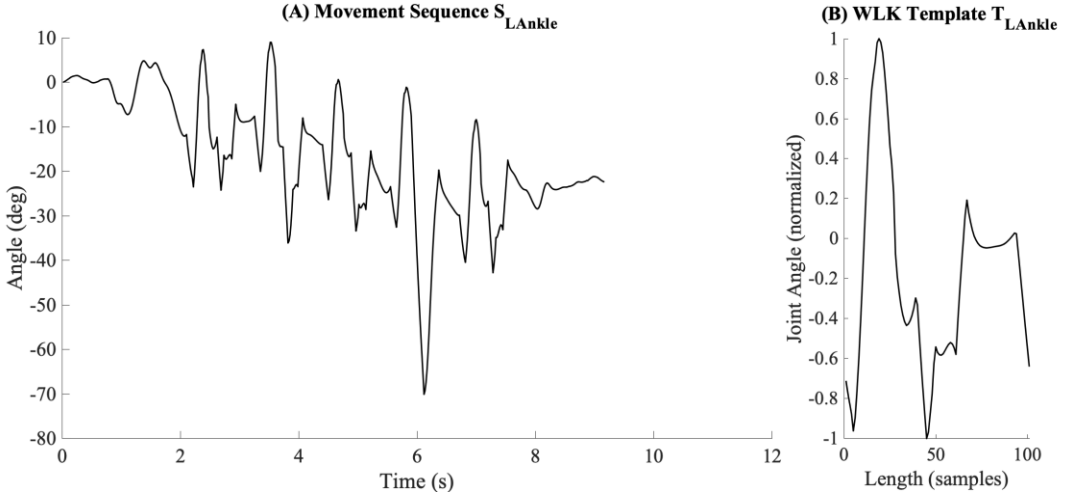


Figure E.2 A representative unnormalized movement sequence $S_{LAnkle}$ for the flexion angle of the left ankle during a walking bout (**A**) along with the corresponding step template $T_{LAnkle}$ generated from this sequence for the left ankle (**B**).

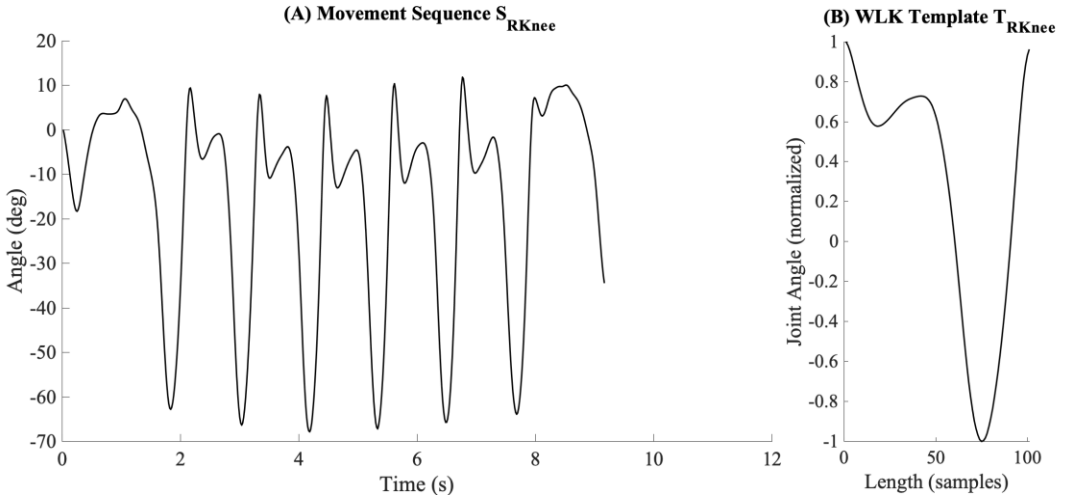


Figure E.3 A representative unnormalized movement sequence $S_{RKnee}$ for the flexion angle of the right knee during a walking bout (**A**) along with the corresponding step template $T_{RKnee}$ generated from this sequence for the right knee (**B**).

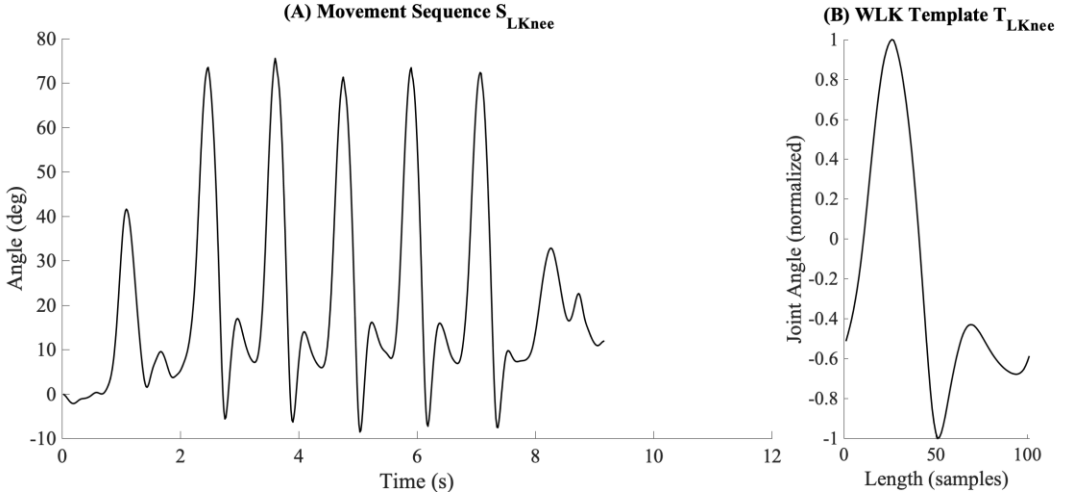


Figure E.4 A representative unnormalized movement sequence $S_{LKnee}$ for the flexion angle of the left knee during a walking bout (**A**) along with the corresponding step template $T_{LKnee}$ generated from this sequence for the left knee (**B**).

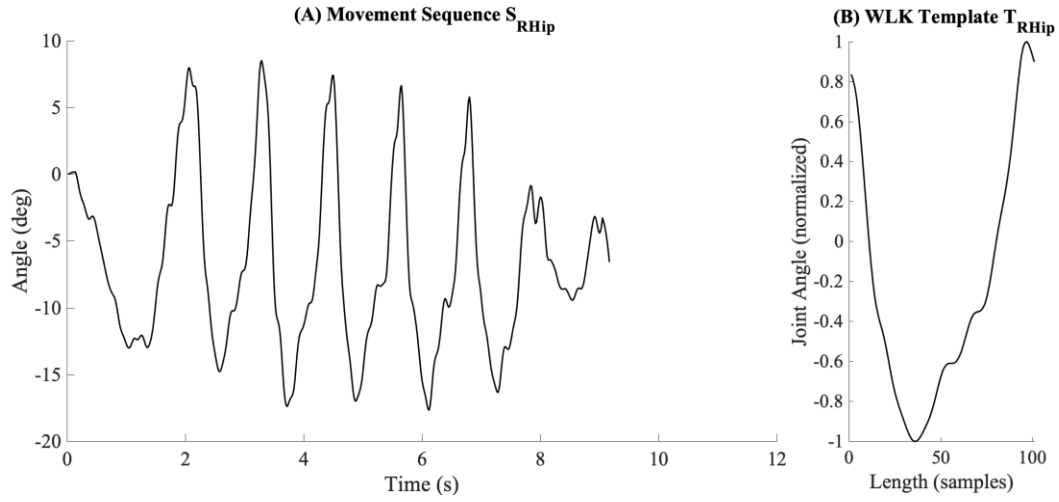


Figure E.5 A representative unnormalized movement sequence $S_{RHip}$ for the flexion angle of the right hip during a walking bout (**A**) along with the corresponding step template $T_{RHip}$ generated from this sequence for the right hip (**B**).

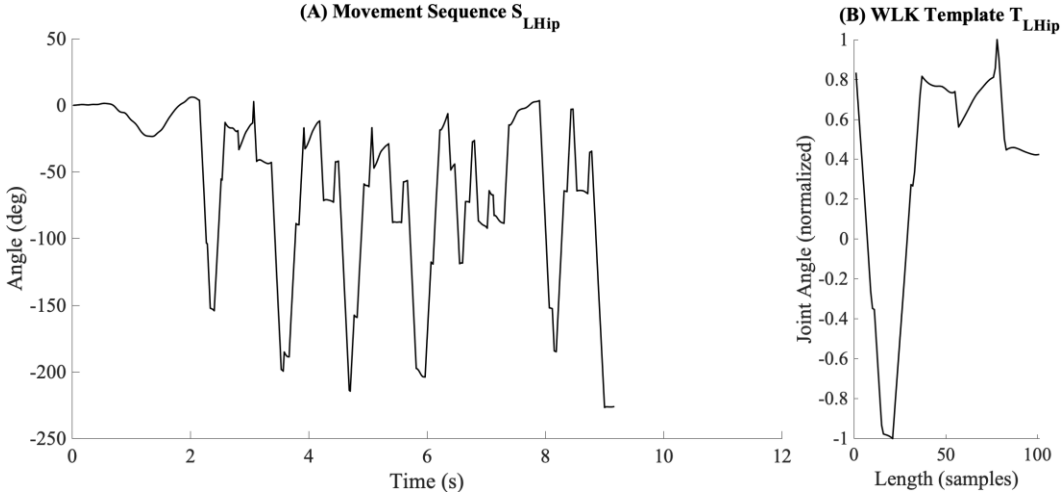


Figure E.6 A representative unnormalized movement sequence $S_{LHip}$ for the flexion angle of the left hip during a walking bout (**A**) along with the corresponding step template $T_{LHip}$ generated from this sequence for the left hip (**B**).

# Appendix F
# Sensitivity-Based Confusion Matrices Resulting from the Classification of Loaded and Unloaded Movement Sequences

Table F.1 Sensitivity-based confusion matrices for the classification of twelve childcare-inspired motions based on (A) unloaded and (B) loaded movement sequences from novel participants using the tested and tuned mDTW kNN model. All values are expressed as percentages relative to the total number of classifications for each childcare-inspired motion. Bolded cells denote correct classifications. The twelve motions analyzed were: heels-up squatting (HS), flatfoot squatting (FS), dorsiflexed kneeling (DK), plantarflexed kneeling (PK), sitting on an adult sized chair (ACS), sitting on a child sized chair (CCS), single arm supported kneeling and double arm supported kneeling (SS), crossed leg sitting (CLS), side sitting and side leaning to the left or the right (SS), stooping (STP), standing (STD), and walking (WLK). *Target Class represents the correct class of each template or sequence. **Output Class represents the class predicted by the classifier.

**A**

Tuned Parameter kNN on Novel Subject Unloaded Movement Sequences

| Target Class* \ Output Class** | DK | PK | FS | HS | CCS | ACS | SK | STP | STD | CLS | SS | WLK |
|---|---|---|---|---|---|---|---|---|---|---|---|---|
| DK | **59.1** | 9.1 | 0.0 | 2.3 | 13.6 | 4.5 | 4.5 | 0.0 | 0.0 | 0.0 | 6.8 | 0.0 |
| PK | 2.2 | **84** | 0.0 | 0.0 | 0.0 | 0.0 | 4.4 | 0.0 | 0.0 | 0.0 | 8.9 | 0.0 |
| FS | 9.3 | 0.0 | **32.6** | 23.3 | 0.0 | 0.0 | 0.0 | 34.9 | 0.0 | 0.0 | 0.0 | 0.0 |
| HS | 7.0 | 0.0 | 32.6 | **41.9** | 2.3 | 0.0 | 0.0 | 16.3 | 0.0 | 0.0 | 0.0 | 0.0 |
| CCS | 0.0 | 0.0 | 2.3 | 9.1 | **70.5** | 18.2 | 0.0 | 0.0 | 0.0 | 0.0 | 0.0 | 0.0 |
| ACS | 0.0 | 0.0 | 0.0 | 2.4 | 26.2 | **71.4** | 0.0 | 0.0 | 0.0 | 0.0 | 0.0 | 0.0 |
| SK | 20.0 | 9.4 | 0.0 | 1.2 | 4.7 | 3.5 | **48.2** | 0.0 | 0.0 | 0.0 | 12.9 | 0.0 |
| STP | 0.0 | 0.0 | 9.3 | 4.7 | 0.0 | 4.7 | 4.7 | **76.7** | 0.0 | 0.0 | 0.0 | 0.0 |
| STD | 0.0 | 0.0 | 0.0 | 2.4 | 2.4 | 4.8 | 0.0 | 4.8 | **76.2** | 0.0 | 7.1 | 2.4 |
| CLS | 0.0 | 2.4 | 0.0 | 0.0 | 4.8 | 2.4 | 0.0 | 0.0 | 0.0 | **64.3** | 26.2 | 0.0 |
| SS | 5.5 | 8.6 | 1.8 | 2.5 | 6.1 | 5.5 | 1.2 | 0.6 | 0.0 | 10.4 | **57.7** | 0.0 |
| WLK | 0.0 | 0.0 | 0.0 | 0.0 | 0.0 | 0.0 | 0.0 | 0.0 | 0.0 | 0.0 | 0.0 | **0** |

**B**

Tuned Parameter *k* NN on Novel Subject Loaded Movement Sequences

| Target Class \ Output Class | DK | PK | FS | HS | CCS | ACS | SK | STP | STD | CLS | SS | WLK |
|---|---|---|---|---|---|---|---|---|---|---|---|---|
| DK | **67.4** | 4.7 | 0.0 | 0.0 | 4.7 | 14.0 | 4.7 | 0.0 | 0.0 | 0.0 | 4.7 | 0.0 |
| PK | 0.0 | **74** | 0.0 | 0.0 | 0.0 | 0.0 | 11.9 | 0.0 | 0.0 | 0.0 | 14.3 | 0.0 |
| FS | 4.5 | 2.3 | **38.6** | 27.3 | 4.5 | 2.3 | 0.0 | 20.5 | 0.0 | 0.0 | 0.0 | 0.0 |
| HS | 0.0 | 4.5 | 31.8 | **36.4** | 6.8 | 0.0 | 0.0 | 20.5 | 0.0 | 0.0 | 0.0 | 0.0 |
| CCS | 0.0 | 0.0 | 0.0 | 2.5 | **65.0** | 27.5 | 2.5 | 2.5 | 0.0 | 0.0 | 0.0 | 0.0 |
| ACS | 0.0 | 0.0 | 2.5 | 0.0 | 35.0 | **60.0** | 0.0 | 0.0 | 0.0 | 0.0 | 2.5 | 0.0 |
| SK | 0.0 | 0.0 | 0.0 | 0.0 | 0.0 | 0.0 | **0.0** | 0.0 | 0.0 | 0.0 | 0.0 | 0.0 |
| STP | 0.0 | 0.0 | 0.0 | 0.0 | 0.0 | 0.0 | 0.0 | **0.0** | 0.0 | 0.0 | 0.0 | 0.0 |
| STD | 0.0 | 0.0 | 2.3 | 4.7 | 2.3 | 0.0 | 2.3 | 4.7 | **76.7** | 0.0 | 2.3 | 4.7 |
| CLS | 2.9 | 0.0 | 8.8 | 0.0 | 2.9 | 0.0 | 0.0 | 0.0 | 0.0 | **58.8** | 26.5 | 0.0 |
| SS | 5.7 | 5.7 | 4.9 | 4.9 | 5.7 | 2.4 | 7.3 | 0.0 | 0.0 | 15.4 | **48.0** | 0.0 |
| WLK | 0.0 | 0.0 | 0.0 | 0.0 | 0.0 | 0.0 | 0.0 | 0.0 | 0.0 | 0.0 | 0.0 | **0** |

# Appendix G
# Labels Assigned to each Movement Class for Classification Model A – Developed with a Combination of Laboratory-Based Templates and Continuous Windows of Pseudo-Childcare Activities

Table G.1 All permutations of movement classes assigned to movement templates and continuous motion windows labeled and included within the algorithm development, testing, and validation datasets for Model A. The twelve motions analyzed were: heels-up squatting (HS), flatfoot squatting (FS), dorsiflexed kneeling (DK), plantarflexed kneeling (PK), sitting on an adult sized chair (ACS), sitting on a child sized chair (CCS), single arm supported kneeling and double arm supported kneeling (SS), crossed leg sitting (CLS), side sitting and side leaning to the left or the right (SS), stooping (STP), standing (STD), and walking (WLK). The phase of motion labels correspond to: ascent (_A), ascent descent (_AD), ascent walk (_AW), descent (_D), descent ascent (_DA), descent static (_DS), static (_S), static ascent (_SA), walking (_W), and walking descent (_WD).

| | | | | | | | | | |
|---|---|---|---|---|---|---|---|---|---|
| ACS_A | CCS_A | CLS_A | DK_A | FS_A | HS_S | PK_A | STP_A | SS_A | SK_A |
| ACS_A_STD | CCS_AD | CLS_A_STD | DK_A_STD | FS_A_STD | HS_A_FS_D | PK_A_STD | STP_A_CCS_D | SS_A_STD | SK_A_STD |
| ACS_AW | CCS_A_STD | CLS_A_STP_D | DK_A_STP_D | FS_A_STP_D | HS_A_STD | PK_A_STP_D | STP_AD | SS_AW | SK_A_STP_D |
| ACS_D | CCS_AW | CLS_AW | DK_AW | FS_AW | HS_A_STP_D | PK_AD | STP_A_HD_D | SS_CLS_S | SK_AW |
| ACS_DA | CCS_D | CLS_DK_S | DK_D | FS_D | HS_AW | PK_CLS_S | STP_A_PK_D | SS_DK_S | SK_CLS_S |
| ACS_DS | CCS_DA | CLS_DK_S | DK_DA | FS_DA | HS_DK_S | PK_DK_S | STP_A_STD | SS_DK_S | SK_DK_S |
| ACS_STD_D | CCS_DS | CLS_DA | DK_D_SS_S | FS_DS | HS_D | PK_DK_S | STP_AW | SS_DA | SK_DK_S |
| ACS_S | CCS_STD_D | CLS_D_SS_S | DK_DS | FS_HS_S | HS_DA | PK_DA | STP_CCS_D | SS_D_CLS_S | SK_DA |
| ACS_SA | CCS_STP_A | CLS_DS | DK_PK_S | FS_STD_D | HS_DS | PK_DS | STP_DK_D | SS_DS | SK_D_SS_S |
| ACS_WD | CCS_S | CLS_PK_S | DK_STD_D | FS_SS_S | HS_D_SS_S | PK_STD_D | STP_D | SS_FS_S | SK_DS |
| | CCS_SA | CLS_STD_D | DK_SS_S | FS_S | HS_FS_S | PK_STP_A | STP_DA | SS_HS_S | SK_PK_S |
| WALK_STD | CCS_WD | CLS_STP_A | DK_S | FS_SA | HS_STD_D | PK_SS_S | STP_DS | SS_PK_S | SK_S_D |
| WALK_W | | CLS_SS_S | DK_SA | FS_WD | HS_STD_D | PK_S | STP_SK_D | SS_STD_D | SK_SS_S |
| | | CLS_S | DK_S_SK_A | | HS_SA | PK_SA | STP_SS_D | SS_STD_D | SK_S |
| STD_STD | | CLS_SA | DK_SK_S | | HS_WD | PK_SK_S | STP_STD_D | SS_SA | SK_SA |
| STD_W | | CLS_SK_S | DK_WD | | | PK_WD | STP_S | SS_SK_D | SK_S_DK_A |
| | | CLS_WD | | | | | STP_SA | SS_WD | SK_WD |
| | | | | | | | STP_WD | | |

# Appendix H
# Labels Assigned to each Movement Class for Classification Model B – Which was Developed Using Continuous Windows of Pseudo-Childcare Activities

Table H.1 All permutations of movement classes assigned to movement templates and continuous motion windows labeled and included within the algorithm development, testing, and validation datasets for Model B. The twelve motions analyzed were: heels-up squatting (HS), flatfoot squatting (FS), dorsiflexed kneeling (DK), plantarflexed kneeling (PK), sitting on a child sized chair (CCS), single arm supported kneeling and double arm supported kneeling (SS), crossed leg sitting (CLS), side sitting and side leaning to the left or the right (SS), stooping (STP), standing (STD), and walking (WLK). The phase of motion labels correspond to: ascent (_A), ascent descent (_AD), ascent walk (_AW), descent (_D), descent ascent (_DA), descent static (_DS), static (_S), static ascent (_SA), walking (_W), and walking descent (_WD).

| | | | | | | | | |
|---|---|---|---|---|---|---|---|---|
| CCS_A | CLS_A | DK_A | FS_A | HS_S | PK_A | STP_A | SS_A | SK_A |
| CCS_AD | CLS_A_STD | DK_A_STD | FS_A_STD | HS_A_FS_D | PK_A_STD | STP_A_CCS_D | SS_A_STD | SK_A_STD |
| CCS_A_STD | CLS_A_STP_D | DK_A_STP_D | FS_A_STP_D | HS_A_STD | PK_A_STP_D | STP_AD | SS_AW | SK_A_STP_D |
| CCS_AW | CLS_AW | DK_AW | FS_AW | HS_A_STP_D | PK_AD | STP_A_HD_D | SS_CLS_S | SK_AW |
| CCS_D | CLS_DK_S | DK_D | FS_D | HS_AW | PK_CLS_S | STP_A_PK_D | SS_DK_S | SK_CLS_S |
| CCS_DA | CLS_DK_S | DK_DA | FS_DA | HS_DK_S | PK_DK_S | STP_A_STD | SS_DK_S | SK_DK_S |
| CCS_DS | CLS_DA | DK_D_SS_S | FS_D_SS_S | HS_D | PK_DK_S | STP_AW | SS_DA | SK_DK_S |
| CCS_STD_D | CLS_D_SS_S | DK_DS | FS_DA | HS_DA | PK_DA | STP_CCS_D | SS_D_CLS_S | SK_DA |
| CCS_STP_A | CLS_DS | DK_PK_S | FS_DS | HS_D_SS_S | PK_DS | STP_DK_D | SS_DS | SK_D_SS_S |
| CCS_S | CLS_PK_S | DK_STD_D | FS_HS_S | HS_DS | PK_STD_D | STP_D | SS_FS_S | SK_DS |
| CCS_SA | CLS_STD_D | DK_SS_S | FS_STD_D | HS_D_SK_S | PK_STP_A | STP_DA | SS_HS_S | SK_PK_S |
| CCS_WD | CLS_STP_A | DK_S | FS_SS_S | HS_FS_S | PK_SS_S | STP_DS | SS_PK_S | SK_S_D |
| | CLS_SS_S | DK_SA | FS_S | HS_STD_D | PK_S | STP_SK_D | SS_STD_D | SK_SS_S |
| WALK_STD | CLS_S | DK_S_SK_A | FS_SA | HS_S | PK_SA | STP_SS_D | SS_STD_D | SK_S |
| WALK_W | CLS_SA | DK_SK_S | FS_WD | HS_SA | PK_SK_S | STP_STD_D | SS_SA | SK_SA |
| | CLS_SK_S | DK_WD | | HS_SK_S | PK_WD | STP_S | SS_SK_D | SK_S_DK_A |
| STD_STD | CLS_WD | | | HS_WD | | STP_SA | SS_WD | SK_WD |
| STD_W | | | | | | STP_WD | | |

# Appendix I
# Confusion Matrix Resulting from the Classification of Continuous Movement Windows in the Testing of Model Bb

Table I.1 Confusion matrix obtained from the classification of continuous movement windows from a single trial of a pseudo-childcare activity in a simulated childcare environment using a mDTW kNN model (model Bb). This model was developed using only the continuous windows of pseudo-childcare movements collected for Chapter 6. All values represent the number of windows classified within each Output Class. Bolded cells denote correct classifications. The motions classes present in these data were: flatfoot squatting ascent to walking (FS_AW), flatfoot squatting walking to descent (FS_WD), flatfoot squatting descent to ascent (FS_DA), crossed leg sitting descent (CLS_D), crossed leg sitting descent to static (CLS_DS), crossed leg sitting static (CLS_S), crosse leg sitting static to ascent (CLS_SA), crossed leg sitting ascent to walking (CLS_AW), walking (WLK_W), walking to standing (WLK_STD), and standing to walking (STD_W), The motions predicted in these data additionally included dorsiflexed kneeling static (DK_W), side sitting static (SS_S), supported kneeling static (SK_S), and child chair sitting static (CCS_S) *Target Class represents the correct class of each template or sequence. **Output Class represents the class predicted by the classifier.

Model *Bb* Classification of Testing Movement Windows

| *Target Class | | | | | | | | | | | | | | | | | | |
|---|---|---|---|---|---|---|---|---|---|---|---|---|---|---|---|---|---|---|
| | FS_AW | **0** | 0 | 0 | 0 | 0 | 0 | 1 | 0 | 0 | 0 | 0 | 0 | 0 | 1 | 1 | 0 | 0 |
| | FS_WD | 0 | **0** | 0 | 0 | 0 | 0 | 1 | 0 | 0 | 0 | 1 | 0 | 0 | 0 | 0 | 0 | 0 |
| | FS_DA | 0 | 0 | **0** | 0 | 0 | 0 | 2 | 0 | 0 | 0 | 0 | 0 | 0 | 0 | 0 | 0 | 0 |
| | CLS_WD | 0 | 0 | 0 | **0** | 0 | 0 | 0 | 0 | 0 | 0 | 0 | 0 | 0 | 0 | 1 | 0 | 0 |
| | CLS_D | 0 | 0 | 0 | 0 | **1** | 0 | 0 | 0 | 0 | 0 | 0 | 0 | 0 | 0 | 0 | 1 | 0 |
| | CLS_DS | 0 | 0 | 0 | 0 | 0 | **0** | 0 | 0 | 0 | 0 | 0 | 0 | 0 | 0 | 0 | 1 | 0 |
| | CLS_S | 0 | 0 | 0 | 0 | 0 | 0 | **184** | 0 | 0 | 0 | 0 | 0 | 0 | 0 | 11 | 1 | 12 |
| | CLS_SA | 0 | 0 | 0 | 0 | 0 | 0 | 1 | **0** | 0 | 0 | 0 | 0 | 0 | 0 | 0 | 0 | 0 |
| | CLS_A | 0 | 0 | 0 | 0 | 0 | 0 | 2 | 0 | **0** | 0 | 0 | 0 | 0 | 0 | 1 | 0 | 0 |
| | CLS_AW | 0 | 0 | 0 | 0 | 0 | 0 | 0 | 0 | 0 | **0** | 0 | 0 | 0 | 0 | 0 | 1 | 0 |
| | WLK_W | 0 | 0 | 0 | 0 | 0 | 0 | 0 | 0 | 0 | 0 | **0** | 0 | 0 | 2 | 1 | 0 | 0 |
| | WLK_STD | 0 | 0 | 0 | 0 | 0 | 0 | 0 | 0 | 0 | 0 | 0 | **0** | 0 | 0 | 1 | 0 | 0 |
| | STD_W | 0 | 0 | 0 | 0 | 0 | 0 | 1 | 0 | 0 | 0 | 0 | 0 | **0** | 0 | 0 | 0 | 0 |
| | DK_S | 0 | 0 | 0 | 0 | 0 | 0 | 0 | 0 | 0 | 0 | 0 | 0 | 0 | **0** | 0 | 0 | 0 |
| | SS_S | 0 | 0 | 0 | 0 | 0 | 0 | 0 | 0 | 0 | 0 | 0 | 0 | 0 | 0 | **0** | 0 | 0 |
| | SK_S | 0 | 0 | 0 | 0 | 0 | 0 | 0 | 0 | 0 | 0 | 0 | 0 | 0 | 0 | 0 | **0** | 0 |
| | CCS_S | 0 | 0 | 0 | 0 | 0 | 0 | 0 | 0 | 0 | 0 | 0 | 0 | 0 | 0 | 0 | 0 | **0** |
| | | FS_AW | FS_WD | FS_DA | CLS_WD | CLS_D | CLS_DS | CLS_S | CLS_SA | CLS_A | CLS_AW | Walk_W | Walk_STD | STD_W | DK_S | SS_S | SK_S | CCS_S |

**Output Class